CRYSTAL-FIELD AND MÖSSBAUER APPLICATIONS TO THE STUDY OF SITE DISTRIBUTION AND ELECTRONIC PROPERTIES OF FERROUS IRON IN MINERALS WITH EMPHASIS ON CALCIC AMPHIBOLES, ORTHOPYROXENE AND CORDIERITE

Thesis by

Don Steven Goldman

In Partial Fulfillment of the Requirements

for the Degree of

Doctor of Philosophy

California Institute of Technology

Pasadena, California

1977

(Submitted May 2, 1977)

ACKNOWLEDGEMENTS

Specific acknowledgements are given at the end of each chapter. In addition, I want to thank Arden Albee, who first took on the burden of my inexperience and for providing microprobe time when funding was scarce (which was nearly always). Wayne Dollase kindly provided experimental time with his Mössbauer spectrometer, without which much of the work done in this thesis would not have been possible, and provided helpful discussion throughout the course of this study. The continuous enthusiasm and pure enjoyment for the field of mineralogy that is characteristic of George Rossman made this thesis project even more enjoyable for me. His advice and direction have been appreciated many times. I would also like to thank my parents, who have always provided me with an opportunity to extend my education. I want to thank my wife, Sandi, for typing a portion of this thesis, but most important of all, for her love, inspiration and patience during my graduate years at Cal Tech.

ABSTRACT

The electronic absorption spectroscopy of ferrous iron is sensitive to the geometry of the coordination site in which it resides. This sensitivity enables ferrous iron in multiple sites in a mineral to be distinguished. The spectra of ferrous iron in the M(2) site in orthopyroxene, $(Mg,Fe)SiO_3$, are used as a model for the spectroscopic properties of iron in a distorted site. The splitting of the $^5\underline{T}_{2g}$ ground state is observed to be 2350 cm^{-1} enabling a theoretical point-charge model to be developed using $\underline{C}_{2v}$ symmetry. The intensity of the near infrared bands due to the splitting of the $^5\underline{E}_g$ state are found to linearly correlate with the concentration of ferrous iron in the M(2) site. From this correlation, calibrations are established for the intensities of the near infrared bands so that quantitative site distributions can be determined for single orthopyroxene crystals from optical spectra. Thermally induced cation disorder allows assignments to be made for spin-allowed and spin-forbidden ferrous iron bands originating from both the M(1) and M(2) sites.

The electronic absorption and Mössbauer spectra of calcic amphiboles, $Ca_2(Mg,Fe)_5Si_8O_{22}(OH)_2$, are reinterpreted to include previously neglected contributions from ferrous iron in the calcium-rich M(4) site. Bands due to ferrous iron in M(1), M(2) and M(3) sites are examined in the electronic spectra and the intensity of the Fe^{2+}/Fe^{3+} intervalence charge-transfer band is found to linearly correlate with the ferric iron content. Next-nearest neighbor variations of ferric iron and aluminum are found to affect the ferrous iron peak parameters in the Mössbauer spectra of calcic amphiboles which impairs the capability of determining accurate site distributions.

Ferrous iron is found to be present in the channel cavities and the octahedral site in cordierite, $(Mg,Fe)_2Al_4Si_5O_{18}$, osumilite, $K(Mg,Fe)_2Al_3(Si_{10}Al_2)O_{30}$, and beryl, $Be_3Al_2Si_6O_{18}$. In cordierite, two types of water are suggested to be present in the channel cavities that differ in crystallographic orientation and relationship to other channel constituents, whereas osumilite is found to be virtually anhydrous. In cordierite, cation migration within the channels is suggested to occur after dehydration which could explain the observed change in the lattice geometry. The blue color in these minerals is suggested to be due to intervalence charge-transfer between ferrous iron and channel ferric iron. Electronic spectra suggest that structural state variations occur in osumilite, whereas significant variations in cordierite are not apparent. Ferric iron in tetrahedral coordination in osumilite is indicated from Mössbauer spectra.

The effect of site size and distortion on the spectroscopic properties of ferrous iron in terms of band position, intensity and polarization anisotropy is examined. As a non-centrosymmetric site becomes larger, absorption bands migrate to longer wavelengths (lower energy), become more intense, and exhibit greater polarization anisotropy among each other. For these sites, intensification is correlated with a decrease in the quadrupole splitting determined from Mössbauer spectra. The spectroscopy of ferrous iron in large sites is distinctly different from that observed from ferrous iron in smaller sites.

PREFACE

An important result of mineralogical research over the past few decades is the realization that ferromagnesium ions are distributed differently among multiple sites in minerals. The differences in site distribution are related to the different geometrical configurations of each site. Crystallographic analysis has provided quantitative site distribution information. However, this technique is least sensitive when a variety of different ions occupy the same site or when the ferromagnesium ion is a minor constituent of that site. Electronic absorption and Mössbauer (^{57}Fe gamma resonance) spectroscopies are sensitive to the presence of ferrous iron in geometrically distinct sites, but only the latter technique, in general, has provided quantitative site distributions. As spectroscopic techniques, they are subject to interpretational error in assigning spectral peaks to ferrous iron in specific sites. One way by which these complications can be minimized is to correlate the spectral data from both techniques combined with electron microprobe data for the same specimen, and to compare these results for a number of different specimens. This approach has been applied to study the site distribution of ferrous iron in: orthopyroxene, $(Mg,Fe)SiO_3$; calcic amphiboles, $Ca_2(Mg,Fe)_5Si_8O_{22}(OH)_2$; cordierite, $(Mg,Fe)_2Al_4Si_5O_{18}$; osumilite, $K(Mg,Fe)_2Al_3(Si_{10}Al_2)O_{30}$; and beryl, $Be_3Al_2Si_6O_{18}$. It is hoped that by combining independent spectroscopic data and using stoichiometry constraints from electron microprobe data, consistent and understandable site distributions of ferrous iron will be obtained in these minerals.

The overall objective of this research is to examine the possibility

of determining quantitative information from electronic absorption spectra of single mineral crystals. Three types of information will be sought. First, the intensities of the electronic absorption bands due to ferrous iron in a particular site in a mineral containing multiple sites will be correlated to the amount of ferrous iron in that site determined from electron microprobe and Mössbauer data (orthopyroxene; Chapter 4). Second, the intensities of the electronic absorption bands in the visible region that are attributed to intervalence charge-transfer between adjacent ferric and ferrous ions and that are responsible for the color and pleochroism in most minerals will be correlated to the ferric iron content of the mineral determined from electron microprobe and Mössbauer data (calcic amphiboles; Chapter 7). Third, the intensities of water absorption bands in the electronic absorption spectra will be correlated to the total amount of water in the mineral determined from thermogravimetric analysis (cordierite; Chapter 8).

Another major objective of this research is to examine the effect of site distortion on the electronic structure and spectroscopic properties of ferrous iron in minerals. These properties include crystal-field splitting, molar absorptivity and polarization anisotropy among the various bands arising from a particular ferrous ion. This discussion will also be extended to include variations in the Mössbauer parameters as sites become more distorted. Correlating these properties to the type of distortion of the coordination site will establish a further basis for using both spectroscopic techniques as diagnostic tools in site distribution studies.

The research presented herein was initiated with calcic amphibole

samples in which electronic absorption and Mössbauer data suggested the presence of ferrous iron in the large and highly distorted M(4) site, which is predominantly occupied by calcium. These interpretations from spectroscopic data conflict with previous work done on the site distribution of ferrous iron in calcic amphiboles. It became necessary to obtain a better understanding of the spectroscopic properties of ferrous iron in a large, distorted site to evaluate the discrepancy in spectral assignments. For this reason, the spectroscopic study of orthopyroxene was undertaken. Orthopyroxene is ideal for this purpose because of its simpler chemistry and smaller number of sites than calcic amphiboles. In addition, the calcic amphibole M(4) site and the orthopyroxene M(2) site are both large sites and have similar distortions consisting of an elongation of two cis metal-oxygen bond lengths. The spectroscopic properties of ferrous iron in the orthopyroxene M(2) site provided the basis to support the initial conclusions from the calcic amphibole spectral study.

It became apparent during the course of these investigations that the spectroscopic properties of ferrous iron in the large sites, such as in calcic amphiboles and orthopyroxenes, are different than those of ferrous iron in the smaller six-coordinate sites. For this reason, it became necessary to understand the spectroscopic properties of ferrous iron in the smaller sites. The six-coordinate sites in cordierite, osumilite and beryl meet these criteria in that they are smaller than the large pyroxene and amphibole sites. The main distortion in these smaller sites is due to a reduction of one cis metal-oxygen bond angle from 90^{o} to nearly 70^{o}, although all of the metal-oxygen bond lengths

are nearly equal. In the course of this study, the presence of ferrous iron in the channel cavities in cordierite, osumilite and beryl was indicated from both Mössbauer and electronic absorption spectra.

The spectroscopic properties of ferrous iron in a variety of six-coordinate sites are correlated to the distortion of the site in which it resides. The resulting correlations are presented in Chapter 11. It is hoped that they may be used as a basis to interpret or re-interpret the spectra of other minerals that contain ferrous iron.

TABLE OF CONTENTS

CHAPTER 1

IDENTIFICATION OF A MID-INFRARED ELECTRONIC ABSORPTION BAND OF Fe^{2+} IN THE DISTORTED M(2) SITE OF ORTHOPYROXENE, $(Mg,Fe)SiO_3$

Published: Chemical Physics Letters, 41, 474-475.
Co-author: George R. Rossman

ABSTRACT

An electronic absorption band of Fe^{2+} in the distorted, six-coordinate M(2) site of the common mineral orthopyroxene, $(Mg,Fe)SiO_3$, is identified at 2350 cm^{-1}. This band is attributed to the $A_1 \rightarrow B_2$ transition within the split $^5T_{2g}$ state of Fe^{2+} in C_{2v} symmetry.

Electronic absorption bands can be expected to occur in the mid-infrared region arising from metal ions in sites of low symmetry. They are generally masked by strong interferences due to absorptions from ligands and solvents. Silicate minerals provide useful substances for the study of the mid-infrared region because their spectra are comparatively free of vibrational activity in this region, high concentrations of metal ions can be obtained, and large crystals are generally available. The near-infrared spectra of Fe^{2+} have been extensively studied in minerals and are characterized by splittings of the octahedral ^5E_g state of up to nearly 6000 cm^{-1}. The possibility of observing large splittings of the octahedral $^5T_{2g}$ ground state has not been examined in these minerals.

The crystal-field splittings of electronic absorption bands due to Fe^{2+} in the distorted six-coordinate M(2) site of the orthorhombic mineral orthopyroxene, $(Mg,Fe)SiO_3$, are of the largest known in the spectroscopy of ferrous iron. Iron-oxygen bond distances in this site vary from 2.037 to 2.519 Å [1]. Absorption bands of Fe^{2+} in this site at about 11,000 cm^{-1} and 5400 cm^{-1} have been well-documented by Bancroft and Burns [2], Burns [3], and Runciman et al. [4]. In a theoretical treatment based on C_{2v} symmetry, Runciman et al. [4] assigned these bands to the $^5A_1 \rightarrow {}^5A_1$ and $^5A_1 \rightarrow {}^5B_1$ transitions of Fe^{2+} in the M(2) site, respectively. Both of these transitions arise from the splitting of the octahedral ^5E_g state. A third feature at 3100 cm^{-1} was observed and assigned to the $^5A_1 \rightarrow {}^5B_2$ transition of Fe^{2+} in the M(2) site on the basis of its polarization properties [4]. Because the half-width of the 3100 cm^{-1} band ($\sim$175 cm^{-1}) seemed unreasonably narrow for a ligand field transition of Fe^{2+}, a number of orthopyroxene samples containing different M(2) iron contents were studied. The 3100 cm^{-1} band is totally absent in these samples and, hence, does not originate from Fe^{2+}.

In the course of this study, a band at 2350 cm^{-1} was observed with a half-width of ~1100 cm^{-1}. The spectra in Figure 1 indicate that the 2350 cm^{-1} band is more intense in samples with higher iron concentrations and appears to correlate in intensity with the 5400 cm^{-1} band which has been previously assigned to M(2) Fe^{2+}. The intensity correlation of these two bands shown in Figure 2 indicates that the 2350 cm^{-1} band is also due to Fe^{2+} in the M(2) site. The 1100 cm^{-1} half-width of the 2350 cm^{-1} band is reasonable for an electronic transition of Fe^{2+} and is similar to the half-width of the 5400 cm^{-1} band. However, because 2350 cm^{-1} is an unusual energy to observe an electronic transition and because of the presence of vibrational transitions in this region, a vibrational origin due to the substitution of Fe for Mg cannot be discounted. To study this possibility, the spectra of pyroxenes containing similar concentrations of metal ions with the same charge and similar atomic weights (Mn^{2+} and Co^{2+}) were obtained. These spectra are featureless in the 2100-4000 cm^{-1} region indicating that the 2350 cm^{-1} band is due to an electronic transition of Fe^{2+} in the M(2) site.

The 2350 cm^{-1} band is assigned to a transition within the split $^5T_{2g}(O_h)$ state of Fe^{2+} in the M(2) site. Based on the analysis in Runciman et al. [4], this band is assigned to the $^5A_1 \rightarrow {}^5B_2$ transition in C_{2v} symmetry. The orthopyroxene spectra will be analyzed with a C_{2v} point-charge model in a forthcoming paper.

The spectra of a number of additional substances are being examined for mid-infrared Fe^{2+} electronic absorptions. Several other minerals are known to exhibit large splittings of the octahedral ^5E_g state. However, mid-infrared Fe^{2+} absorption has not been found in these minerals.

We thank J. Ito of the University of Chicago for supplying us with the synthetic magnesium, cobalt and manganese pyroxenes.

REFERENCES

[1] S. Ghose, Z. Kristallogr. 122 (1965) 81.

[2] G. M. Bancroft and R. G. Burns, Amer. Mineral. 58 (1967) 1278.

[3] R. G. Burns, "Mineralogical Applications of Crystal Field Theory," Cambridge University Press (1970) pp. 87-92.

[4] W. A. Runciman, D. Sengupta and M. Marshall, Amer. Mineral. 58 (1975) 444.

FIGURE CAPTIONS

Figure 1. Absorption spectra in the near- and mid-infrared regions of orthopyroxenes containing various concentrations of Fe^{2+}. .....synthetic $MgSiO_3$, 0.0% Fe; - - - - - bronzite from Bamble, Norway, 7.6% Fe; ——— hypersthene from Summit Rock, Oregon, 19.4% Fe. The bands at 11,000 cm^{-1}, 5400 cm^{-1} and 2350 cm^{-1} are assigned to electronic transitions of Fe^{2+} in the M(2) site. The shoulder at ~8500 cm^{-1} arises from Fe^{2+} in the M(1) site [3]. Polarization: $\underset{\sim}{E} \parallel \underline{c}$ (γ). Room temperature. Crystal thickness = 0.50 mm.

Figure 2. Intensity correlation of the bands at 5400 cm^{-1} and 2350 cm^{-1} from the three spectra presented in Figure 1.

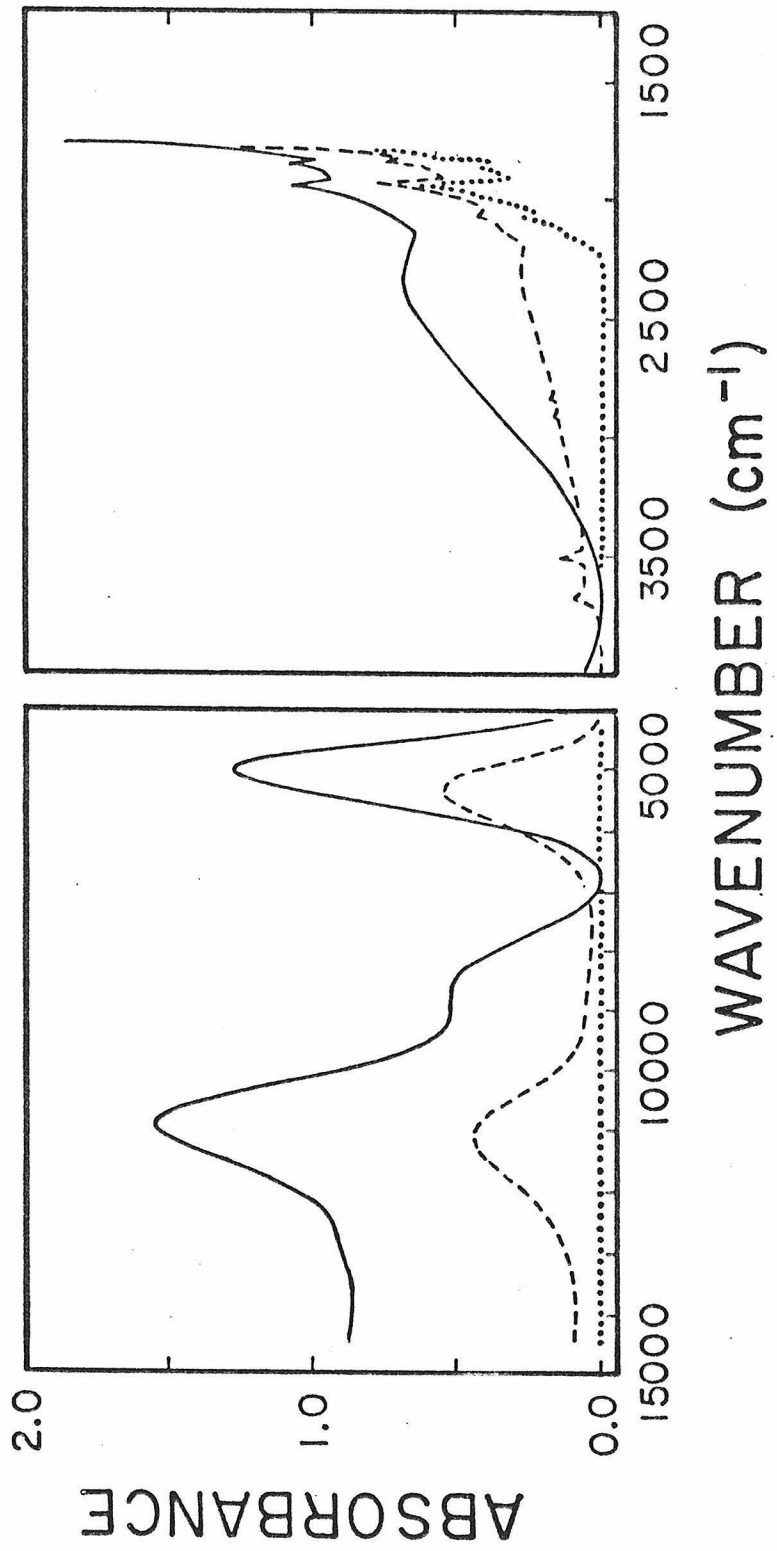
ABSORBANCE
2.0
1.0
0.0
15000
10000
5000
3500
2500
1500
WAVENUMBER (cm⁻¹)

Figure 1

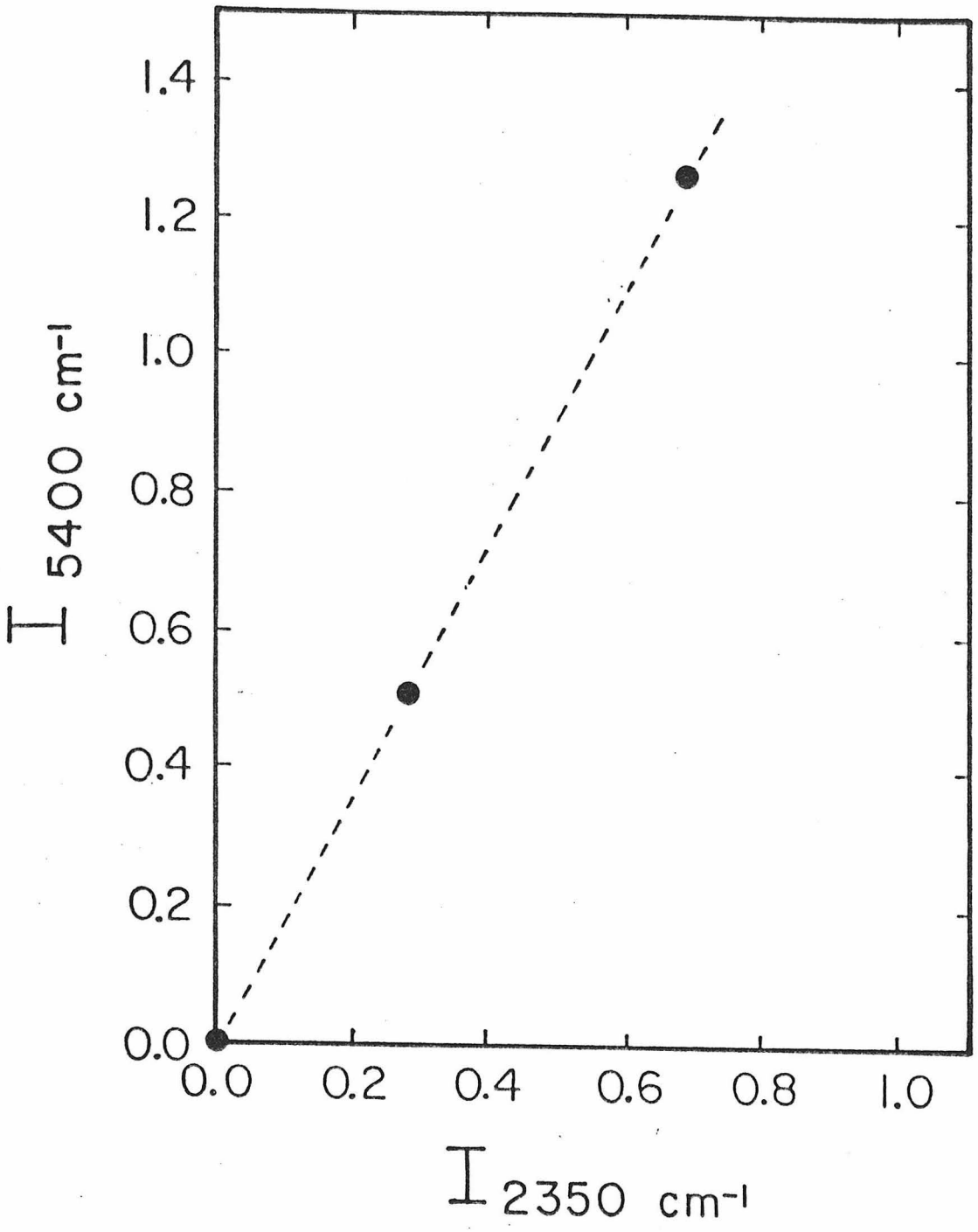

Figure 2.

CHAPTER 2

THE SPECTRA OF IRON IN ORTHOPYROXENE REVISITED: THE SPLITTING OF THE GROUND STATE

Published: The American Mineralogist, 62, 151-157.
Co-author: George R. Rossman

ABSTRACT

The three allowed electronic transitions of Fe^{2+} in the distorted M(2) site of orthopyroxene have been experimentally observed in absorption spectra, including a mid-infrared band at 2350 cm^{-1} that arises from a transition within the split $^5\underline{T}_{2\underline{g}}$ ground state in the low-symmetry crystalline field. These bands are analyzed with a theoretical point-charge model that is different from previously reported methods, but which results in a more acceptable energy level scheme for Fe^{2+} in this site.

INTRODUCTION

For many years, mineral spectroscopists have attempted to explain the spectra of Fe^{2+} in a variety of coordination environments with idealized crystal-field point-charge models. Hence, a variety of interpretations and assignments have been made for the spectra of Fe^{2+}, even in the same mineral. The electronic absorption spectrum of ferrous iron in the M(2) site of orthopyroxene, $(Mg,Fe)SiO_3$, has been the subject of many investigations aimed at understanding the polarization properties and the crystal-field splittings among the various bands that result from iron in a low-symmetry, coordination environment. White and Keester (1966) assigned a band at 11,000 cm^{-1} in the spectrum of enstatite to Fe^{2+} in octahedral coordination and assigned a band at about 5400 cm^{-1} to Fe^{2+} in tetrahedral coordination. It was subsequently suggested by Bancroft and Burns (1967) and later accepted by White and Keester (1967) that both bands arise from Fe^{2+} in the distorted, six-coordinate M(2) site. Runciman, Sengupta and Marshall (1973) pointed out an incorrect classification of C_{2v} states used in the previous studies to explain the polarization properties of these bands. They presented spectra of enstatite and analyzed the results in a crystal-field analysis that was also based upon a C_{2v} model, but with a different classification of states. Because of the large energy splittings and the polarization characteristics exhibited by these bands, the spectra of Fe^{2+} in the M(2) site of orthopyroxene are used as the model for the study of the spectra of iron in a variety of low-symmetry environments.

The degeneracies within the octahedral $^5T_{2g}$ and ^5E_g states of Fe^{2+} are removed in C_{2v} symmetry producing five states, among which a maximum of three allowed, electric dipole transitions are possible, depending upon the symmetry of the ground state. For this reason, a third absorption band was sought in

previous studies. White and Keester (1966) observed a band at 3100 cm^{-1} and attributed it to a vibrational overtone of the silicate lattice. Bancroft and Burns (1967) assigned this 3100 cm^{-1} band to Fe^{2+} in the M(2) site. Runciman et al.(1973) determined the polarization properties of a band at 3100 cm^{-1} and also assigned it to Fe^{2+} in the M(2) site.

It was pointed out by Goldman and Rossman (1976) that the half-width of the 3100 cm^{-1} band is an order of magnitude smaller than the other M(2) Fe^{2+} bands. This suggested a vibrational origin and led them to examine a number of orthopyroxenes to determine the origin of this band. It was found that this band does not arise from M(2) Fe^{2+}. In the course of that investigation, they found a band at 2350 cm^{-1} which was correlated with M(2) Fe^{2+} content, had the correct polarization properties for the C_{2v} model proposed by Runciman, et al. (1973), and had a half-width similar to those of the other M(2) Fe^{2+} bands.

The crystal-field analysis of the orthopyroxene spectral data of Runciman et al.(1973) is quantitatively incorrect due to the incorporation of the incorrectly assigned 3100 cm^{-1} band. The crystal-field analysis was re-done, using their equations with the correct energy of the mid-infrared band of 2350 cm^{-1}. However, an unacceptable energy level scheme resulted from these calculations. As will be discussed, the calculated value for the splitting of the $^5T_{2g}$ state was unreasonably large and the value for 10 Dq (Δ) was unreasonably small. These results suggest a fundamental problem in this computational method.

Orthopyroxene is the only documented sample in which all three C_{2v} allowed transitions are observed. In addition, it is the only sample in which a mid-infrared absorption band of Fe^{2+} within the split $^5T_{2g}$ ground state has been confirmed. Therefore, it is essential to quantitatively understand these data. For this reason, the orthopyroxene spectral data will be reanalyzed with a

quantitatively different $\underline{C}_{2\underline{v}}$ point-charge model. It will be shown that this model results in a more acceptable and understandable energy level scheme while still explaining the observed absorption anisotropy of the various bands.

EXPERIMENTAL METHOD

Self-supporting sections of bronzite from Bamble, Norway were cut parallel and perpendicular to $\underline{c}$ using external crystal morphology for orientation. An additional (001) section was set in epoxy on a microscope slide, thinned and polished to about 100 μm for measurement of the intense α band at 930 nm. The thickness of this section was determined by ratioing the intensity of the 1800 nm β band with that from the self-supporting section. Euhedral crystals, tabular along (100), of a hypersthene from Summit Rock, Oregon (Kleck, 1970) were sufficiently thin so that only polishing was necessary prior to obtaining their spectra. The orientation in all cases was confirmed by conoscopic interference figures. All spectra presented herein were obtained at room temperature although the mid-infrared spectra of the Bamble bronzite were also obtained at 12^{o}K using a Cryogenic Technology, Inc. cryogenic refrigerator. Other experimental details are similar to those presented in Rossman (1975 a,b). Chemical analyses were obtained with an automated MAC5-SA3 electron microprobe using the technique of Bence and Albee (1968) for data reduction (Table 1).

Each spectrum and its polarizer baseline were digitized using a Calma X-Y digitizer. A plotting program was written for the IBM 370/155 to correct each spectrum for its polarizer baseline, to normalize the intensity to represent a desired crystal thickness and to plot a smooth curve through all data points using a second-order polynomial interpolation function.

CRYSTAL STRUCTURE AND OPTICAL ORIENTATION

Ghose (1965) analyzed the crystal structure of a hypersthene, $Mg_{.93}Fe_{1.07}Si_2O_6$, with space-group Pbca; $\underline{a}$ = 18.310 Å, $\underline{b}$ = 8.927 Å, and $\underline{c}$ = 5.226 Å. The optical orientation is $\alpha = \underline{b}$, $\beta = \underline{a}$, and $\gamma = \underline{c}$. All atoms have C_1 point-group symmetry. (100) and (010) ORTEP (Johnson, 1965) projections of the M(2) site are presented in Figure 1. The position of the metal ion in Figure 1 represents an M(2) site that contains 90 percent Fe^{2+}. The principal distortion of this site from octahedral geometry results from an elongation of the M(2)-O(6) and M(2)-O(3) bonds with a reduction in the O(6)-M(2)-O(3) angle to 72.2°.[1]

SPECTROSCOPIC DATA

The room temperature spectra of the Bamble bronzite are presented in the 15000-4000 cm^{-1} region in Figure 2 to illustrate the absorption bands due to Fe^{2+} in the M(2) site. Bancroft and Burns (1967) and Burns (1970) reported room temperature, polarized spectra in the 25000-4000 cm^{-1} region of a bronzite sample from this locality, and the reader is referred to these studies for the spectroscopic details that occur above 15000 cm^{-1}. Mössbauer analysis of that sample (Bancroft, Burns and Howie, 1967) indicated that greater than 90 percent of the total Fe^{2+} is in the M(2) site. In fact, a quadrupole-split doublet due to Fe^{2+} in M(1) was not detected. The spectra in Figure 2 differ[2] from those previously reported in the intensities of the α, β, and γ components of the band at 11,000 cm^{-1}. Also, the spectra in Figure 2 and in Bancroft and Burns (1967) do not show the broad absorption band of low intensity at about 8500 cm^{-1} described and assigned to Fe^{2+} in the M(1) site by Burns (1970). If these differences are inherent to the samples studied, the variation in the intensity of the 8500 cm^{-1} band suggests that slightly different distributions

of Fe^{2+} between the M(1) and M(2) sites occur for different samples of bronzite from the Bamble, Norway locality.

The previous studies of orthopyroxene spectra indicated that the band near 11,000 cm^{-1} is predominantly α-polarized and the band at 5400 cm^{-1} is predominantly β-polarized. In agreement with these studies, the spectra of bronzite in Figure 2 indicate that the intensity ratios among the α, β, and γ components of the band near 11,000 cm^{-1} are 0.86:0.10:0.04 and for the band near 5400 cm^{-1} are 0.12:0.70:0.18.

The mid-infrared spectra of the orthopyroxenes has also been a subject of debate. White and Keester (1966) attributed a band at 3100 cm^{-1} to a vibrational overtone of the silicate lattice. Bancroft and Burns (1967), Burns (1970) and Runciman et al.(1973) assigned this band to Fe^{2+} in M(2). Goldman and Rossman (1976) subsequently found that the 3100 cm^{-1} band was incorrectly assigned to Fe^{2+}. They showed that it was absent from all of the samples which they analyzed and, hence, did not correlate with M(2) Fe^{2+} content.

In the course of their study, Goldman and Rossman found an absorption band in the mid-infrared at 2350 cm^{-1} (Figure 3). They assigned this band to Fe^{2+} in the M(2) site based on the observations that this band 1) has a half-width similar to the near-infrared M(2) Fe^{2+} bands, 2) is polarized in γ as expected from the analysis of Runciman et al., 3) correlates exactly with the M(2) Fe^{2+} concentration as measured by the intensity of the 5400 cm^{-1} band, and 4) is absent in synthetic Mg, Ni and Co orthopyroxenes.

Runciman et al. indicated that a mid-infrared band due to Fe^{2+} in the M(2) site must be polarized mostly in γ to conform to a C_{2v} point-group which explains the α and β-polarized bands at 11,000 cm^{-1} and 5400 cm^{-1}, respectively. The α, β and γ spectra of the Bamble bronzite have been obtained at 12°K to determine the polarization rations for the 2350 cm^{-1} band. The low temperature diminishes the overlap of the 2350 cm^{-1} band with the vibrational

overtones that occur below 2200 cm^{-1} so that more accurate intensity ratios can be obtained. The resulting ratios for the α, β and γ bands at 2350 cm^{-1} are 0.28:0.20:0.52. Therefore, this band is predominantly γ-polarized with some α and some β due to the different orientations of the C_{2v} crystal-field axes and the crystallographic axes as will be discussed in the next section. Coincidentally, these polarization ratios are nearly identical to the ratios determined for the 3100 cm^{-1} band by Runciman et al. (1973) which were used to compare the theoretical intensities calculated from the selected C_{2v} crystal-field axes with the experimental intensities.

POINT GROUP AND BAND ASSIGNMENTS

The crystallographic point group symmetry of the M(2) site is C_1. In this point group, all transitions are allowed in each polarization. However, the 11,000 cm^{-1}, 5400 cm^{-1} and 2350 cm^{-1} bands are strongly polarized indicating that the Fe^{2+} ion experiences an effective electrostatic symmetry higher than C_1. Runciman et al. suggested that the spectroscopic symmetry is C_{2v} and proceeded to develop their model based upon this symmetry. They pointed out errors made in earlier studies in the assignment of the various absorption bands to specific transitions of Fe^{2+} in C_{2v} symmetry. This process utilizes the descent-in-symmetry method from O_h to D_{4h} to C_{2v}. Problems arose because the assignment of experimentally determined energy values to the specific symmetry states of C_{2v} by reducing the overall symmetry from D_{4h} is not unique and depends upon the type of rhombic distortion. There are four types of rhombic distortions that can be applied to a D_{4h} polyhedron, each resulting in a distinct C_{2v} polyhedron whose symmetry elements (a two-fold rotation axis and two mirror planes) are related differently to the original symmetry elements of the D_{4h} polyhedron. Figure 4 illustrates the four C_{2v} types in which each type

is designated by the only symmetry elements that remain from $\underline{D}_{4\underline{h}}$ (Wilson, Decius and Cross, 1955). In addition, the section of each $\underline{C}_{2\underline{v}}$ type viewed along the former $\underline{C}_4$ axis of $\underline{D}_{4\underline{h}}$ is presented to facilitate a comparison of the distortions.

Idealized energy level schemes for each $\underline{C}_{2\underline{v}}$ type have been constructed from the correlation tables in Wilson, Decius and Cross and are presented in Figure 5 in which the descent-in-symmetry from $\underline{O}_{\underline{h}}$ to $\underline{C}_{2\underline{v}}$ is given. The polarization properties of the allowed transitions have been determined using the character table for $\underline{C}_{2\underline{v}}$ in Cotton (1963).

The appropriate $\underline{C}_{2\underline{v}}$ model for the M(2) site is $\underline{C}_2$" due to the orientation of an approximate two-fold rotation axis between the O(1)-O(4) and O(6)-O(3) oxygen pairs. The XZ plane of $\underline{C}_{2\underline{v}}(\underline{C}_2$") symmetry (Figure 4) was approximated in the orthopyroxene M(2) coordination polyhedron by the nearly planar group of the M(2) metal ion and the O(1), O(3), O(4) and O(6) oxygens (Runciman et al, 1973). Hence, the 11,000 cm^{-1}, 5400cm^{-1} and 2350 cm^{-1} absorption bands are assigned from Figure 5 to the $\underline{A}_1 \rightarrow \underline{A}_1$, $\underline{A}_1 \rightarrow \underline{B}_1$ and $\underline{A}_1 \rightarrow \underline{B}_2$ transitions of Fe^{2+} in the M(2) site. Each of these transitions is allowed in only one of the crystal-field directions. However, the crystal-field directions are not aligned with the principal vibration directions of the indicatrix. Therefore, components of each transition will occur in all vibration directions, and the transitions to $\underline{A}_1$, $\underline{B}_1$ and $\underline{B}_2$, polarized in Z, X, and Y, are expected to occur mostly in α, β and γ, respectively.

Runciman et al. (Table 1, set 1) calculated theoretical intensity ratios of the α, β and γ components for these transitions of 0.85:0.02:0.14, 0.05:0.67:0.29 and 0.10:0.33:0.58, respectively. Our measured ratios for the Bamble bronzite for these bands are 0.86:0.10:0.04, 0.12:0.70:0.18 and 0.28:0.20:0.52, respectively. The general agreement between the theoretical and

experimental intensity ratios for the three M(2) Fe^{2+} bands is certainly suggestive of a C_{2v} spectroscopy. These data could not be explained using either C_1 or C_2 point-group symmetry.

Upon considering the orientation of the five d-orbitals in each of the C_{2v} polyhedra in Figure 4, a general ordering scheme of the various states is readily obtained. For instance, by assuming tetragonal compression between O_h and D_{4h} (Figure 5), A_{1g} is expected to be at higher energy than B_{1g} in D_{4h} symmetry. As a consequence, A_1 is expected to be at higher energy than B_1 in C_{2v}(C_2"). In the same manner, the energy level of the two C_{2v} states derived from the E_g state of D_{4h} were obtained for the distortions presented in Figure 4. Generally, the relative energy levels of these states are reversed if 1) the elongation in the XY plane is along Y in C_2,σ_v; 2) the dihedral angle about X is greater than 90° in C_2,σ_d; 3) the elongation in the XZ plane is along X in C_2'; and 4) the dihedral angle about Z is greater than 90° in C_2".

The O(3)-M(2)-O(6) and O(1)-M(2)-O(4) angles about the crystal-field Z axis of the M(2) site are both less than 90°. Therefore, A_2 is expected to be at a lower energy than B_2 from the arguments presented above. However, Runciman *et al.* calculated just the reverse, that A_2 lies above B_2 in the energy level scheme. This discrepancy will be examined in the following section.

CRYSTAL FIELD ANALYSIS

Crystal-field analysis of absorption spectra is a systematic method by which the polarization properties of the bands can be explained and possible energy level schemes evaluated. Runciman *et al.* described a general crystal-field treatment and applied it to the spectra of enstatite. This method will be

used to analyze the spectra of bronzite presented in this paper in light of the assignment of a third $\underline{C}_{2v}$ band of Fe^{2+} in the M(2) site at 2350 cm^{-1}. However, it will be shown that this method does not result in a satisfactory energy level scheme, and for this reason, the bronzite data will be re-analyzed using a different crystal-field treatment. First, it is helpful to review the pertinent aspects of the crystal-field method of Runciman et al.

Runciman et al. (1973) derived a crystal-field potential using a $\underline{C}_{2v}$ ($\underline{C}_2$") model. Fourth and higher order harmonic terms were excluded from the potential, after extracting octahedral terms, because an exact solution for their coefficients would require more data than are available in the spectra. Hence, Δ and two additional fitting parameters that relate to the coefficients of the $\underline{Y}_2^0$ and $\underline{Y}_2^{\pm 2}$ harmonic terms were fitted. $\Delta(10\underline{D}_q)$ refers to the energy separation between the octahedral $^5\underline{T}_{2g}$ and $^5\underline{E}_g$ states initially needed to produce the observed splittings of the $\underline{C}_{2v}$ states, and which also accounts for the effect of configuration interaction between the two $\underline{A}_1$ states. It is important to realize that this method does not incorporate the specific bond length and bond angle distortions of the $\underline{C}_{2v}$ site within the potential and therefore, does not distinguish between sites of different $\underline{C}_{2v}$($\underline{C}_2$") coordination geometries.

The values of Δ and of the forbidden $\underline{A}_1 \rightarrow \underline{A}_2$ transition have been calculated from the energy expressions given in Runciman et al. using the following bronzite data from Figures 2 and 3: $\underline{A}_1 \rightarrow \underline{A}_1$ = 10930 cm^{-1}; $\underline{A}_1 \rightarrow \underline{B}_1$ = 5400 cm^{-1}, and $\underline{A}_1 \rightarrow \underline{B}_2$ = 2350 cm^{-1}. The energy values of Δ and of the $\underline{A}_1 \rightarrow \underline{A}_2$ transition are calculated to be 4934 cm^{-1} and 6178 cm^{-1}, respectively. These results indicate that the splitting of the $^5\underline{T}_{2g}$($\underline{O}_h$) state is also 6178 cm^{-1} because $\underline{B}_2$ is at lower energy than $\underline{A}_2$. However, from the discussion in the previous section, a dihedral angle about Z of less than 90° leads to the prediction that $\underline{A}_2$ is at lower energy than $\underline{B}_2$. As will be shown subsequently, $\underline{A}_2$ transforms as an XY

wavefunction in $\underline{C}_{2v}(\underline{C}_2")$ and $\underline{B}_2$ transforms as a YZ wavefunction. An acute dihedral angle about Z increases the potential about YZ relative to XY and thus, $\underline{A}_2$ is expected to lie beneath $\underline{B}_2$. Therefore, the O(6)-M(2)-O(3) angle of 72.2^{o} and the O(1)-M(2)-O(4) angle of 83^{o} suggest that the energy level scheme resulting from the method of Runciman et al. is incorrect. For this reason, the bronzite data will be re-analyzed using a crystal-field treatment that incorporates fourth-order contributions of the distortion into the potential and also considers the effect of specific bond lengths and angles.

The bronzite data have been re-analyzed using the operator-equivalent method described in Hutchings (1964) to derive energy expressions for the various $\underline{C}_{2v}(\underline{C}_2")$ states using the Z axis in Figure 1 as the axis of quantization. Contributions from the $\underline{Y}_2^0$, $\underline{Y}_2^{\pm 2}$, $\underline{Y}_4^0$, $\underline{Y}_4^{\pm 2}$ and $\underline{Y}_4^{\pm 4}$ harmonic terms remain in the potential after subtracting the octahedral terms. The number of fitting parameters in addition to Δ are reduced to two by deriving the potential in terms of one specified bond length, which in this case is taken to be the average metal-oxygen distance, $\bar{a}$; one fitting parameter is related to the second order terms and the other is related to the fourth order terms. The method assumes that each ligand constitutes a point charge. Hence, there are three fitting parameters and the spectra can be analyzed as before. The potential, written in operator-equivalent notation, consists of an octahedral term, Δ, and

$$M\left[\frac{A}{3}\hat{O}_2^0 + B\hat{O}_2^2\right] + N\left[\frac{C}{8}\hat{O}_4^0 + 5D\hat{O}_4^2 + \frac{35C}{4}\hat{O}_4^4\right]$$

where

$$M = \frac{-q\langle r^2\rangle}{14\bar{a}^3} \qquad N = \frac{q\langle r^4\rangle}{504\bar{a}^5}$$

$\hat{O}_2^0$, $\hat{O}_2^2$, $\hat{O}_4^0$ and $\hat{O}_4^4$ are the operator equivalents of the associated spherical harmonic terms and A, B, C, D and E are determined by the bond angles and bond

lengths of the site. The M(2) site possesses six unequal metal-oxygen bond lengths, from which three bond lengths must be selected to conform to a $\underline{C}_{2v}$ point-group symmetry. Therefore, the averages of the following bond lengths are used: M(2)-O(6), M(2)-O(3); M(2)-O(1), M(2)-O(4), and M(2)-O(2), M(2)-O(5).

The energy expressions for the two $\underline{A}_1$ states are the eigenvalues of the following configuration interaction matrix:

$\langle d_{y^2} \rangle$	$\langle d_{(x^2-z^2)} \rangle$
$M(A+3B) + \frac{9}{8}N(3C+40D+70E) + 0.6\Delta$	$M(B-A)\sqrt{3} + N(C+8D-14E)\ 15\sqrt{3/8}$
$M(B-A)\sqrt{3} + N(C+8D-14E)\ 15\sqrt{3/8}$	$-M(A+3B) + \frac{3}{8}N(19C-120D+70E) - 0.4\Delta$

Table 2 lists the wavefunctions and energies of the other three states.

The solutions for the bronzite data are: $\Delta = 6522\ cm^{-1}$; $\underline{A}_1 \rightarrow \underline{A}_2 = 354\ cm^{-1}$; $M = -636\ cm^{-1}$; and $N = 9.5\ cm^{-1}$. The energy level scheme based upon these calculations is presented in Figure 6. As predicted from the acute dihedral angles about Z for the M(2) site, the energy level of $\underline{A}_2$ is calculated below $\underline{B}_2$ and the overall splitting of the $^5\underline{T}_{2g}(\underline{O}_h)$ state, determined by the $\underline{A}_1 \rightarrow \underline{B}_2$ transition energy, is only $2350\ cm^{-1}$. This much smaller splitting of the $^5\underline{T}_{2g}(\underline{O}_h)$ state than previously calculated supports the contention by Faye (1972) that the splitting of this state is either small or roughly similar from a large variety of mineral spectra. It is unlikely that Faye's suggestion can be accurately tested below $2000\ cm^{-1}$ due to the presence of vibrational absorptions in that region. However, the identification of the Fe^{2+} band at $2350\ cm^{-1}$ represents the largest confirmed splitting of the $^5\underline{T}_{2g}(\underline{O}_h)$ ground state known to us. Also, the magnitude of splitting indicated by this band arises from one of the largest, distorted six-coordinate mineral sites. These observations suggest

that the splitting of the $^5T_g(O_h)$ state is probably not greater than 2000 cm^{-1} in most minerals, although further data are needed, especially in the 2000-4000 cm^{-1} region, to examine this possibility further.

The calculated value of Δ for Fe^{2+} in the M(2) site is 6522 cm^{-1}. This value is reasonable upon considering the dependence of Δ on $1/\bar{a}^5$ (Figgis, 1966). To determine a value of Δ for Fe^{2+} in a more regular, six-coordinate site so that the $1/\bar{a}^5$ dependence can be evaluated for the bronzite data, use is made of a study conducted by Faye (1972). Faye indicated that the barycenter energy of the states derived from the splitting of the $^5E_g(O_h)$ state is approximately 10,000 cm^{-1} for many of the more regular, six-coordinate sites (i.e., the M(1) sites in orthopyroxene, olivine, etc.) which have $\bar{a}$ values of about 2.1 Å. Since the barycenter energy is determined by the transitions from the ground state, any splitting of the $^5T_{2g}(O_h)$ state results in a barycenter energy that is larger than Δ (see Figure 6). Therefore, assuming that a Δ of 9500 cm^{-1} is produced from a site with $\bar{a}$ = 2.1 Å, a $1/\bar{a}^5$ dependence predicts a Δ of about 7200 cm^{-1} for Fe^{2+} in the orthopyroxene M(2) site using 2.22 Å for $\bar{a}$ (Ghose, 1965). Although there appears to be general agreement between the values of Δ calculated from the spectral data and from the $1/\bar{a}^5$ dependence, it should be realized that this dependence assumes octahedral geometry. The validity of calculating a value for Δ based upon the average of six M-O bonds lengths in a distorted coordination site is subject to question, especially when four M-O bonds are typically 2.1 Å in length whereas the remaining two bonds are extremely long at greater than 2.4 Å. However, using $\bar{a}$ in these calculations may be the most appropriate way in which the analysis of the spectral data from distorted coordination sites can be compared. From the analysis of the bronzite spectra, it is concluded that by incorporating the fourth-order contributions into the potential and by considering the effect of bond length and bond angle distortions of the M(2) site, a more reasonable C_{2v} energy level scheme is obtained which still explains the polarization properties of the various bands.

Finally, it must be pointed out that the β and γ components of the band near 11,000 cm^{-1} and the α and γ components of the band near 5400 cm^{-1} do not occur at the same energy at which the main components occur (Figure 2). These differences may result from weak spin-orbit coupling interactions. Ham, Schwarz and O'Brien (1969) in a study of Fe^{2+} doped into octahedrally-coordinated sites in MgO suggested that spin-orbit interactions, affected by Jahn-Teller distortions, produce a splitting of the $^5T_{2g}$ state of approximately 100 cm^{-1}. Runciman et al. pointed out that spin-orbit splittings of Fe^{2+} in the M(2) site are expected to be small due to a quenching effect of a low-symmetry environment. It is therefore conceivable that the small differences ($\sim$100cm^{-1}) in the energy locations of the various components of the bands near 11,000 cm^{-1} and 5400 cm^{-1} are due to spin-orbit interactions, although more data are required to evaluate this possibility.

CONCLUSIONS

A third, low-energy absorption band arising from an electronic transition among the components of the $T_{2g}(O_h)$ state of Fe^{2+} was identified by correlating the absorption spectra of a series of orthopyroxenes of various M(2) Fe^{2+} concentrations. The energy of this band provided the experimental basis for a crystal field model of the energy levels of Fe^{2+} in the M(2) orthopyroxene site which is consistent with qualitative crystal-field considerations based on angular distortions. This model differs from previous studies through the incorporation of specific bond distances and angles of the M(2) site, and the inclusion of the fourth-order terms of the crystal-field potential. Most minerals show splitting of the $E_g(O_h)$ state of Fe^{2+} which range up to 6000 cm^{-1} as a result of distortion from octahedral geometry. However, orthopyroxene is the only example among these minerals in which a transition within the split $T_{2g}(O_h)$ ground state is confirmed. Orthopyroxene, therefore, provides an important spectroscopic and theoretical basis for the discussion of the electronic structure of Fe^{2+} in other distorted sites.

ACKNOWLEDGMENTS

We are indebted to Jeff Hare, Caltech, for numerous discussions concerning the point charge calculations and crystal-field interpretations of the orthopyroxene spectra. We thank Jack Huneke for the hypersthene sample from Oregon.

REFERENCES

Bancroft, G. M. and R. G. Burns (1967) Interpretation of the electronic spectra of iron in pyroxenes. Am. Mineral. 52, 1278-1287.

Bancroft, G. M., R. G. Burns and R. A. Howie (1967) Determination of the cation distribution in the orthopyroxene spectra by the Mössbauer effect. Nature 213, 1221-1223.

Bence, A. E. and A. L. Albee (1968) Empirical correction factors for the electron microanalysis of silicate and oxides. J. Geol. 76, 382-403.

Burns, R. G. (1970) Mineralogical Applications of Crystal Field Theory, Cambridge University Press.

Cotton, F. A. (1963) Chemical Applications of Group Theory, Wiley-Interscience.

Faye, G. H. (1972) Relationship between crystal-field splitting parameter, "Δ_{VI}", and M_{host}-O bond distance as an aid in the interpretation of absorption spectra of Fe^{2+}-bearing materials, Canad. Mineral. 11,473-487.

Figgis, B. N. (1966) Introduction to Ligand Fields, Interscience Publishers.

Ghose, S. (1965) Mg^{2+}-Fe^{2+} order in an orthopyroxene, $Mg_{0.93}Fe_{1.07}Si_2O_6$. Z. Kristallogr. 122, 81-99.

Goldman, D. S. and G. R. Rossman (1976) Identification of a mid-infrared electronic absorption band of Fe^{2+} in the distorted M(2) site of orthopyroxene, $(Mg,Fe)SiO_3$. Chem. Phys. Lett. 41, 474-475.

Ham, F. S., Schwarz, W. M. and M.C.M. O'Brien (1969) Jahn-Teller effects in the far-infrared, EPR, and Mössbauer spectra of MgO:Fe^{2+}. Phys. Rev. 185,

Hutchings, M. T. (1964) Point-charge calculations of energy levels of magnetic ions in crystalline electric fields. Solid State Phys. 16, 227-273.

Johnson, C. K. (1965) ORTEP, a FORTRAN thermal ellipsoid plotting program for crystal structure illustrations. U. S. Nat. Tech. Inform. Serv. ORNL-3794.

Kleck, W. C. (1970) Cavity minerals at Summit Rock, Oregon. Am. Mineral. 55, 1396-1404.

Rossman, G. (1975a) Joaquinite: The nature of its water content and the question of four coordinated ferrous iron. Am. Mineral. 60, 435-440.

Rossman, G. (1975b) Spectroscopic and magnetic studies of ferric iron hydroxy sulfates: Intensification of color in ferric iron clusters bridged by a single hydroxide ion. Am. Mineral. 60, 698-704.

Runciman, W. A., D. Sengupta and M. Marshall (1973) The polarized spectra of iron in silicates. I. Enstatite. Am. Mineral. 58, 444-450.

White, W. B. and K. L. Keester (1966) Optical absorption spectra of iron in the rock-forming silicates. Am. Mineral. 51, 774-791.

White, W. B. and K. L. Keester (1967) Selection rules and site assignments for the spectra of ferrous iron in pyroxenes. Am. Mineral. 52,1508-1514.

Wilson, E. B., J. C. Decius and P. C. Cross (1955) Molecular Vibrations. McGraw Hill, New York.

FOOTNOTES

1. Specific bond distances for the M(2) site from the metal ion to the O(1), O(2), O(3), O(4), O(5) and O(6) oxygens are (in angstroms) 2.119, 2.066, 2.519, 2.175, 2.037 and 2.405, respectively (Ghose, 1965).
2. These differences arise from the nature of the experimental methods used to obtain the spectra. The spectra of Bancroft and Burns (1967) and Burns (1970) were obtained with microscope spectrophotometers which necessarily mix polarization components due to the strongly convergent light in the optical system. The quantitative aspects of this problem will be dealt with in Chapter 4.

FIGURE CAPTIONS

Figure 1. (100) and (010) ORTEP projections of the M(2) coordination site in orthopyroxene (hypersthene) based upon the atomic coordinates given by Ghose (1965). Both projections are drawn to the same scale.

Figure 2. Room temperature spectra of bronzite ($Fs_{14.0}$) from Bamble, Norway illustrating the absorption bands due to Fe^{2+} in the M(2) site. ..... α spectrum; ------β spectrum; ——— γ spectrum. Crystal thickness = 0.10 mm. Optic orientation: $\alpha = \underline{b}$, $\beta = \underline{a}$, $\gamma = \underline{c}$.

Figure 3. Room temperature γ spectrum (———) of hypersthene ($Fs_{39.5}$) from Summit Rock, Oregon, and the γ spectrum (------) of bronzite ($Fs_{14.0}$) from Bamble, Norway which indicate that the bands at 5400 cm^{-1} and at 2350 cm^{-1} are correlated in intensity and arise from Fe^{2+} in the M(2) site. Crystal thickness = 0.50 mm.

Figure 4. Four types of $\underline{C}_{2\underline{v}}$ polyhedra resulting from rhombic distortions of a $\underline{D}_{4\underline{h}}$ polyhedron. Each $\underline{C}_{2\underline{v}}$ figure is designated by the only symmetry elements that remain from $\underline{D}_{4\underline{h}}$. For each $\underline{C}_{2\underline{v}}$ figure, the sections viewed along the former $\underline{C}_4$ axis of $\underline{D}_{4\underline{h}}$ and the X,Y,Z axes are also shown where Z corresponds to the two-fold rotation axis.

Figure 5. Correlation diagram showing the idealized descent-in-symmetry from $\underline{O}_{\underline{h}}$ to $\underline{C}_{2\underline{v}}$. The polarization properties of the allowed transitions represent the axial labelings and the distortions presented in Figure 4. The effect of configuration interaction between the two

$\underline{A}_1$ states in $\underline{C}_{2\underline{v}}$ symmetry is ignored. Also, tetragonal compression between $\underline{O}_{\underline{h}}$ and $\underline{D}_{4\underline{h}}$ and the barycenter "rule" for the split states are assumed. $\underline{C}_{2\underline{v}}(\underline{C}_2{}'')$ is applicable to the orthopyroxene M(2) site.

Figure 6. Energy level scheme of Fe^{2+} in the M(2) site using a $\underline{C}_{2\underline{v}}(\underline{C}_2{}'')$ theoretical point-charge model.

TABLE 1. MICROPROBE ANALYSES

SAMPLE	1	2
	Weight Percent of Oxides	
SiO_2	57.83	53.30
TiO_2	-	.19
Al_2O_3	.09	.23
MgO	32.86	19.67
MnO	-	.51
FeO	9.77	25.02
CaO	.26	1.76
	100.81	100.68
	Formula Proportions(#cations = 4)	
Si	2.00	2.00
Al(VI)	-	.01
Mg	1.70	1.10
Ti	-	.01
Mn	-	.02
Fe	.28	.79
Ca	.01	.07

1. Bronzite, Bamble, Norway
2. Hypersthene, Summit Rock, Oregon

TABLE 2. $\underline{C}_{2\underline{v}}$ CRYSTAL-FIELD LEVELS

State	Wavefunction	Energy
B_1	$\sqrt{3}XZ$	$-M(A+3B) - 6N(C-10D) + 0.6\Delta$
B_2	$\sqrt{3}YZ$	$M(3B-A) - 6N(C+10D) - 0.4\Delta$
A_2	$\sqrt{3}XY$	$2AM + \frac{3}{2}N(C-70E) - 0.4\Delta$

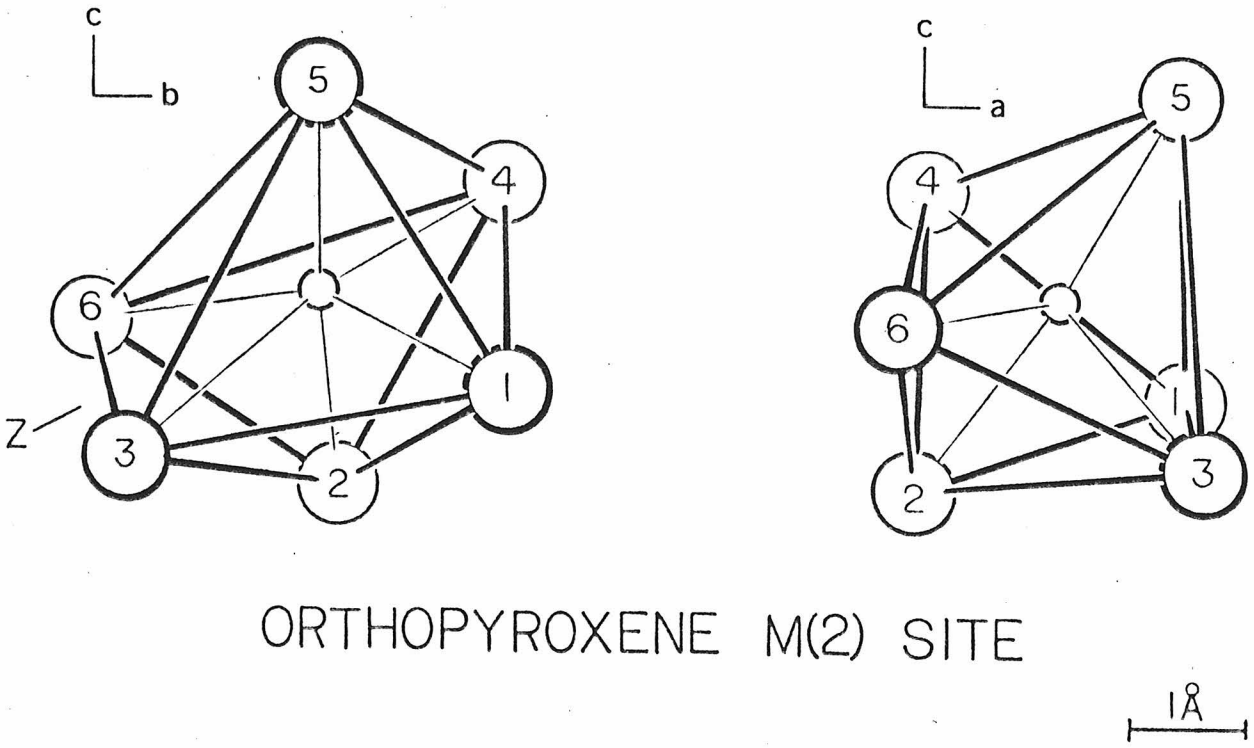

Figure 1

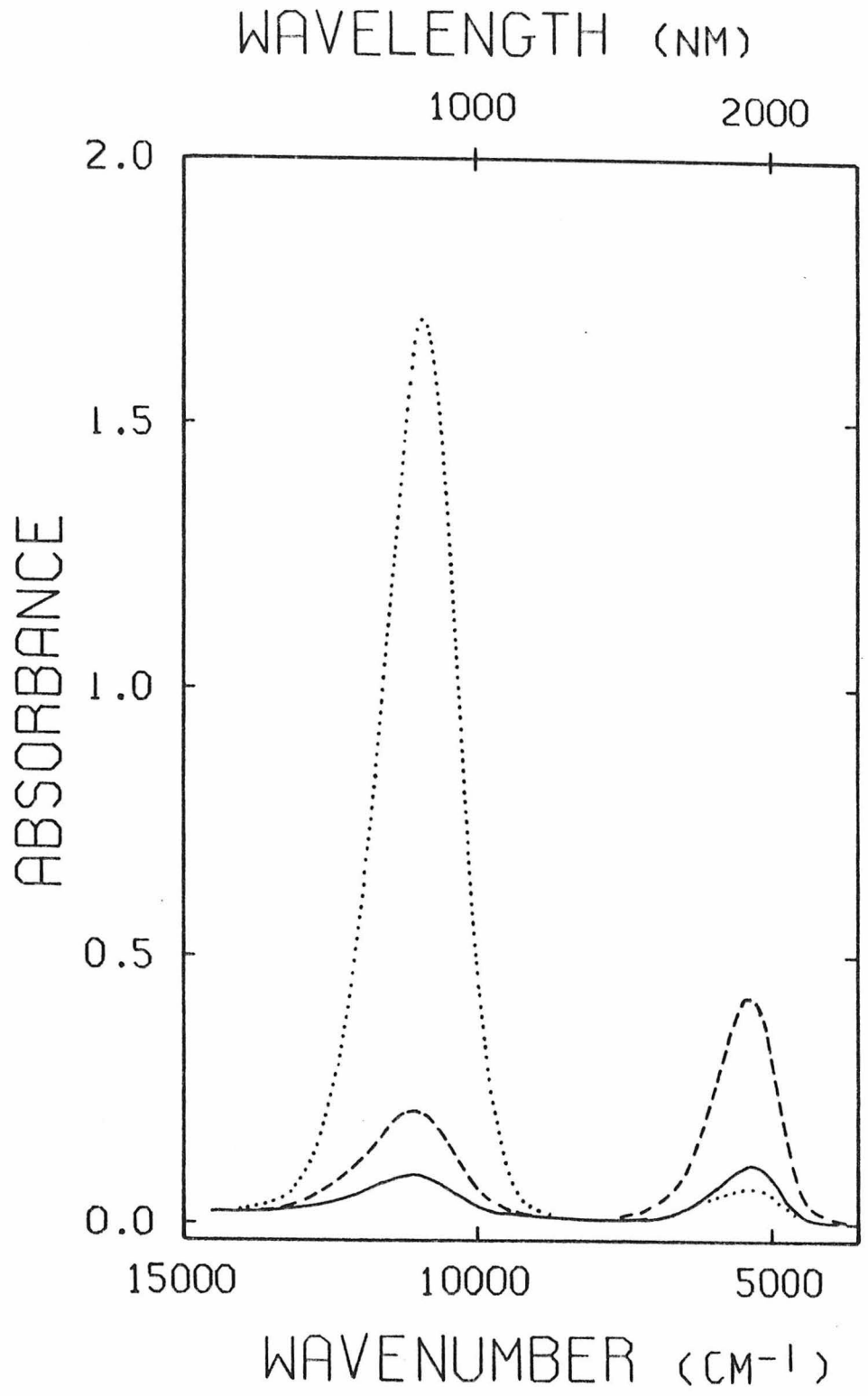
WAVELENGTH (NM)
1000
2000
2.0
1.5
1.0
0.5
0.0
ABSORBANCE
15000
10000
5000
WAVENUMBER (CM-1)

Figure 2

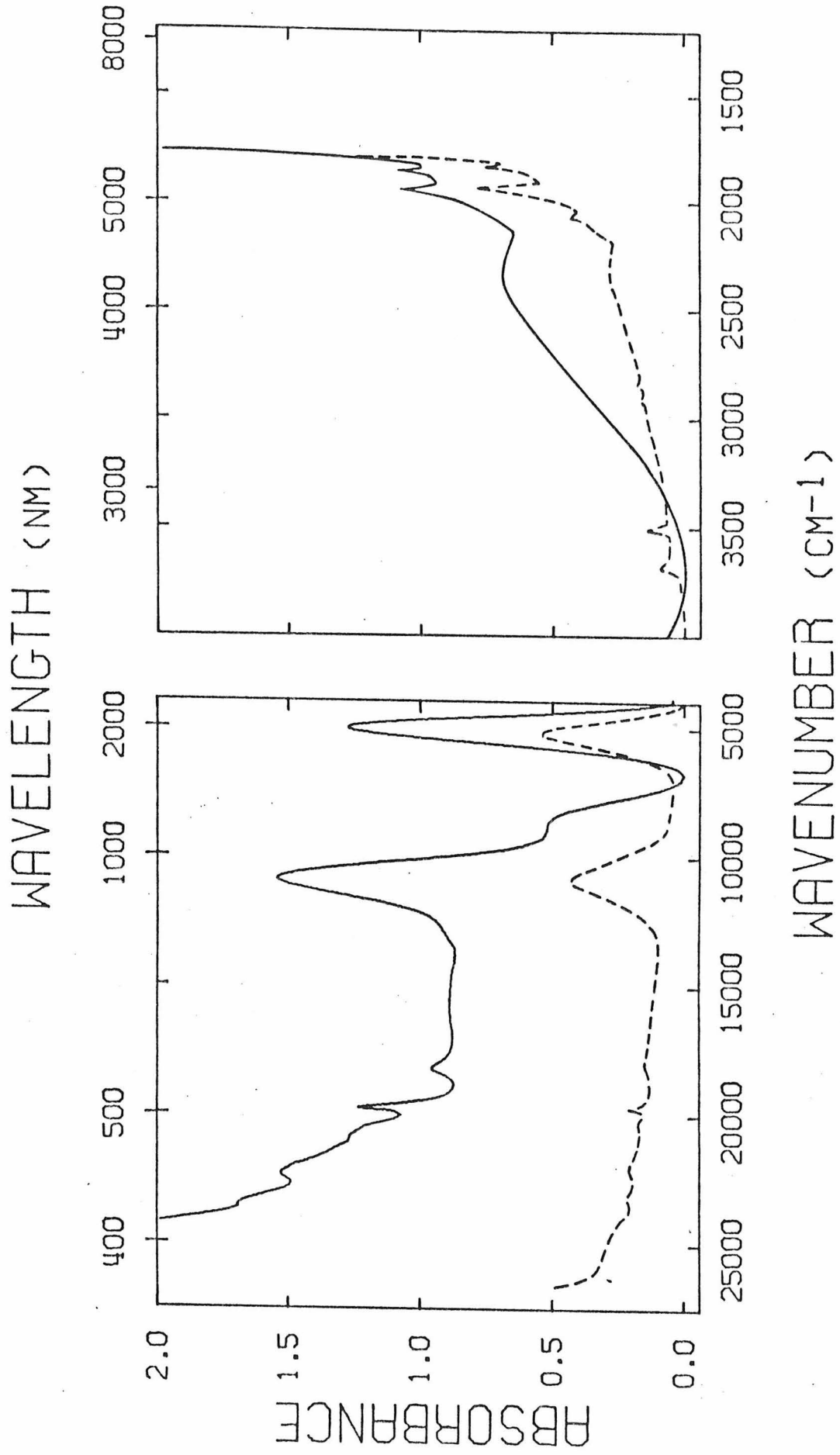
WAVELENGTH (NM)
400
500
1000
2000
25000
20000
15000
10000
5000
WAVENUMBER (CM-1)
3000
4000
5000
8000
3500
3000
2500
2000
1500
ABSORBANCE
2.0
1.5
1.0
0.5
0.0

Figure 3

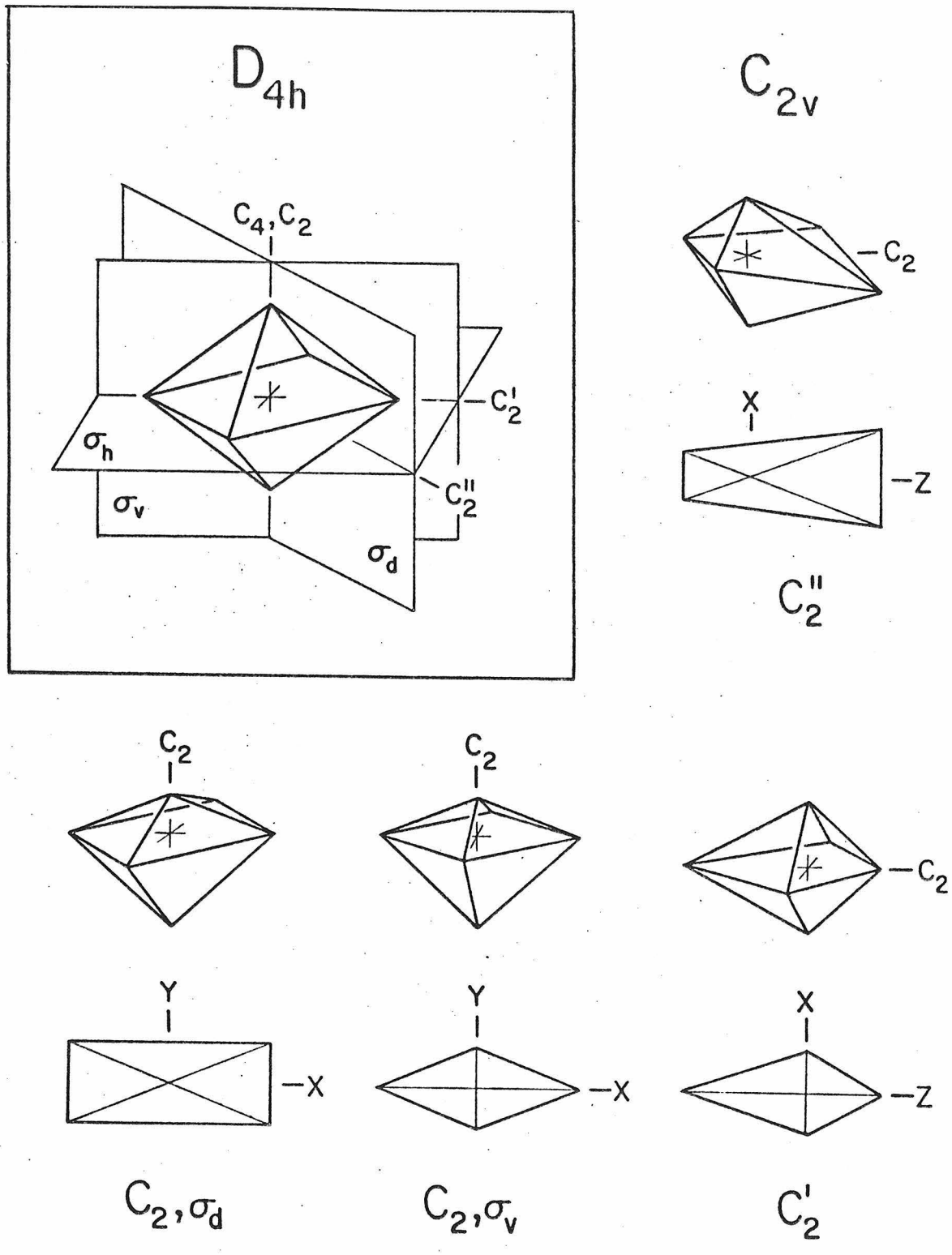

Figure 4

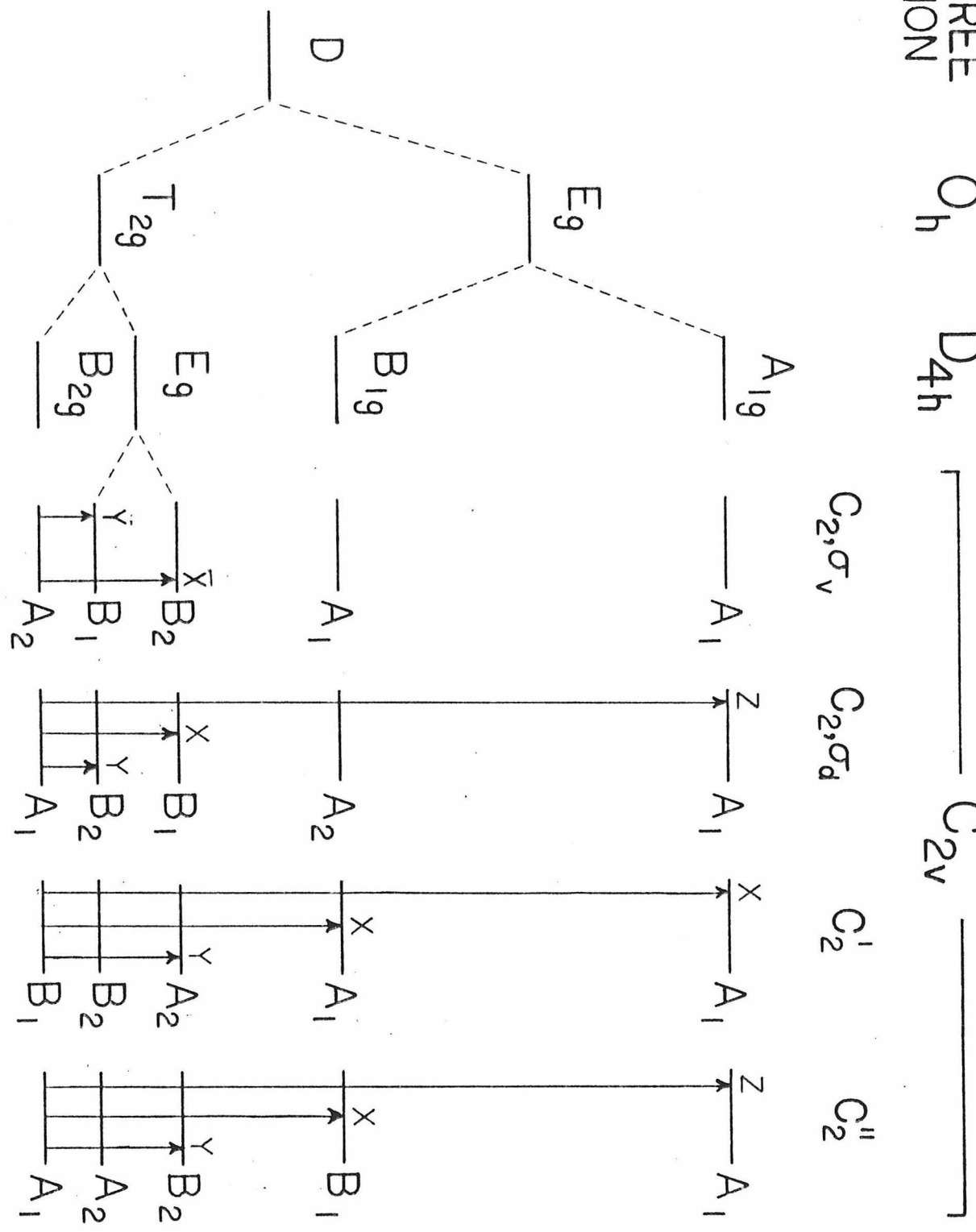
FREE ION
O_h
D_{4h}
C_{2v}
D
E_g
T_{2g}
A_{1g}
B_{1g}
B_{2g}
E_g
C_{2,σ_v}
C_{2,σ_d}
C_2'
C_2''
A_1
A_2
B_1
B_2
X
Y
Z

Figure 5

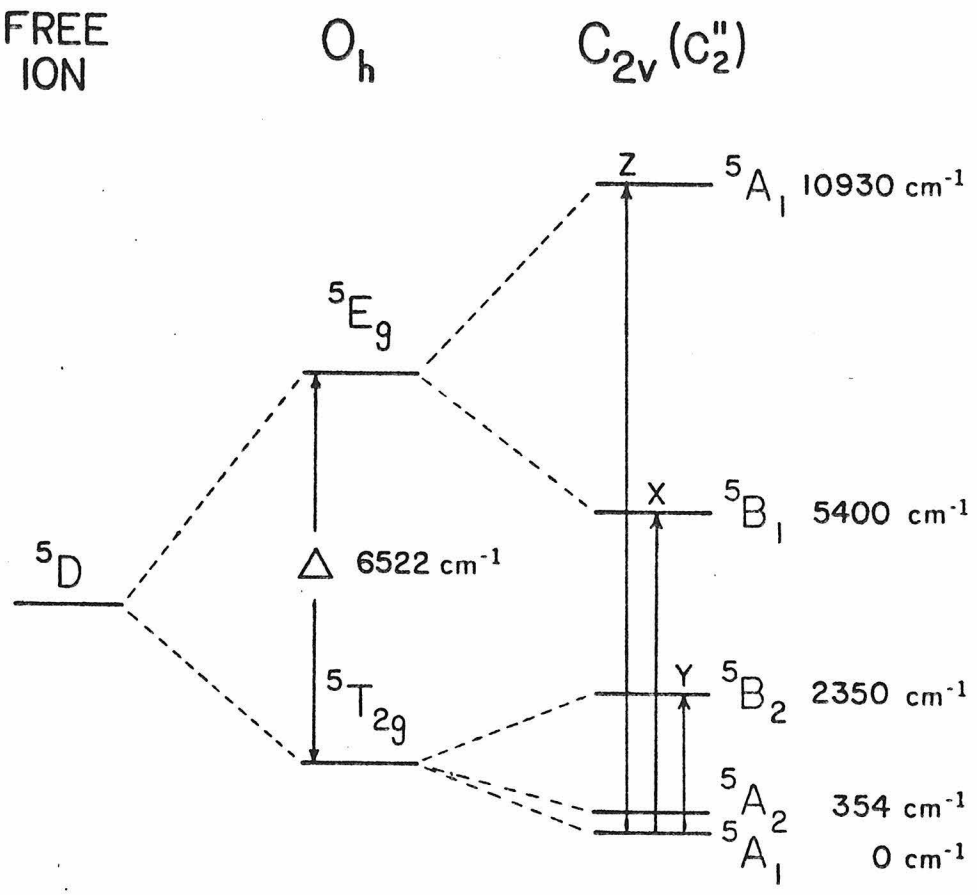
FREE ION
O_h
$C_{2v}(C_2'')$
^5D
^5E_g
$^5T_{2g}$
Δ 6522 cm^{-1}
Z
$^5A_1$ 10930 cm^{-1}
X
$^5B_1$ 5400 cm^{-1}
Y
$^5B_2$ 2350 cm^{-1}
$^5A_2$ 354 cm^{-1}
$^5A_1$ 0 cm^{-1}

Figure 6

CHAPTER 3

THE SPECTRA OF IRON IN ORTHOPYROXENE REVISITED: THE SPLITTING OF THE GROUND STATE.

SUPPLEMENT:

THE POINT-CHARGE MODEL

The Spectra of Iron in Orthopyroxene Revisited: The Splitting of the $^5T_{2g}$ Ground State

Supplement:

THE POINT-CHARGE MODEL

Introduction

The operator-equivalent point-charge method used to derive energy expressions for specified crystal-field states in the analysis of electronic absorption spectra is described in detail in Hutchings (1964). Hutchings includes the necessary formulas to derive the crystal-field potential and to rewrite it in terms of the operator equivalents. Extensive tables are presented that contain the various matrix elements of the operator equivalents for coupled wavefunctions so that expressions for the crystal-field states can be determined. The operator-equivalent method, as applied to the spectra of Fe^{2+} in the M(2) site of orthopyroxene by Goldman and Rossman (1977), will now be outlined. It is hoped that the reader will gain sufficient familiarity with the procedural aspects of this method so that it could be applied to spectra arising from a variety of coordination geometries.

THE CRYSTAL-FIELD POTENTIAL

The general expression for the crystal-field potential in terms of spherical harmonics at point (r,θ,ϕ) is

$$V(r,\theta,\phi) = \sum_{n=o}^{\infty} \cdot \sum_{m=-n}^{n} r^n \gamma'_{nm} Y_n^m (\theta,\phi) \qquad (1)$$

where

$$\gamma'_{nm} = \sum_j \frac{4\pi}{(2n+1)} \frac{q_j}{R_j^{(n+1)}} (-1)^m Y_n^{-m} (\theta_j, \phi_j). \qquad (2)$$

Therefore, γ'_{nm} results from a summation of harmonic contributions from all j point charges in the coordination site.

Figure 1 represents the idealized geometry of a C_{2v} coordination site containing a dihedral two-fold rotation axis. Z coincides with the two-fold axis of the site and the two mirror planes are located in XZ and YZ and are mutually orthogonal. In equation 2, θ is the angular measure of point j from Z and ϕ is the angular measure of point j from X about Z. Hence, points 1 through 6 have (r,θ,ϕ) coordinates (a_1,θ_1,π), $(a_1,\theta_1,0)$, (a_2,θ_2,π) $(a_2,\theta_2,0)$, $(a_3,\theta_3,\frac{\pi}{2})$ and $(a_3,\theta_3,\frac{3\pi}{2})$, respectively.

The derivation of the Y_2^0 spherical harmonic contribution to the crystal-field potential serves to illustrate the procedure to derive the remaining terms. Given that (Hutchings, 1964, table 3)

$$Y_2^0 = \frac{1}{4}\left(\frac{5}{\pi}\right)^{\frac{1}{2}} (3\cos^2\theta - 1)$$

and assuming that each point contributes the same charge, q, equation 2 over all six points in figure 1 becomes

$$\gamma'_{20} = \left(\frac{\pi}{5}\right)^{\frac{1}{2}} q \sum_j \left(\frac{3\cos^2\theta_j - 1}{a_j^3}\right) \qquad (3)$$

Substituting γ'_{20} into equation 1, the contribution to the potential from Y_2^0 is

$$V_{20} = \left(\frac{\pi}{5}\right)^{\frac{1}{2}} qr^2 \left[\sum_j \frac{(3\cos^2\theta_j - 1)}{a_j^3}\right] Y_2^0 \quad . \qquad (4)$$

In this way, the remaining terms in the potential are derived. Excluding harmonic terms with $n > 4$ (Figgis, 1966, p. 32), contributions from the Y_2^0, $Y_2^{\pm 2}$, Y_4^0, $Y_4^{\pm 2}$ and $Y_4^{\pm 4}$ harmonic terms occur in this potential.

The potential is now rewritten in terms of the operator equivalents. The operators that are formed, which operate on the angular part of the wavefunctions, possess the same transformation properties under rotation as the potential. Hence, they allow for the matrix elements of the crystal-field potential between coupled wavefunctions that are specified by one particular value of angular momentum (LL_Z) to be evaluated. Rewriting Y_2^0 in cartesian coordinates brings

$$Y_2^0 = \frac{1}{4}\left(\frac{5}{\pi}\right)^{\frac{1}{2}}\left(\frac{3z^2-r^2}{r^2}\right)$$

In operator equivalents, Y_2^0 becomes (Hutchings, 1964, table 8)

$$Y_2^0 = \frac{1}{4r^2}\left(\frac{5}{\pi}\right)^{\frac{1}{2}} \alpha_J \langle r^2 \rangle \, [3L_z^{\,2} - L(L+1)] = \frac{1}{4r^2}\left(\frac{5}{\pi}\right)^{\frac{1}{2}} \alpha_J \langle r^2 \rangle \, O_2^0 \qquad (5)$$

where α_J is a constant multiplicative factor which is equal to $-\frac{2}{21}$ for $3d^6$ ions such as Fe^{2+} (Hutchings, 1964, table 7), and O_2^0 is the standard notation for the operator equivalent of Y_2^0. Substituting equation 5 into equation 4 brings

$$V_{20} = -\frac{1}{42} q \langle r^2 \rangle \left[\sum_j \frac{(3\cos^2\theta_j - 1)}{a_j^{\,3}}\right] O_2^0 \quad . \qquad (6)$$

Continuing for the remaining terms, the potential is then entirely rewritten using the operator equivalents.

In C_{2v} symmetry with Z as a dihedral axis, three electronic transitions are allowed; $A_1 \rightarrow A_1$, $A_1 \rightarrow B_1$ and $A_1 \rightarrow B_2$. Hence, spectral analysis provides three parameters whereas five coefficients occur in the potential. After subtracting

the octahedral terms from the potential in order to solve for $\Delta(=10\ Dq)$, the five coefficients that still remain are reduced to two by rewriting each a_j in terms of $\bar{a}$, the average metal-ligand bond distance (or any other specified distance). For O_2^0, equation 6 becomes

$$v_{20} = -\frac{1}{42}\frac{q\langle r^2\rangle}{\bar{a}^3}\left[\sum_j\left(\frac{3\cos^2\theta_j-1}{(a_j/\bar{a})^3}\right) - v_{20}^{oct}\right]O_2^0 \qquad (7)$$

Since $a_1=a_2=a_3=\bar{a}$, $\theta_1=\theta_2=\frac{\pi}{4}$, $\theta_3=\theta_4=\frac{3\pi}{4}$, and $\theta_5=\theta_6=\frac{\pi}{2}$ in octahedral geometry (Figure 1), the summation in equation 6 over all six points is zero, and $v_{20}^{oct}=0$. Hence, there are no octahedral contributions to be extracted from v_{20} and the summation in equation 7 within the brackets results in a numerical value for the A coefficient used in Goldman and Rossman (1977). Similarly, the remaining terms in the potential are:

$$(v_2^2 + v_2^{-2}) = -\frac{1}{14}\frac{q\langle r^2\rangle}{\bar{a}^3}\left[\sum_j\left(\frac{\sin^2\theta_j\cos^2\phi_j-\sin^2\theta_j\sin^2\phi_j}{(a_j/\bar{a})^3}\right)\right]O_2^2 \qquad (8)$$

$$v_4^0 = \frac{1}{4032}\frac{q\langle r^4\rangle}{\bar{a}^5}\left[\sum_j 2\cdot\left(\frac{35\cos^4\theta_j-30\cos^2\theta_j+3}{(a_j/\bar{a})^5}\right)+14\right]O_4^0 \qquad (9)$$

$$(v_4^2 + v_4^{-2}) = \frac{5}{504}\frac{q\langle r^4\rangle}{\bar{a}^5}\left[\sum_j\frac{(\sin^2\theta_j\cos^2\phi_j-\sin^2\theta_j\sin^2\phi_j)(7\cos^2\theta_j-1)}{(a_j/\bar{a})^5}-7\right]O_4^2 \qquad (10)$$

$$(v_4^4 + v_4^{-4}) = \frac{35}{2016}\frac{q\langle r^4\rangle}{\bar{a}^5}\left[\sum_j\left(\frac{\sin^4\theta_j\cos^4\phi_j+\sin^4\theta_j\sin^4\phi_j}{(a_j/\bar{a})^5}\right)-3\right]O_4^4 \qquad (11)$$

where the numerical values of the bracketed terms in equations 8 through 11 are the B through E coefficients in Goldman and Rossman (1977), respectively.

Certain terms that occur in the general expressions for the B, D and E coefficients are zero in C_{2v} symmetry and these terms have been omitted.

Because of the presence of mirror planes in XZ and YZ in Figure 1, bond distances from the metal ion to points 1 and 2 are identical (as are the distances to points 3 and 4, and 5 and 6). However, the crystallographic point-group symmetry of the M(2) coordination site in orthopyroxene is C_1 in which there are six unequal metal-oxygen bond distances. To conform to a C_{2v} symmetry with Z along the bisector of the O(3)-M(2)-O(6) angle, the averages of the bond lengths from M(2) to O(6) and O(3), O(1) and O(4), and O(2) and O(5) are used as a_1,a_2 and a_3 which have values of 2.462Å, 2.147Å and 2.052Å, respectively. $\bar{a}$ has a value of 2.220Å (Ghose, 1965). Because the O(6)-M(2)-O(3) angle is 72.2° and the O(1)-M(2)-O(4) angle is 83°, θ_1 and θ_2 (Figure 1) are 36.1° and 138.5°, respectively. θ_3 is set at 90°. Using these values for θ_j and a_j and the values for ϕ_j shown in Figure 1, the coefficients A,B,C,D and E, calculated from equations 7 through 11, are 0.38066, -1.05474, 14.5148, 0.48616 and 0.56845, respectively.

The C_{2v} potential is written by defining two parameters

$$M = -\frac{1}{14}\frac{q\langle r^2\rangle}{\bar{a}^3} \quad \text{and} \quad N = \frac{1}{504}\frac{q\langle r^4\rangle}{\bar{a}^5} \ ,$$

and substituting A,B,C,D and E for the bracketed terms in equations 7 through 11, respectively. The potential, V, consists of an octahedral portion, and

$$M\left[\frac{A}{3}O_2^0 + BO_2^2\right] + N\left[\frac{C}{8}O_4^0 + 5DO_4^2 + \frac{35}{4}EO_4^4\right] \qquad (12)$$

Hence, there are three parameters, Δ, M and N, to be fitted from the spectra.

d - ORBITAL WAVEFUNCTIONS

Using the octahedral form of the C_{2v} potential

$$V^{oct'} = \frac{q\langle r^4\rangle}{8\bar{a}^5}\left[-\frac{1}{36}O_4^0 + \frac{5}{9}O_4^2 + \frac{5}{12}O_4^4\right] \quad ,$$

the five linear combinations of the d orbitals that transform as A_1, A_2, B_2, B_1 and A_1 in the C_{2v} symmetry group are found. This involves determining the elements of the 5 x 5 matrix of d orbitals. For instance, neglecting the common factor $(5/4\pi)^{\frac{1}{2}}$, the matrix element for $\langle Y_2^0|V^{oct}|Y_2^0\rangle$ is found using Hutchings (1964, table 9). In this case, L=2 and L_Z=0. Letting $\frac{q\langle r^4\rangle}{8\bar{a}^5} = \delta$ in $V^{oct'}$, table 9 in Hutchings (1964) indicates that

$$-\frac{1}{36}\delta\langle 0|O_4^0|0\rangle = (-\frac{1}{36}\delta)(72) = -2\delta$$

$$\frac{5}{9}\delta\langle 0|O_4^2|0\rangle = (\frac{5}{9}\delta)(0) = 0$$

$$\frac{5}{12}\delta\langle 0|O_4^4|0\rangle = (\frac{5}{12}\delta)(0) = 0$$

so that the matrix element for $\langle Y_2^0|V^{oct'}|Y_2^0\rangle$ is -2δ . Upon determining the remaining matrix elements, it is found that Y_2^0, Y_2^2 and Y_2^{-2} and Y_2^1 and Y_2^{-1} mix. The appropriate linear combinations are then determined in the conventional manner (Ballhausen, 1962) and the following wavefunctions are obtained:

$$d_{y^2} = \frac{1}{2}(2y^2-x^2-z^2) = -\frac{1}{2}Y_2^0 - \frac{1}{2}\sqrt{\frac{3}{2}}(Y_2^2 + Y_2^{-2})$$

$$d_{xz} = \sqrt{3}xz = \frac{1}{\sqrt{2}}(Y_2^1 - Y_2^{-1})$$

$$d_{yz} = \sqrt{3}yz = \frac{1}{\sqrt{2}}(Y_2^1 + Y_2^{-1})$$

$$d_{xy} = \sqrt{3}xy = \frac{1}{\sqrt{2}}(Y_2^2 - Y_2^{-2})$$

$$d_{x^2-z^2} = \frac{\sqrt{3}}{2}(x^2-z^2) = -\frac{\sqrt{3}}{2}Y_2^0 + \frac{1}{2}\frac{1}{\sqrt{2}}(Y_2^2 + Y_2^{-2})$$

which transform as A_1, B_1, B_2, A_2 and A_1, respectively, in C_{2v} symmetry. Applying $V^{oct'}$ to the above wavefunctions remembering that $\delta = 0.75\Delta$ (Figgis, 1966, page 35), the energy of d_{y^2} and d_{xz} is 0.6Δ and the energy of d_{xy}, d_{yz} and $d_{x^2-z^2}$ is -0.4Δ. Therefore, d_{y^2} (A_1) and $d_{xz}(B_1)$ arise from the splitting of the octahedral ^5E_g state of Fe^{2+} as is indicated in the correlation tables for $C_{2v}(C_2'')$ in Wilson, Decius and Cross (1955).

ENERGY EXPRESSIONS

The energy expressions for the five d wavefunctions in C_{2v} symmetry are found by applying the C_{2v} potential in equation 12 to each one of the wavefunctions using table 9 in Hutchings to evaluate the matrix elements. The expression for the A_2 state is

$$\frac{1}{2}\langle Y_2^2 - Y_2^{-2}|V|Y_2^2 - Y_2^{-2}\rangle$$

$$= \langle Y_2^2|V|Y_2^2\rangle - \langle Y_2^2|V|Y_2^{-2}\rangle$$

$$= \langle Y_2^{-2}|V|Y_2^{-2}\rangle - \langle Y_2^{-2}|V|Y_2^2\rangle \quad .$$

Taking the first term

$$\langle 2 \left| \frac{MA}{3} O_2^0 \right| 2 \rangle = \frac{MA}{3}(6) = 2MA$$

$$\langle 2 \left| MBO_2^2 \right| 2 \rangle = MB(0) = 0$$

$$-\langle 2 \left| \frac{MA}{3} O_2^0 \right| -2 \rangle = \frac{MA}{3}(0) = 0$$

$$-\langle 2 \left| MBO_2^2 \right| -2 \rangle = -MB(0) = 0$$

and the second term

$$\langle 2 \left| \frac{NC}{8} O_4^0 \right| 2 \rangle = \frac{NC}{8}(12) = \frac{3}{2}NC$$

$$\langle 2 \left| 5NDO_4^2 \right| 2 \rangle = 5ND(0) = 0$$

$$\langle 2 \left| \frac{35}{4} NEO_4^4 \right| 2 \rangle = \frac{35}{4}NE(0) = 0$$

$$-\langle 2 \left| \frac{NC}{8} O_4^0 \right| -2 \rangle = \frac{NC}{8}(0) = 0$$

$$-\langle 2 \left| 5NDO_4^2 \right| -2 \rangle = 5ND(0) = 0$$

$$-\langle 2 \left| \frac{35}{4} NEO_4^4 \right| -2 \rangle = \frac{35}{4}NE(12) = -105NE$$

and remembering that $\langle d_{xy} | V^{oct'} | d_{xy} \rangle = -0.4\Delta$, the entire energy expression for the A_2 state is

$$2MA + \frac{3}{2}NC - 105NE - 0.4\Delta$$

which is given in Goldman and Rossman (1977, table 2). In this way, energy expressions for the remaining four states are determined.

Since the two A_1 states have the same transformational symmetry, they can mutually interact. To account for this configurational interaction, a 2x2 matrix is formed for d_{y^2} and $d_{x^2-z^2}$. The two eigenvalues of this configuration interaction matrix are the resulting energies of the two A_1 states. The energy expression for the two A_1 states derived from the configuration interaction matrix is

$$\left[\frac{9}{16}(3C+40D+70E) + \frac{3}{16}(19C-120D+70E)\right]N + 0.1\Delta \pm$$

$$\left\{\frac{1}{4}\Delta^2+[(A+3B)^2+3(B-A)^2]M^2 - \left[\frac{3}{8}(19C-120D+70E)(A+3B)\right.\right.$$

$$\left. - \frac{9}{8}(3C+40D+70E)(A+3B) - \frac{45}{4}(C+8D-14E)(B-A)\right]M\cdot N$$

$$+\left[\frac{9}{256}(19C-120D+70E)^2 + \frac{81}{256}(3C+40D+70E)^2 + \frac{675}{64}(C+8D-14E)^2\right.$$

$$\left. - \frac{27}{128}(3C+40D+70E)(19C-120D+70E)\right]N^2 + (A+3B)\cdot\Delta\cdot M$$

$$\left. + \left[\frac{9}{8}(3C+40D+70E) - \frac{3}{8}(19C-120D+70E)\right](0.5\Delta)N\right\}^{\frac{1}{2}}$$

where the (+) combination is the energy of the upper A_1 state derived from $E_g(O_h)$. The energy expression for the A_1 ground state is then subtracted from the expressions for the excited A_1, B_1 and B_2 states. The three resulting expressions are equivalent to the experimentally determined energies for the $A_1 \rightarrow A_1$, $A_1 \rightarrow B_1$ and $A_1 \rightarrow B_2$ electronic transitions of Fe^{2+} in C_{2v} symmetry. Hence, there are three equations containing three unknowns, Δ, M and N, and the point-charge model can be solved exactly.

REFERENCES

Ballhausen, C. J. (1962) Introduction to Ligand Field Theory. McGraw Hill, New York.

Figgis, B. N. (1966) Introduction to Ligand Fields. Interscience Publishers.

Ghose, S. (1965) Mg^{2+}-Fe^{2+} order in an orthopyroxene, $Mg_{0.93}Fe_{1.07}Si_2O_6$. Z. Kristallogr. 122, 81-99.

Goldman, D. S. and G. R. Rossman (1977) The spectra of orthopyroxene revisited: the splitting of the ground state. Amer. Mineral. 62, 151-157.

Hutchings, M. T. (1964) Point-charge calculations of energy levels of magnetic ions in crystalline electric fields. Solid State Phys. 16, 227-273.

Wilson, E. B., J. C. Decius and P. C. Cross (1955) Molecular Vibrations, McGraw Hill, New York.

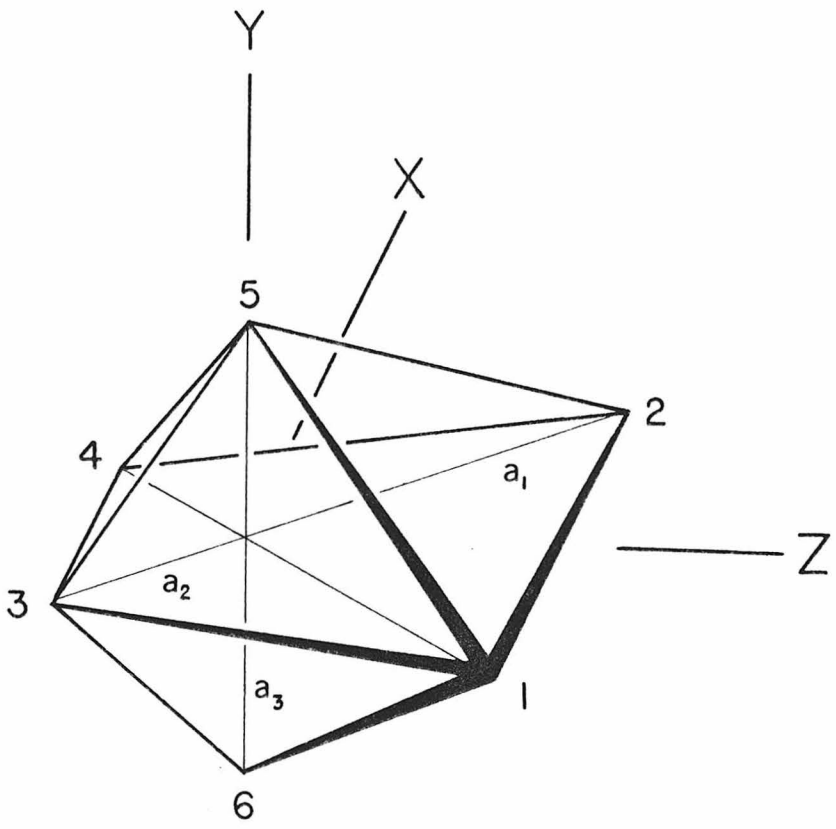

Figure 1. Idealized C_{2v} coordination site in which Z, the two-fold rotation axis, is a dihedral axis. Points 1 through 6 have (r,θ,ϕ) coordinates of (a_1,θ_1,π), $(a_1,\theta_1,0)$, (a_2,θ_2,π), $(a_2,\theta_2,0)$, $(a_3,\theta_3,\pi/2)$ and $(a_3,\theta_3,3\pi/2)$, respectively.

CHAPTER 4

DETERMINATION OF QUANTITATIVE CATION DISTRIBUTION IN ORTHOPYROXENE FROM ELECTRONIC ABSORPTION SPECTRA

ABSTRACT

Electronic absorption, Mössbauer and electron microprobe data are correlated for iron-bearing orthopyroxenes. The correlation provides a means of quantitatively determining the distribution of Fe^{2+} among the M(1) and M(2) sites of orthopyroxene crystals from electronic spectra and electron microprobe analysis. A spin-allowed transition of Fe^{2+} in the M(1) site is identified at about 13,000 cm^{-1} in γ, ε values for spin-allowed Fe^{2+} absorption bands in the near-infrared region are determined, and the origins of spin-forbidden transitions in the visible region are examined.

INTRODUCTION

The distribution of ferrous iron between the two non-equivalent six-coordinate sites in orthopyroxene, $(Mg,Fe)SiO_3$, has been extensively analyzed, using Mössbauer spectroscopy and X-ray structural refinements, because of its potential applications in geothermometry. Ghose (1965) found that Fe^{2+} preferentially occupies the large, highly-distorted M(2) site. Evans *et al.* (1967) observed that the distribution of Fe^{2+} between the M(1) and M(2) sites is dependent upon temperature. Ghose and Hafner (1967) showed that Fe^{2+} is more strongly partitioned into the M(2) site in slowly cooled metamorphic rocks than in quickly cooled volcanic rocks. These observations suggested that the cation distribution depends on the rate of cooling, which led Virgo and Hafner (1969, 1970) and Saxena and Ghose (1971) to determine rate constants for the Fe^{2+} - Mg order-disorder process.

Electronic absorption spectra are also sensitive to the site distribution of ferrous iron in orthopyroxene. The spectroscopic features of Fe^{2+} in the M(1) and M(2) sites differ in energy and intensity due to the structural dissimilarities of the two sites (Burns, 1970; Goldman and Rossman, 1976, 1977). Previous electronic absorption studies of orthopyroxenes have not provided quantitative site distribution information. The purpose of this study is to establish a method from which a quantitative site distribution can be determined from electronic absorption spectra of single orthopyroxene crystals. The advantages of this method are that 1) it can be used to analyze

orthopyroxene crystals in a thin-section in which the textural relationships among the various phases are retained, and 2) it can be used to analyze the site distribution in single orthopyroxene crystals to examine the petrologic implications of compositional zonation.

The method results from correlating the intensity of the absorption bands due to Fe^{2+} in the M(2) site in the electronic spectra with the molar concentration of Fe^{2+} in this site, which is determined from Mössbauer spectra (taken at 77 K) and electron microprobe analysis. A linear correlation between the spectroscopic techniques over the compositional range spanned depends on the constancy of the ratio of the recoil-free fractions for both sites in the Mössbauer spectra and the constancy of molar absorptivity for Fe^{2+} in the M(2) site in the electronic absorption spectra. Virgo and Hafner (1968) and Burnham et al. (1971) indicated that differences in recoil-free fraction for Fe^{2+} between both sites are small and assumed that the ratio is equal to one. The linearity of absorbance with concentration in electronic spectra is generally found in solution chemistry and has also been found for Fe^{2+} in silicate garnets (White and Moore, 1972).

EXPERIMENTAL METHODS

The electronic absorption spectra of the bronzite from Bamble, Norway are presented in Goldman and Rossman (1977). The spectra of a bronzite from the Barton garnet mine (Cal Tech ref. 3403) and the hypersthene from Summit Rock, Oregon (Kleck, 1970) have been obtained on polished, self-supporting (010) and (100) slabs. To obtain the intense band in α near 11,000 cm^{-1} on scale for spectroscopic measurement, the (100) slabs were epoxied onto a glass slide, thinned to less than 0.05 mm and spectroscopically examined. The epoxy was then dissolved in n,n-dimethylformamide, the samples were removed and their thicknesses were determined directly. The thickness of the slab of eulite from Greenland used to obtain the β spectrum was determined similarly, except on a (001) orientation. Methods of sample preparation and data reduction have been described in Goldman and Rossman (1977). Electron microprobe analyses of samples 1, 2 and 3 (Table 1) have been taken within the area in which the optical spectra were obtained. The chemical analysis of the eulite sample is given in Virgo and Hafner (1969). Site distributions from 77 K Mössbauer spectra have been determined directly from the area ratios.

SPECTROSCOPIC CONSIDERATIONS

Spin-allowed bands

The electronic absorption spectra of the spin-allowed transitions due to Fe^{2+} in the M(2) site are best illustrated in the spectra of a bronzite ($Fs_{14.0}$) from Bamble, Norway (Goldman and Rossman, 1977, Figure 2). The Mössbauer spectrum of that sample taken at 77 K as a part of the present study indicates that 96.1 percent of the iron is in the M(2) site. Bands assigned to the $^5\underline{A}_1 \rightarrow {}^5\underline{A}_1$, $^5\underline{A}_1 \rightarrow {}^5\underline{B}_1$ and $^5\underline{A}_1 \rightarrow {}^5\underline{B}_2$ transitions occur at 10,930, 5400 and 2350 cm^{-1} and are polarized mostly in $\alpha(\underline{b})$, $\beta(\underline{a})$ and $\gamma(\underline{c})$, respectively. The transitions to the $^5\underline{A}_1$ and $^5\underline{B}_1$ states are considered to originate from a removal of the degeneracy of the octahedral $^5\underline{E}_g$ state due to the low symmetry of the site and similarly, the $^5\underline{B}_2$ state is considered to arise from the splitting of the octahedral $^5\underline{T}_{2g}$ state.

An absorption band near 8600 cm^{-1} that is polarized mostly in γ has been assigned to Fe^{2+} in the M(1) site by Burns (1970). Burns considered this band to represent the transition to the lower energy component of the split $^5\underline{E}_g$ state. The higher energy component was considered to be beneath the main band in γ due to Fe^{2+} in the M(2) site. It is important to understand the extent to which the M(1) absorptions will interfere with the calibrations for the M(2) peak intensities. For this reason a series of experiments were performed to more clearly identify the location of the higher energy M(1) band. In the course of that study, the origin of the spin-forbidden bands in the 15,000-25,000 cm^{-1} region was also examined. These experiments make

use of the ability to disorder the iron distribution between the M(1) and M(2) sites by heating single crystals to temperatures above 500 ^{o}C and then by quickly quenching the sample.

The γ spectrum of a bronzite ($Fs_{29.5}$) from Gore Mountain, New York is presented in Figure 1a. The Mössbauer spectrum of this sample taken at 77 K indicates that 94.9 percent of the iron is in the M(2) site, and consistent with this result, the intensity of the M(1) band near 8600 cm^{-1} is weak. The oriented slab used to obtain this spectrum was sealed in an evacuated fused silica tube and placed in a furnace at 850^{o}C for 24 hours to disorder Fe^{2+} between the two sites. After heating, the sample was removed from the furnace, quickly quenched in liquid nitrogen, and spectroscopically examined at room temperature (Figure 1b). The reduction in the intensity of the M(2) feature near 5400 cm^{-1} with the increase in the intensity of the M(1) feature near 8600 cm^{-1} is an independent spectroscopic verification of the cation disordering phenomenon previously described from Mössbauer spectroscopy (Virgo and Hafner, 1969; Saxena and Ghose, 1971). The absorption tail originating from the ultraviolet region has moved further into the visible region and the intensity of the Fe^{2+}/Fe^{3+} intervalance charge-transfer band near 17,000 cm^{-1} (Burns, 1970, page 72) appears to have increased after heating. In particular, the transmission valley near 13,500 cm^{-1} (Figure 1a) is replaced by absorption after heating (Figure 1b), which is attributed to the presence of the higher energy $^{5}\underline{E}_{g}$ component of Fe^{2+} in the M(1) site. This band becomes evident in a difference plot (Figure 1c) in which the unheated spectrum was subtracted

from the heated spectrum. The higher energy M(1) band is clearly evident in the 77 K γ spectrum (Figure 1d) of a volcanic hypersthene ($Fs_{39.5}$) from Summit Rock, Oregon that has been heated at 900 and then 800 °C, each for 48 hours. From these observations, the upper $^5\underline{E}_g$ component for Fe^{2+} in the M(1) site is estimated to have an energy of 13,000 cm^{-1}, which produces a barycenter (mean) energy of both components of 10,800 cm^{-1}.

Spin-forbidden bands

Five narrow bands of low intensity occur in γ at 23,470, 22,400, 20,800, 19,760 and 18,250 cm^{-1} (Figure 1a). They are considered to arise from spin-forbidden transitions of Fe^{2+} in the M(2) site. After heating (Figure 1b) the bands at 23,470 and 22,400 cm^{-1} have diminished in intensity as shown in the difference plot (Figure 1c), supporting their assignment to the M(2) site. After heating, new bands appear at 20,500 and 19,700 cm^{-1} that are attributed to Fe^{2+} in the M(1) site. At greater M(1) concentrations (Figure 1d), another band near 21,370 cm^{-1} appears that is attributed to Fe^{2+} in the M(1) site. Site assignments are summarized in Figure 1c in which absorptions due to Fe^{2+} in the M(1) and M(2) sites are annotated with arrows pointing up and down, respectively.

THE CALIBRATION

The spectra of the two bronzites and the hypersthene sample form the basis for the calibration of optical intensities. The 77 K Mössbauer spectrum of the hypersthene sample indicates that 82.1 percent of the total iron content resides in the M(2) site. The β spectrum of a eulite (Fs_{86}) from Greenland containing nearly full Fe^{2+} occupancy of the M(2) site is also included which has bands at 10,850 and 4890 cm^{-1}. The cation distribution in this sample was determined by both X-ray and Mössbauer analyses in Burnham et al.

In order to calculate the concentration of Fe^{2+} in the M(2) site for any sample, the density must be known. It would be particularly advantageous to obtain the density of a crystal in a thin section without having to extract it. Howie (1963) showed that the density of orthopyroxene regularly increases with increasing iron content. Therefore, an equation can be determined to relate density to iron content, enabling densities to be calculated from electron microprobe analyses of orthopyroxene crystals in a thin-section. From the thirty-eight chemical analyses and density measurements in Howie (1963), two in Deer et al. (1966), and using the density measurement for the Bamble sample in Gibbons (1974), the following least-squares equation is obtained:

$$D(g/l) = 13.37\ (\pm .02)\ (\text{wt. \% FeO}) + 3186.13\ (\pm .47) \qquad (1)$$

where D is the density in grams per liter and FeO is the total iron content in the sample. The densities of the Gore Mountain and Summit Rock samples were determined from equation 1, whereas

the density of the Greenland sample was calculated from the chemistry and cell axes given in Burnham *et al*. The Fe^{2+} concentration in each site and the intensities of the M(2) electronic absorption features are listed in Table 2.

The intensities of α, β and γ polarized components of the $^5A_1 \rightarrow {}^5A_1$ and $^5A_1 \rightarrow {}^5B_1$ transitions in the 10,500-11,000 and 4900-5400 cm^{-1} regions are correlated with the Fe^{2+} concentrations in the M(2) site in Figures 2 and 3, respectively. The spectral intensities are linearly related to Fe^{2+} concentration in the range up to 10 moles/liter of Fe^{2+} in the M(2) site determined from the Summit Rock hypersthene, which represents nearly 66 percent occupancy of the M(2) site by Fe^{2+}. The intensity of the band in β for the eulite sample in the 4900-5400 cm^{-1} region also falls on the linear trend determined by the other samples (Figure 3). Therefore, molar absorptivity for this band is a constant across the entire composition range of Fe^{2+} in the M(2) site and is equal to 9.65 from a least-squares solutions of the four samples. The slight curvature of the band in β in the 10,500-11,000 cm^{-1} region (Figure 2) is attributed to a weak M(1) component that is superimposed on the main β peak in the eulite sample. A weak component of the 8600 cm^{-1} M(1) band that is dominantly polarized in γ, also occurs in β in this sample. Molar absorptivity (ε) values for all bands in Figures 2 and 3 have been determined from least-squares solutions of the data and are presented in Table 3. From these results, the M(2) iron concentration can be determined from any band using the following:

$$Fe^{2+}_{M(2)} \text{ (moles/liter)} = \frac{Abs}{T \cdot \varepsilon} \qquad (2)$$

where Abs is the optical absorbance (log Io/I), T is the thickness (in centimeters) and ε is the molar absorptivity for that band given in Table 3. Equation 2 can be rewritten to give the iron content in weight percent as:

$$Fe^{2+}_{M(2)} \text{ (wt. \%)} = \frac{Abs \cdot (5584.7)}{T \cdot \varepsilon \cdot D} \qquad (3)$$

where D is the density determined from equation 1. To determine the iron content as FeO, replace 5584.7 by 7184.7 in equation 3. The values determined from these equations are then subtracted from the total iron content to obtain the M(1) Fe^{2+} content.

The ε value for the M(1) band near 8600 cm^{-1} in the γ spectrum of the Summit Rock hypersthene (Goldman and Rossman, 1977, Figure 3) is calculated to be 4.6. An ε value of 4.7 is calculated for this band from the Gore Mountain bronzite after heating (Figure 1b) using equation 2.

The band in α in the 10,000-11,000 cm^{-1} region is the most sensitive means for determining the cation distribution and is about four times as intense as the band in β in the 5000-5500 cm^{-1} region. For a 30 μm thick orthopyroxene crystal which contains 0.5% FεO, all of which is in the M(2) site, the absorbance in α at about 11,000 cm^{-1} would be about 0.03 which is readily detectible in the spectra. For the Bamble bronzite in a thin-section, this indicates that about a 5 percent change in the M(2) iron content can be detected at this thickness from the spectra. Similarly, a 2 percent change in the M(2) iron content of the Summit Rock hypersthene can be detected.

TECHNICAL PROBLEMS

It is particularly important to accurately determine the thickness of the crystal, especially when it is in thin section. For example, by incorporating oriented sections of quartz into the thin-section, the final thickness after polishing can be obtained using the appropriate refractive index of quartz with the Duc de Chalnes method (see Bloss, 1961, page 48). If a universal stage is used for orientation, the appropriate thickness corrections must be made. It is also important to realize that the calibrations presented in this paper are derived from a spectrophotometer that is not equipped with polarizing microscopes in the sample and reference chambers used in some laboratories. Therefore, additional convergent light problems necessarily introduced by the microscope optical system which mix polarization intensities of the various absorption bands in the electronic spectra are avoided.

The effect of convergence in the optical path can best be understood in an example of a typical spectroscopic experiment. This is illustrated in Figure 4. A polarized beam of light, with a convergence angle θ, interacts with an oriented crystal in the $\alpha\beta$ plane in which α and β have absorbances per unit thickness of 0.0 and 1.0, respectively. The resulting intensity leaving the sample is:

$$I = I_{\beta}\cos^2\theta + I_{\alpha}\sin^2\theta \qquad (4)$$

Ratioing this intensity to that in the reference chamber (I_o) in a dual-beam spectrometer results in:

$$Abs/t = -\log\ (I/I_o) = -\log\left[(I_{\beta}/I_o)\ \cos^2\theta + (I_{\alpha}/I_o)\ \sin^2\theta\right] \qquad (5)$$

Integrating this equation to account for the total convergence as:

$$2\int_{o}^{\theta} 10^{-Abs/t} d\theta = 2\int_{o}^{\theta} \left(\frac{I\beta}{I_o}\right) \cos^2\theta d\theta + 2\int \left(\frac{I\alpha}{I_o}\right) \sin^2\theta d\theta \qquad (6)$$

results in

$$Abs/t = -\log \left\{ \tfrac{1}{2} \frac{\sin\theta\cos\theta}{\theta} \left[\frac{I_\beta}{I_o} - \frac{I_\alpha}{I_o} \right] + \tfrac{1}{2} \left[\frac{I_\beta}{I_o} + \frac{I_\alpha}{I_o} \right] \right\} \qquad (7)$$

Using equation 7, the reduction in the intensity of the β feature as the convergence angle increases is shown in Figure 5. Therefore, with a 30^{o} convergence angle, the β feature will only be about 75 percent of its true intensity. The convergence angle in the Cary 17I spectrometer used in this study is less than 3^{o}.

CONCLUSION

The linear correlation of band intensity with the concentration of Fe^{2+} in the M(2) site enables quantitative cation distributions to be determined from electronic spectra and microprobe analyses for single orthopyroxene crystals. The linearity of the correlation suggests that the molar absorptivity of Fe^{2+} in the M(2) site and the ratio of the recoil-free fractions for Fe^{2+} in both sites are constant over the compositional range examined. Site populations can now be determined for orthopyroxene crystals in petrographic thin-section without sacrificing important textural relationships among the coexisting phases. This technique may be particularly useful in studying the site distribution in zoned or partially exsolved orthopyroxene crystals.

ACKNOWLEDGMENTS

I thank J. Huneke (Cal Tech) and S. Ghose (U. of Washington) for providing the hypersthene and eulite crystals used in this study. I also thank J. Huneke for the use of his apparatus to evacuate and seal fused silica tubes containing the orthopyroxene crystals and W. A. Dollase (UCLA) for obtaining the 77 K Mössbauer spectra.

REFERENCES CITED

Bloss, F.D. (1966) An Introduction to the Methods of Otical Crystallography. Holt, Rinehart and Winston, New York.

Burnham, C.W., Y. Ohashi, S.S. Hafner and D. Virgo (1971) Cation distribution and atomic thermal vibrations in an iron-rich orthopyroxene. Am. Mineral. 56, 850-875.

Burns, R.G. (1970) Mineralogical Applications of Crystal Field Theory. Cambridge University Press.

Deer, W.A., R.A. Howie and J. Zussman (1966) An Introduction to the Rock-Forming Minerals. John Wiley and Sons.

Evans, B.J., S. Ghose and S.S. Hafner (1967) Hyperfine splitting of Fe^{57} and Mg-Fe order-disorder in orthopyroxene ($MgSiO_3$-$FeSiO_3$) solid solution. J. Geol. 75, 306-322.

Ghose, S. (1965) Mg^{2+}-Fe^{2+} order in an orthopyroxene, $Mg_{0.93}Fe_{1.07}Si_2O_6$. Zeis. Kristallogr. 122, 81-99.

Ghose, S. and S. Hafner (1967) Mg^{2+}-Fe^{2+} distribution in metamorphic and volcanic orthopyroxenes. Zeis. Kristallogr. 125, 157-162.

Gibbons, R.V. (1974) Experimental effects of high shock pressure on materials of geologic and geophysical interest. Ph.D. Thesis. California Institute of Technology.

Goldman, D.S. and G.R. Rossman (1976) Identification of a mid-infrared electronic absorption band of Fe^{2+} in the distorted M(2) site of orthopyroxene, $(Mg,Fe)SiO_3$. Chem. Phys. Lett. 41 (3), 474-475.

Goldman, D.S. and G.R. Rossman (1977) The spectra of iron in orthopyroxene revisited: The splitting of the ground state. Am. Mineral. 62, 151-157.

Howie, R.A. (1963) Cell parameters of orthopyroxenes. Mineral. Soc. Amer., Spec. Pap. 1, 213-222.

Kleck, W.C. (1970) Cavity minerals at Summit Rock, Oregon. Am. Mineral. 55, 1396-1404.

Saxena, S.K. and S. Ghose (1971) Mg^{2+}-Fe^{2+} order-disorder and the thermodynamics of the orthopyroxene crystalline solution. Am. Mineral. 56, 532-559.

Virgo, D. and S.S. Hafner (1968) Re-evaluation of the cation distribution in orthopyroxenes by the Mössbauer effect. Earth Planet Sci. Lett. 4, 265-269.

Virgo, D. and S.S. Hafner (1969) Fe^{2+}, Mg order-disorder in heated orthopyroxenes. Mineral. Soc. Amer. Spec. Pap. 2, 67-81.

Virgo, D. and S.S. Hafner (1970) Fe^{2+}, Mg order-disorder in natural orthopyroxenes. Am. Mineral. 55, 201-223.

White, W.B. and R.K. Moore (1972) Interpretation of the spin-allowed bands of Fe^{2+} in silicate garnets. Am. Mineral. 57, 1692-1710.

TABLE 1. Microprobe analyses

	1	2	3	4
SiO_2	57.83	52.83	53.30	47.38
TiO_2	-	0.07	0.19	-
Al_2O_3	0.09	2.94	.23	0.79
MgO	32.86	25.08	19.67	3.83
FeO	9.77	18.82	25.02	48.57
MnO	-	0.17	.51	-
CaO	0.26	.44	1.76	.84
	100.81	100.35	100.68	101.41

Formula proportions (# cations = 4)

Si	2.00	1.92	2.00	1.98
Al^{IV}	-	.08	-	.02
Al^{VI}		.05	.01	.02
Ti	-	-	.01	-
Mg	1.70	1.36	1.10	.24
Fe	.28	.57	.79	1.70
Mn	-	.01	.02	-
Ca	.01	.02	.07	.04

1 Bronzite Bamble, Norway
2 Bronzite Barton garnet mine, Gore Mountain, New York
3 Hypersthene Summit Rock, Oregon
4 Eulite (XYZ) Greenland (Virgo and Hafner, 1969)

TABLE 2. Optical intensities*

	SAMPLE 1	2	3	4	
α	172	347	410	-	10,500 -
β	20	44	54	90	11,000 cm^{-1}
γ	8	20	27	-	region
α	6	15	15	-	4,900 -
β	42	85	99	138	5,400 cm^{-1}
γ	11	20	26	-	region
Fe conc. (moles/1)					
M(1)	0.2	0.5	2.2	11.5	
M(2)	4.3	8.5	10.0	14.7	

* absorbance per centimeter crystal thickness

TABLE 3. Molar absorptivity (ε) for M(2) Fe^{2+}

Region	α	β	γ
10,500 - 11,000 cm^{-1}	40.83	5.24	2.51
4,900 - 5,400 cm^{-1}	1.59	9.65	2.48

FIGURE CAPTIONS

1. Room temperature γ electronic absorption spectra of a bronzite from Gore Mountain, New York taken before heat-treatment (a) and after heating in a vacuum at 850 ^{o}C for 24 hours (b). The unheated spectrum was subtracted from the heated spectrum to produce the difference plot (c) in which features due to Fe^{2+} in the M(1) and M(2) sites are denoted by arrows pointing up and down, respectively. The γ spectrum taken at 77 K of a hypersthene from Summit Rock, Oregon (d) which was heated in a vacuum at 900 and then 800 ^{o}C for 48 hours clearly shows the two spin-allowed M(1) absorptions near 8600 and 13,000 cm^{-1}.
2. Correlation of the intensities of the M(2) bands in the 10,500-11,000 cm^{-1} region with the concentration of Fe^{2+} in the M(2) site.
3. Correlation of the intensities of the M(2) bands in the 4900-5400 cm^{-1} region with the concentration of Fe^{2+} in the M(2) site.
4. A typical optical absorption experiment in which plane polarized light with a convergence angle θ interacts with a crystal in the $\alpha\beta$ plane.
5. The reduction in the intensity of an absorbance band in an optical experiment as a function of the convergence angle, θ. The β and α absorbances are initially assumed to be 1.0 and 0.0, respectively.

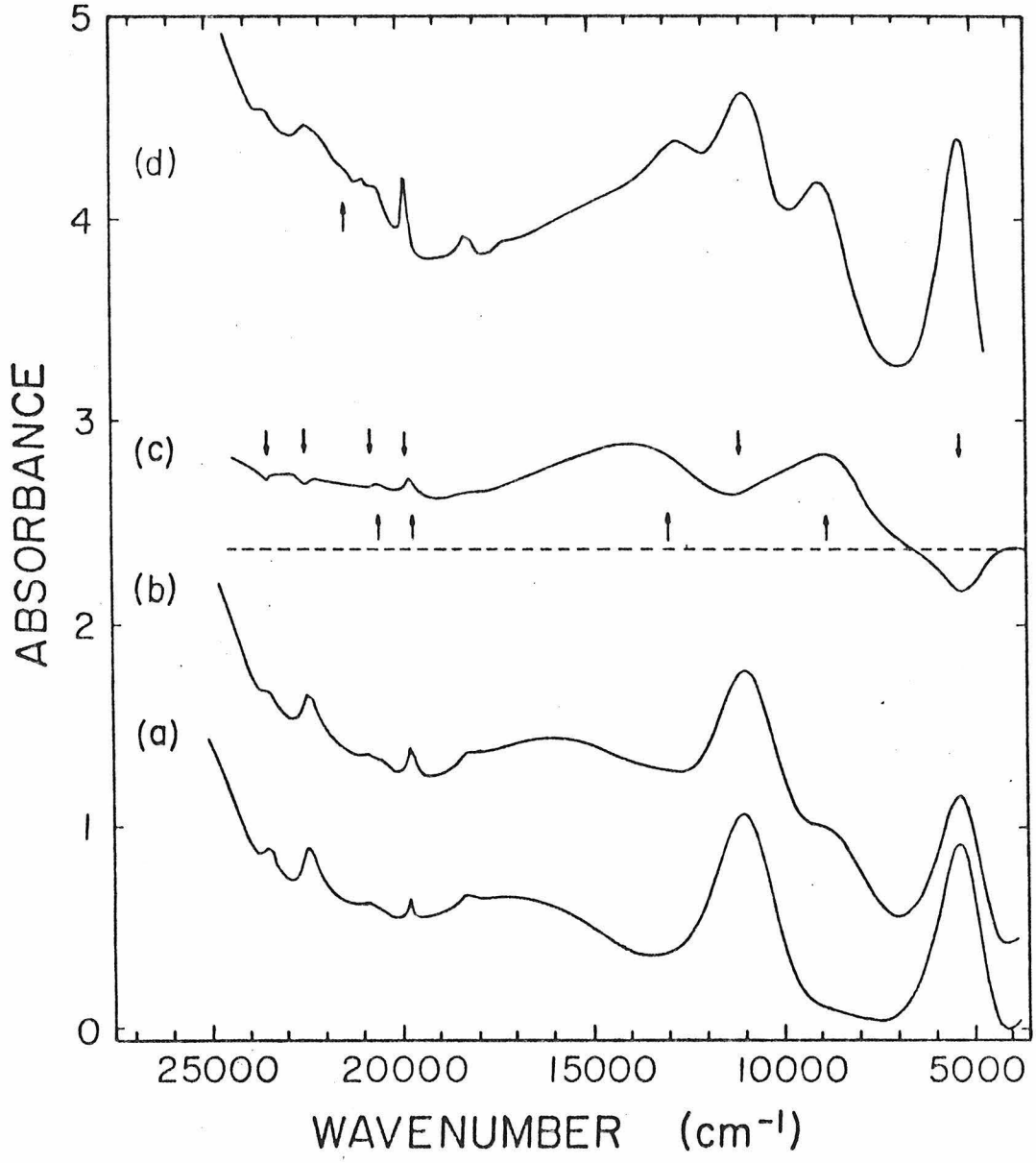
5
4
3
2
1
0
ABSORBANCE
(d)
(c)
(b)
(a)
25000
20000
15000
10000
5000
WAVENUMBER (cm⁻¹)

Figure 1

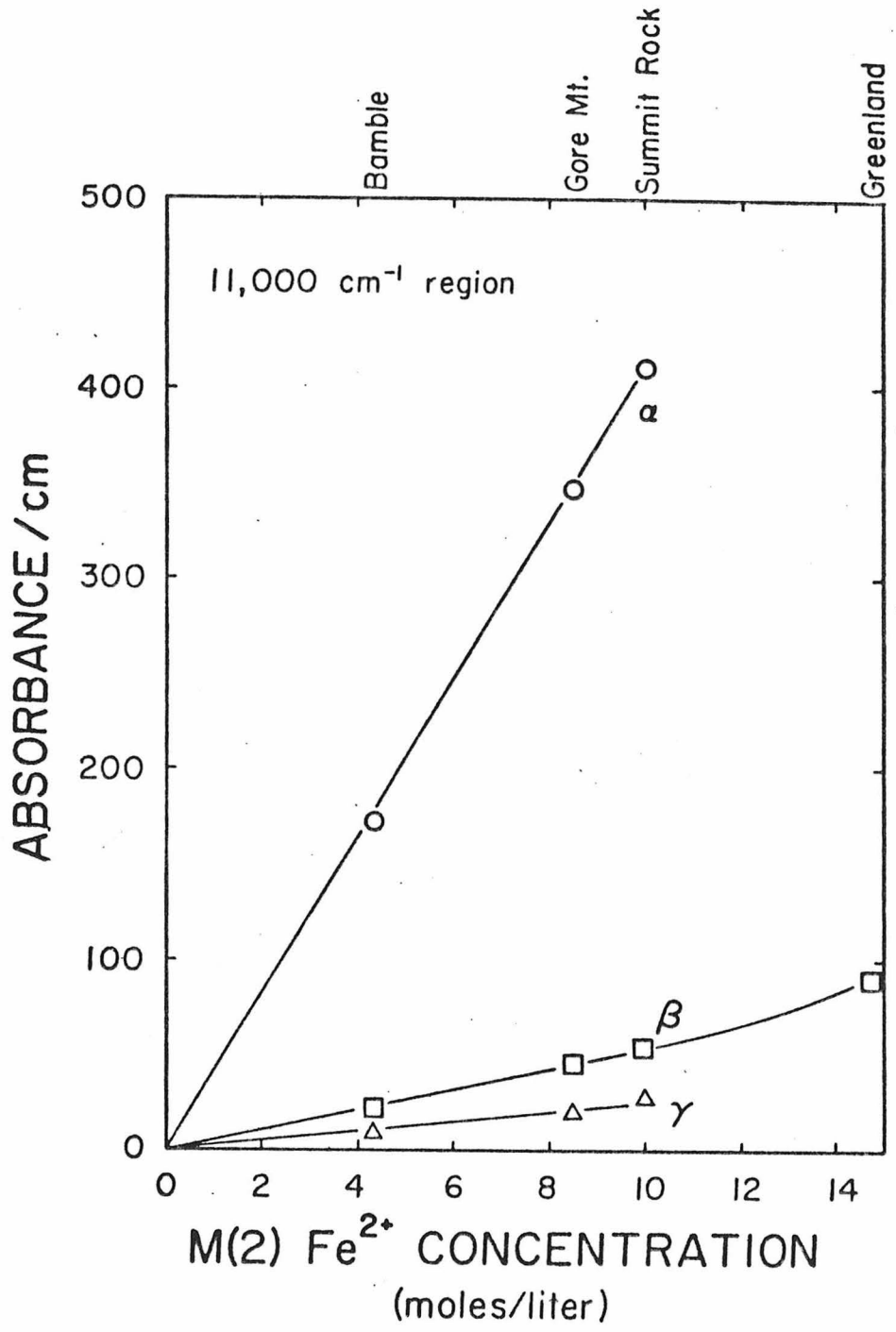
Bamble
Gore Mt.
Summit Rock
Greenland
11,000 cm⁻¹ region
α
β
γ
ABSORBANCE / cm
0
100
200
300
400
500
0
2
4
6
8
10
12
14
M(2) Fe2+ CONCENTRATION
(moles/liter)

Figure 2

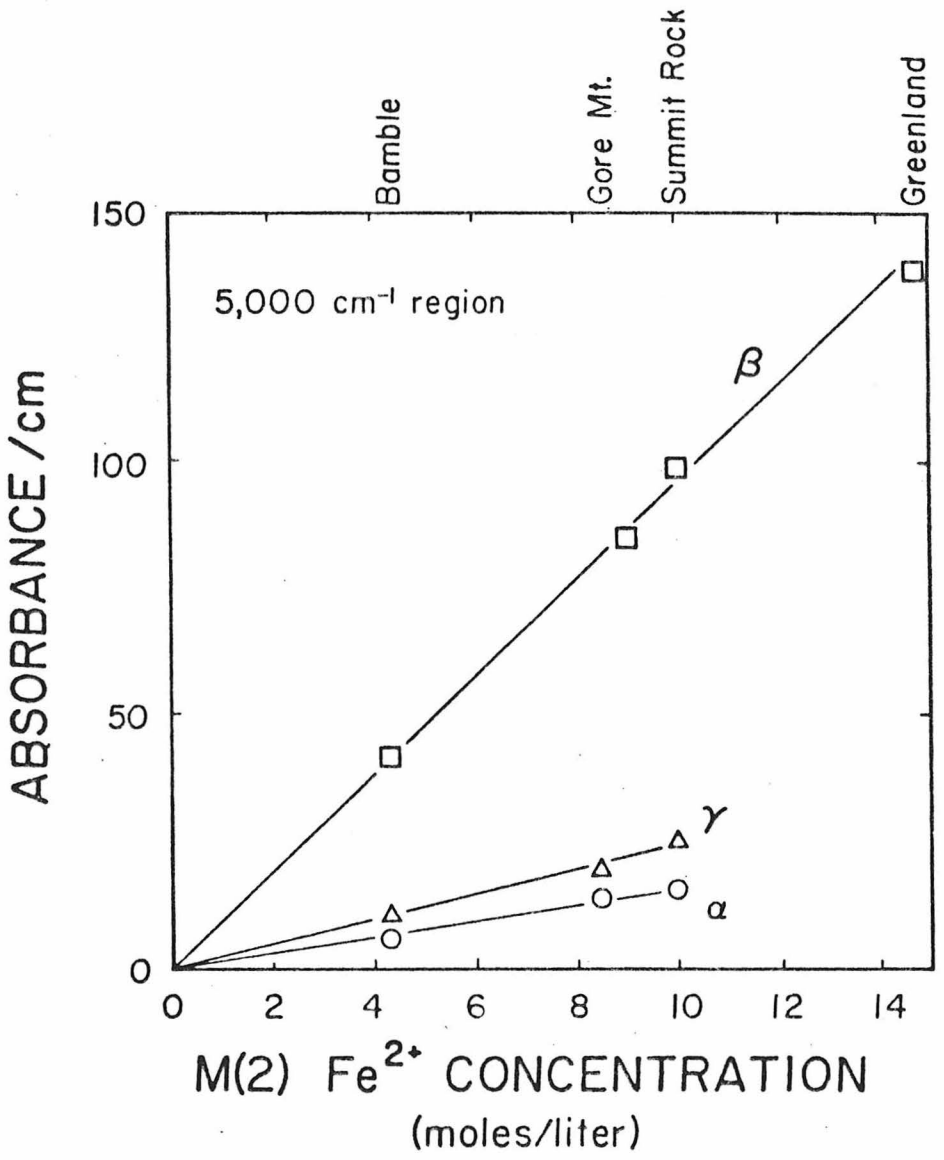
Bamble
Gore Mt.
Summit Rock
Greenland
150
100
50
0
5,000 cm⁻¹ region
β
γ
α
ABSORBANCE /cm
0
2
4
6
8
10
12
14
M(2) Fe2+ CONCENTRATION
(moles/liter)

Figure 3

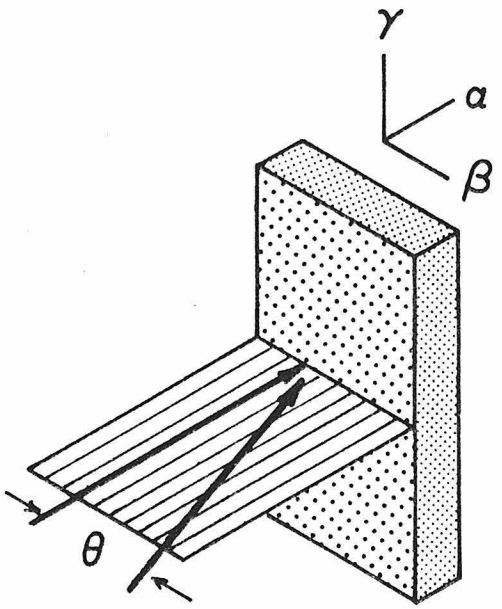

Figure 4

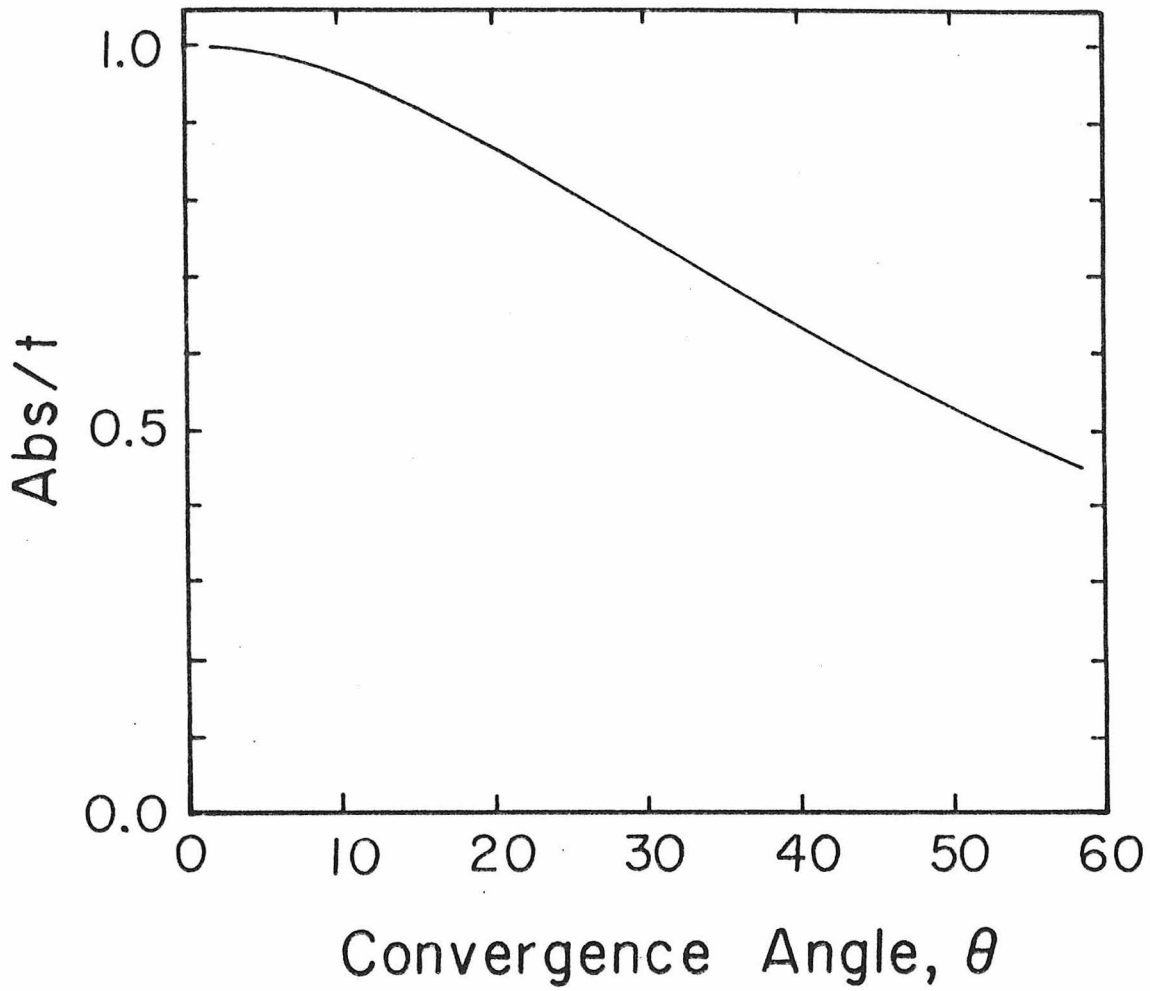

Figure 5

CHAPTER 5

THE IDENTIFICATION OF Fe^{2+} IN THE M(4) SITE OF CALCIC AMPHIBOLES

Published: The American Mineralogist, 62, 205-216
Co-author: George R. Rossman

ABSTRACT

Evidence is presented for the occurrence of Fe^{2+} in the predominantly Ca-filled M(4) site of calcic amphiboles. Absorption bands in the electronic spectra at 1030 nm in β and at 2470 in α provide a sensitive means for identifying Fe^{2+} in this site. The large ε value for the 1030 band, the large energy separation between both bands, and the similarity to the spectra of Fe^{2+} in large, highly distorted coordination sites in other minerals provide the basis for the M(4) site assignment. The energy splittings and polarization anisotropy of these bands are analyzed using a point-charge model based on $\underline{C_{2v}}$ symmetry. Spectral data indicate that the Fe^{2+} content in the M(4) site significantly varies among the calcic amphiboles.

INTRODUCTION

Little is known about the Fe^{2+} content of the M(4) site of calcic amphiboles. M(4) Fe^{2+} has been difficult to identify because calcium generally occupies 85-95% of this site (Leake, 1968) and therefore, only a small percentage of the total iron in most samples can occupy the M(4) site. Hence, it is difficult to analyze for M(4) Fe^{2+} in the complex Mössbauer spectra, and to detect small quantities of Fe^{2+} in a predominantly Ca-filled M(4) site by crystallographic analysis. The purpose of this paper is to identify Fe^{2+} in the M(4) site with electronic absorption spectra and to show that this technique is sensitive to small concentrations of Fe^{2+} in this site.

The electronic absorption spectra of the calcic amphiboles consist of a superposition of absorption bands that arise from ferrous iron in several sites of different coordination geometries. Amphiboles contain three sites, M(1), M(2) and M(3), that more closely resemble regular octahedra than the fourth site, M(4), that is highly distorted from octahedral geometry. Fe^{2+} in the M(4) site of calcic amphiboles has not been previously identified in absorption spectra. Burns (1970) presented absorption spectra of two actinolites, $Ca_2(Mg,Fe)_5Si_8O_{22}(OH)_2$, in the 350-1500 nm region in which all Fe^{2+} features

were attributed to Fe^{2+} in the M(1), M(2), and M(3) sites. It can be inferred from this discussion and from Burns (1965) that the main band at about 1035 nm arises from Fe^{2+} in the M(2) site. White and Keester (1966) assigned a band in the 2300-2500 nm region to Fe^{2+} in tetrahedral coordination also in a spectrum of actinolite. Both of these bands occur in the spectra of the orthorhombic amphiboles of the anthophyllite-gedrite series, $(Mg,Fe,Al)_7(Si,Al)_8O_{22}(OH)_2$; however, Mao and Seifert (1973) assigned both bands to Fe^{2+} in the M(4) site.

The high degree of distortion of the M(4) site is expected to produce large crystal-field splittings analogous to the spectra of Fe^{2+} in the distorted M(2) site of orthopyroxene, $(Mg,Fe)_2Si_2O_6$. Burns (1970), Runciman et al., (1973), and Goldman and Rossman (1977) studied a variety of orthopyroxenes in which bands at about 930 nm and 1850 nm were assigned to transitions to excited states derived from the splitting of the octahedral $^5\underline{E}_{\underline{g}}$ state. These interpretations provide a basis for the analysis of the calcic amphibole spectra. A third absorption band at 2350 cm^{-1} was identified in orthopyroxene (Goldman and Rossman, 1976) and assigned to a transition within the split $^5\underline{T}_{2\underline{g}}(\underline{O}_{\underline{h}})$ state of Fe^{2+} in the M(2) site. Polarized spectra will be presented to examine if a similar band arising from Fe^{2+} in the M(4) site occurs in the 1200-4000 cm^{-1} region.

Sample Description

Tremolite: Mt. Bity, Malagasay Republic (Lacroix, 1910); CIT #8038; a 2 cm prismatic, euhedral crystal that is green, transparent and free of inclusions. Microprobe analyses of various chips from the crystal show a range of iron

content from 1.6 to 2.8 wt % FeO, but the microprobe analysis of the sample used for optical spectra indicated 2.06% FeO and the wet chemical analysis of the Mössbauer sample indicated 2.09% FeO.

Actinolite: Zillerthal, Tyrol, Austria; CIT #4916; dark green, prismatic, euhedral laths up to 15 mm long and up to 4 mm across the basal section in a talc-mica schist. The absorption spectra were taken in areas on the oriented slabs that were free of micaceous inclusions common to these samples. The microprobe analyses are similar to those reported for actinolites from this locality in Leake (1968).

(Fluoro)Pargasite: Pargas, Finland; CIT #2573; large crystal clusters in which the individual crystals are black, tabular along (010), and have other well-developed crystal faces. These crystals occur in marble and commonly have calcite inclusions. The spectra were obtained in inclusion-free areas. The composition of this sample differs from those reported for other pargasites from this locality in Leake (1968).

These minerals did not show chemical zonation in the area in which the optical spectra were taken on the (100) slabs.

Experimental methods

All spectral data presented in this paper have been obtained at room temperature on self-supporting (010) and (100) slabs. The method of preparation and data analysis have been described (Goldman and Rossman, 1976b).

The Mössbauer spectrum was obtained at room temperature using a MCA unit driven by a conventional loudspeaker drive system with moving source geometry. A 16 mc ^{57}Co source in a palladium matrix was used which produced a minimum line width of 0.27 mm/sec. The velocity increment was approximately 0.04 mm/sec/channel and was calibrated with laboratory standards. The sample concentration was approximately 1 mg Fe/cm^2. The sample was ground under acetone, meshed to obtain a grain size from 43-74 μm and set in lacquer in the bottom of a shallow

1" diameter plastic dish. Nearly 3×10^6 counts per channel were accumulated and the spectrum was analyzed using the computer program MOSFT (W. A. Dollase, personal communication). Other experimental details are similar to Dollase (1973).

The Mössbauer spectrum of the Mt. Bity tremolite was analyzed for six peaks which included two quadrupole doublets from Fe^{2+}(AA',BB') and one quadrupole doublet from Fe^{3+}(CC'). The half-widths for the two components of each doublet were constrained to be equal, although the half-widths of the different doublets were allowed to vary. Due to the small percentage of Fe^{3+} in this sample, the position of peak C was fixed, the areas of C and C' were constrained to be equal and their half-widths were specified. The sinusoidal variation of the background was also fitted. The resulting parameters are given in Table 2. A χ^2 value for the 200 channels analyzed is 196.

The electron microprobe analyses (Table 1) of the three amphiboles have been obtained within the areas in which the optical spectra were obtained on the (100) slabs. The analyses of the Mt. Bity and Zillerthal samples were normalized to charge assuming 23 oxygens and that all Fe is Fe^{2+}. Mössbauer data presented in this paper for the Mt. Bity sample and the analyses given in Leake (1968) for actinolites from the Zillerthal area indicate that less than 10% of the total Fe is Fe^{3+}. Using an Fe^{3+}/Fe ratio of 0.10 does not change these formula proportions. The formula proportions for the Pargas sample have been obtained similarly. Changing the Fe^{3+}/Fe ratio up to 0.30 does not appreciably change the resulting formula proportions. The sum of Al^{VI}, Fe, Mg, Ti and Mn is close to 5.0 and the sum of Ca, K and Na is approximately 3.0 with Fe^{3+}/Fe ratios of less than 0.30.

CRYSTAL STRUCTURE

Calcic amphiboles are monoclinic with space-group $C_{2/m}$. The M(1), M(2) and M(4) sites have point-group symmetry C_2 and the M(3) site has point-group symmetry C_{2h}.

The structural differences between the M(1), M(2) and M(3) sites and the M(4) site suggest that the spectroscopic features of ferrous iron in these sites will markedly differ. (c*-b) and (a-c) ORTEP (Johnson, 1965) projections of the M(1), M(2) and M(3) sites of actinolite are presented in Figure 1. These sites approach octahedral geometry, with similar average metal-oxygen (M-O) bond distances of 2.105 Å, 2.098 Å, and 2.098 Å, respectively (Mitchell, Bloss and Gibbs, 1971). In comparison, the M(4) site of actinolite shown in Figure 2 is highly distorted and is eight-coordinate when occupied by calcium.

Ideally, absorption spectra would be analyzed using the specific bond angles and bond lengths of a particular metal ion in a coordination polyhedron. For a metal ion in a site that is occupied predominantly by a different metal ion, these structural details are not known, as is the case for Fe^{2+} in the M(4) site of actinolite. The projections of the actinolite M(4) site relate primarily the position of calcium. The C_2 point-group does not constrain Fe^{2+} to occupy the calcium position; the only constraint is that it must, on the average, occupy a position on the two-fold rotation axis parallel to b. The position of Fe^{2+} in the M(4) site of monoclinic amphiboles has been determined in grunerite, $Fe_7Si_8O_{22}(OH)_2$ (Finger, 1969). A comparison of the two sites (Figure 2) indicates that Fe^{2+} is displaced on the two-fold axis toward the O(2) oxygens relative to the calcium position. An important consequence of this displacement is the increase of the Fe^{2+} -O(5) bond distances to nearly 3.3 Å. For this reason, the grunerite site is considered as a highly distorted, six-coordinate site (Papike et al., 1969) with the principal distortions being due

to 1) an elongation of the Fe^{2+}-O(6) bonds with a reduction in the O(6)-Fe^{2+}-O(6) bond angle; 2) a twisting of the O(6)-O(6) bond about b relative to the O(2)-O(2) bond; 3) a relative compression of the Fe^{2+}-O(4) bonds; and 4) a removal of the center of symmetry. The grunerite M(4) site will be used as the structural model to analyze the bands due to Fe^{2+} in the M(4) site of actinolite. This assumes that Fe^{2+} occupies a "grunerite position" in the actinolite M(4) site.

DESCRIPTION OF SPECTRA

The spectra of the Mt. Bity tremolite are presented in Figure 3 to illustrate the features that characterize most calcic amphibole spectra. These spectra will serve as a basis for the identification, assignment and crystal-field analysis of the absorption bands due to Fe^{2+} in the M(4) site. Many of the features shown in Figure 3 have been described and assigned in previous studies.

White and Keester (1966) presented an unpolarized spectrum of an actinolite and assigned an absorption band at 1020 nm to Fe^{2+} in six-fold coordination, a sharp band at 1399 nm to the first vibrational overtone of the OH^- stretching mode and a set of sharp bands at 2320 nm and 2392 nm to infrared combination modes. Burns (1970) presented the spectra of two actinolites and assigned absorption bands at 727 nm in γ and at 661 nm in β to Fe^{2+}/Fe^{3+} intervalence charge-transfer (IVCT) and described four sharp absorption bands in α at about 1400 nm arising from OH^- vibrational overtones. Burns attributed the

absorptions in the 800-1300 nm region to Fe^{2+} in the M(1), M(2) and M(3) sites. The band assigned by White and Keester to tetrahedral Fe^{2+} is located in α at approximately 2470 nm (4050 cm^{-1}) in Figure 3. The correct interpretation of this band is crucial for the site assignment to be discussed in the next section.

In addition to the features discussed in previous investigations, the sharp peaks of low intensity in the 400-550 nm region in Figure 3 are identified as spin-forbidden, electronic transitions of Fe^{2+} and Fe^{3+}. Sharp bands at 2297 nm and 2384 nm in β and at 2315 nm and 2387 nm in γ correspond to the locations of the combination bands described by White and Keester.

Fe^{2+} in M(4)

The prominent absorption bands at 1030 nm in β and at 2470 in α are assigned to transitions of Fe^{2+} in the M(4) site. The evidence supporting this assignment is derived from 1) the similarity to the spectra of Fe^{2+} in the M(4) sites of the Mg-Fe amphiboles and in the M(2) sites of ortho- and clinopyroxene, 2) the intensity correlation between these bands, 3) the barycenter energy of the two bands, and 4) the intensity of the 1030 nm band.

Similarity of Spectra

The locations of the 1030 nm and 2470 nm bands are similar to those reported for other large, distorted sites. The spectra of Fe^{2+} in the M(4) sites of cummingtonite-grunerites (Burns, 1970) show a dominant absorption band in the 1000 nm region. In the spectra of anthophyllite and gedrite, Mao and Seifert (1973) assigned bands near 1000 nm and 2500 nm to Fe^{2+} in the M(4) site. Fe^{2+} in the distorted M(2) sites of orthopyroxene (Burns, 1970; Runciman, Sengupta and Marshall, 1973; Goldman and Rossman, 1976, 1977) and

clinopyroxene (Bell and Mao, 1972; Burns, Abu-Eid and Huggins, 1972) also have bands in the 1000 nm and 1800-2500 nm regions. Therefore, it is apparent that these large, distorted sites produce a crystal-field splitting of about 5500 cm^{-1} which results in one band in the 1000 nm region and the other in the 2000 nm region. Absorption bands due to Fe^{2+} in the smaller pyroxene M(1) sites do not occur above 1200 nm. If it can be shown that these two bands arise from the same Fe^{2+} ion, then these observations support an M(4) site origin for the two calcic amphibole bands and exclude their origin from the M(1), M(2) and M(3) sites.

Band Correlations

Sections of the Mt. Bity tremolite were heated in air at 535°C for 8 hours. After the sample was heated, the 1030 nm band in β retained only 50 percent of its unheated intensity (Figure 4). A similar value is obtained for the 2470 nm band, although the vibrational absorptions superimposed upon this band preclude an exact determination of the reduction factor. These data suggest that both the 1030 nm and 2470 nm bands arise from the same Fe^{2+} ion.

The spectra of two additional calcic amphiboles have been obtained to verify that both bands originate from the same Fe^{2+} ion. Spectra of an actinolite are presented in Figure 5 in which the 1030 and 2470 nm bands are approximately 3.1 times as intense as the analogous bands in Figure 3. Stoichiometry considerations for this sample (Table 2) indicate that there is an excess of Al^{VI}, Mg, Cr, Mn and Fe that cannot be accommodated in the five M(1), M(2) and M(3) sites in the half-unit cell. Hence, the excess must be accommodated in M(4), which has only 1.82 of 2.0 possible sites occupied by Ca. In addition, there is not enough Ca and Na to completely fill the M(4) site. Furthermore, the spectra of pargasite, $NaCa_2(Mg,Fe^{2+})_4(Al,Fe^{3+})Si_6Al_2O_{22}(OH,F,Cl)_2$, (Figure 6)

indicate that the absence of the 1030 nm band is correlated with the absence of the 2470 nm band. Regardless of the Fe^{3+}/Fe^{2+} ratio assumed for this sample, the resulting formulas from the microprobe analysis indicate that the M(4) site is fully occupied by Ca and that the sum of the remaining octahedral cations is approximately 5.0. In summary, these spectra indicate that both absorption bands are either simultaneously present or absent and hence, they must arise from the same Fe^{2+} ion.

Barycenter Energy

The M(2) Fe^{2+} absorption bands at about 930 nm and 1850 nm in orthopyroxene are derived from the splitting of the $^5\underline{E}_{\underline{g}}(0_{\underline{h}})$ state due to the low symmetry of this site. Based upon the interpretation of Runciman et al., Mao and Seifert concluded that the similar bands in anthophyllite and gedrite were due to the splitting of this state. The results of a study by Faye (1972) support these interpretations, and hence, support the assignment of the 1030 nm and 2470 nm bands as electronic transitions to the separated $^5\underline{E}_{\underline{g}}(0_{\underline{h}})$ components of Fe^{2+} in the M(4) site. Faye correlated the barycenter energy of the two components with the average M-O bond length of six-coordinate sites in a variety of minerals. Upon slightly modifying the average M-O bond distance to account for the effect of the substitution of other metal ions into each site, it was found that the barycenter energy decreased linearly with increasing average M-O bond length. Using the average for the six M-O bond lengths in the grunerite M(4) site of 2.29 Å (Finger, 1969), a barycenter energy of 6880 cm^{-1} is predicted from Faye's correlation. This is the same value that is obtained from the tremolite spectra in Figure 3. For comparison, the smaller M(2) site in the orthopyroxene, bronzite, having an average M-O bond distance of 2.22 Å, has a barycenter energy of about 8160 cm^{-1}. In addition, Faye's correlation argues against the possibility that the 2470 nm band and

hence, the 1030 nm band, arise from Fe^{2+} in the M(1), M(2) or M(3) sites. The predicted barycenter energies of absorption bands arising from these sites, having average M-O bond lengths of about 2.1 Å, are about 10,000 cm^{-1}, which precludes the occurrence of one component at 2500 nm (4000 cm^{-1}). The remaining Fe^{2+} bands in the near-infrared region occur between 850 nm and 1150 nm. Taking these limits as the maximum extent of the ^5E_g splitting for Fe^{2+} in the M(1), M(2) or M(3) sites, a barycenter energy of 10,200 cm^{-1} is obtained. The agreement with Faye's correlation supports their assignment to Fe^{2+} in the M(1), M(2) or M(3) sites. It is concluded that both the 1030 nm and the 2470 nm absorption bands in the spectra of calcic amphiboles arise from Fe^{2+} in the M(4) site and that these bands result from the splitting of the $^5E_g(O_h)$ state in the low-symmetry environment.

Intensity Considerations

The intensification of absorption features in distorted sites lacking centers of symmetry is a well-known phenomenon (Burns, 1970; White and Keester, 1967). The greater intensity of the 1030 nm band in β, in comparison with other Fe^{2+} features in the 800-1300 nm region provides an indication that this band is due to Fe^{2+} in a non-centrosymmetric site. Although the M(1) and M(2) sites lack centers of symmetry, they are not nearly as distorted or non-centrosymmetric as the M(4) site. Therefore Fe^{2+} in the M(4) site is the most likely candidate for the 1030 nm band. This assignment, indicated by the band position, can be evaluated by comparing the absolute intensity of the 1030 nm band (expressed in terms of molar absorptivity, ε_{1030}) with ε values from site of various coordination geometries. Although an accurate value for ε_{1030} cannot be determined because the Fe^{2+} content of the M(4) site is not known, electron microprobe and Mössbauer analyses of the Mt. Bity tremolite provide constraints to derive a lower limit.

An absolute lower limit for ε_{1030} of 16 is obtained from the formula, assuming all iron is Fe^{2+} and that all of it contributes to the band. However, the presence of Fe^{2+}/Fe^{3+} IVCT bands in γ and β in the 600-750 nm region, as well as aspects of the Mössbauer spectrum (below) indicate that some iron is Fe^{3+}. If the 1030 nm band is due to Fe^{2+} in M(4), the presence of 1.95 formula units of calcium in this site implies an ε_{1030} of at least 80, assuming that Fe^{2+} occupies the remainder of the site.

The Mössbauer data for the Mt. Bity tremolite provide further constraints on the lower limit of ε_{1030}. The room temperature Mössbauer spectrum of this sample (Figure 7) shows two distinct peaks in the high velocity region (2.0-2.5 mm/sec) that are attributable to Fe^{2+} in at least two distinct environments. The presence of Fe^{3+} in this sample is suggested in the +0.5 mm/sec region, although a distinct peak is not observed.

The Mössbauer studies of the calcic amphiboles by Bancroft, Maddock and Burns (1967), Häggström, Wäppling and Annersten (1969), Burns and Greaves (1971) and Bancroft and Brown (1975) have assumed that Ca, Na and K completely fill the M(4) site, and hence, peak assignments have been made only for Fe^{2+} in the M(1), M(2) and M(3) sites, with the peaks having the smallest quadrupole splitting assigned to Fe^{2+} in the M(2) site. Fe^{2+} in the M(4) site has been identified in the Mössbauer spectra of cummingtonites and grunerites (Bancroft, Burns and Maddock, 1967; Hafner and Ghose, 1971). These spectra are characterized by two distinct quadrupole doublets: the outer doublet has a quadrupole splitting of about 2.7-2.8 mm/sec and is assigned to Fe^{2+} in the M(1), M(2) and M(3) sites; the inner doublet has a quadrupole splitting of 1.5-1.8 mm/sec and is assigned

to Fe^{2+} in the M(4) site.

Making the reasonable assumption that the band at 1030 nm is due to Fe^{2+} in one site only, the existence of two doublets in the spectrum of Mt. Bity tremolite establishes that ε_{1030} must be greater than 16, i.e. at least 27 if the band is due to the site giving rise to peaks AA', and at least 40 if it is due to the site giving rise to BB'. If the Mössbauer peaks in question represent more than one site, the value of ε_{1030} could only be higher.

Thus, if we assign AA' to M(1) and M(3), and BB' to M(2) in accordance with previous work on calcic amphiboles, we obtain minimum values of ε_{1030} equal to (a) 40 if the band is due to M(2); (b) 27 if it is due to M(1) or M(3), and (c) very large (well over 40) if it is due to M(4). If we assign peaks BB' to M(4) and AA' to M(1), M(2) and M(3), we obtain minimum values for ε_{1030} of (a) 40 if the band is due to M(4), and (b) 27 if it is due to M(1), M(2) or M(3).

The ε values for Fe^{2+} absorption bands in other sites (Table 3) can be compared with the lower limit determined for ε_{1030}. The smaller sites such as the M(1) sites in olivine and orthopyroxene have ε values of less than 10 even though these sites have different distortions and departures from centrosymmetry. The larger sites in the pyroxenes and amphiboles have larger ε values. Based on this comparison, and ε value for the 1030 nm band of greater than 27 is consistent with an assignment to Fe^{2+} in the M(4) site, but probably inconsistent with assignment to any other site.

Other Considerations

Due to similar types of distortions of the calcic amphibole M(4) site and the orthopyroxene M(2) site involving elongation of two adjacent M-O bonds and due to the similar crystal-field splittings of the $^5\underline{E}_g(O_h)$ state for these minerals, the spectra of the Mt. Bity tremolite were obtained in the 1200-4200 cm^{-1} region (Figure 8) to search for a low energy absorption band analogous to the 2350 cm^{-1} band in orthopyroxene. The absorption bands in the 3600-3750 cm^{-1} region arise from OH^- stretching motions, and the absorptions below 2000 cm^{-1} also have a vibrational origin. Another band due to M(4) Fe^{2+} does not occur in this region above 2000 cm^{-1}.

It was shown that both the 1030 nm band in β and the 2470 band in α in the spectra of pargasite are absent. The absorption band in α at 1030 nm is also absent in Figure 6, although it is present in both the tremolite and actinolite spectra. Furthermore, this band was reduced in intensity in the heat-treated tremolite spectra. To examine the possibility that this band may be due to Fe^{2+} in the M(4) site, the intensities for the α and β bands at 1030 nm were compared for fourteen calcic amphibole samples (Figure 9). The trend of these data suggests that the α and β bands are correlated. Consequently, the absorption band at 1030 nm in α is assigned to M(4) Fe^{2+}. The possibility that the α band results from the mixing of intensities from the intense β peak due to experimental problems does not appear likely because there is little evidence for mixing of polarization intensities in the 2000-2500 nm region.

CRYSTAL-FIELD ANALYSIS

The crystallographic point-group symmetry of the calcic amphibole M(4) site is $\underline{C}_2$ with the two-fold rotation axis parallel to $\underline{b}$ which bisects the O(6)-M(4)-O(6) and O(2)-M(4)-O(2) bond angles. For spectroscopic analysis, the Z crystal-field axis is taken along $\underline{b}$ to coincide with the axis of highest symmetry of the site. The relative ordering of the crystal-field states and the polarization properties of the allowed transitions for $\underline{C}_2$ in which Z is a dihedral axis are presented in Figure 10. The classification of states is derived from the "descent in symmetry" method from $\underline{O}_h$ to $\underline{D}_{4h}$ to $\underline{C}_{2v}(\underline{C}_2'')$ to $\underline{C}_2(\underline{C}_2'')$ using the correlation tables in Wilson, Decius and Cross (1955) and the polarization properties of the allowed transitions are obtained from the character table for $\underline{C}_2$ in Cotton (1963). Tetragonal compression between $\underline{O}_h$ and $\underline{D}_{4h}$ and acute dihedral angles about Z are used based on the structural data. The upper two states and the lower three states are derived from the octahedral $^5\underline{E}_g$ and $^5\underline{T}_{2g}$ states of Fe^{2+}, respectively. Although $\underline{C}_2$ explains the polarization of the 1030 nm band mostly in Z(β), it cannot explain the complete polarization of the 2470 nm band in α. This transition is expected to occur in both α(X) and γ(Y). Therefore, the polarization properties of these bands are indicative of a higher, effective electrostatic symmetry.

The effective electrostatic symmetry of the calcic amphibole M(4) site is taken to be $\underline{C}_{2v}(\underline{C}_2'')$ based upon the similar interpretation of the analogous bands in the spectra of orthopyroxene by Runciman et al., and Goldman and Rossman (1977), and anthophyllite and gedrite by Mao and Seifert. From the classification of states and the allowed transitions for $\underline{C}_{2v}$, the 1030 nm and 2470 nm absorption bands are assigned to the $\underline{A}_1 \rightarrow \underline{A}_1$ and $\underline{A}_1 \rightarrow \underline{B}_1$ transitions, respectively. The $\underline{A}_1 \rightarrow \underline{B}_2$ transition within the split $^5\underline{T}_{2g}(\underline{O}_h)$ state, which was identified at 2350 cm^{-1} in the spectra of orthopyroxene, does not occur at energies greater than 2000 cm^{-1}. For $\underline{C}_{2v}$ symmetry, this transition is expected to be polarized in γ(Y) as shown in Figure 10.

The operator-equivalent method described by Hutchings (1964) to derive energy expressions for the crystal-field states was used by Goldman and Rossman (1977) to analyze the spectra of Fe^{2+} in the M(2) site of orthopyroxene. In orthopyroxene, all three allowed transitions of $\underline{C}_{2\underline{v}}$ were observed experimentally and hence, the three crystal-field fitting parameters were calculated; $\Delta(= 10\ \underline{D}_{\underline{q}})$, M and N. From these parameters, the energy of the forbidden $\underline{A}_1 \rightarrow \underline{A}_2$ transition was calculated. However, the energy of the $\underline{A}_1 \rightarrow \underline{B}_2$ transition due to Fe^{2+} in the M(4) site of calcic amphiboles is not known, although the mid-infrared spectra of the Mt. Bity tremolite indicate that it does not occur above 2000 cm^{-1}. Using this value as an upper limit for the $\underline{A}_1 \rightarrow \underline{B}_2$ transition, the following results are obtained: Δ = 4629 cm^{-1} and $\underline{A}_1 \rightarrow \underline{A}_2$ = 976 cm^{-1}. If $\underline{A}_1 \rightarrow \underline{B}_2$ occurs at 1400 cm^{-1}, the crystal-field parameters change as follows: Δ = 4760 cm^{-1}, and $\underline{A}_1 \rightarrow \underline{A}_2$ = 524 cm^{-1}.

The value determined for Δ, the energy separation between the octahedral $^5\underline{T}_{2\underline{g}}$ and $^5\underline{E}_{\underline{g}}$ states, in the 4600-4800 cm^{-1} range has been obtained from the point-charge model in which the crystal-field potential was derived in terms of the average M-O bond distance of the M(4) site. Although a Δ of this magnitude for a six-coordinate site at first seems low, its value is acceptable upon considering orthopyroxene spectral data. The $\underline{A}_1 \rightarrow \underline{A}_1$, $\underline{A}_1 \rightarrow \underline{B}_1$ and $\underline{A}_1 \rightarrow \underline{B}_2$ transitions of bronzite occur at 10,930 cm^{-1}, 5400 cm^{-1} and 2350 cm^{-1}, respectively. Using the average M-O bond distance of the M(2) site of 2.22 Å, Δ was calculated to be 6522 cm^{-1}. In comparison, the smaller Δ value for M(4) Fe^{2+} in calcic amphiboles reflects the larger size of the M(4) site as expected from the $1/r^5$ dependence of Δ. The energies of the transitions to the $\underline{A}_1$ and $\underline{B}_1$ states are about 1000 cm^{-1} and 1400 cm^{-1} smaller than the energies of the analogous transitions in orthopyroxene, respectively. This indicates that the energy of the $\underline{E}_{\underline{g}}(\underline{O}_{\underline{h}})$ state, from which $\underline{A}_1$ and $\underline{B}_1$ are derived, is also at

least 1000 cm^{-1} lower in the calcic amphibole M(4) site and hence, Δ is expected to be reduced from the orthopyroxene value by about this magnitude. Therefore, a Δ for M(4) Fe^{2+} in the 4600-4900 cm^{-1} range is reasonable.

Goldman and Rossman (1977) indicated that the O-M-O bond angles about the crystal-field Z axis plays a significant role in determining the energy of the $\underline{A}_1 \rightarrow \underline{B}_2$ transition within the split $^5\underline{T}_{2\underline{g}}(\underline{O}_{\underline{h}})$ state. The O(6)-M(4)-O(6) angle of 62° is 10° smaller than the O(6)-M(2)-O(3) angle in orthopyroxene. The smaller angle about Z is expected to raise the energy of the $\underline{A}_1 \rightarrow \underline{B}_2$ transition. However, the two elongated M-O bonds in orthopyroxene are about 2.5 Å, whereas they are nearly 2.8 Å in grunerite. This longer bond distance explains the lower energy of $\underline{A}_1 \rightarrow \underline{B}_2$ transition in the amphibole M(4) site.

Finally, it was suggested that Fe^{2+} in the M(4) site also produces a band in α at 1030 nm. Since $\underline{A}_1 \rightarrow \underline{A}_1$ is expected to be polarized entirely in β, the presence of the α band at 1030 nm is difficult to explain. Similarly, in the spectra of M(2) Fe^{2+} in orthopyroxene, the polarization intensities of the subsidiary components of the main bands were not accounted for using the most intuitively reasonable selection for the $\underline{C}_{2\underline{v}}$ axes, although the polarization intensities of the main bands were correctly explained. It must be remembered that these results are based upon a theoretical treatment that is highly idealized, both with regard to the presumed effective symmetry and the assumption of equivalent point-charge contributions from each of the ligands. Nevertheless, on a comparative level, the crystal-field analyses of the calcic amphibole and orthopyroxene spectral data produce consistent results.

CONCLUSION

The electronic absorptions arising from ferrous iron in the M(4) site of calcic amphiboles have been identified. The absorption bands due to M(4) Fe^{2+} occur at 1030 nm in β, with some intensity in α, and at 2470 nm in α. The spectra of a wide variety of calcic amphiboles indicate that the Fe^{2+} content in the M(4) site is variable. In particular, M(4) Fe^{2+} has been found in absorption spectra of all actinolite samples studied in this laboratory. The indication from the absorption spectra that the M(4) Fe^{2+} content exhibits significant variation may be important petrologically due to the temperature and pressure dependencies of the various elemental partitions that involve iron, either between coexisting minerals, or among the crystallographically distinct sites within each mineral.

ACKNOWLEDGMENTS

We wish to thank J. D. Hare (Caltech) and R. G. Burns (MIT) for discussing many aspects of the spectroscopic interpretation. We also appreciate the use of the Mössbauer spectrometer made available to us by W. A. Dollase (UCLA) and the many discussions with him that ensued concerning the analysis of the Mössbauer spectrum.

REFERENCES

Bancroft, G.M. and J. R. Brown (1975) A Mössbauer study of coexisting hornblendes and biotites: Quantitative Fe^{3+}/Fe^{2+} ratios. Amer. Mineral. 60, 265-272.

Bancroft, G.M., R.G. Burns and R.A. Howie (1967) Determination of the cation distribution in the orthopyroxene series by the Mössbauer effect. Nature 213, 1221-1223.

Bancroft, G.M., R.G. Burns and A.G. Maddock (1967) Determination of the distribution in the cummingtonite-grunerite series by Mössbauer spectra. Am. Mineral. 52, 1009-1026.

Bancroft, G.M., A.G. Maddock and R.G. Burns (1967) Applications of the Mössbauer effect to silicate mineralogy. Part I. Iron silicates of known crystal structure. Geochim. Cosmochim. Acta 31, 2219-2246.

Bell, P.M. and H.K. Mao (1972) Crystal-field effects of iron and titanium in selected grains of Apollo 12, 14, and 15 rocks, glasses, and fine fractions. Proc. Third Lunar Sci. Conf., Geochim. Cosmochim. Acta, Suppl. 3, Vol. 1, 545-553.

Birle, J.D., G.V. Gibbs, P.B. Moore and G.V. Smith (1968) Crystal structures of natural olivines. Am. Mineral. 53, 807-824.

Burns, R.G. (1965) Electronic spectra of silicate minerals: applications of crystal field theory to aspects of geochemistry. Ph.D. thesis, Univ. Calif., Berkeley.

Burns, R.G. (1970) Mineralogical Applications of Crystal Field Theory, Cambridge University Press.

Burns, R.G., R.M. Abu-Eid and F.E. Huggens (1972) Crystal field spectra of lunar pyroxenes. Proc. Third Lunar Sci. Conf., Geochim. Cosmochim. Acta, Suppl. 3, Vol. 1, 533-543.

Burns, R.G. and C. Greaves (1971) Correlations of infrared and Mössbauer site population measurements of actinolites. Am. Mineral. 56, 2010-2033.

Bush, W.R., S.S. Hafner and D. Virgo (1970) Some ordering of iron and magnesium at the octahedrally coordinated sites in a magnesium-rich olivine. Nature 227, 1339-1341.

Cotton, F. A. (1963) Chemical Applications of Group Theory Wiley-Interscience Publ., New York.

Dollase, W. A. (1973) Mössbauer spectra and iron distribution in the epidote-group minerals. Zeits. Kristallogr. 138, 41-63.

Faye, G. H. (1972) Relationship between crystal-field splitting parameter, "Δ_{VI}", and M_{host}-O bond distance as an aid in the interpretation of absorption spectra of Fe^{2+} materials. Canad. Mineral. 11, 473-487.

Finger, L. W. (1969) The crystal structure and cation distribution of a grunerite. Min. Soc. Sp. Paper No. 2, 95-100.

Goldman, D. S. and G. R. Rossman (1976) Identification of a mid-infrared electronic absorption band of Fe^{2+} in the distorted M(2) site of orthopyroxene, $(Mg,Fe)SiO_3$. Chem. Phys. Lett. 41, 474-475.

Goldman, D. S. and G. R. Rossman (1977) The spectra of iron in orthopyroxene revisited: the splitting of the ground state. Am. Mineral. 62, 151-157.

Hafner, S.S. and S. Ghose (1971) Iron and magnesium distribution in cummingtonites $(Fe,Mg)_7Si_8O_{22}(OH)_2$. Zeits. Kristallagr. 133, 361-376.

Häggström, L., R. Wäppling and H. Annersten (1969) Mössbauer study of oxidized iron silicate minerals, Phys. Stat. Solid. 33, 741-748.

Hutchings, M. T. (1964) Point-charge calculations of energy levels of magnetic ions in crystalline electric fields. Solid State Phys. 16, 227-273.

Johnson, C. K. (1965) ORTEP, a FORTRAN thermal ellipsoid plot program for crystal structure illustrations. U. S. Nat. Tech. Inform. Serv. ORNL-3794.

Kuno, H. (1954) Study of orthopyroxenes from volcanic rocks. Am. Mineral. 39, 30-46.

Lacroix, A. (1910) Mineralogie de la France et de ses Colonies, Tome IV, page 786.

Leake, B. E. (1968) A catalog of analyzed calciferous and subcalciferous amphiboles together with their nomenclature and associated minerals. Geol. Soc. Am. Sp. Paper No. 98.

Mao, H. K. and F. Seifert (1973) A study of crystal-field effects of iron in the amphiboles anthophyllite and gedrite. Carnegie Inst. Washington Year Book 73, 500-503.

Mitchell, J. T., F. D. Bloss and G. V. Gibbs (1971) Examination of the actinolite structure and four other $C_{2/m}$ amphiboles in terms of double bonding. Zeits. Kristallogr. 133, 273-300.

Papike, J. J. and M. Ross (1970) Gedrite: crystal structures and intracrystalline cation distributions. Am. Mineral. 55, 304-305.

Papike, J. J., M. Ross and J. Clark (1969) Crystal-chemical characterization of clinoamphiboles based on five new structure refinements. Min. Soc. Am. Sp. Paper No. 2, 117-136.

Runciman, W. A., D. Sengupta and M. Marshall (1973) The polarized spectra of iron in silicates. I. Enstatite. Am. Mineral. 58, 444-450.

White, W. B. and K. L. Keester (1966) Optical absorption spectra of iron in the rock-forming silicates. Am. Mineral. 51, 774-791.

White, W. B. and K. L. Keester (1967) Selection rules and assignments for the spectra of ferrous iron in pyroxenes. Am. Mineral. 52, 1508-1514.

White, W.B. and R.K. Moore (1972) Interpretation of the spin-allowed bands of Fe^{2+} in silicate garnets. Amer. Mineral. 57, 1692-1710

Wilson, E. B., J. C. Decius and P. C. Cross (1955) Molecular Vibrations. McGraw-Hill Publ., New York.

TABLE 1. MICROPROBE ANALYSES

SAMPLE	1	2	3
	Weight percent of oxides		
SiO_2	57.65	57.01	42.91
TiO_2	.07	-	.88
Al_2O_3	1.31	1.06	12.69
Cr_2O_3	-	.24	-
MgO	23.62	21.36	14.44
MnO	-	.22	.09
FeO	2.06	5.72	10.25
CaO	13.42	12.30	13.00
Na_2O	.61	.41	2.45
K_2O	.20	.05	1.57
F	.21	.06	1.66
Cl	.04	-	-
	99.19	98.43	99.94
-O≡F	.09	.03	.70
-O≡Cl	.01	-	-
	99.09	98.40	99.24
	Formula Proportions*		
Si	7.81	7.87	6.28
Al(IV)	.19	.13	1.72
Al(VI)	.02	.04	.47
Mg	4.77	4.40	3.15
Ti	.01	-	.10
Cr	-	.03	-
Mn	-	.03	.01
Fe	.23	.66	1.26
	5.03	5.16	4.99
Ca	1.95	1.82	2.03
Na	.16	.11	.69
K	.03	.01	.29

1. Tremolite, Mount Bity, Malagasay Republic
2. Actinolite, Zillerthal, Tyrol, Austria
3. Fluoro-pargasite, Pargas, Finland

*The formula proportions are obtained by normalizing the total positive charge to 46 assuming all Fe is Fe^{2+}.

TABLE 2. MÖSSBAUER PARAMETERS

PEAKS	ISOMER* SHIFT	QUADRUPOLE SPLITTING	HALF-WIDTH	% AREA
AA' Fe^{2+}	1.14	2.82	.32	51.4(±0.92)
BB' Fe^{2+}	1.17	1.84	.34	41.4(±1.22)
CC' Fe^{3+}	0.48	0.74	.53	7.2(±1.20)

*Relative to Fe° in mm/sec

TABLE 3. ε VALUES FOR COMMON MINERALS

MINERAL	SITE	BAND (cm^{-1})	ε(ℓ/mole cm)	REFERENCE*
OLIVINE	M(1)	10,930	2.4	(1),{1},[2],[3]
(FAYALITE)	M(2)	9,290	8.6	
ORTHOPYROXENE (BRONZITE)	M(2)	10,930	41	(4),{4},[5]
ORTHOPYROXENE (ORTHOFERROSILITE)	M(1)	8,560	∿10	(1),{6},[5]
Mg-Fe AMPHIBOLE (GEDRITE)	M(4)	∿10,600	∿20	(7),{8},[8]
Mg-Fe AMPHIBOLE (GRUNERITE)	M(4)	9,980	∿80	(1),{9},[9]
GARNET (PYROPE-ALMANDINE)	8-fold	7,830	1.1	(10),{10}
CORDIERITE	6-fold	8,200	4	(11),{11},[11]

1. Burns (1970)
2. Bush et al. (1970)
3. Birle et al. (1968)
4. Goldman and Rossman (1977)
5. Bancroft, Burns and Howie (1967)
6. Kuno (1954)
7. Mao and Seifert (1973)
8. Papike and Ross (1970)
9. Bancroft, Burns and Maddock (1967)
10. White and Moore (1972)
11. Goldman and Rossman (in preparation)

* ( ) = Spectral Data [ ] = Site Population Data { } = Chemcical Data

Figure Captions

Figure 1. (c*-b) and (a-c) ORTEP projections of the M(1), M(2) and M(3) coordination sites in actinolite based on the atomic coordinates given in Mitchell *et al.* (1971). All figures have been drawn to the same scale. Bond distances are given on page 142.

Figure 2. (c*-b) and (a-c) ORTEP projections of the M(4) coordination sites in actinolite and grunerite based on the atomic coordinates given in Mitchell *et al.* (1971) and Finger (1969), respectively. These projections illustrate the different positioning of iron in the grunerite site from calcium in the actinolite site. All figures are drawn to the same scale. Bond distances are given on page 142.

Figure 3. Room temperature spectra of tremolite from Mt. Bity, Malagasay Republic. α spectrum (. . . . .), β spectrum (-------), and γ spectrum (————). $\gamma \wedge \underline{c} = 17^{o}$. Crystal thickness = 1.0 mm.

Figure 4. Spectra of tremolite from Mt. Bity, Malagasay Republic before heating (————) and after heating in air at 535^{o}C for 8 hours (-------). The bands at 1030 nm in β and 2470 nm in α are reduced to nearly half of their original intensity after heating which suggests a common Fe^{2+} origin. Crystal thickness = 1.0 mm. The β-spectra have been displaced vertically for clarity.

Figure 5. Room temperature spectra of actinolite from Zillerthal, Tyrol, Austria. α spectrum (. . . . .), β spectrum (------), and γ spectrum (————). $\gamma \wedge \underline{c} = 16^{o}$. Crystal thickness = 1.0 mm.

Figure 6. Room temperature spectra of pargasite from Pargas, Finland. α spectrum (. . . . .), β spectrum (--------), and γ spectrum (———). $\gamma \wedge \underline{c} = 24^{o}$. Crystal thickness = 0.10 mm.

Figure 7. Mössbauer spectrum of tremolite, Mt. Bity, Malagasay Republic, taken at room temperature. The spectrum is presented relative to ^{57}Co in Fe^{o}.

Figure 8. Room temperature, mid-infrared spectra of tremolite from Mt. Bity, Malagasy Republic, showing that a second M(4) Fe^{2+} absorption band does not occur in this region above 2000 cm^{-1}. α spectrum (. . . . .), β spectrum (---------), and γ spectrum (————). $\gamma \wedge \underline{c} = 17^{o}$. Crystal thickness = 1.0 mm.

Figure 9. Intensity correlation of the calcic amphibole absorption bands in β and α at 1030 nm suggesting that the α-band is also due to Fe^{2+} in the M(4) site. All points represent room temperature spectra normalized to 1.0 cm thickness.

Figure 10. Energy level schemes for $\underline{C}_2$ and $\underline{C}_{2\underline{v}}$ symmetries in which the crystal-field Z axis is a dihedral axis. The $\underline{C}_{2\underline{v}}$ energy level scheme explains the polarization properties of the M(4) Fe^{2+} absorption bands. $\underline{C}_2$, the crystallographic point-group symmetry of the M(4) site, cannot explain the polarization of the 2470 nm band in α.

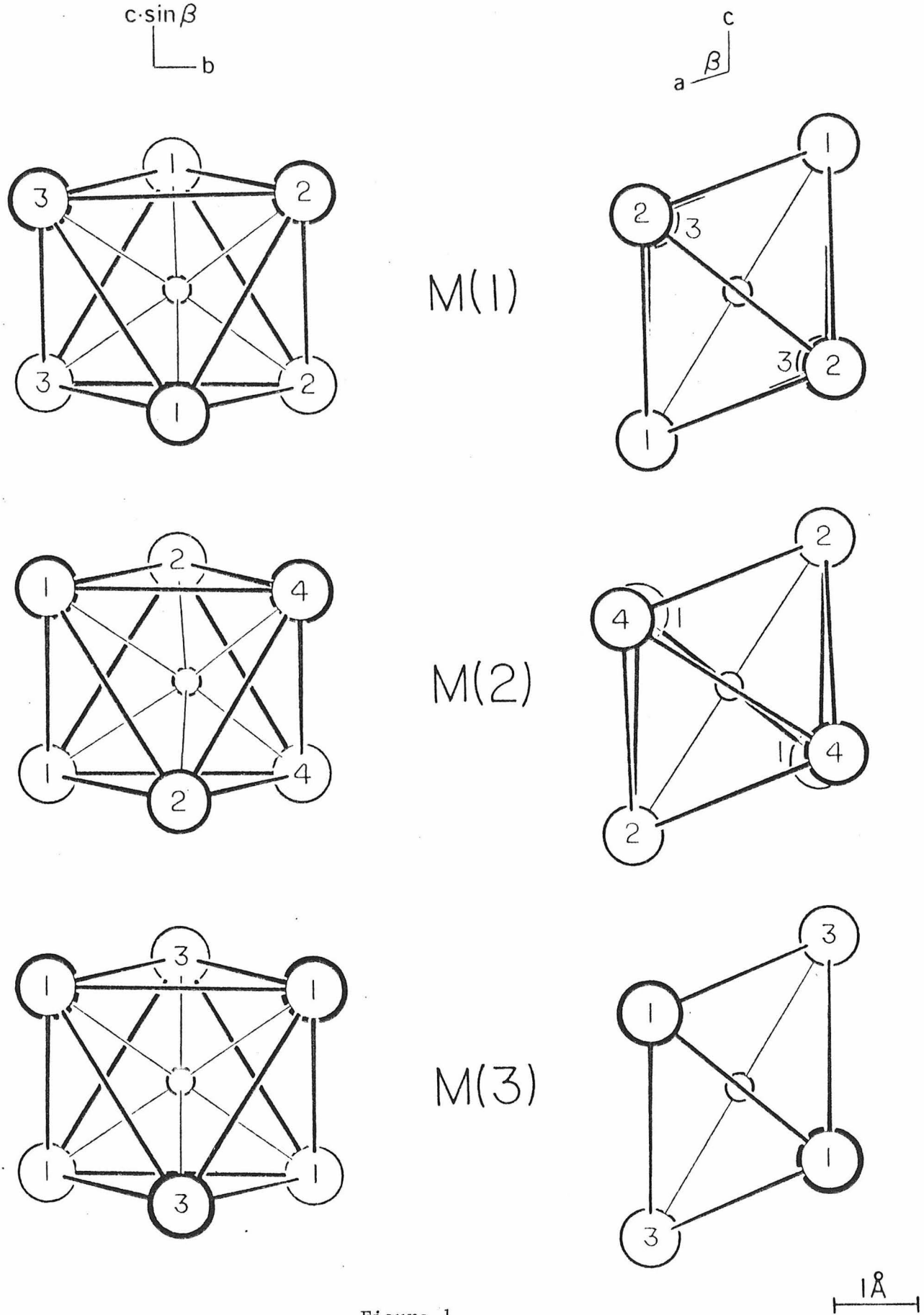

Figure 1

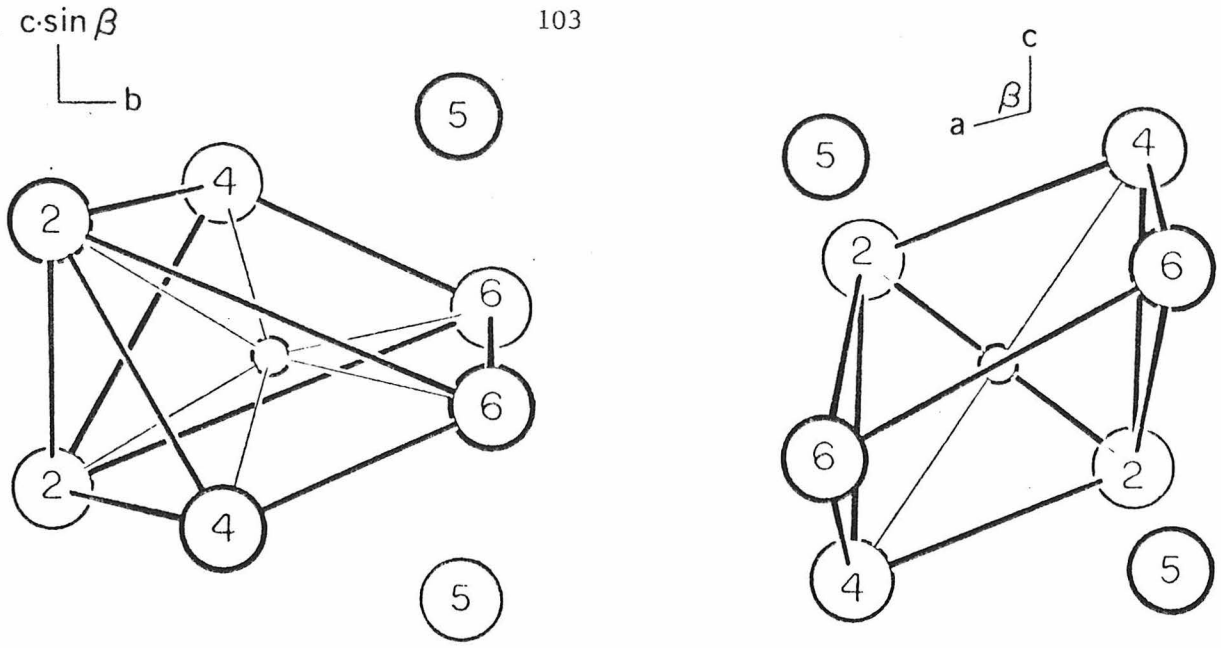

ACTINOLITE M(4) SITE

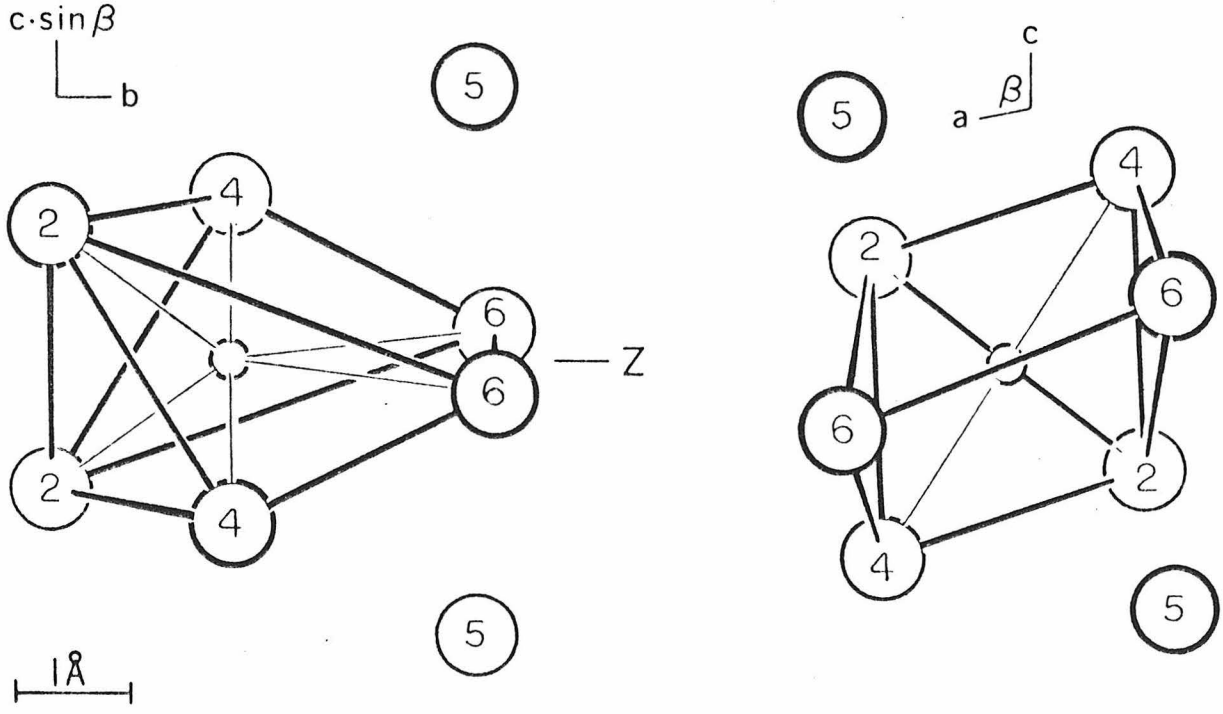

GRUNERITE M(4) SITE

Figure 2

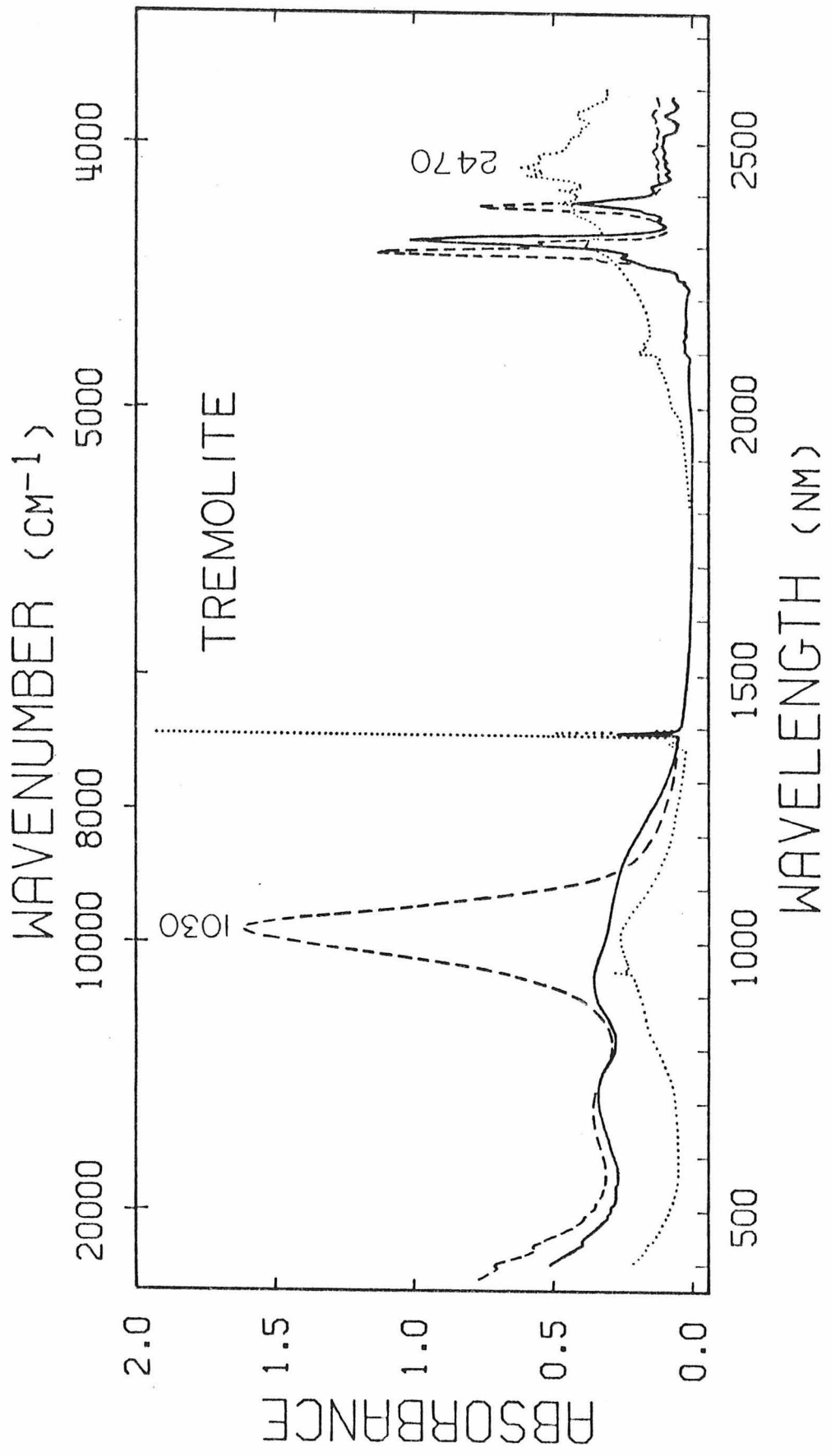
WAVENUMBER (CM-1)
20000
10000
8000
5000
4000
WAVELENGTH (NM)
500
1000
1500
2000
2500
ABSORBANCE
0.0
0.5
1.0
1.5
2.0
TREMOLITE
1030
2470

Figure 3

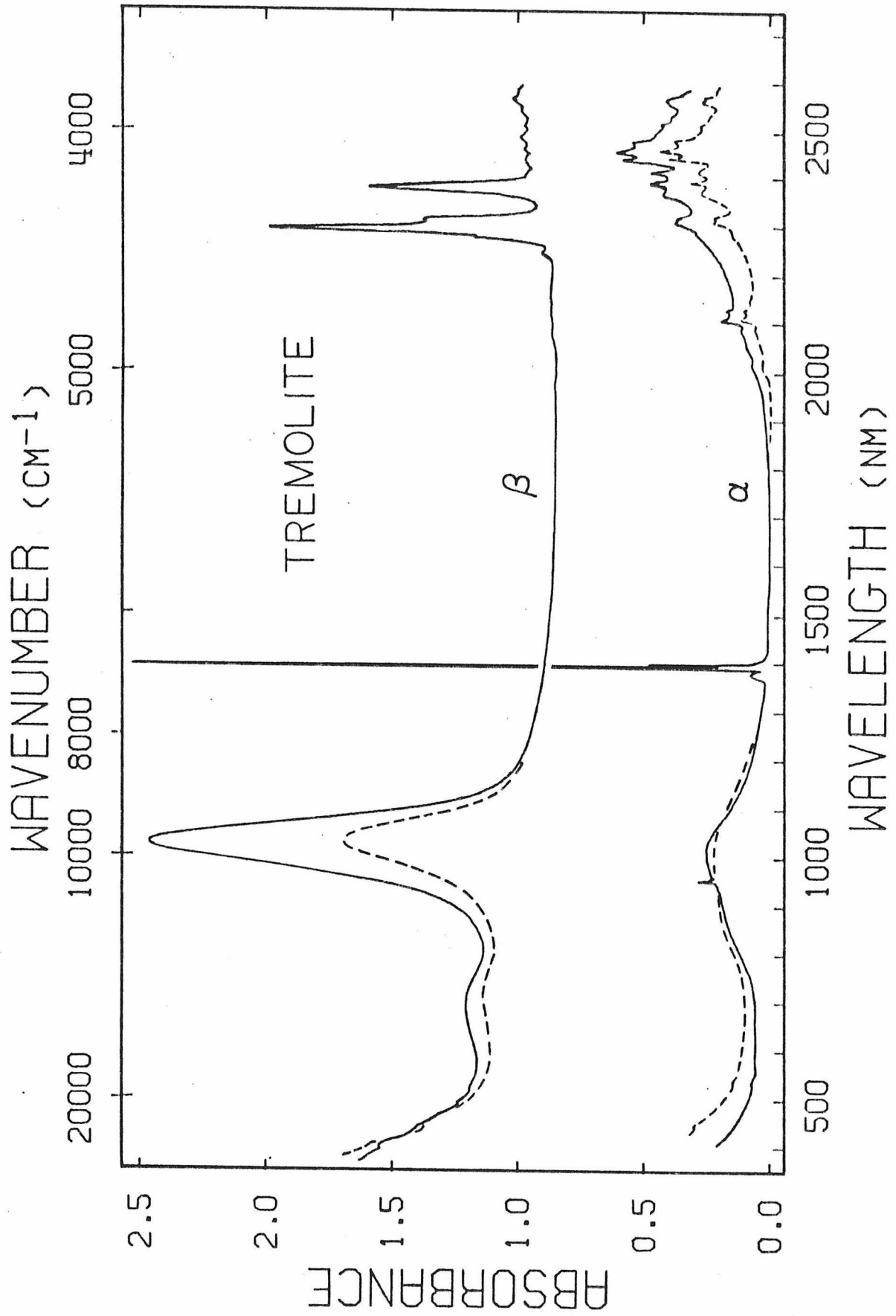
WAVENUMBER (CM-1)
20000
10000
8000
5000
4000
WAVELENGTH (NM)
500
1000
1500
2000
2500
ABSORBANCE
0.0
0.5
1.0
1.5
2.0
2.5
TREMOLITE
β
α

Figure 4

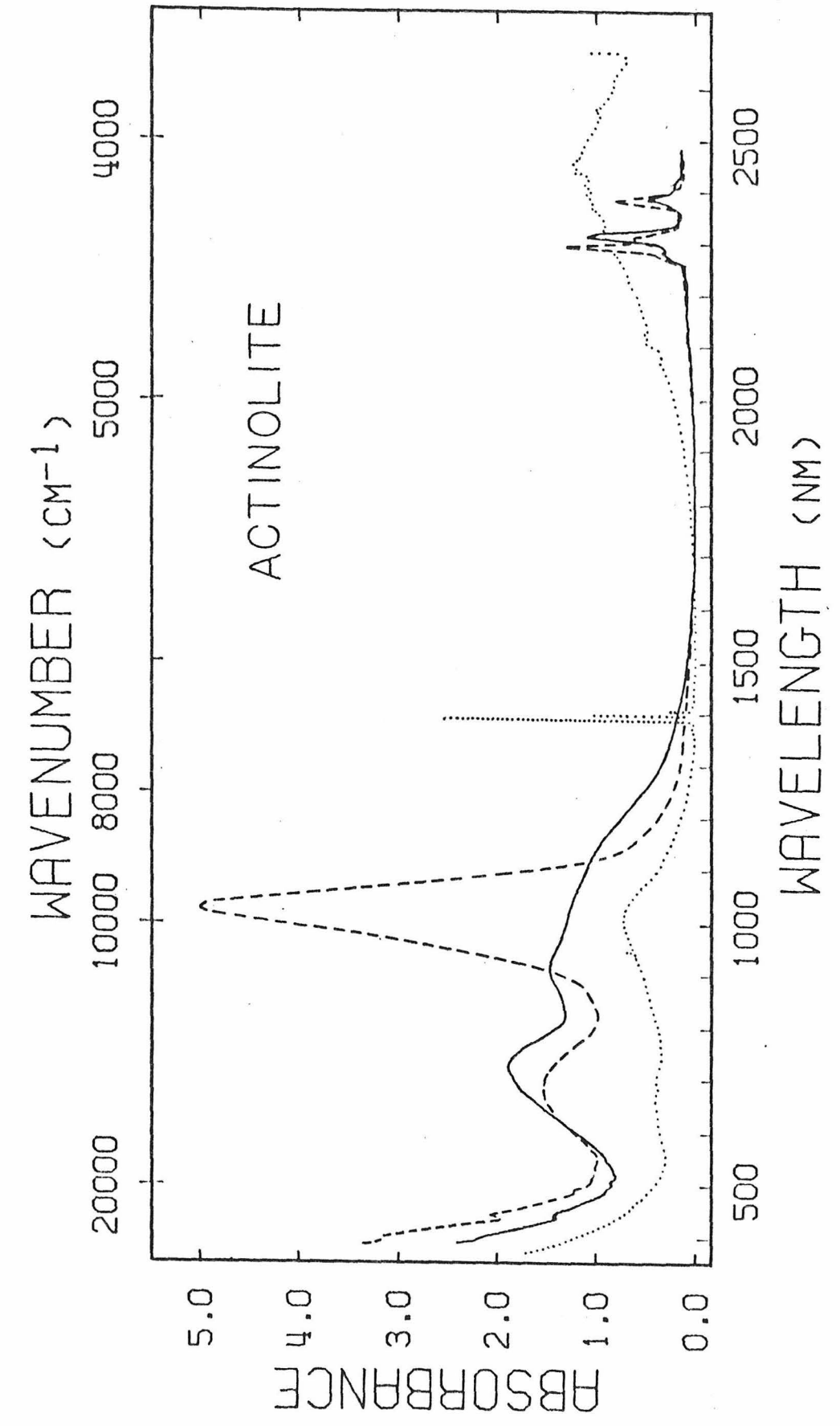
ACTINOLITE
WAVENUMBER (CM-1)
20000
10000
8000
5000
4000
WAVELENGTH (NM)
500
1000
1500
2000
2500
ABSORBANCE
0.0
1.0
2.0
3.0
4.0
5.0

Figure 5

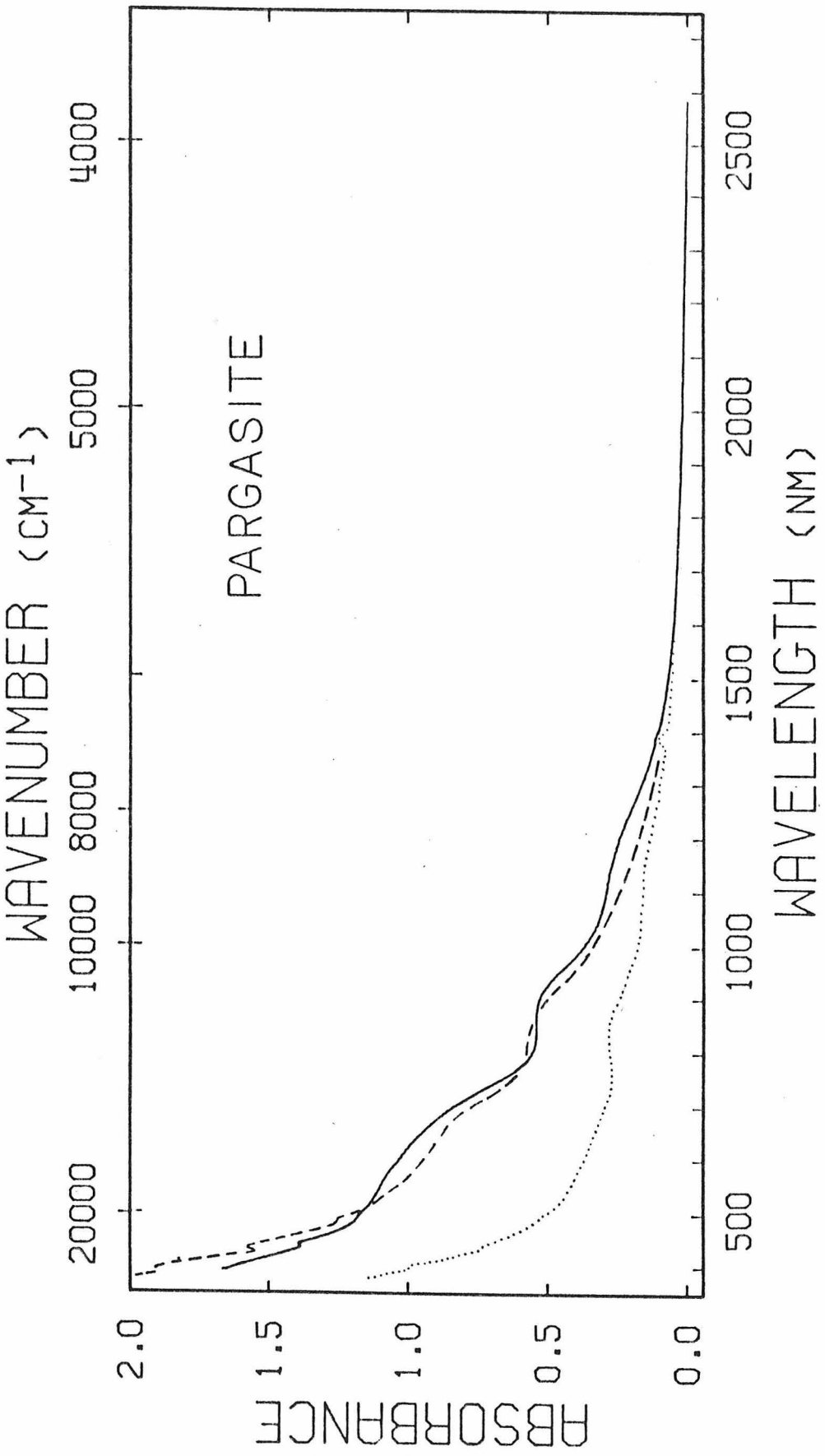
PARGASITE
WAVENUMBER (CM-1)
20000
10000
8000
5000
4000
WAVELENGTH (NM)
500
1000
1500
2000
2500
ABSORBANCE
2.0
1.5
1.0
0.5
0.0

Figure 6

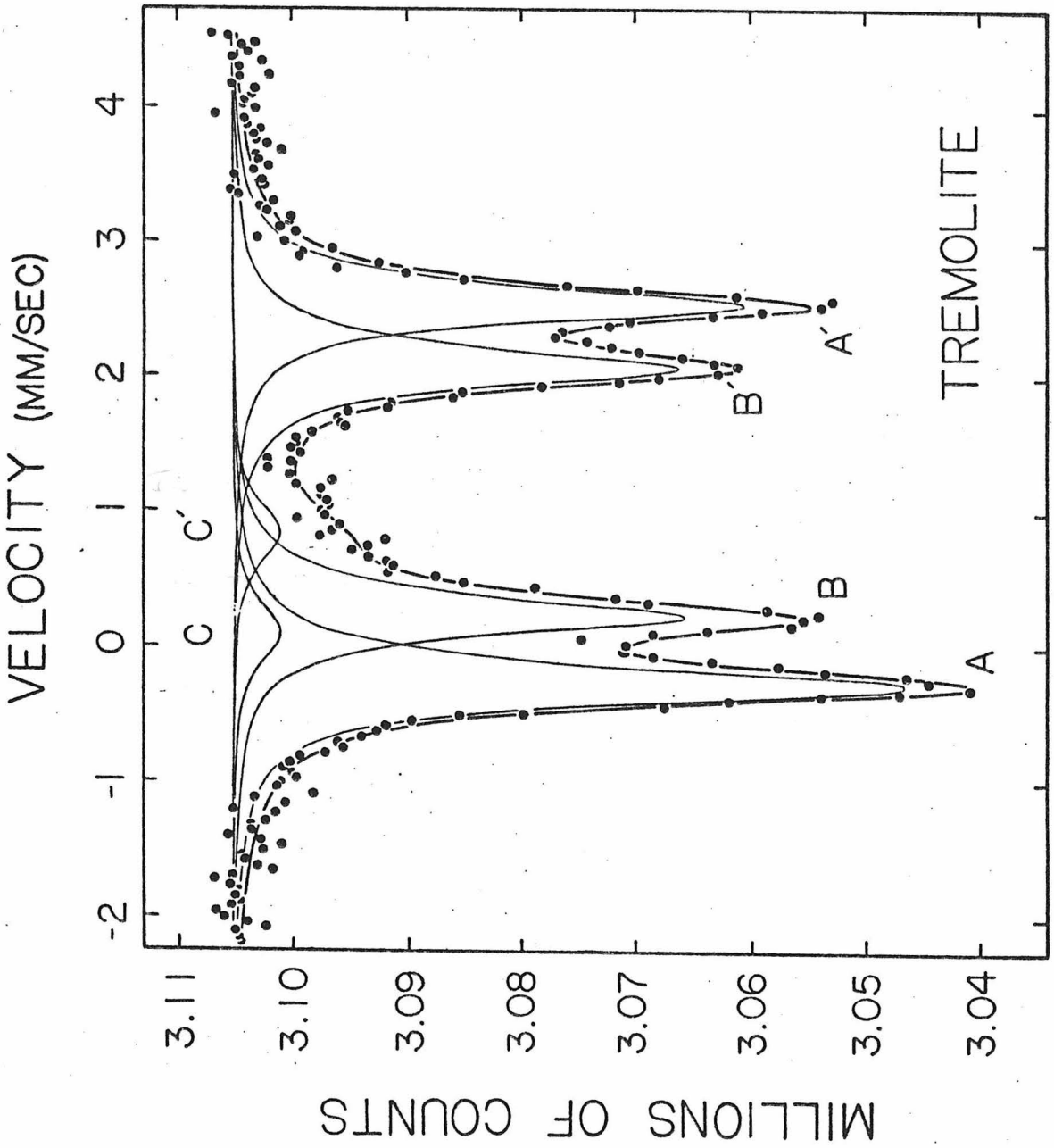
TREMOLITE
A
A'
B
B'
C
C'
VELOCITY (MM/SEC)
-2
-1
0
1
2
3
4
MILLIONS OF COUNTS
3.04
3.05
3.06
3.07
3.08
3.09
3.10
3.11

Figure 7

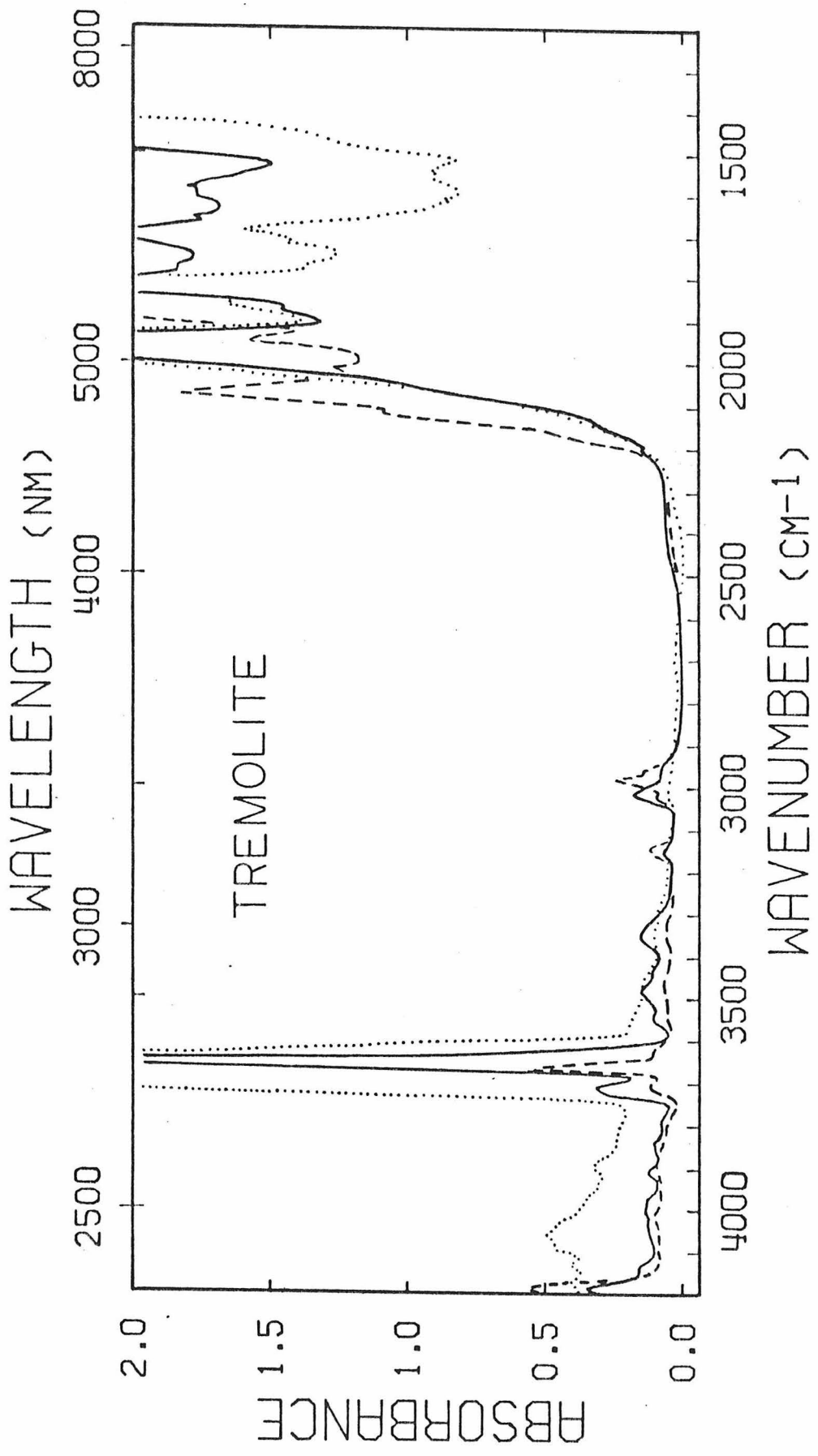
WAVELENGTH (NM)
8000
5000
4000
3000
2500
TREMOLITE
WAVENUMBER (CM-1)
1500
2000
2500
3000
3500
4000
ABSORBANCE
2.0
1.5
1.0
0.5
0.0

Figure 8

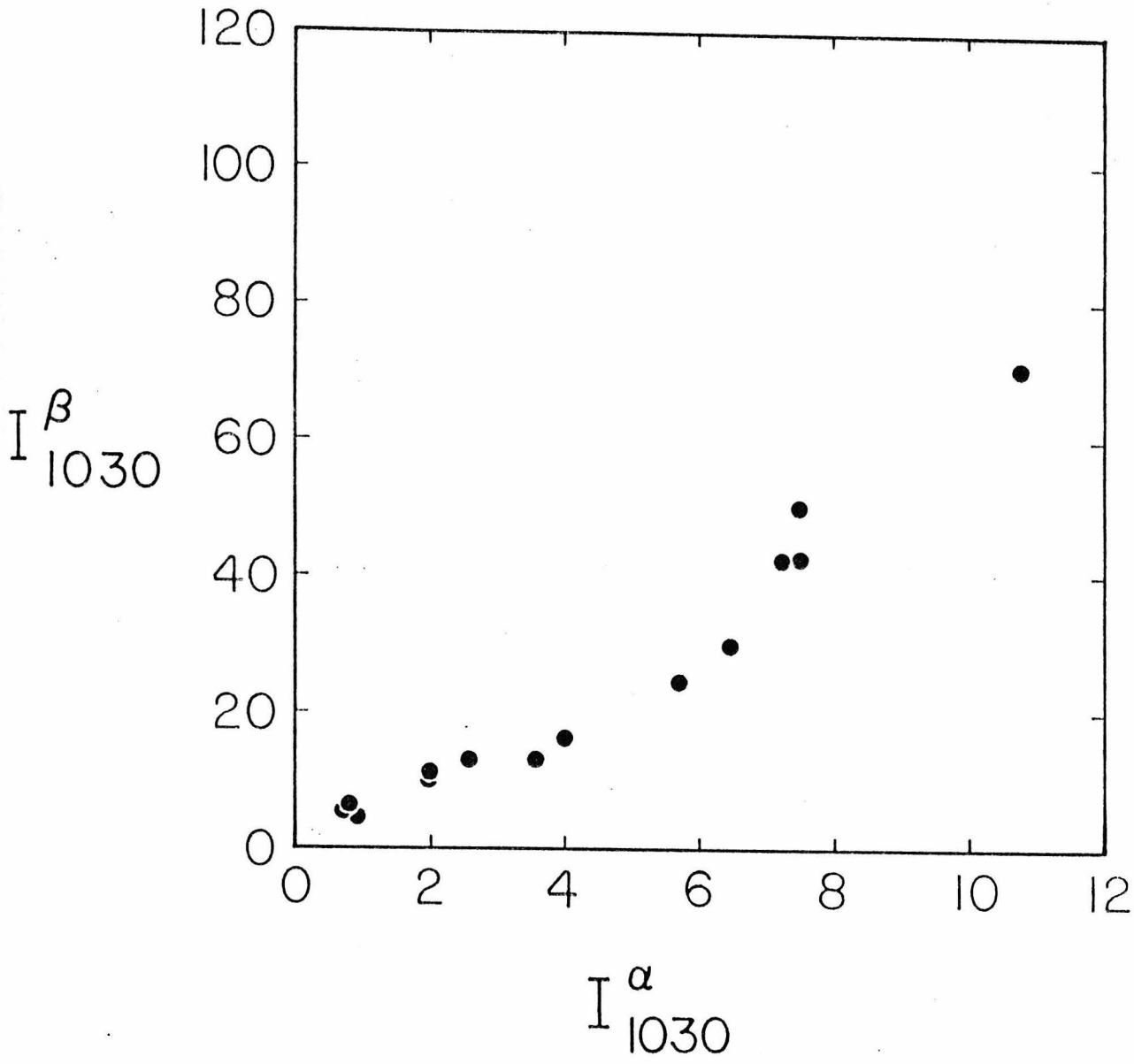

Figure 9

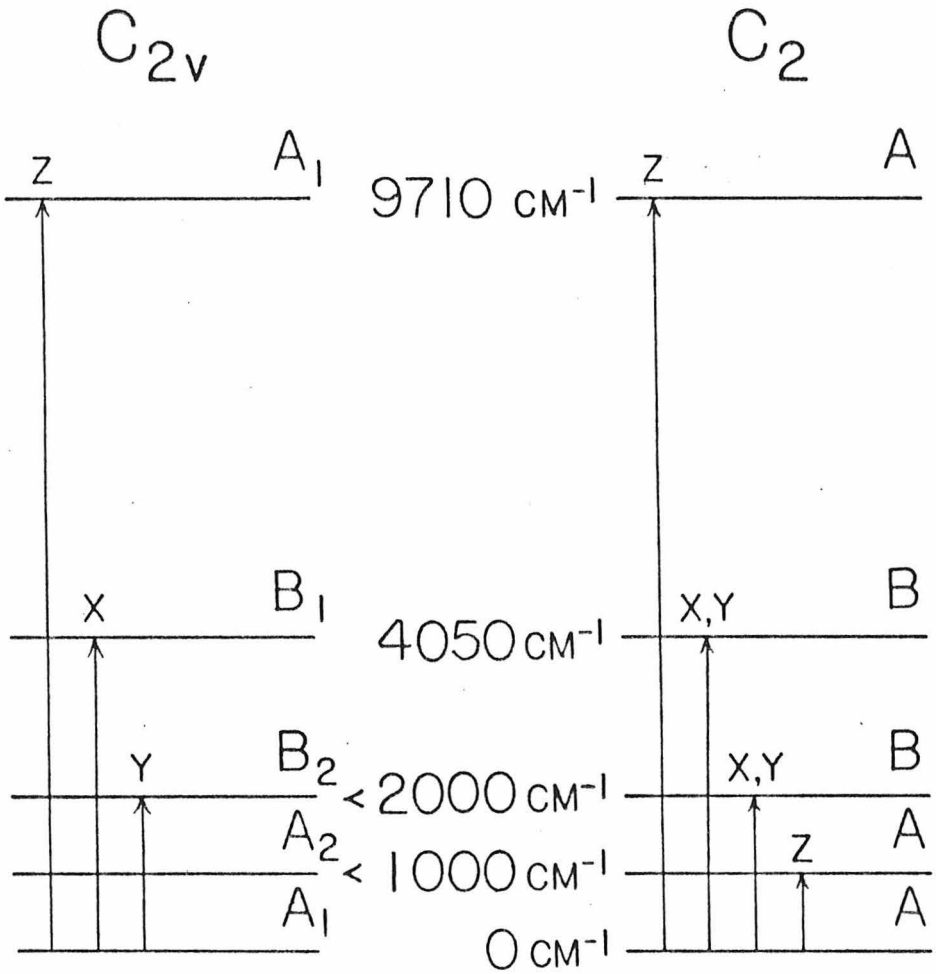
C2v
C2
Z
A1
9710 cm-1
Z
A
X
B1
4050 cm-1
X,Y
B
Y
B2
< 2000 cm-1
X,Y
B
A2
< 1000 cm-1
Z
A
A1
0 cm-1
A

Figure 10

CHAPTER 6

A RE-EVALUATION OF THE MÖSSBAUER SPECTROSCOPY OF CALCIC AMPHIBOLES

Submitted to The American Mineralogist

ABSTRACT

The Mössbauer spectra of calcic amphiboles have been reassessed to examine the validity of previous peak assignments. A brief review of previously established peak assignments for cummingtonite-grunerite, calcic and sodic amphiboles is presented. The Mössbauer spectra of tremolite-actinolites are reinterpreted in terms of Fe^{2+} in the M(1) and M(3) sites (quadrupole splitting, $\Delta \sim 2.8$ mm/sec), the M(2) site ($\Delta \sim 2.2$ mm/sec) and the M(4) site ($\Delta \sim 1.8$ mm/sec). From a number of spectra, these assignments indicate that Fe^{2+} prefers to enter the M(4) site prior to the M(1) and M(3) sites, and it discriminates against the M(2) site. This is the same ordering scheme found in cummingtonite-grunerites. Evidence is presented to show that increasing the Al and Fe^{3+} contents in calcic amphiboles reduces Δ for Fe^{2+} in the M(1), M(2) and M(3) sites from the values in tremolite-actinolites, and separates the M(1) and M(3) doublets. It is suggested that next-nearest neighbor effects on the already closely overlapping peaks limits the accuracy of determining site populations from Mössbauer spectra.

INTRODUCTION

In a recent study of the electronic absorption spectra of calcic amphiboles, Goldman and Rossman (1977) identified features due to Fe^{2+} in the Ca-rich M(4) site, and found that these features are characteristic of tremolite-actinolites (TA), $Ca_2(Mg,Fe)_5Si_8O_{22}(OH)_2$. They also presented a Mössbauer spectrum of a tremolite which is unlike other reported spectra of calcic amphiboles (DeCoster et al., 1963; Bancroft et al., 1967a; Häggström et al., 1969; Burns and Greaves, 1971; Bancroft and Brown, 1975; Goodman and Wilson, 1976) because it has two distinct, well-separated Fe^{2+} quadrupole doublets. As shown in Figure 1, it bears a striking similarity to the Mössbauer spectra of cummingtonite-grunerites (CG), $(Mg,Fe)_7Si_8O_{22}(OH)_2$. However, the peak assignments for these amphibole groups differ considerably. In particular, the inner doublet in CG spectra has been assigned to Fe^{2+} in the M(4) site (Bancroft et al., 1967 a,b) whereas it has been assigned to Fe^{2+} in the M(2) site in TA spectra (Burns and Greaves), and possible contributions from Fe^{2+} in the M(4) site, in general, have not been considered. The resulting difference in quadrupole splitting, Δ, for Fe^{2+} in the M(2) sites of these amphibole groups is surprisingly large (0.9-1.0 mm/sec), considering their structural similarity. In addition to the similarity of the Mössbauer spectra of tremolite and grunerite, the similarity of their electronic absorption spectra (Figure 1) suggests that Fe^{2+} occurs in similar types of sites. The arrows point to absorption bands near 1000 nm in β polarization and 2500 nm in α polarization that are due to Fe^{2+} in the M(4) site in both samples.

A notable difference exists in the Mössbauer spectra of CG and TA amphiboles when they are examined across their compositional range. CG spectra retain a two doublet character across their compositional range. The transmission valleys between the inner and outer doublets in tremolite are replaced by resonant

absorption at higher iron contents (Burns and Greaves), and are generally absent in more chemically complex amphiboles, such as hornblendes (Bancroft and Brown), where an asymmetric Fe^{2+} resonant envelope is typically observed.

This paper (1) briefly traces the interpretation of the Mössbauer spectra of CG, calcic and sodic amphiboles, and amphiboles intermediate in composition between calcic and sodic amphiboles,(2) evaluates the peak assignments in TA spectra with particular emphasis on identifying peaks due to Fe^{2+} in the M(4) site, and suggests a new peak assignment scheme that better explains the change in the Fe^{2+} resonant envelope with increasing iron content, and (3) examines the effect of additional chemical complexities on the spectral parameters in calcic amphiboles.

EXPERIMENTAL METHODS

The experimental methods used to obtain the Mössbauer, optical and chemical data have been presented previously (Goldman and Rossman, 1977). All quadrupole splitting and isomer shift values for the Mössbauer data discussed in this paper are room temperature values unless otherwise specified. All Mössbauer spectra are presented relative to metallic iron. Only the fitted envelopes to the Mössbauer spectra in Figures 1 and 3 are presented, but these spectra were analyzed to obtain Fe^{2+}/Fe^{3+} ratios in order to calculate the formula proportions from the electron microprobe data in Table 4. The half-widths of all Fe^{2+} peaks in Figures 4 and 6 were constrained to be equal and the half-widths of the two ferric peaks were also constrained to be equal. Because of the low Fe^{3+} content of the actinolite sample in Figure 4, it was necessary to specify the half-widths of the ferric peaks and the location of the low velocity component. Sample locations and electron microprobe analyses are tabulated in Table 4. All site population data reported herein are obtained directly from the area ratios. X-ray precession photographs of the tremolite sample did not show the presence of an exsolved cummingtonite phase.

CUMMINGTONITE-GRUNERITE SERIES

The Mössbauer spectra of CG are generally characterized by two well-separated doublets (Figure 1) with the outer and inner doublets having Δ values of about 2.8 and 1.5-1.8 mm/sec, respectively. Bancroft et al. (1967a,b) gave four reasons for assigning the inner doublet to Fe^{2+} in the M(4) site and the outer doublet to Fe^{2+} in the M(1), M(2) and M(3) sites. First, X-ray studies (Ghose, 1961; Fischer, 1966) indicated that Fe^{2+} prefers to enter the large, highly distorted M(4) site. Consistent with this result, the inner doublet is more intense than the outer doublet in cummingtonite. Second, the area ratio of the inner to outer doublet in grunerite is approximately the value expected for Fe^{2+} in the M(4) site from the site multiplicities. Third, Δ is expected to be smaller for Fe^{2+} in the distorted M(4) site in comparison to Δ for Fe^{2+} in the more regular M(1), M(2) and M(3) sites. Fourth, the half-width of the outer doublet is always larger than that of the inner doublet, consistent with a close superposition of Fe^{2+} absorptions from the M(1), M(2) and M(3) sites.

The Fe^{2+} distribution determined from Mössbauer spectra of CG (Hafner and Ghose, 1971) have been collated with X-ray site refinements (Ghose, 1961; Fischer, 1966; Finger, 1969) for two samples, and the comparison is presented in Table 1. There is excellent agreement for Klein 1, but poor agreement for DH7-482 which was not discussed by Hafner and Ghose, nor was the discrepancy between the results of the two X-ray studies for this sample explained.

CALCIC AMPHIBOLES

Bancroft et al. (1967a) presented a Mössbauer spectrum of an actinolite which contains two visually identifiable peaks in the high velocity region with the inner peak occurring as a shoulder of lower intensity on the outer peak. The doublets associated with these peaks were assigned to Fe^{2+} in the M(2) site ($\Delta \sim 2.0$ mm/sec) and the M(1) and M(3) sites ($\Delta \sim 2.8$ mm/sec), respectively, because of the slightly greater distortion of the M(2) site. They attributed the large difference in Δ for Fe^{2+} in the structurally similar M(2) sites in CG and TA to the presence of Ca, rather than Fe^{2+} or Mg, in the neighboring M(4) sites, which is a premise also adopted by Häggström et al. (1969).

Burns and Greaves (1971) added a third Fe^{2+} doublet in analyzing actinolite Mössbauer spectra indicating that statistical tests warranted its addition. They also presented spectra to show that the three doublets become more distinguishable at 77 K. Assuming that Ca, Na and K occupy most of the M(4) sites, they assigned the three doublets to Fe^{2+} in the M(1), M(3) and M(2) sites, in order of decreasing Δ. The M(1) assignment was made because this site is considered to be least distorted of the three sites, these peaks are the most intense in the spectra, there are two M(1) sites to one M(3) site, and Fe^{2+} should discriminate against the smaller M(2) site, which is favored by Fe^{3+}. The remaining peaks were assigned based on their similarity to sodic amphibole Mössbauer assignments (Bancroft and Burns, 1969) in which the M(2) doublet is least intense due to the preferred occupancy of Fe^{3+} and Al in this site. Bancroft and Brown (1975) also used these assignments in their hornblende study, but reversed the Fe^{3+} and M(2) Fe^{2+} peaks in the low velocity region so that Δ of the Fe^{2+} doublets decreases with decreasing isomer shift, δ, as for Fe^{2+} in the M(4) site in CG spectra (Bancroft et al., 1967a). They noted that this reversal did not change the resulting Fe^{2+} site population or the Fe^{3+}/Fe^{2+} ratio.

Goodman and Wilson (1976) analyzed their hornblendes with doublets assigned to Fe^{2+} in the M(1), M(3), M(2) and M(4) sites, in order of decreasing Δ, and Fe^{3+} in octahedral and tetrahedral coordinations.

The peak assignments for calcic amphiboles have been tested in two experiments reported by Burns and Greaves. They examined the Mössbauer spectrum of synthetic ferrotremolite, $Ca_2Fe^{2+}_5Si_8O_{22}(OH)_2$, expecting to find M(1):M(2):M(3) area ratios of 2:2:1 based on the site multiplicities. However, separate peaks due to Fe^{2+} in each of these sites, similar to those reported for their other samples, were not obtained. The outer and intermediate peaks were assigned to Fe^{2+} in the M(1) site and the M(2) and M(3) sites, respectively. In addition, an inner shoulder appears in the high velocity region which occurs at lower velocities than the M(2) peaks in other samples. Although a complementary shoulder was not observed in the low velocity region, computer fitting resulted in a Δ of 1.37 mm/sec for this doublet, which they assigned to Fe^{2+} in the M(4) site, noting that this assignment raised crystal-chemical problems given the assumed stoichiometry of the synthetic sample.

The Fe^{2+} site distribution of an actinolite (USNM 44973) has been determined by both X-ray (Mitchell *et al.*, 1971) and Mössbauer (Burns and Greaves, sample 6) methods, and the results are compared in Table 2. There is an exact agreement for the M(3) site, but poor agreement for the M(1) and M(2) sites. However, as pointed out by Burns and Greaves, the sum of the formula units of Fe^{2+} and Fe^{3+} from the X-ray study is greater than the value specified by the chemical analysis of this sample. Mitchell *et al.* also constrained all Mn^{2+} to the M(4) site whereas some Fe^{2+} may be included in this result due to the similar scattering factors of the two ions. In addition, they constrained the Fe^{3+} and Al to the M(2) site,

whereas Burns and Greaves concluded that these ions occur in a number of different sites. These problems make it difficult to evaluate the discrepancy between both methods.

"INTERMEDIATE" AMPHIBOLES

The intermediate amphiboles referred to in this study are considered to be intermediate in composition between the sodic and calcic amphiboles and include: richterites, $Na(Na,Ca)(Mg,Fe^{2+})_5Si_8O_{22}(OH)_2$; edenites, $NaCa_2(Mg,Fe^{2+})_5(Si_7Al)O_{22}(OH)_2$; and paragasite-ferrohastingsites, $NaCa_2(Mg,Fe^{2+})_4(Al,Fe^{3+})(Si_6Al_2)O_{22}(OH)_2$. A Mössbauer spectrum of synthetic ferro-richterite taken at 77 K (Virgo, 1972) exhibits one visually apparent doublet from Fe^{2+} ($\Delta\sim3.09$ mm/sec) and one doublet from Fe^{3+}. The Fe^{2+} envelope was fitted with two doublets assigned to Fe^{2+} in the M(1) and M(3) sites and the M(2) site in order of decreasing Δ.

Semet (1973) studied the Mössbauer spectra of magnesiohastingsite synthesized at generally the same pressure and temperature, but with different values of oxygen fugacity which resulted in different proportions of Fe^{2+} and Fe^{3+}. Two doublets were fitted to the asymmetric Fe^{2+} envelope and assigned to Fe^{2+} in the M(1) and M(3) sites ($\Delta\sim2.7$ mm/sec) and the M(2) site ($\Delta\sim2.0$ mm/sec).

SODIC AMPHIBOLES

The Mössbauer spectra of sodic amphiboles have been studied by Gibb and Greenwood (1965), Whitfield and Freeman (1967), Bancroft et al. (1968), Bancroft and Burns (1969) and Ernst and Wai (1970). The Fe^{2+} envelope in the high velocity region is either asymmetric, or it has a prominent inner shoulder on the more intense outer peak. Bancroft et al. (1968) and Bancroft and Burns fitted two Fe^{2+} doublets to their spectra and assigned them to the M(1) site ($\Delta \sim 2.8$ mm/sec) and the M(3) and M(2) sites ($\Delta \sim 2.3$ mm/sec). For a glaucophane, $Na_2(Mg,Fe^{2+})_3(Al,Fe^{3+})_2\ Si_8O_{22}(OH)_2$ (Bancroft and Burns, sample 1), this assignment resulted in an Fe^{2+} site population that agrees with a structural refinement of that specimen (Papike and Clark, 1968) in which Al and Fe^{3+} were constrained to the M(2) site. For one sample (Bancroft and Burns, sample 7), the sum of Al and Fe^{3+} (1.79) is not sufficient to assume that these ions completely occupy the M(2) site, and hence, a substantial proportion of the total Fe^{2+} ($\sim$25 percent) could enter this site. They fit this spectrum with three Fe^{2+} doublets assigned to the M(1), M(3) and M(2) sites with Δ values of 2.79, 2.40 and 2.00 mm/sec, respectively, and found that about 17 percent of the total Fe^{2+} was in the M(2) site. However, for other samples in which the sum of Al and Fe^{3+} is greater than about 1.9, they were unable to fit three Fe^{2+} doublets without imposing additional constraints in the fitting process that were not considered justified.

DISCUSSION

Cummingtonite-grunerites

Perhaps the most important characteristic of CG Mössbauer spectra is the nearly exact superposition of Fe^{2+} peaks from the M(1), M(2) and M(3) sites, which prevents their distinction even in computer analysis. The commonly quoted model of Ingalls (1964) predicts that Δ decreases with increasing distortion of a site from octahedral geometry. Using the maximum variation of metal-oxygen (M-O) bond lengths as a measure of distortion, the M(4) site is much more distorted than the other sites (Table 3), and Δ for Fe^{2+} in this site is 1.0 - 1.3 mm/sec smaller (Bancroft et al., 1967a). Although this result is predicted by the Ingalls' model, it does not appear to explain the superposition of Fe^{2+} peaks from the other sites where the M(1) and M(2) sites are more distorted than the centrosymmetric M(3) site.

The M(1), M(2) and M(3) sites become slightly larger with increasing total iron content (Table 3), but these modifications do not systematically change Δ of Fe^{2+} in these sites across the series (Figure 2a). In contrast, the M(4) site retains about the same average M-O bond length across the series, but Δ of Fe^{2+} in this site decreases with increasing Fe^{2+} content in the M(4) site (Figure 2b) and also with increasing total Fe^{2+} content (Figure 2c). An explanation for the M(4) trends may relate to structural modifications that the M(4) site experiences across the series. These modifications appear to result, in part, from readjusting the fit of the tetrahedral chain to the expanding octahedral chain with increasing iron content, as suggested by Hafner and Ghose. The O(6) oxygens of the M(4) site each bridge two corner-shared tetrahedra. Furthermore, structural projections of the M(4) site indicate that the position of Fe^{2+} in cummingtonite[1/] (Fischer, 1966) is further from the O(2) oxygens and the adjacent M(1) site than in grunerite (Finger, 1969). Both types of

modifications result in a further distortion of the site, particularly by increasing the M(4) - O(6) bond lengths (Table 3), which makes the site less centrosymmetric. It is likely that these modifications are also responsible for changing the absolute intensity (i.e. molar absorptivity, ε) of the M(4) absorption band near 1000 nm in β polarization in the electronic absorption spectra of these minerals, because band intensities are related to the degree of centrosymmetry of the site. The ε value for this band in cummingtonite (sample 118125, Ghose and Weidner, 1972) is about 120 (Goldman, unpublished data) whereas it is about 150 for the grunerite sample in Figure 1.

The anomalous sample in Figure 2b contains 23.7 mole percent Mn^{2+} and much of this is in the M(4) site (Bancroft et al., 1967a,b); but this sample falls near the smooth trend in Figure 2c. Combining the Fe^{2+} and Mn^{2+} components (i.e. 43.7 mole percent), this sample falls on the trend in Figure 2c. This supports the suggestion of Hafner and Ghose that the octahedral-tetrahedral chain fit, which is controlled by the overall composition of the mineral, is dominantly responsible for changing the value of Δ for Fe^{2+} in the M(4) site.

Tremolite-actinolites Fe^{2+} in M(2)

The non-coincidence of Fe^{2+} peaks from the M(1), M(2) and M(3) sites in TA Mössbauer spectra is perhaps their most surprising characteristic. Bancroft et al. (1967a) and Häggström et al. (1969) suggested that Δ of Fe^{2+} in the M(2) site is reduced due to Ca in the neighboring M(4) sites. Next-nearest neighbor effects involving Ca have been invoked to explain certain anomalies in the Mössbauer spectra of clinopyroxenes synthesized along the hedenbergite ($CaFeSi_2O_6$) - ferrosilite ($Fe_2Si_2O_6$) join by Dowty and Lindsley (1973). They found that the area of the M(2) doublet was larger than expected from the stoichiometry of each specimen (assuming Ca only occurs in the M(2) site) when only one doublet was fitted for each site. They concluded that some of the M(1) intensity overlaps and augments the M(2) peak intensities due to the changing occupancy of the surrounding M(2) sites from Ca to Fe^{2+} across the join. By fitting four M(1) doublets and one M(2) doublet for samples of intermediate composition, M(1)/M(2) ratios were in better, but not exact, agreement with the expected stoichiometry. Consistent with this model, only one M(1) doublet was analyzed in hedenbergite (Δ = 2.22 mm/sec) and ferrosilite (Δ=2.49 mm/sec). Hence, Δ for Fe^{2+} in the clinopyroxene M(1) site is reduced by about 0.3 mm/sec upon changing the occupancy of the three adjacent M(2) sites from Fe^{2+} to Ca. However, the 0.9-1.0 mm/sec difference in Δ between the inner and outer Fe^{2+} peaks in actinolites is difficult to explain using these arguments because the M(2) site shares only two edges with neighboring Ca sites. Note that the M(1) site also shares an edge with the M(4) site. Considering the close structural (Clark et al., 1969; Cameron et al., 1973; Mitchell et al., 1971; Sueno et al., 1973) and topological similarity of the clinopyroxene M(1) and actinolite M(2) sites, it also becomes difficult to explain the large difference in Δ to a significant difference in geometric distortion.

An assignment of the doublet having a Δ of 2.16 mm/sec in the spectrum of synthetic ferrotremolite (Burns and Greaves) to Fe^{2+} in the M(2) site is consistent with the hedenbergite M(1) site data. This is expected due to the similar structural and next-nearest neighbor configurations of the two sites. The similar area ratio of this doublet to the outer doublet in synthetic ferrotremolite further supports an M(2) site origin. However, the peaks of this doublet would occur in the transmission valleys between the inner and outer Fe^{2+} doublets in tremolite, corresponding to the position of the intermediate doublet analyzed by Burns and Greaves and assigned to Fe^{2+} in the M(3) site. Based on the synthetic ferrotremolite and clinopyroxene data, it is suggested that the intermediate doublet in TA spectra does arise mostly from Fe^{2+} in the M(2) site. This possibility necessitates a reassignment of the other Fe^{2+} resonance. The outer doublet ($\Delta \sim 2.8$ mm/sec) is assigned to Fe^{2+} in the M(1) and M(3) sites and the inner doublet ($\Delta \sim 1.8$ mm/sec) is assigned to Fe^{2+} in the M(4) site. The basis for these assignments will be discussed in the next section.

The M(2) doublet in the Mössbauer spectra of intermediate and sodic amphiboles has a Δ of approximately 2.0 mm/sec (Bancroft and Burns, 1969; Semet, 1973). This value is approximately 0.2 mm/sec smaller than Δ for the proposed M(2) doublet in TA spectra. It can be seen from Table 3 that the M(2) site becomes smaller and more distorted in the sequence cummingtonite-actinolite-glaucophane as it accommodates more Al and Fe^{3+} (Papike and Clark). The relative distortion of the M(2) site in hornblende occurs between actinolite and glaucophane in this sequence (Robinson et al., 1973). Therefore, as more Al and Fe^{3+} enter the calcic amphibole crystal structure, Δ for Fe^{2+} in the M(2) site is expected to be reduced from the TA value.

Fe^{2+} in M(4)

A fundamental assumption used to arrive at peak assignments in calcic amphibole spectra is that Ca, Na and K occupy most of the M(4) sites, and therefore, peaks due to Fe^{2+} in the M(4) site have not been sought. However, the occurrence of M(4) Fe^{2+} for the actinolites reported by Burns and Greaves is indicated from their stoichiometry and optical spectra. The sum of Al^{vi}, Ti, Fe^{2+}, Fe^{3+}, Mg and Mn ranges from 5.07 to 5.39 for six of seven samples, whereas a total of five M(1), M(2) and M(3) sites are available for these ions. The excess is most likely accommodated in the M(4) sites, which have a maximum of 1.83 of two possible sites occupied by Ca. An indication that some of these excess ions in the M(4) site are Fe^{2+} comes from the electronic absorption spectra of their samples 1 and 5 in Burns (1970). These spectra have intense bands at 1030 nm in β polarization. This band has been shown to be due to Fe^{2+} in the M(4) site by Goldman and Rossman (1977). The large size of the M(4) site also produces Fe^{2+} absorption bands in the 2500 nm region in both tremolite and grunerite optical spectra (Figure 1), and anthophyllite-gedrite spectra (Mao and Seifert, 1973). These results suggest that the inner doublet observed in the Mössbauer spectrum of tremolite is predominantly due to Fe^{2+} in the M(4) site.

As suggested earlier, an assignment of the inner doublet in tremolite (Δ = 1.84 mm/sec) to Fe^{2+} in the M(2) site is not supported by the synthetic clinopyroxene or ferrotremolite data. The M(4) assignment is supported from cummingtonite-grunerite data (Figures 2b,c), which show that Δ for Fe^{2+} in the M(4) site increases from 1.5 mm/sec to about 1.8 mm/sec as the total iron and the M(4) iron contents decrease. From an extrapolation of these data, a Δ of about 1.8 mm/sec is expected for Fe^{2+} in the M(4) site in tremolite.

Ca generally occupies 85-95 percent of the M(4) sites in calcic amphiboles (Leake, 1968). The M(4) doublet should therefore become relatively less intense as the iron content in the other sites increases. To examine this possibility, the fitted resonant envelope of the tremolite spectrum in Figure 1 can be compared to those of two additional amphiboles of the TA series in Figure 3. These samples have been selected based on their different iron contents and the observation of M(4) Fe^{2+} bands in their electronic absorption spectra. The Fe^{2+} content and the locations of the inner Fe^{2+} peaks in tremolite are annotated on each Mössbauer spectrum. These spectra show that as the Fe^{2+} content increases in the M(1), M(2) and M(3) sites, there is a progressive reduction in the relative intensity of the inner doublet, which is visually distinct in tremolite, but barely discernible in ferrotremolite. This observation supports the assignment of the inner doublet to Fe^{2+} in the M(4) site. The reduction in the relative intensity of the M(4) doublet with increasing iron content also provides an explanation for the disappearance of the transmission valley between the inner and outer doublets observed in tremolite. The chemical, Mössbauer and electronic absorption data for the samples reported by Burns and Greaves are consistent for an M(4) assignment for the inner doublet.

Fe^{2+} in M(1) and M(3)

The outer Fe^{2+} doublet ($\Delta \sim 2.7$-2.8 mm/sec) is interpreted differently among the various amphibole groups. It is assigned to the M(1), M(2) and M(3) sites in CG (Bancroft et al., 1967a,b), to the M(1) and M(3) sites in the intermediate amphiboles (Virgo, 1972; Semet, 1973), and to the M(1) site in sodic amphiboles (Bancroft and Burns, 1969). Absorptions from Fe^{2+} in the M(1) site occur in the outer doublet region in each of these groups. However, there appears to be a progressive separation of the M(3) doublet from the M(1) doublet as more Fe^{3+} and Al enter the crystal structure. The cause of this separation is unlikely to be due to significant differences in geometric distortions of the M(3) site between cummingtonite and glaucophane because these sites are structurally similar (Table 3). TA have compositions that occur between CG and the intermediate amphiboles in this progression. The outer doublet in TA is therefore assigned to Fe^{2+} in the M(1) and M(3) site because absorptions from these sites remain superimposed (or nearly superimposed) between CG and the intermediate amphiboles.

It is likely that the separation of the M(1) and M(3) doublets will increase in calcic amphiboles as more Fe^{3+} and Al preferentially enter the adjacent M(2) sites. The separation appears to reach a limiting value of ~ 0.4 mm/sec in glaucophane (Bancroft and Burns, 1969) in which the M(2) site is almost fully occupied by Fe^{3+} and Al. The assignment made above is therefore more safely applied to calcic amphiboles, such as TA, in which these compositional problems are less severe.

Temperature dependency

The temperature dependence of Δ is one way by which the proposed peak assignments for TA can be evaluated. Hafner and Ghose (1971) showed that Δ for Fe^{2+} in the CG M(1), M(2) and M(3) site increases from 2.8 to about 3.1 mm/sec as the temperature decreases to 77 K, whereas Δ for Fe^{2+} in the M(4) site remains nearly constant. The Mössbauer spectrum of an actinolite taken at 77 K is presented in Figure 4 to examine the temperature dependency of the three Fe^{2+} doublets.[3/] The stoichiometry (Table 1) and electronic absorption spectra of this sample indicate the presence of Fe^{2+} in the M(4) site. The outer doublet has a Δ of 3.10 mm/sec, which is 0.3 mm/sec larger than its typical room temperature value. A similar Δ at 77 K was found for the outer doublet in synthetic ferrorichterite, which was assigned to Fe^{2+} in the M(1) and M(3) sites (Virgo, 1972). The intermediate Fe^{2+} doublet in Figure 4 has a Δ of 2.50 mm/sec, which is about 0.3 mm/sec larger than the room temperature value of the proposed M(2) doublet in synthetic ferrotremolite (Burns and Greaves). The similarity in the temperature dependency of the outer and intermediate doublets in TA Mössbauer spectra to that found for the outer doublet in CG spectra supports their assignment to Fe^{2+} in the M(1) and M(3) sites and the M(2) site, respectively. The inner Fe^{2+} doublet in Figure 4 has a Δ of 1.86 mm/sec which can be compared to the room temperature value of 1.84 mm/sec determined for the inner doublet in tremolite (Goldman and Rossman, 1977). The lack of a temperature dependence for the inner doublet in TA spectra supports its assignment to Fe^{2+} in the M(4) site, based on the CG data. Although Bancroft and Burns indicated that Δ for Fe^{2+} in the sodic amphibole M(2) site does not appear to have a significant temperature dependency, it must be remembered that this site is much more distorted than the TA M(2) site (Table 3), and a comparison between these groups is likely to be less valid.

Site preferences

The observation from Figure 1 that Fe^{2+} is nearly equally distributed between the M(4) site and the other sites in tremolite suggests that Fe^{2+} will attempt to occupy available M(4) sites prior to Mg. The presence of a transmission valley between the M(1) and M(3) doublet and the M(4) doublet suggests that Fe^{2+} discriminates against the M(2) site. These observations indicate that Fe^{2+} prefers to enter the M(4) site prior to the M(1) and M(3) sites, and discriminates against the M(2) site. This is the same ordering scheme found in cummingtonite (Ghose, 1961; Fischer, 1966) and grunerite (Ghose and Hellner, 1959; Finger, 1969) from X-ray studies. In addition, this ordering scheme is consistent for a suite of tremolite-actinolites as shown in Figures 1 and 3 and from the spectra in Burns and Greaves. These interpretations provide an additional reason for the disappearance of the transmission valleys between the inner and outer doublets as the iron concentration increases. The change in the appearance of the Fe^{2+} envelope involves a progressively less intense M(4) doublet and a continuously more intense M(2) doublet as the iron concentration increases.

Peak variations

It was suggested earlier that the substitution of Al and Fe^{3+} into the calcic amphibole crystal structure produces a separation of the M(1) and M(3) doublets, and reduces Δ for Fe^{2+} in the M(2) site. The Mössbauer spectra of the hornblendes studied by Bancroft and Brown are likely examples of this process. The stoichiometry of most of their samples (Dodge et al., 1968) suggests that there is not sufficient Fe^{2+} in the M(4) site to be an important contribution to the Mössbauer spectra. This is also indicated from the electronic absorption spectra of two of those samples taken as a part of this study. The Δ values for the doublets assigned to Fe^{2+} in the M(1), M(3) and M(2) sites are approximately 2.8, 2.4 and 2.0 mm/sec, respectively. The possibility that hornblendes may also have Fe^{2+} in the M(4) site suggests that four Fe^{2+} doublets may be required for certain samples, such as those reported by Goodman and Wilson (1976). However, such fits should be viewed with caution without supporting evidence from chemical and electronic absorption data for the occurrence of Fe^{2+} in the M(4) site. Nevertheless, the observation of a distinct inner Fe^{2+} peak or shoulder in a calcic amphibole Mössbauer spectrum probably signifies the presence of Fe^{2+} in the M(4) site.

It is also possible that Al and Fe^{3+} influence the peak parameters for the outer Fe^{2+} doublet in hornblendes. As shown in Figure 5, the Mössbauer data for the hornblendes reported by Bancroft and Brown correlate with the Al and Fe^{3+} Fe^{3+} contents of these samples (Dodge et al., 1968; Burns and Greaves,1971). These trends show that Δ for the outer doublet decreases with increasing Al, Fe^{3+} and (Al + Fe^{3+}) contents. Although variations in the Na content of the M(4) site may be involved in these correlations, the Mössbauer spectrum of a low-Fe richterite (Goldman, unpublished data) is virtually identical to the tremolite spectrum in Figure 1 which indicates that significant variations

of the Na content in the M(4) site does not affect the peak positions of Fe^{2+} in the M(1), M(3) or M(4) sites.

The trends in Figure 5 also suggest that two different mechanisms are responsible for producing the variation in Δ, because the Al in these samples is mostly in tetrahedral coordination and bonding occurs through one Al-O-(Fe,Mg) bridge, whereas the Fe^{3+} is most likely in octahedral coordination and bonding with adjacent octahedral sites occurs by sharing a common edge. An indication that the amount of tetrahedral Al is the dominant factor comes from the Mössbauer and structural data for the intermediate and sodic amphiboles. In glaucophane, the M(2) site is almost fully occupied by Al and Fe^{3+} (Papike and Clark) and there is very little tetrahedral Al, but Δ of the outer peaks is about 2.8 mm/sec (Bancroft and Burns). In synthetic magnesiohastingsite, less than half of the M(2) sites could be occupied by Al and Fe^{3+}, but there is significant tetrahedral Al. Δ of the outer peaks is about 2.7 mm/sec (Semet). It appears likely that the amount of tetrahedral Al affects the fit of the octahedral and tetrahedral chains. This fit, in response to changing composition, was discussed earlier as a possible cause for the variation in Δ of Fe^{2+} in the M(4) site in CG spectra.

Regardless of the mechanisms responsible for producing the trends in Figure 5, the result would be a progressive "collapse" of the Fe^{2+} envelope, if the locations of the inner peaks remain about the same. This can be seen in the Mössbauer spectrum of a pargasite in Figure 6.[4/] This pargasite was selected because its electronic absorption spectra indicate the presence of Fe^{2+} in the M(4) site. The Δ values for the outer, intermediate and inner doublets are 2.59, 2.26, and 1.88 mm/sec, respectively. The smaller Δ of the outer doublet does result in a "collapse" of the Fe^{2+} envelope, because the inner doublet remains at about the same position as in tremolite (Figure 1, Δ = 1.84 mm/sec). This produces a much closer overlap of all Fe^{2+} peaks, and therefore, the ability to determine accurate

site distributions by assuming that one peak represents Fe^{2+} in only one site is further impaired.

It was found that convergence in the computer fitting of the pargasite spectrum in Figure 6 was obtained, using only half-width constraints, only if all of the Fe^{2+} peaks in the low velocity region occurred at lower velocities than the Fe^{3+} peaks. The positioning of the inner Fe^{2+} peak and the low velocity Fe^{3+} peak in this region is similar to the fits for hornblendes in Bancroft and Brown, but reversed from the fits for actinolites in Burns and Greaves. Bancroft and Brown preferred their placement of these peaks, because it resulted in decreasing δ values as the Δ decreases for the Fe^{2+} peaks. It is true that as Δ for Fe^{2+} in the M(4) site in cummingtonite-grunerites decreases, δ also decreases (Bancroft et al., 1967a,b). However, the δ values for the inner and outer doublets for tremolite in Figure 1 show just the reverse, being 1.17 and 1.14 mm/sec, respectively (Goldman and Rossman, 1977). Δ for the inner doublet in Figure 6 is sufficiently close to the expected value for M(4) Fe^{2+} based on the tremolite spectrum that it was felt that imposing additional constraints to reverse the M(4) and Fe^{3+} peaks in the low velocity region was unnecessary. Bancroft and Brown indicated that the same Fe^{2+} site population and the same Fe^{2+}/Fe^{3+} ratios were obtained with either positioning within the error of measurement.

The effect of next-nearest neighbor chemical variations in calcic amphiboles has been discussed in terms of reducing Δ for Fe^{2+} in the M(1), M(2) and M(3) sites as more trivalent ions enter the crystal structure. It is realized that Fe^{2+} in a particular site may experience a variety of next nearest neighbor environments within a crystal structure which would tend to broaden the spectral region in which it absorbs. Fitting one peak to this broadened region for iron in that site will lead to erroneous site distributions, as shown for synthetic clinopyroxenes by Dowty and Lindsley. Because of the chemical complexities

that are characteristic of calcic amphiboles, and the large number of sites available for Fe^{2+}, these problems may always be inherent to the method. Hence, a compromise between the number of peaks that can be fitted to a complex Mössbauer spectrum and the ability to decipher the origin of each peak must be reached. Figure 7 summarizes the conclusions reached in this paper regarding the site assignments for calcic amphibole Mössbauer spectra.

ACKNOWLEDGMENTS

The manuscript benefited greatly from the comments of W. A. Dollase (UCLA) and G. R. Rossman (Caltech). The author also is indebted to W. A. Dollase for making his spectrometer available during the course of this study and to F. C. W. Dodge (U.S.G.S., Menlo Park) for supplying a number of hornblende samples.

REFERENCES CITED

Bancroft, G.M., A.G. Maddock and R.G. Burns (1967a) Applications of the Mössbauer effect to silicate mineralogy - I. Iron silicates of known crystal structure. Geochim. Cosmochim. Acta 31, 2219-2246.

Bancroft, G.M., R.G. Burns and A.G. Maddock (1967b) Determination of the cation distribution in the cummingtonite-grunerite series by Mössbauer spectra. Amer. Mineral. 52, 1009-1026

Bancroft, G.M., A.G. Maddock and R.G. Burns (1968) Applications of the Mössbauer effect to silicate mineralogy - II Iron silicates of unknown and complex crystal structures. Geochim Cosmochim. Acta 32, 547-559.

Bancroft, G.M. and R.G. Burns (1969) Mössbauer and absorption spectral study of alkali amphiboles. Miner. Soc. Amer. Spec. Pap. 2, 137-150.

Bancroft, G.M. and J.R. Brown (1975) A Mössbauer study of coexisting hornblendes and biotites: Quantitative Fe^{3+}/Fe^{2+} ratios. Amer. Mineral. 60, 265-272.

Buckley, A.N. and R.W.T. Wilkins (1971) Mössbauer and infrared study of a volcanic amphibole. Amer. Mineral. 56, 90-100.

Burns, R.G. (1970) Mineralogical Applications of Crystal Field Theory. Cambridge University Press.

Burns, R.G. and C. Greaves (1971) Correlations of infrared and Mössbauer site population measurements of actinolites. Amer. Mineral. 56, 2010-2033.

Cameron, M., S. Sueno, C.T. Prewitt and J.J. Papike (1973) High temperature crystal chemistry of acmite, diopside, hedenbergite, jadeite, spodumene, and ureyite. Amer. Mineral. 58, 594-618.

Clark, J.R., D.E. Appleman and J.J. Papike (1969) Crystal-chemical characterization of clinopyroxenes based on eight new structure refinements. Mineral. Soc. Amer. Spec. Pap. 2, 31-50.

DeCoster, M., H. Pollack and S. Amelinckx (1963) A study of Mössbauer absorption in iron silicates. Phys. Stat. Solids 3, 283-288.

Dodge, F.C.W., J.J. Papike and R.E. Mays (1968) Hornblendes from granitic rocks of the central Sierra Nevada batholith, California. J. Petrol. 9, 378-410.

Dowty, E. and D.H. Lindsley (1973) Mössbauer spectra of synthetic hedenbergite-ferrosilite pyroxenes. Amer. Mineral. 58, 850-868.

Ernst, W.G. and C.M. Wai (1970) Mössbauer, infrared, X-ray and optical study of cation ordering and dehydrogenation in natural and heat-treated sodic amphiboles. Amer. Mineral. 55, 1226-1258.

Finger, L.W. (1969) The crystal structure and cation distribution of a grunerite. Mineral. Soc. Amer. Spec. Pap. 2, 95-100.

Fischer, K.F. (1966) A further refinement of the crystal structure of cummingtonite, $(Mg,Fe)_7(Si_4O_{11})_2(OH)_2$. Amer. Mineral. 51, 814-818.

Ghose, S. (1961) The crystal structure of a cummingtonite. Acta Crystallogr. 14, 622-627.

Ghose, S. and E. Hellner (1959) The crystal structure of a grunerite and observations of the Mg-Fe distribution. J. Geol. 67, 691-701.

Ghose, S. and J.R. Weidner (1972) Mg^{2+}-Fe^{2+} order-disorder in cummingtonite, $(Mg,Fe)_7Si_8O_{22}(OH)_2$: A new geothermometer. Earth Planet. Sci. Lett. 16, 346-354.

Gibb, T.C. and N.N. Greenwood (1965) Chemical applications of the Mössbauer effect. Part 2. Oxidation states of iron in crocidolite and amosite. Trans. Faraday Soc. 61, 1317-1323.

Goldman, D.S. and G.R. Rossman (1977) The identification of Fe^{2+} in the M(4) site in calcic amphiboles. Amer. Mineral. 62, 205-216.

Goodman, B.A. and M.J. Wilson (1976) A Mössbauer study of the weathering of hornblende. Clay Minerals 11, 153-163.

Hafner, S.S. and S. Ghose (1971) Iron and magnesium distribution in cummingtonites, $(Fe,Mg)_7Si_8O_{22}(OH)_2$. Zeits. Kristallogr. 133, 301-326.

Häggström, L., R. Wäppling and H. Annersten (1969) Mössbauer study of oxidized iron silicate minerals. Phys. Stat. Solids 33, 741-748.

Ingalls, R. (1964) Electric field gradient tensor in ferrous compounds. Phys. Rev. 133, A787-795.

Kamineni, D.C. (1973) X-ray and Mössbauer characteristics of a cummingtonite from Yellowknife, District of MacKenzie. Canad. Mineral. 12, 230-232.

Leake, B.E. (1968) A catalogue of analyzed calciferous and subcalciferous amphiboles together with their nomenclature and associated minerals. Geol. Soc. Amer. Prof. Pap. 98.

Mao, H.K. and F. Seifert (1973) A study of the crystal-field effects of iron in the amphiboles anthophyllite and gedrite. Carnegie Inst. Wash. Year Book 73, 500-502.

Mitchell, J.T., F.D. Bloss and G.V. Gibbs (1971) Examination of the actinolite structure and four $C_{2/m}$ amphiboles in terms of double bonding. Zeits. Kristallogr. 133, 273-300.

Papike, J.J. and J.R. Clark (1968) The crystal structure and cation distribution of glaucophane. Amer. Mineral. 53, 1156-1173.

Robinson, K., G.V. Gibbs, P.H. Ribbe and M.R. Hall (1973) Cation distribution in three hornblendes. Amer. J. Sci. 273-A, 522-535.

Semet, M. (1973) A crystal-chemical study of synthetic magnesiohastingsite. Amer. Mineral. 58, 480-494.

Sueno, S., M. Cameron, J.J. Papike and C.T. Prewitt (1973) The high-temperature crystal chemistry of tremolite. Amer. Mineral. 58, 649-664.

Virgo, D. (1972) Preliminary fitting of ^{57}Fe Mössbauer spectra of synthetic Mg-Fe richterites. Carnegie Inst. Wash. Year Book 71, 513-516.

Whitfield, H.J. and A.G. Freeman (1967) Mössbauer study of amphiboles. J. Inorg. Nucl. Chem. 29, 903-914.

Table 1. Fe^{2+} site occupancies* for a cummingtonite and grunerite

Sample	X-ray M(1,2,3)	X-ray M(4)	Mössbauer M(1,2,3)	Mössbauer M(4)
DH7-482	1.16 0.62	1.34[a] 1.88[b]	1.02	1.48[d]
Klein 1	4.16	1.98[c]	4.21	1.93[d]

* formula units; a. Ghose, 1961; b. Fischer, 1966; c. Finger, 1969; d. Hafner and Ghose, 1971

Table 2. Site occupancies* for an actinolite

method	M(1)	M(2)	M(3)	M(4)
X-ray[a]	1.22 Fe^{2+} 0.78 Mg	0.92 Fe^{2+} 0.32 Fe^{3+} 0.68 Mg	0.58 Fe^{2+} 0.42 Mg	1.76 Ca 0.16 Mn 0.08 Na
Mössbauer[b]	1.53 Fe^{2+}	0.40 Fe^{2+}	0.58 Fe^{2+}	-

* formula units
a. Mitchell, Bloss and Gibbs (1971)
b. Burns and Greaves (1971)

Table 3. Metal-oxygen bond distances for the M sites in amphiboles

bond	cummingtonite[a]	grunerite[b]	actinolite[c]	glaucophane[d]
M(1)-O(1)	2.07Å	2.082Å	2.090Å	2.078Å
M(1)-O(2)	2.14	2.160	2.115	2.082
M(1)-O(3)	2.10	2.122	2.114	2.100
mean	2.10	2.121	2.105	2.087
max. var.	0.07	0.078	0.025	0.022
M(2)-O(1)	2.14	2.161	2.151	2.038
M(2)-O(2)	2.08	2.128	2.114	1.943
M(2)-O(4)	2.04	2.075	2.022	1.849
mean	2.08	2.121	2.098	1.943
max. var.	0.10	0.086	0.129	0.189
M(3)-O(1)	2.11	2.118	2.100	2.103
M(3)-O(3)	2.08	2.103	2.093	2.077
mean	2.10	2.113	2.098	2.094
max. var.	0.03	0.015	0.007	0.026
M(4)-O(2)*	2.17	2.135	2.388	2.411
M(4)-O(4)	2.02	1.988	2.301	2.337
M(4)-O(6)	2.70	2.757	2.561	2.446
M(4)-O(5)	-	-	2.816	2.798
mean	2.30	2.293	2.517	2.498
max. var.	0.66	0.769	0.515	0.461

a. Fischer (1966)
b. Finger (1969)
c. Mitchell, Bloss and Gibbs (1971)
d. Papike and Clark (1968)
* The M(4)-O bond lengths in cummingtonite and grunerite represent the position primarily of Fe^{2+}, whereas they represent the positions primarily of Ca and Na in actinolite and glaucophane, respectively.

Table 4. Electron microprobe analyses

	1	2	3	4	5	6
oxide			weight percent of oxides			
SiO_2	57.65	51.97	56.99	48.61	54.68	39.82
TiO_2	0.07	-	0.01	-	0.05	2.18
Al_2O_3	1.31	-	0.92	1.86	2.45	16.06
Cr_2O_3	-	-	0.08	-	0.69	-
MgO	23.62	8.61	20.66	3.83	20.47	14.98
FeO	2.06	36.96	5.48	30.27	5.87	9.09
MnO	-	0.82	0.22	2.22	0.30	0.08
CaO	13.42	1.01	12.15	10.59	12.16	12.43
Na_2O	0.61	0.04	0.85	0.26	0.73	2.46
K_2O	0.20	-	0.02	0.15	0.06	0.67
Cl	0.04	0.05	0.01	0.04	-	0.02
F	0.21	-	-	-	0.33	-
$\sum$ (-O≡F,Cl)	99.09	99.45	97.38	97.88	97.65	97.80
Fe^{3+}/Fe^{t} (Mössbauer)	0.10	n.d.	0.12	0.18	0.08	0.34
			formula proportions*			
Si	7.81	8.00	7.92	7.59	7.66	5.77
Al^{iv}	0.19	-	0.08	0.34	0.34	2.23
Al^{vi}	0.02	-	0.07	-	0.06	0.52
Ti	0.01	-	-	-	0.01	0.24
Cr	-	-	0.01	-	0.08	-
Mn	-	0.11	0.03	0.29	0.04	0.01
Fe^{2+}	0.21	4.76	0.56	3.24	0.63	0.72
Fe^{3+}	0.02	-	0.08	0.71	0.06	0.37
Mg	4.77	1.98	4.28	0.89	4.27	3.23
Ca	1.95	0.17	1.81	1.77	1.82	1.93
Na	0.16	0.01	0.23	0.08	0.20	0.69
K	0.03	-	-	0.03	0.01	0.12

1. Tremolite, Mt. Bity, Malagasay Republic (CIT 8038)
2. Grunerite, Smallwood mine, Heath Lake, Canada (CIT 7223)
3. Actinolite, Berkeley, California (CIT 299)
4. Ferrotremolite, Biwabik iron formation, Babbitt, Minnesota (UCLA MS2625)
5. Actinolite, Chester, Vermont (CIT 6191)
6. Pargasite, Chelan, Washington (CIT 1188)

* the formula proportions are obtained by normalizing the total positive charge to 46 including both ferric and ferrous iron

FOOTNOTES

1. The M(4) site of this sample contains 84 percent Fe^{2+} (Fischer, 1966).
2. The M(4) site of this sample contains nearly 99 percent Fe^{2+} (Finger, 1969).
3. The computed values for Δ, δ, and the relative area of each Fe^{2+} doublet are: 3.10, 1.26 mm/sec, 52.1%; 2.50, 1.26 mm/sec, 20.0%; 1.86, 1.23 mm/sec, 20.2%. The values for the Fe^{3+} doublet are: 0.41, 0.64 mm/sec, 7.8%. The ferrous and ferric half-widths are 0.36 and 0.46 mm/sec, respectively, and χ^2 for the 200 channels analyzed is 274.
4. The computed values for Δ, δ, and the relative area of each Fe^{2+} doublet are: 2.59, 1.15 mm/sec, 30.6%; 2.26, 1.14 mm/sec, 23.0%; 1.88, 1.10 mm/sec, 12.6%. The values for the Fe^{3+} doublet are: 0.55, 0.61 mm/sec, 33.8%. The ferrous and ferric half-widths are 0.31 and 0.49 mm/sec, respectively, and χ^2 for the 210 channels analyzed is 240.

FIGURE CAPTIONS

1. Mössbauer and electronic absorption spectra of a tremolite from the Malagasay Republic and a grunerite from Canada taken at room temperature. Fe^{2+} in the M(4) sites of these amphiboles is suggested to produce the intense electronic absorption band near 1000 nm in β polarization and 2500 nm in α polarization and the inner quadrupole doublet in the Mössbauer spectra. The FeO value represents only Fe^{2+}. The electronic spectra of tremolite and grunerite represent crystal thicknesses of 1.0 and 0.1 mm, respectively.

2. Variations in the quadrupole splitting at room temperature in the cummingtonite-grunerite series.

   a. quadrupole splitting of the outer doublet with the total iron content.

   b. quadrupole splitting of the inner doublet with the iron content in the M(4) site.

   c. quadrupole splitting of the inner doublet with the total iron content.

   The open circles, filled circles, triangles and x's represent data from Hafner and Ghose (1971), Bancroft et al. (1967a,b), Buckley and Wilkins (1971) and Kamineni (1973), respectively. The sample labeled Mn has 23.7 mole percent Mn^{2+}.

3. Mössbauer spectra of an actinolite from California and a ferrotremolite from Minnesota taken at room temperature which show that as the total Fe^{2+} content (given as FeO) increases, the relative intensity of the inner Fe^{2+} doublet is reduced. The arrows mark the locations of the inner Fe^{2+} peaks in the tremolite spectrum in Figure 1.

4. Mössbauer spectrum of an actinolite from Vermont taken at 77 K showing the increased peak separation. The FeO content represents only Fe^{2+} and the arrows mark the locations of the inner Fe^{2+} peaks in the tremolite spectrum in Figure 1.
5. Correlations between the quadrupole splitting of the outer Fe^{2+} doublet and the Al_2O_3 and Fe_2O_3 contents in the hornblendes reported by Bancroft and Brown (1975). Chemical data are from Dodge et al.(1968) and Burns and Greaves (1971).

6. Mössbauer spectrum of a pargasite from Washington taken at room temperature. The FeO content represents only Fe^{2+} and the arrows mark the locations of the inner Fe^{2+} peaks in the tremolite spectrum in Figure 1. The electronic absorption spectra of this sample indicate the presence of Fe^{2+} in the M(4) site.
7. Summary of the values of quadrupole splitting for Fe^{2+} in calcic amphiboles. The lower values in each range for Fe^{2+} in the M(1), M(2) and M(3) sites represent samples having more Al and Fe^{3+}.

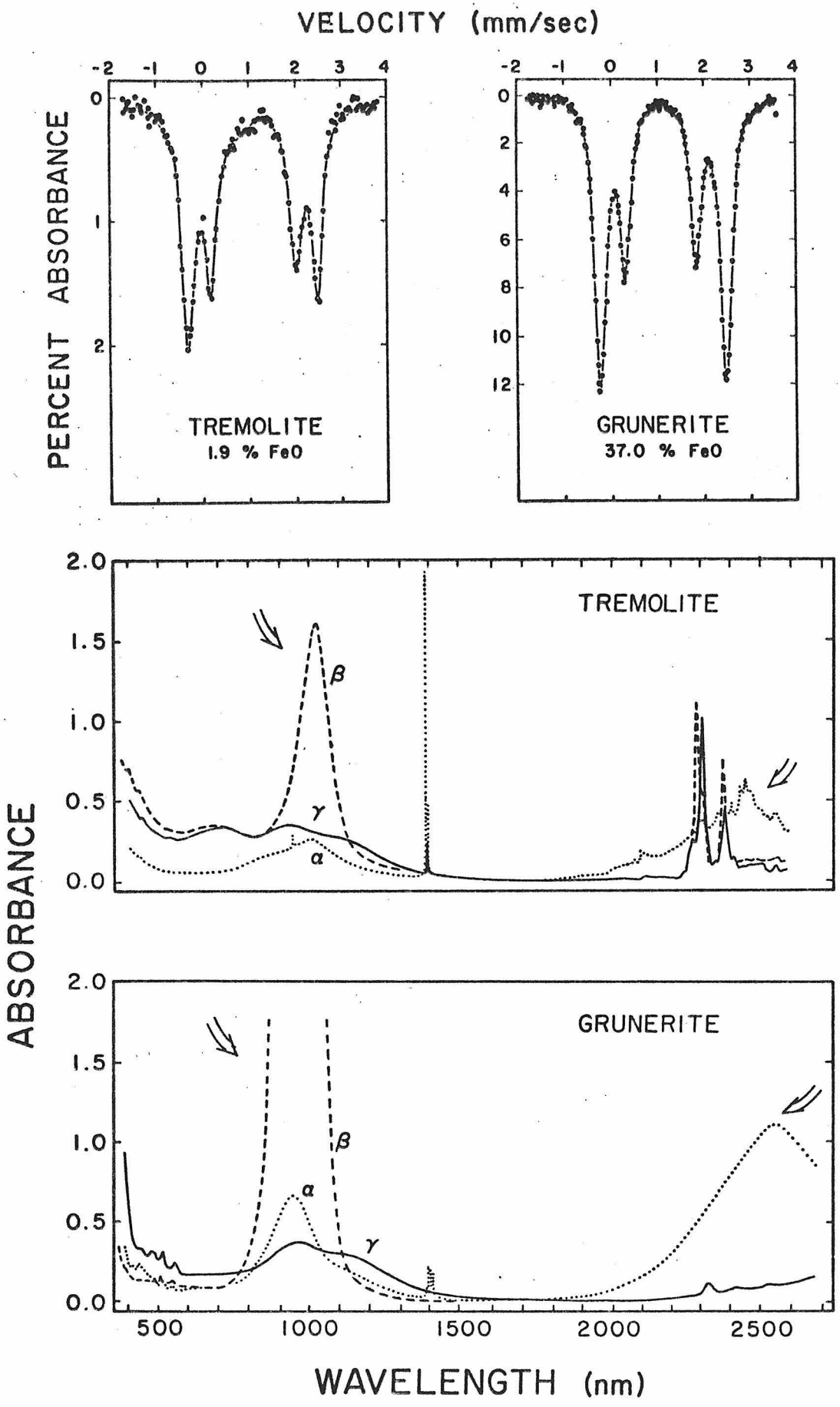
VELOCITY (mm/sec)
-2 -1 0 1 2 3 4
PERCENT ABSORBANCE
TREMOLITE
1.9 % FeO
GRUNERITE
37.0 % FeO
ABSORBANCE
TREMOLITE
GRUNERITE
β
γ
α
WAVELENGTH (nm)
500 1000 1500 2000 2500

Figure 1

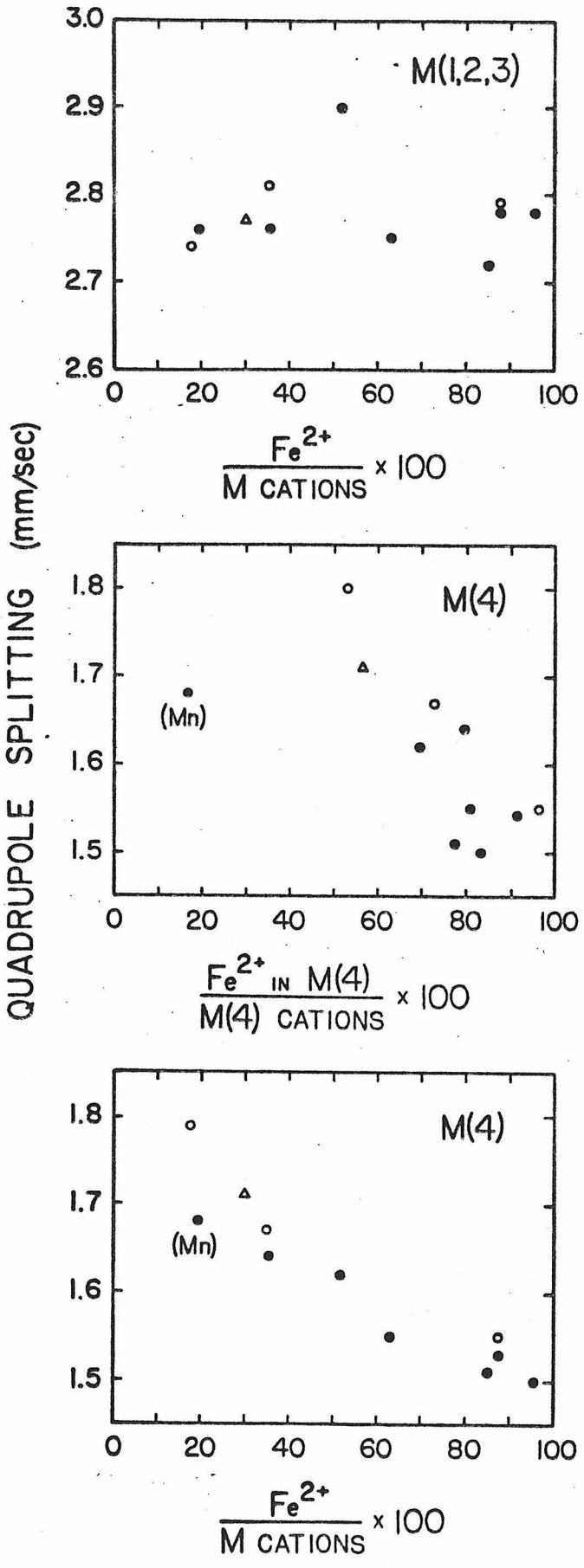
QUADRUPOLE SPLITTING (mm/sec)
M(1,2,3)
M(4)
(Mn)
M(4)
(Mn)
$\frac{Fe^{2+}}{M\ CATIONS} \times 100$
$\frac{Fe^{2+}\ IN\ M(4)}{M(4)\ CATIONS} \times 100$
$\frac{Fe^{2+}}{M\ CATIONS} \times 100$

Figure 2

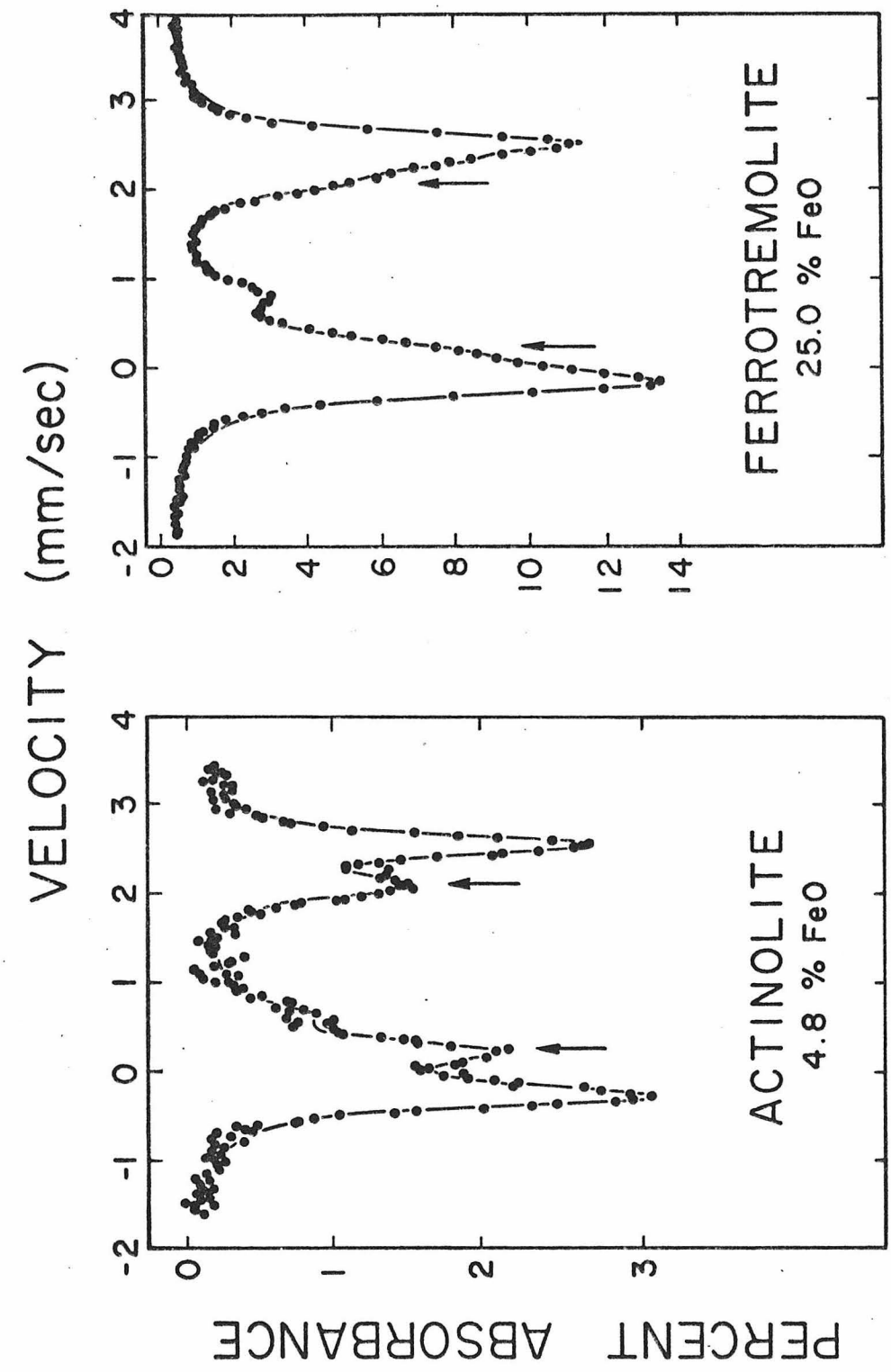
PERCENT ABSORBANCE
VELOCITY (mm/sec)
ACTINOLITE
4.8 % FeO
FERROTREMOLITE
25.0 % FeO

Figure 3

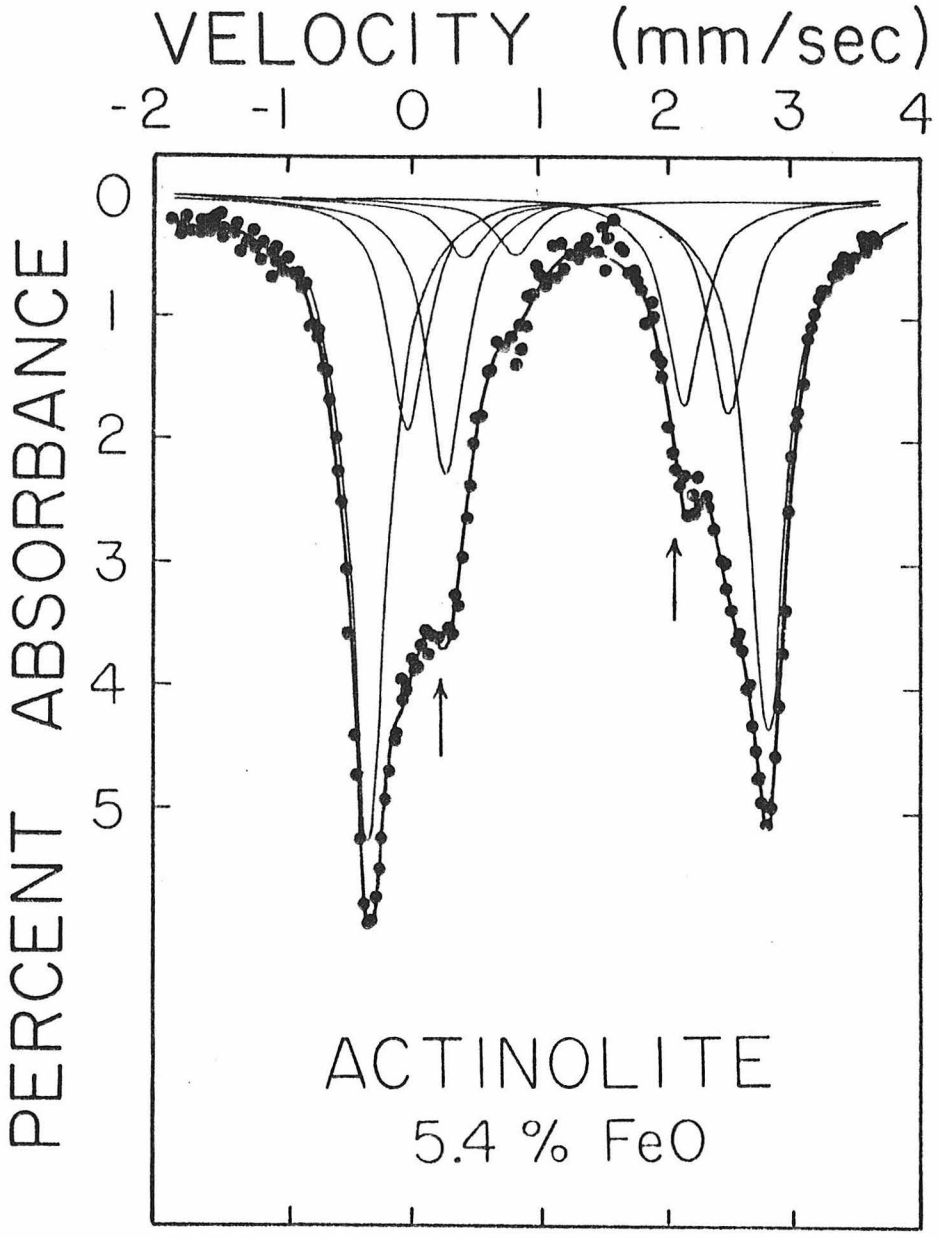
VELOCITY (mm/sec)
-2 -1 0 1 2 3 4
PERCENT ABSORBANCE
0
1
2
3
4
5
ACTINOLITE
5.4 % FeO

Figure 4

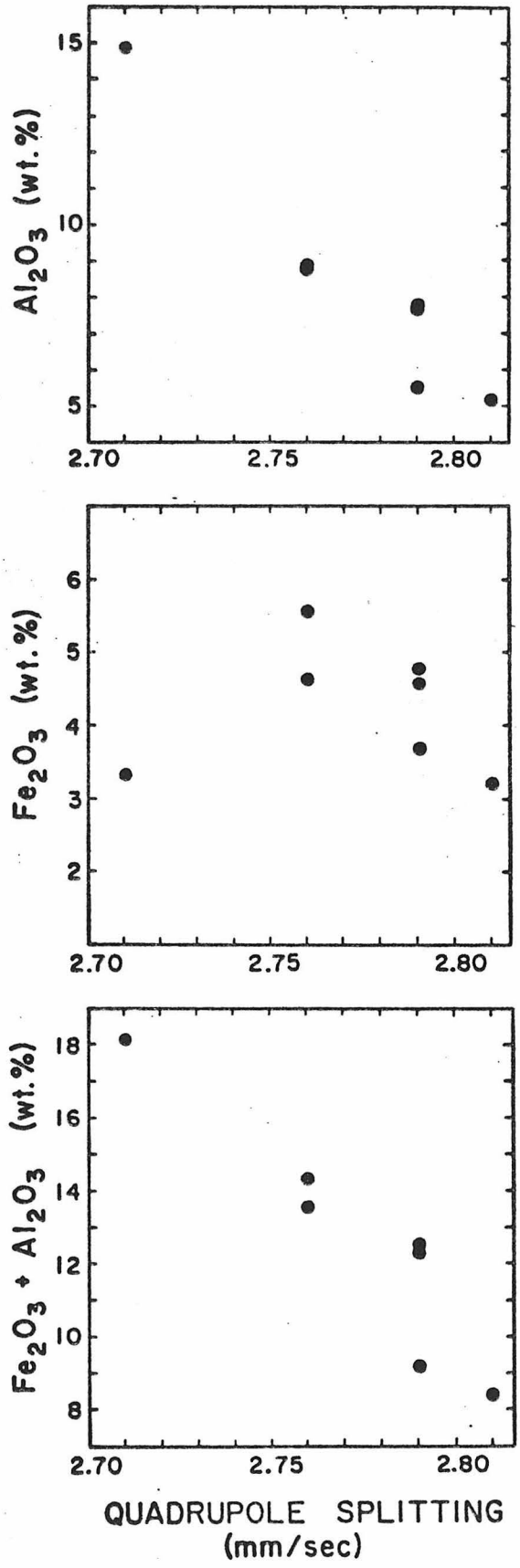
Al_2O_3 (wt.%)
15
10
5
2.70
2.75
2.80
Fe_2O_3 (wt.%)
6
5
4
3
2
2.70
2.75
2.80
$Fe_2O_3 + Al_2O_3$ (wt.%)
18
16
14
12
10
8
2.70
2.75
2.80
QUADRUPOLE SPLITTING
(mm/sec)

Figure 5

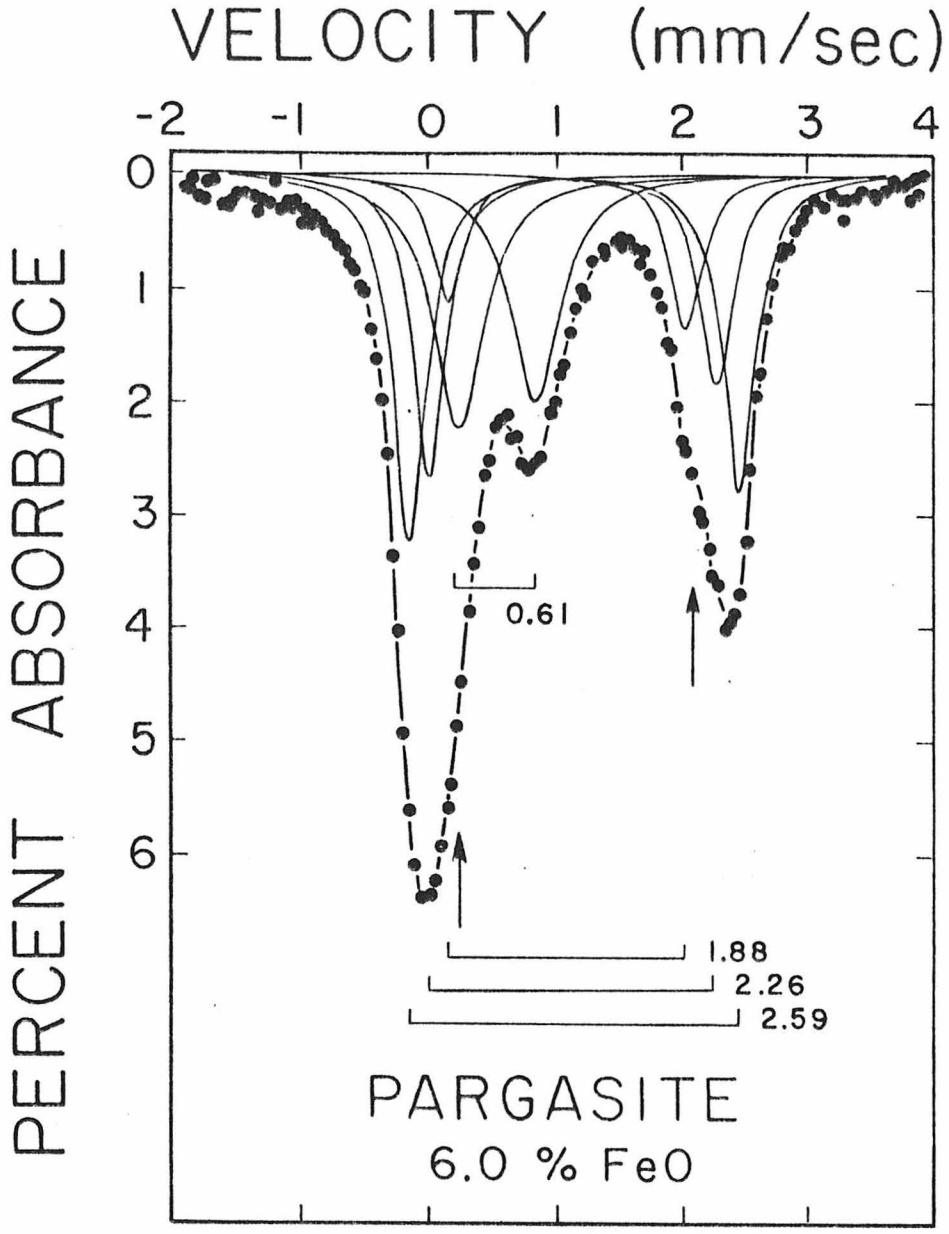
VELOCITY (mm/sec)
-2
-1
0
1
2
3
4
PERCENT ABSORBANCE
0
1
2
3
4
5
6
0.61
1.88
2.26
2.59
PARGASITE
6.0 % FeO

Figure 6

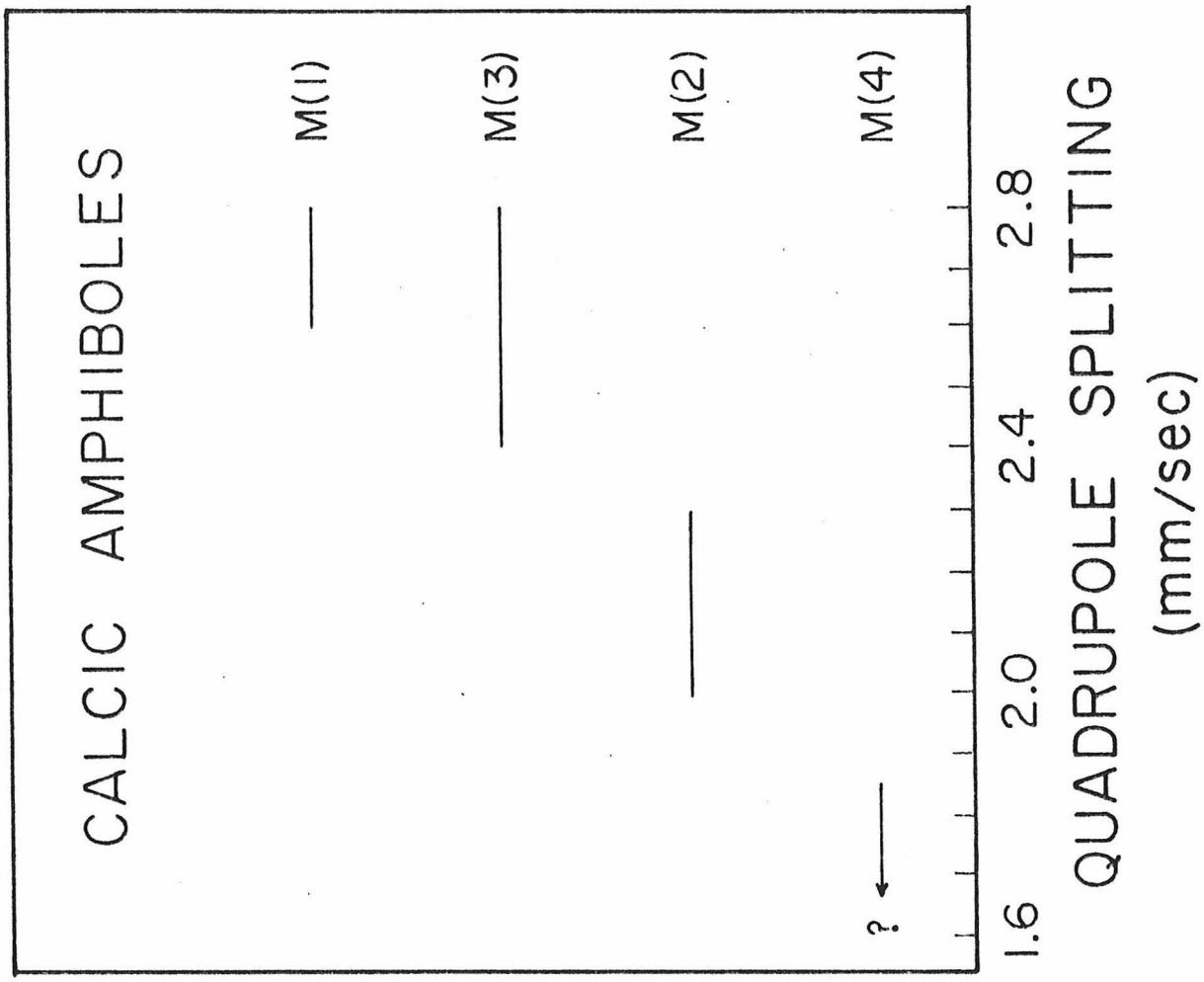
CALCIC AMPHIBOLES
M(1)
M(3)
M(2)
M(4)
?
1.6
2.0
2.4
2.8
QUADRUPOLE SPLITTING
(mm/sec)

Figure 7

CHAPTER 7

OTHER SPECTROSCOPIC FEATURES OF CALCIC AMPHIBOLES

ABSTRACT

Absorption bands in the 800-1300 nm region in the electronic spectra of calcic amphiboles are examined in regard to possible assignments to the M(1), M(2) and M(3) sites. The spectra of Fe^{3+}, Cr^{3+} and Mn^{3+} in calcic amphiboles are presented. The intensity of the Fe^{2+}/Fe^{3+} intervalence charge-transfer band at about 730 nm in γ is found to correlate with the Fe^{3+} concentration.

INTRODUCTION

The study of Fe^{2+} in the electronic absorption spectra of calcic amphiboles has mainly focused on the origin of the band near 1030 nm in β polarization, because of its dominance in most spectra. Goldman and Rossman (1977) presented evidence to show that this band, a weak component of this band in α, and a band near 2470 nm in α are due to Fe^{2+} in the M(4) site. Bands originating from Fe^{2+} in the remaining M sites are considered to occur in the 800-1300 nm region. This study discusses possible site assignments for those bands, and presents spectra of other ions (e.g. Cr^{3+}, Fe^{3+} and Mn^{3+}) in calcic amphiboles. The relationship between Fe^{3+} content and the intensity of the Fe^{2+}/Fe^{3+} intervalence charge-transfer bands in the visible region is also explored.

EXPERIMENTAL METHODS

α and γ spectra were obtained on (010) slabs and the β spectra were obtained on (100) slabs. Samples used in this study include a ferri-richterite from Langban, Sweden (Cal Tech Reference 2482), a chrome tremolite from the Magadi District in Kenya, an actinolite from Cloverdale, California (UCLA MS2843), an Mn-tremolite (hexagonite) from Gouverneur, New York (11/2974), a tremolite from Mt. Bity, Malagasay Republic (CTR8038), an actinolite from Chester, Vermont (CTR6191) and a hornblende from Kragero, Norway (CTR2913). Mössbauer data for the Mt. Bity tremolite occur in Goldman and Rossman (1977) and those for the Chester actinolite are given in Goldman (1977). Electron microprobe data were obtained on crystals from the same hand specimen.

Fe^{2+}

Absorption bands considered to be due to Fe^{2+} in the M(1), M(2) and M(3) sites are most clearly illustrated in the spectra of a pargasite from Finland (Goldman and Rossman, Figure 6), because the features due to M(4) Fe^{2+} are absent. Bands occur at about 870 nm in α and β, 900 and 1100-1300 nm in γ, and at 1150 nm in α. The bands in γ are present in all Fe^{2+}-bearing calcic amphiboles examined, whereas the features in α and β at 870 nm are always less intense than those in γ and are variable in intensity. It is difficult to analyze the relationship of these bands with the band at 1150 nm in α due to the presence of the 1030 nm M(4) band in α in most samples.

The bands in γ are considered to be due to Fe^{2+} mostly in the M(1) site. X-ray (Mitchell et al., 1971) and Mössbauer (Goldman, 1977) analyses of actinolites suggest that Fe^{2+} prefers to enter the M(1) and M(3) sites and discriminates against the M(2) site. Since there are two M(1) sites to every M(3) site, most of the Fe^{2+} among these sites should be in the M(1) site. These results suggest that the bands in γ are probably due to Fe^{2+} mostly in the M(1) site. The M(2) and M(3) sites are slightly smaller than the M(1) site in actinolites (Mitchell et al.). The smaller size of these sites is expected to produce bands at shorter wavelengths, so that Fe^{2+} in either of these sites could be responsible for the band at 870 nm. The variability of these bands with regard to those in γ supports an M(2) assignment. M(2) features are expected to be more intense than absorptions from the centrosymmetric M(3) site (see chapter 11). However, these interpretations must be regarded as tentative without further experimental verification. Although the 870 nm band becomes pronounced in Fe-rich samples, this is consistent with more

Fe^{2+} entering either the M(2) or M(3) site.

Fe^{3+}

The spectra of most calcic amphiboles contain a sharp band at about 440 nm which has been attributed to Fe^{3+} by Goldman and Rossman. This is supported from the β spectrum of a ferri-richterite from Langban, Sweden containing 2.3 percent Fe (Figure 1). A wet-chemical analysis of a richterite from this locality (Deer et al., 1966, page 153) reports only Fe^{3+} to be present. This is confirmed by the absence of any Fe^{2+} features in the 800-1300 nm region in Figure 1. The broader bands at about 800 and 600 nm can be assigned to the $^6A_{2g} \rightarrow {}^4T_{1g}$ and $^6A_{2g} \rightarrow {}^4T_{2g}$ spin-forbidden transitions and the sharp band at 440 nm is assigned to the $^6A_{2g} \rightarrow (^4A_{1g}, {}^4E_g)$ spin-forbidden transition. Assuming that all of the Fe^{3+} resides in one site, the ε values for these bands are 0.6, 0.3 and approximately 3.5, respectively. The ε value for the $(^4A_{1g}, {}^4E_g)$ band is greater than the value expected for completely isolated Fe^{3+} ions (Rossman, 1975), which may suggest Fe^{3+} clustering in calcic amphiboles.

Cr^{3+}

The spectra of a chrome-tremolite from Kenya containing 0.22 percent Cr^{3+} are presented in Figure 2. Cr^{3+} bands are interpreted using the assignments for Cr^{3+} in emerald by Wood (1965). The bands in the 400-500 and 600-700 nm regions are assigned to the $^4A_{2g} \rightarrow {}^4T_{1g}$ and $^4A_{2g} \rightarrow {}^4T_{2g}$ spin-allowed transitions, respectively, and the sharp bands at 687 and 695 nm are assigned to spin-forbidden $^4A_{2g} \rightarrow (^2E_g, {}^2T_{1g})$ transitions. The polarization of the Cr^{3+} bands and the different energies of the components of each main band probably represent the effect of a low

symmetry crystalline field removing the degeneracy of the quartet triplet states, as has been suggested in emerald by Wood.

The ε values for the $^4T_{1g}$ and $^4T_{2g}$ bands in α, β and γ are determined to be 24 and 27, 41 and 41, and 18 and 9, respectively, assuming that the Cr^{3+} is in one site. From ε values of this magnitude, it only requires a few tenths weight percent Cr^{3+} to intensify the green color in calcic amphiboles. Upon examining a number of actinolites for Cr^{3+}, a sample from Cloverdale, California was found to contain dark green veinlets surrounding cracks in a light green actinolite host. Spectra of these different areas (Figure 3) show that the darker green areas are enriched in Cr^{3+} relative to the host. The dark green areas also contain more Fe^{2+}, but it appears that Fe^{2+} became relatively more enriched in the M(4) site than in the other M sites.

Mn^{3+}

The spectra of an Mn-tremolite (hexagonite) from Gouverneur, New York containing 0.6 percent Mn are presented in Figure 4. The bands in the 500-650 nm region that produce the purple color of this sample are due to electronic transition of Mn^{3+}. The multiplicity of bands in this region likely results from Jahn-Teller splitting of the excited ^5E_g state. The ε values for these bands are approximately 3.3. The presence of sharp bands in the 400-500 nm region may represent spin-forbidden transitions of Mn^{3+} or Mn^{2+}, so that the calculated value of ε must be taken as a lower limit due to the possible presence of Mn^{2+}.

Fe^{2+}/Fe^{3+} INTERVALENCE CHARGE-TRANSFER

Absorption bands near 680 nm in β and 730 nm in γ have been attributed to intervalence charge-transfer between Fe^{2+} and Fe^{3+} (Burns, 1970; Faye

and Nickel, 1970). These bands are responsible for the color and pleochroism observed in most calcic amphiboles (without significant Cr^{3+}). Burns suggested that the intensity of these bands is related to the Fe^{3+} content of the sample. A correlation between the Fe^{3+} content and the band intensity would enable Fe^{3+} contents to be determined from polarized optical spectra. To test this possibility, the molar concentrations of Fe^{3+} were determined for three calcic amphiboles using Mössbauer and electron microprobe data. Densities were taken from samples of similar chemistry in Leake (1968). The Fe^{3+} concentration is plotted against the intensity of the 730 nm band in γ in Figure 5. The intensity of the band for sample 2 has been adjusted for the presence of Cr^{3+} using the intensity of the Cr^{3+} band in α and the intensity relationship between the Cr^{3+} bands in α and γ in Figure 2. The resulting correlation in Figure 5 appears to be linear, although the errors in determining intensities are large due to difficulties in estimating the contribution of the absorption tail coming from the ultraviolet region. From this relationship, the molar concentration of Fe^{3+} in calcic amphiboles can be determined from the intensity of the intervalence charge-transfer band in γ using an ε value of 40.

REFERENCES CITED

Burns, R.G. (1970) Mineralogical Applications of Crystal Field Theory. Cambridge University Press.

Deer, W.A., R.A. Howie and J. Zussman (1966) An Introduction to the Rock-Forming Minerals. John Wiley and Sons, Inc., New York.

Faye, G.H. and E.H. Nickel (1970) The effect of charge-transfer processes on the colour and pleochroism of amphiboles. Can. Mineral. 10, 616-635.

Goldman, D.S. (1977) A Re-evaluation of the Mössbauer spectroscopy of calcic amphiboles. Am. Mineral. (submitted).

Goldman, D.S. and G.R. Rossman (1977) The identification of Fe^{2+} in the M(4) site of calcic amphiboles. Am. Mineral. 62, 205-216.

Leake, B.E. (1968) A catalog of analyzed calciferous and subcalciferous amphiboles together with their nomenclature and associated minerals. Geol. Soc. Am. Spec. Pap., No. 98.

Mitchell, J.T., F.D. Bloss and G.V. Gibbs (1971) Examination of the actinolite structure and four other $C_{2/m}$ amphiboles in terms of double bonding. Z. Kristallogr. 133, 273-300.

Rossman, G.R. (1975) Spectroscopic and magnetic studies of ferric iron hydroxy sulfates: Intensification of color in ferric ion clusters bridged by a single hydroxide ion. Am. Mineral.60, 698-704.

Wood, D.L. (1965) Absorption, fluorescence and Zeeman effect in emerald. J. Chem. Phys. 42, 3404-3410.

FIGURE CAPTIONS

1. Room-temperature β spectrum of a ferri-richterite from Langban, Sweden containing 2.3 percent Fe^{3+}. Crystal thickness = 0.2 mm.

2. Room temperature spectra of a chrome tremolite from the Magadi District in Kenya containing 0.2 percent Cr^{3+}. Crystal thickness = 1.0 mm.

3. Room temperature spectra of an actinolite from Cloverdale, California containing dark green regions (dashed lines) in a light green host (solid lines). Crystal thickness = 1.0 mm.

4. Room temperature spectra of a hexagonite from Gouverneur, New York containing 0.6 percent Mn. The spectra suggest that much of this Mn is Mn^{3+}. Crystal thickness = 3.0 mm.

5. Correlation of the intensity of the Fe^{2+}/Fe^{3+} intervalence charge-transfer band at 730 nm in γ and the molar concentration of Fe^{3+} in calcic amphiboles. 1. Tremolite, Mt. Bity, Malagasay Republic. 2. Actinolite, Chester, Vermont. 3. Hornblende, Kragero, Norway.

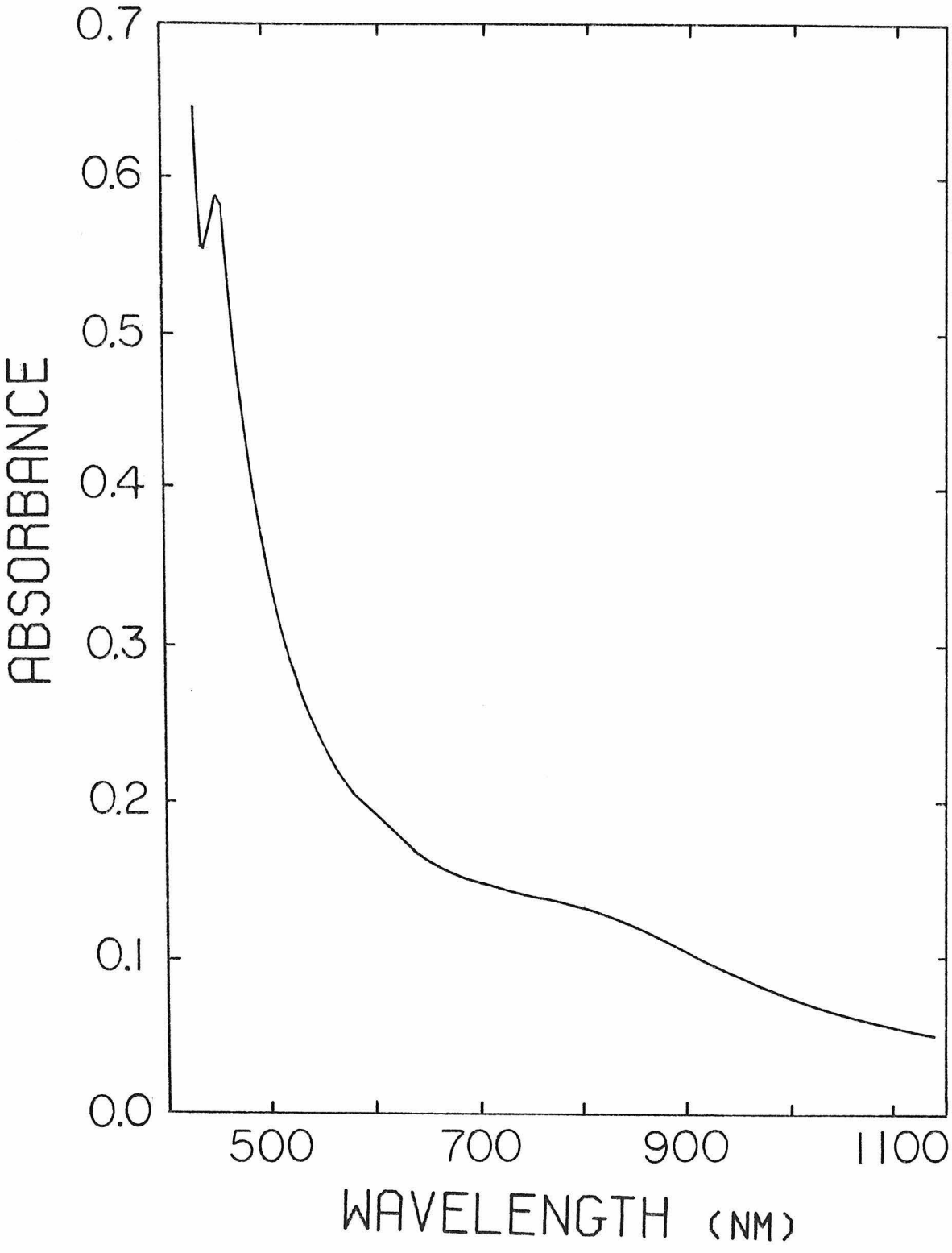
0.7
0.6
0.5
0.4
0.3
0.2
0.1
0.0
ABSORBANCE
500
700
900
1100
WAVELENGTH (NM)

Figure 1

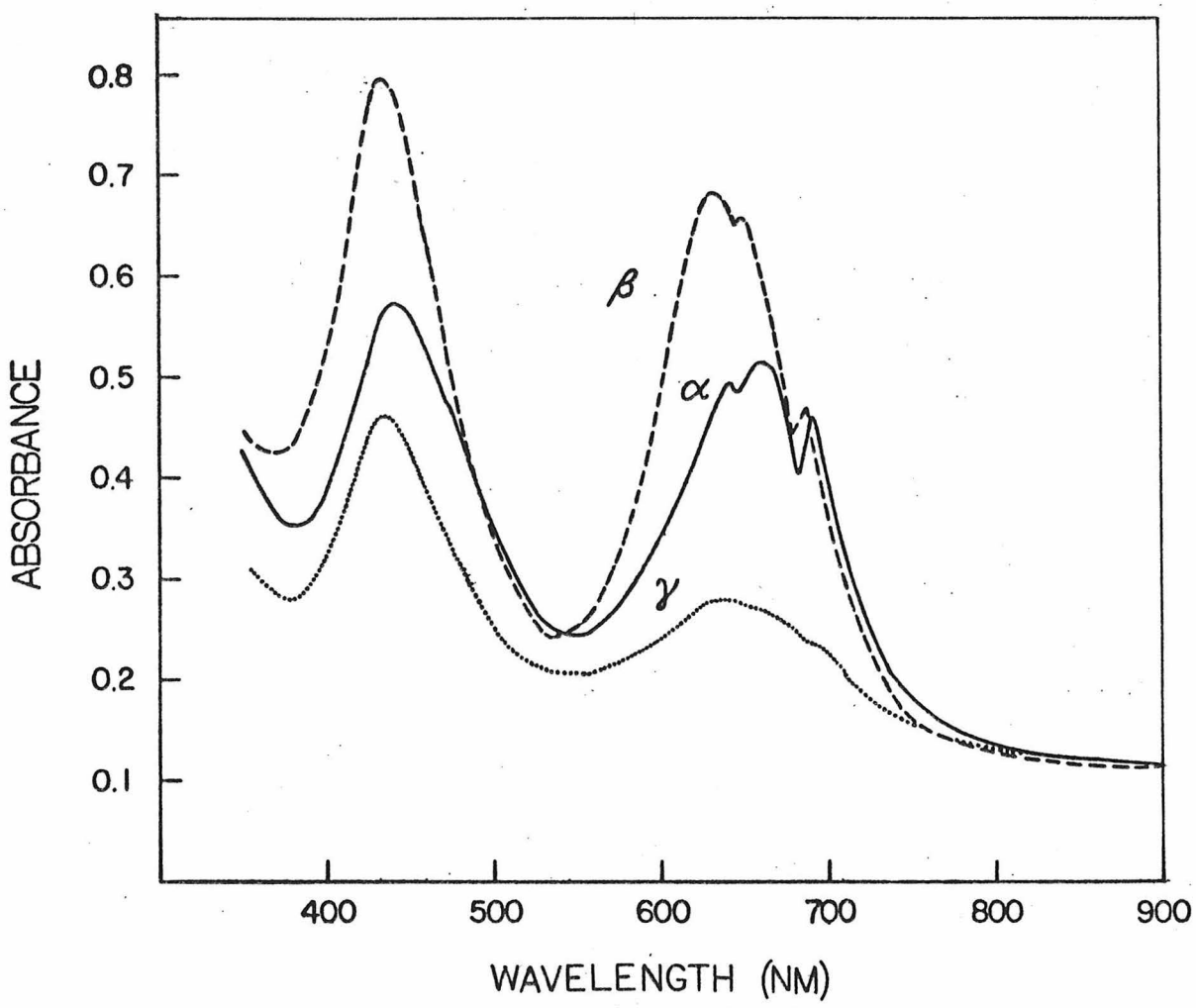
ABSORBANCE
0.8
0.7
0.6
0.5
0.4
0.3
0.2
0.1
β
α
γ
400
500
600
700
800
900
WAVELENGTH (NM)

Figure 2

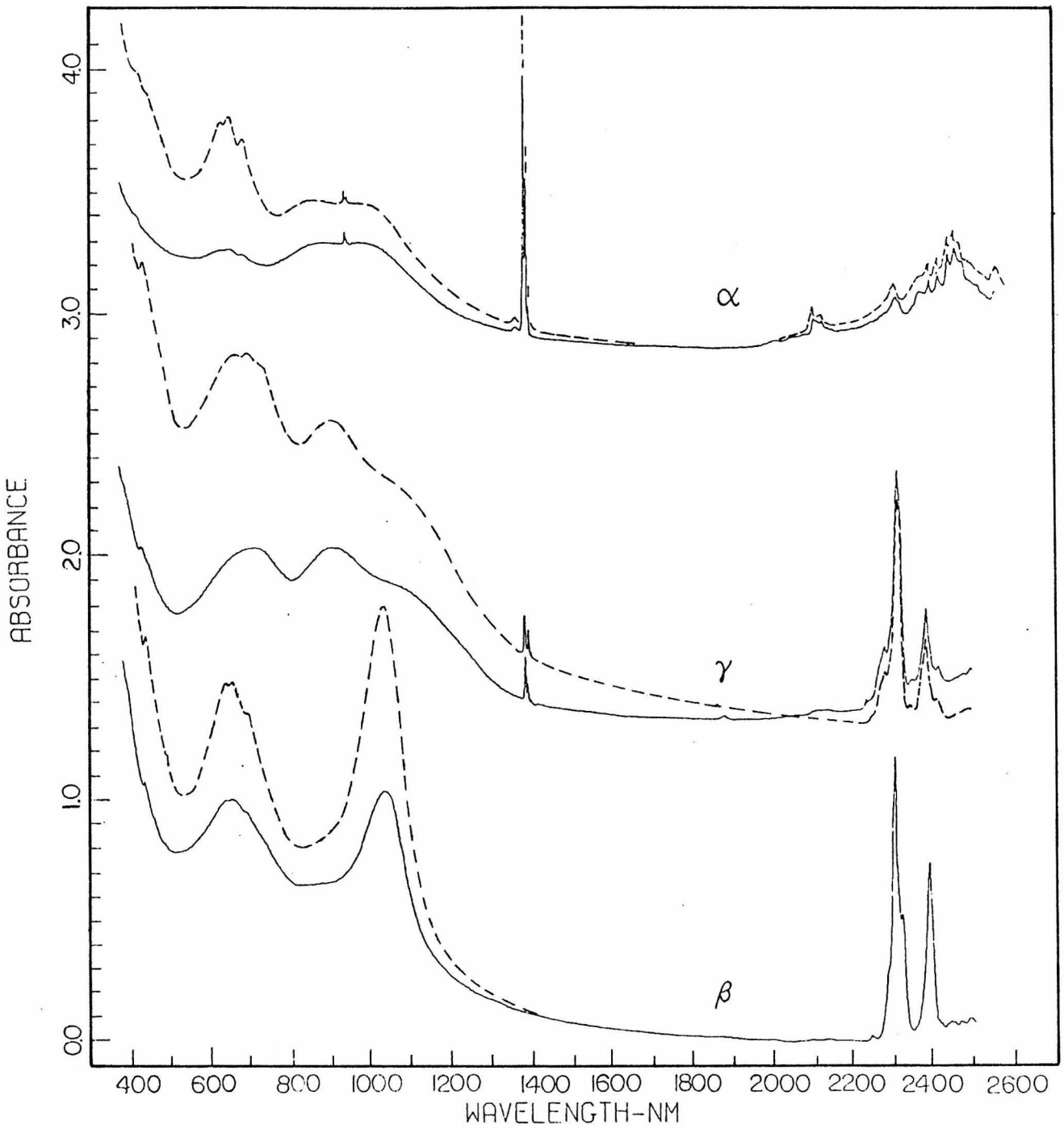
ABSORBANCE
0.0
1.0
2.0
3.0
4.0
400
600
800
1000
1200
1400
1600
1800
2000
2200
2400
2600
WAVELENGTH-NM
α
γ
β

Figure 3

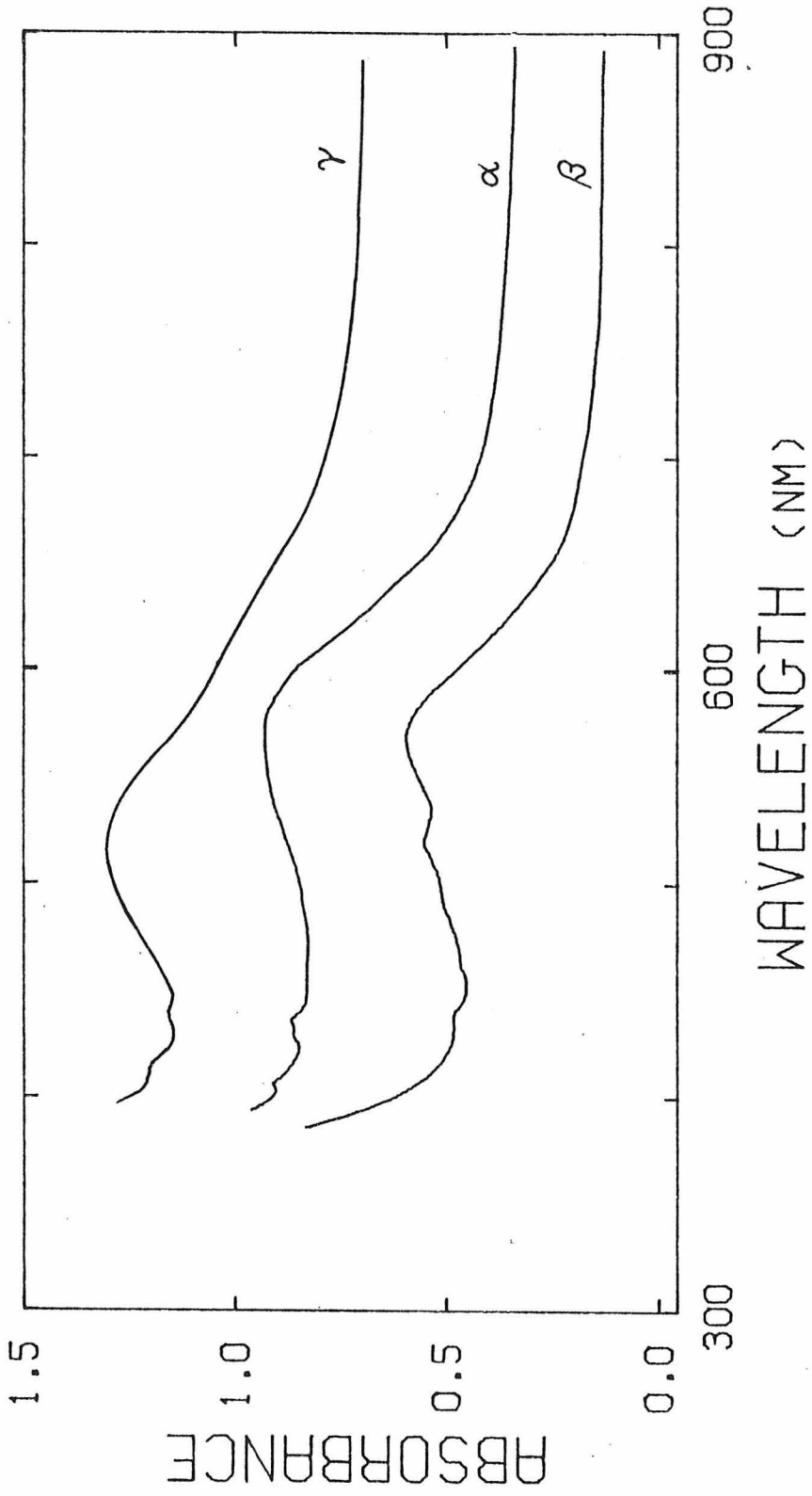

Figure 4

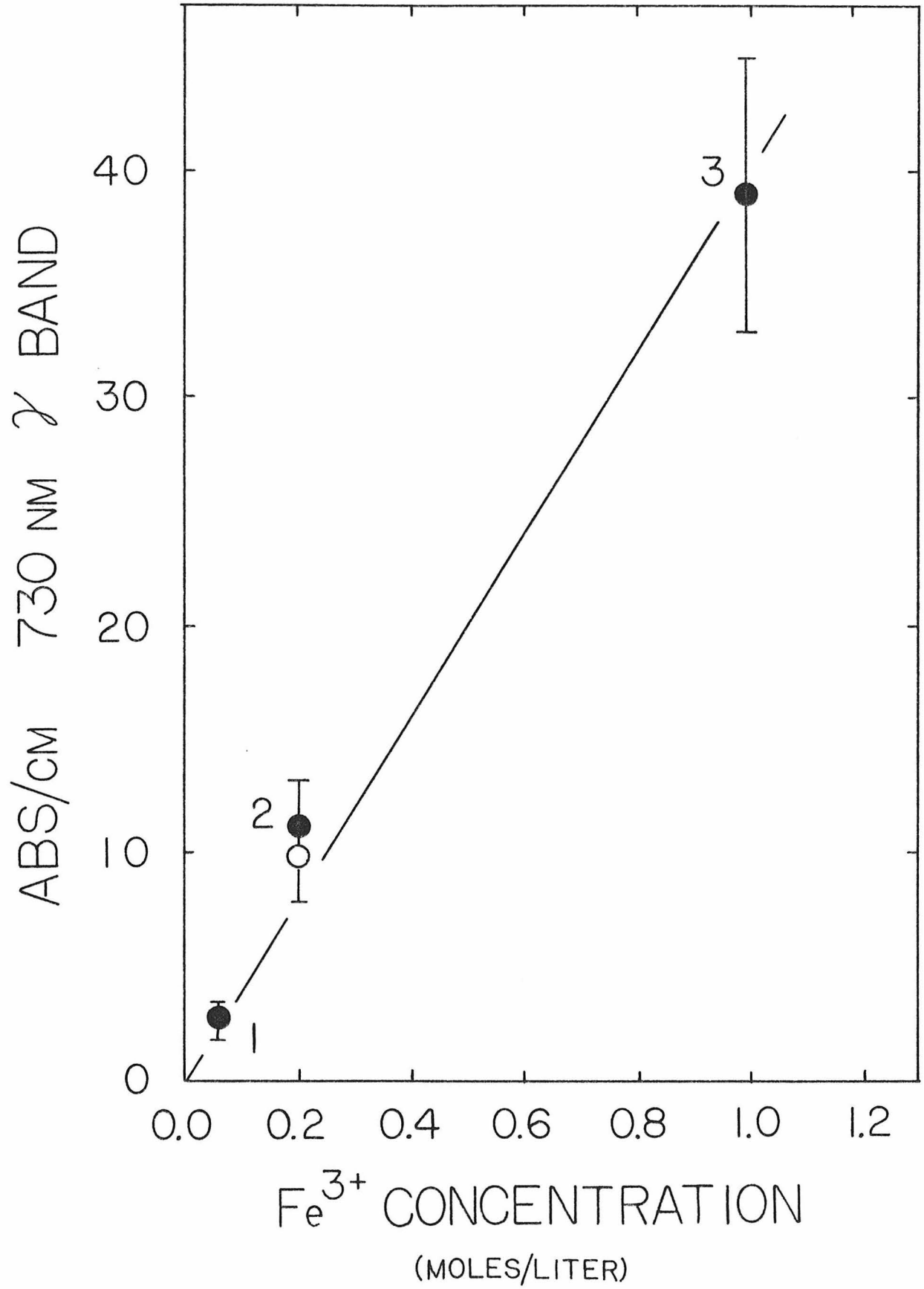
ABS/CM 730 NM γ BAND
0
10
20
30
40
0.0
0.2
0.4
0.6
0.8
1.0
1.2
1
2
3
Fe3+ CONCENTRATION
(MOLES/LITER)

Figure 5

CHAPTER 8

CHANNEL CONSTITUENTS IN CORDIERITE

Submitted to The American Mineralogist
Co-authors: George R. Rossman and W.A. Dollase

ABSTRACT

Chemical, optical and infrared absorption, Mössbauer and X-ray data are reported for eight cordierite samples. Fe^{2+} in the octahedral and channel sites is identified in optical and Mössbauer spectra, which indicate that less than 5 percent of the total iron is Fe^{2+} in the channels. The single-crystal Mössbauer data of Duncan and Johnston (1974) are reinterpreted. Two types of H_2O are identified and are found to be oriented in the (100) plane with their H-H directions parallel to [001] (Type I) and [010] (Type II). Type II H_2O is found to correlate to the amount of cations in the channels. Optical spectra provide a measure of the hexagonality of cordierite, but these measurements are not correlated with the distortion index, Δ. The color and pleochroism are suggested to arise from intervalence charge-transfer between octahedral Fe^{2+} and channel Fe^{3+}. The strong enhancement of intervalence intensity after dehydration is interpreted in terms of migration of Fe^{3+} from the six-membered tetrahedral rings to the walls of the channel cavities. It is proposed that migration of Na^{+} from the rings into the cavities is primarily responsible for changes in the distortion index which accompany dehydration. ε values for the Fe^{2+} and H_2O absorption bands are determined.

INTRODUCTION

The structure of cordierite, $(Mg,Fe)_2Al_4Si_5O_{18}$, consists of six-membered rings of corner-shared Si and Al tetrahedra linked by additional tetrahedra and octahedra. The stacking of the rings forms large cavities that extend parallel to [001] (Gibbs, 1966). Ionic and molecular species such as water, carbon dioxide, argon, helium, and alkaline earth and alkali metal ions have been found in the cavities (Damon and Kulp, 1958; Sugiura, 1959; Smith and Schreyer, 1962; Gibbs, 1966: Farrell and Newnham, 1967; Tsang and Ghose, 1972; Zimmerman, 1972; Cohen et al., 1977).

In a recent Mössbauer study, Duncan and Johnston (1974) concluded that Fe^{2+} also occurs in the channel cavities. Optical absorption spectra should also indicate the occurrence of Fe^{2+} in mulitiple sites. However, the optical spectra of cordierite have previously been interpreted only in terms of Fe^{2+} in the octahedral site (Farrell and Newnham, 1967; Faye et al., 1968; Faye, 1972; Smith and Strens, 1976).[1] This discrepancy between the Mössbauer and optical interpretations of cordierite has not been explained.

This paper reports the findings of a combined optical absorption, Mössbauer and X-ray study of eight cordierite samples to 1) identify octahedral and channel Fe^{2+} in optical and Mössbauer spectra, 2) determine the site distribution of iron, 3) re-interpret the single-crystal Mössbauer data of Duncan and Johnston (1974), 4) identify two types of water in the channels and determine their orientation, 5) evaluate the effect of structural state upon the optical spectra, and 6) examine the origin of color and pleochroism.

EXPERIMENTAL METHODS

Single slabs of cordierite were cut and polished using conoscopic interference figures for orientation. The optic orientation for cordierite given in Strunz *et al*. (1971) is *a*(~17Å) = γ, *b*(~9.7Å) = β and *c*(~9.3Å) = α. Thicknesses for the optical slabs were determined with a micrometer and the thicknesses for the slabs used for infrared spectra were also checked by band intensity ratios and by propping them on their edges, placing them next to a standard of known thickness, and measuring their thickness in a scanning electron microscope. Data reduction for both the optical and Mössbauer spectra have been described previously (Rossman, 1975b; Goldman and Rossman, 1977a). Heating experiments were conducted in air at 200, 500, 800, 900, 1150 and 1250 °C for 15.0, 16.3, 6.3, 0.5, 1.0 and 2.0 hours, respectively. Heating experiments on other slabs of different thicknesses produced nearly identical results. Densities for some samples in Table 1 were calculated from the following:

$$\rho(g/cm^3) = 0.00036[X]^2 + 0.00394[X] + 2.572$$

which is a least-squares solution to the data for 45 samples in Leake (1960) and Strunz *et al*. where X = ($FeO + Fe_2O_3$) in weight percent.

The Mössbauer spectra of single (001) slabs of samples 3 (1.128 mm thick) and 8 (0.180 mm thick) were obtained on a constant acceleration spectrometer with a Kankeleit-type drive system in which the velocity increment was approximately 0.03 mm/sec/ch. The results of Duncan and Johnston (1974) indicate that these thicknesses represent ideally thin absorbers. Approximately 1.8×10^6 and 2.3×10^6 counts per channel were collected in the off-resonance region for these two samples, respectively, and nearly 4.3×10^6 counts were collected for the powder spectrum of sample 3. The velocity calibration was determined

using laboratory foils and the spectra and spectral parameters are reported relative to iron metal at room temperature.

The distortion index (Δ) in Table 1 was determined from repeated scans in the 28.5-30.5^{o} 2θ region in X-ray diffractograms of powdered material where $\Delta = (2\theta_{(131)} - (2\theta_{(421)} + 2\theta_{(511)})/2)$. Electron microprobe data were obtained in the area on the slab that the optical spectra were taken for each of the eight samples and the results are presented in Table 1. Emission spectrograph analyses of samples 2, 5 and 8 indicate less than 0.01 percent boron and beryllium.

CHANNEL Fe^{2+}

Optical spectra assignment

The optical spectra of a low-Fe cordierite (Figure 1) has absorption bands near 995 nm and 1170 nm in α polarization and 935 nm and 570 nm in β and γ polarizations that were assigned to Fe^{2+} in the octahedral site by Farrell and Newnham (1967). Faye et al. (1968) alternatively suggested that the bands near 570 nm, which produce the intense color and pleochroism exhibited by cordierite, originate from intervalence charge-transfer between octahedral Fe^{2+} and tetrahedral Fe^{3+}. Faye (1972) indicated that the barycenter (mean) energy for all bands, approximately 13,000 cm^{-1}, is much larger than expected for the size of the octahedral site. A charge-transfer assignment for the 570 nm band results in a barycenter energy for the remaining bands of about 9800 cm^{-1}, which is in better agreement with spectral data for Fe^{2+} in other sites of this size.

Certain problems remain with the Fe^{2+} assignment because there are too many absorption bands arising from the octahedral site. Only two spin-allowed electronic transitions to the split ^5E_g states are expected in the near-infrared region. The observation of three bands at 935, 995 and 1170 nm suggests that they originate from more than one source. To test this possibility, the intensity relationships among these bands can be compared to those in an Fe-cordierite (sekaninaite) in Figure 2. It is evident that the two bands in α retain the same intensity relationship between each other, which indicates a common origin. These bands are more intense than the bands in β and γ, contrary to the relationship in Figure 1. Hence, the bands in β and γ originate from a different Fe^{2+} source.

Site assignments for the various absorption bands can be clarified utilizing the stoichiometry of each sample, which suggests that most of the iron is in the octahedral site (Table 1). Consequently, only the intensities of the bands

due to octahedral Fe^{2+} are expected to correlate with the total iron content among these samples. The intensities of the band in α near 1170 nm and those in β and γ near 935 nm are plotted against the total iron concentration in Figure 3. Gaussian analyses of the α envelope was performed on five samples and the resulting intensities of the two components are also shown. Their nearly linear correlation with the total iron concentration suggests that they are due to Fe^{2+} in the octahedral site. The erratic variation for the bands in β and γ is consistent with variable amounts of Fe^{2+} in a second site.

The shoulders in β and γ near 1250 nm (Figure 2) are pronounced only in the high-Fe samples. The shoulders are attributed to components of the 1250 nm transition of octahedral Fe^{2+} which is most intense in α.[2] The different γ/β intensity ratios for samples 7 and 8 (Table 1) suggest that a component of the 995 nm α band is present in β and γ. For samples 7 and 8, the intensities of the β and γ bands are corrected for this component using the intensity of the shoulder and the observed intensity relationship for the bands in α (shown in Figure 3 by the partially filled triangles and squares, respectively). The resulting γ/β ratios are more consistent with those for other samples.

The second Fe^{2+} site in cordierite could be either a tetrahedral site or a position in the channel. The nearly linear correlation between Gaussian intensity of octahedral Fe^{2+} absorption bands in α and the total iron concentration suggests that a small amount of Fe^{2+} in the second site produces the intense bands in β and γ. Hence, the molar absorptivity (ε) for Fe^{2+} in this site must be very large, but large ε values can represent Fe^{2+} in either tetrahedral sites or large, distorted sites. Goldman and Rossman (1977b) indicated that Fe^{2+} in large, distorted sites produce absorption bands in both the 1000 and 2000 nm

regions. Bands in the 2000 nm region are less intense and are polarized in a different direction than the band near 1000 nm. The band near 2230 nm in α (Figures 1 and 2) has these characteristics to represent the electronic transition to the remaining $^5\underline{E}_g$ component of Fe^{2+} in the second site. The excellent correlation between this band and those in β and γ (Figure 4) supports their assignment to the second site. Note that the corrected bands in β and γ for samples 7 and 8 fall on the respective trends. The observation that the bands near 950 and 2230 nm are both produced by Fe^{2+} in the second site suggests that the second site is a position in the channel. Fe^{2+} in a tetrahedral site is not expected to produce absorption bands at wavelengths below about 1500 nm. The crystal-field splitting of $\underline{E}_g$ state for channel Fe^{2+} is about 6200 cm^{-1}, which is nearly three times the splitting observed for octahedral Fe^{2+} in cordierite. The barycenter energy for channel Fe^{2+} (~7200 cm^{-1}) suggests an average metal-oxygen bond distance of 2.26 Å for the coordination site from Faye's (1972, Figure 3) correlation.

Duncan and Johnston (1974) determined that 20 percent of the total iron content for sample 4 is Fe^{2+} in the channel cavities. However, a significant but variable channel iron content would not result in a linear correlation for the octahedral Fe^{2+} bands with total iron concentration. To examine the apparent discrepancy between the two spectroscopic techniques, Mössbauer spectra of single crystals of samples 3 and 8 have been obtained to identify channel Fe^{2+} resonance so that the peak locations can be used to determine the site distribution from the powder spectrum of sample 3.

Site distribution from Mössbauer spectra

Mössbauer spectra of (001) slabs of samples 8 and 3 are presented in Figure 5. The spectrum of sample 4 with this orientation appears in Duncan and Johnston (1974, Figure 3). The shoulder near 2.0 mm/sec is pronounced only in

low-Fe samples suggesting that it is due to channel Fe^{2+}, because the channel: octahedral Fe^{2+} ratio is more favorable in these samples. The smaller quadrupole splitting suggested from the Mössbauer spectra is consistent for Fe^{2+} in a distorted channel site. Heating experiments also support this assignment. Duncan and Johnston found that as (001) slabs were heated in air to temperatures up to 1380 °C, Fe^{3+} resonance appeared in the low-velocity region with a concomitant disappearance of the shoulder near 2.0 mm/sec. Our optical spectroscopic examination of slabs heated in air to similar temperatures indicated that proportionately more channel Fe^{2+} was oxidized. The assignment of the shoulder to Fe^{2+}/Fe^{3+} intervalence charge-transfer by Pollack (1976) is unlikely because the charge-transfer optical bands near 570 nm increase upon heating. It is also noted that the intensity ratio of the octahedral Fe^{2+} resonance at 0.1 and 2.4 mm/sec for both single crystal spectra are the same. This indicates that the remaining channel Fe^{2+} peak in the low velocity region does not have significant intensity.

Single crystal orientation affects the probability of observing each quadrupole transition differently, but does not affect their energy (Zory, 1965). Therefore, the position of the shoulder can be used as a guideline to analyze the powder spectrum of sample 3 (Figure 5). The equal intensities of the main peaks indicates a randomly oriented powder. In fitting the spectrum to two doublets with equal area and halfwidth constraints, the channel Fe^{2+} peak in the high velocity region freely converged to within 0.01 mm/sec of the position determined in the single crystal spectrum. The resulting octahedral: channel Fe^{2+} ratio of 17:1 is much different than the 4:1 ratio determined for sample 4 by Duncan and Johnston.[3] Samples 3 and 4 have nearly the same total iron content, but sample 3 has more intense channel Fe^{2+} optical bands, which indicates that the results of Duncan and Johnston are incorrect. They determined the site

distribution in Mössbauer spectra of heated powders assuming only channel Fe^{2+} was oxidized. However, optical spectra of slabs heated to similar temperatures demonstrate the partial oxidation of octahedral Fe^{2+}, as will be discussed in a later section.

Duncan and Johnston determined the orientation of the electric field gradient (EFG) for iron in each site. Their computational method depends on an *a priori* knowledge of the correct site distribution, but the results of this study indicate that the site distribution which they used is incorrect. Therefore, their resulting EFG orientations are also incorrect. This problem will now be reanalyzed.

SINGLE CRYSTAL MÖSSBAUER ANALYSIS

The electric field gradient (EFG) at a particular site within a crystal is a traceless, symmetric, second-order tensor (Zory, 1965). It is described by the magnitudes of the axial components and by their orientation relative to the crystal axes. The principal axes are conventionally chosen so that the magnitudes of the axial components in ascending order are $|V_{xx}| \leq |V_{yy}| \leq |V_{zz}|$ where $(V_{zz} + V_{yy} + V_{xx}) = 0$. Only the relative magnitudes of the axial components are recovered from Mössbauer observations. Therefore, only one variable is needed to describe any inequality among them. This variable is referred to as the asymmetry parameter, η, which is equal to $(V_{xx} - V_{yy})/V_{zz}$. The sign of the EFG is determined by the sign of V_{zz}.

The two absorption lines of a quadrupole split ^{57}Fe doublet represent two separate nuclear transitions ($\pm 3/2 \rightarrow \pm 1/2$ and $\pm 1/2 \rightarrow \pm 1/2$) whose probabilities depend upon the orientation of the gamma-ray beam relative to the EFG at that site. The relative intensities (peak areas) of the two transitions are given by Zory (1965) as; $I(3/2)=4(1+\eta^2/3)^{\frac{1}{2}} +[3+\eta)(g\cdot z)^2 +2\eta(g\cdot x)^2-\eta-1]$ and $I(1/2)=4(1+\eta^2/3)^{\frac{1}{2}} -[(3+\eta)(g\cdot z)^2 + 2\eta(g\cdot x)^2 -\eta-1]$, where $(g\cdot x)$, etc. are the direction cosines of the gamma-ray beam relative to the EFG axes. A positive value of V_{zz} results in the $\pm 3/2 \rightarrow \pm 1/2$ transition lying at higher energies while a negative V_{zz} means that the lower energy line represents this transition.

The EFG orientation is given by specifying the orientation of its orthogonal principal axis set (x,y,z) relative to a conveniently chosen orthogonal reference axis set (a,b,c). For cordierite, the reference axis set may be chosen as coincident with the orthorhombic crystal axes, $\underline{a}$, $\underline{b}$, $\underline{c}$. The orientation is specified by the matrix of direction cosines;

$$\underline{R} = \begin{pmatrix} x\cdot\underline{a} & x\cdot\underline{b} & x\cdot\underline{c} \\ y\cdot\underline{a} & y\cdot\underline{b} & y\cdot\underline{c} \\ z\cdot\underline{a} & z\cdot\underline{b} & z\cdot\underline{c} \end{pmatrix}$$

where $x \cdot \underline{a}$ is the cosine of the angle between principal axis, x, and crystal axis, $\underline{a}$, etc. The EFG orientations at two different, symmetry-related sites are given by;

$$\underline{R}' = \underline{R}\ \underline{S}$$

where $\underline{S}$ is the symmetry operation which relates the site at coordinates u'v'w' to the site at coordinates, uvw, such that;

$$[u'v'w'] = [uvw]\underline{S}.$$

Only those symmetry operations which produce different EFG orientations need be considered; consequently, translational or inversion components of symmetry operations can be ignored. The result of having several different EFG orientations within a crystal is that the equations giving the intensities of the two transitions will then be a sum of terms, as given above, for each of the EFG orientations present. For iron in the octahedral site in cordierite, there are two EFG orientations related by a two-fold rotation about the crystallographic $\underline{c}$ axis.

At a site within the crystal, the EFG must be invariant to the symmetry of that site, i.e. $\underline{R}\ \underline{S}$ must give the same orientation as $\underline{R}$ for each symmetry element of that site. For example, the octahedral site lies on a two-fold axis which is parallel to [100]. As a result, <u>one</u> of the principal axes of the EFG <u>must</u> lie along [100]. For analogous cases see e.g., vivianite, (Greenwood and Gibb, 1971, p. 137), FeF_2 (Wertheim, 1961) or sodium nitroprusside (Grant, <u>et</u>. <u>al</u>., 1969).

A least-squares refinement routine has been programmed to fit the observed Mössbauer intensities to those calculated as a function of the asymmetry parameter, η, and the orientation matrix, $\underline{R}$. For this purpose, the terms $(g \cdot x)$ and $(g \cdot z)$ in the intensity equations given above are replaced with expressions

involving the orientation matrix, viz;

$$\begin{pmatrix} g\cdot x \\ g\cdot y \\ g\cdot x \end{pmatrix} = \underline{R} \begin{pmatrix} g\cdot \underline{a} \\ g\cdot \underline{b} \\ g\cdot \underline{c} \end{pmatrix}$$

where the direction cosines of the gamma-ray beam relative to the reference (crystal) axes are known for each Mössbauer spectrum. This refinement procedure has been applied to the fifteen observed intensities reported by Duncan and Johnston (1974). Although they assigned 79% of the total iron to the octahedral site and 20% to a channel site, this study has concluded that their cordierite has about 95% of the total iron in the octahedral site. Their observations are therefore considered to be due to ^{57}Fe atoms in the set of symmetry equivalent octahedral sites only, with contributions to the area from channel iron being negligible. A constraint on the refinement of the orientation matrix is that one of the principal axes must parallel [100] (a constraint not applied by Duncan and Johnston). The value of the asymmetry parameter will lie between zero and one when the axes are labeled in ascending order. It is computationally expedient to refine η without constraint on its value and then to rearrange the axial labels to give their conventional order. This procedure eliminates having to refine six models differing in the choice of the sign of V_{zz} and which principal axis is constrained to lie along [100].

The results of the refinement of the Duncan and Johnston observations are summarized in Table 2. The model results in $\eta = 0.16 \pm .05$ and V_{zz} being negative. The two symmetry-related orientation matrices are;

$$\begin{pmatrix} 1.0 & 0.0 & 0.0 \\ 0.0 & .9044 & -.4267 \\ 0.0 & .4267 & .9044 \end{pmatrix} \quad \text{and} \quad \begin{pmatrix} 1.0 & 0.0 & 0.0 \\ 0.0 & .9044 & .4267 \\ 0.0 & .4267 & -.9044 \end{pmatrix}$$

which results in the x principal axis of the EFG lying along [100]. The probable error in orientation of the EFG is about 2°.

The line intensities calculated from this model agree with those observed by Duncan and Johnston and show significantly better agreement than their calculated values. It should be pointed out that the EFG axes reported by Duncan and Johnston are not orthogonal. The excellent agreement for our model supports the initial interpretation from optical data that essentially all the Fe^{2+} in cordierite is present in the octahedral site. The success of this fit with an EFG axis constrained parallel to [100] further supports the assignment of this iron to the octahedral site.

Because a small amount of the area of the Mössbauer spectrum is due to Fe^{2+} in a second site, EFG calculations made ignoring this contribution must be somewhat in error. To assess the magnitude of this error, a trial calculation was made as follows. If the EFG orientation (and asymmetry parameter) of the second Fe^{2+} site was the same as that of the octahedral site Fe^{2+}, no error in recovering this orientation from the data would occur. Consequently, a "worst case" EFG orientation (and its symmetry equivalent orientations) was chosen for the channel site Fe^{2+} which gave, as far as possible, a doublet asymmetry always opposed to that of the octahedral site doublet. Then, assuming the channel site Fe^{2+} contributed 5% of the total intensity, its effect was subtracted from the Duncan and Johnston observations. The "corrected" Mössbauer data were then refit by least-squares methods yielding a negative V_{zz}, $\eta = 0.07$, $V_{xx} = \underline{a}$ and $z \wedge \underline{b} = 69°$. The differences between the two sets of results for the octahedral site Fe^{2+}, even assuming the worst orientation of the second site EFG, are small, amounting to only about twice the estimated errors in these parameters.

WATER

Orientation

It was suggested from early studies of water in cordierite that it is present as molecular H_2O and as $(OH)_4$ groups replacing some of the tetrahedral SiO_4 groups (Sugiura, 1959; Iiyama, 1960). Subsequently, Schreyer and Yoder (1964) suggested from infrared spectra that molecular H_2O is the sole hydrous component. Later studies confirmed the presence of molecular H_2O and deciphered its orientation in the channel cavities. Farrell and Newnham (1967) and Tsang and Ghose (1972) concluded that the H_2O molecules are oriented in the (100) plane with their H-H direction parallel to [001] based on infrared and nuclear magnetic resonance spectra (NMR), respectively. However, Cohen et al. (1977) concluded from a combined X-ray and neutron diffraction study of sample 1, that the H_2O molecules are disordered into four positions with their molecular planes near (001).

Combination and overtone modes of H_2O occur near 1900 and 1400 nm, respectively. An examination of these absorption bands among the eight samples studied revealed two independent sets of bands. One set, referred to as Type I, has absorption bands polarized in α at 1401 and 1898 nm. The other set, referred to as Type II, has absorption bands in β at 1406 and 1903 nm. The distinction between these sets of H_2O absorptions can be best seen in Figure 6. The bands near 1900 nm arise from a combination of the fundamental bending (ν_2) and asymmetric stretching (ν_3) modes, and are polarized in the H-H direction of the H_2O molecule (assuming $\underline{C}_{2v}$ symmetry). Hence, the two types of H_2O in cordierite are oriented 90° apart with their H-H directions parallel to [001] (Type I) and [010] (Type II). This result is similar to the findings of Wood and Nassau (1967) from the infrared spectra of beryl. Their nomenclature with regard to orientation has been adopted in this study.

The polarization of the combination band near 1900 nm defines the H-H direction of the H_2O molecule, but does not provide information about the orientation of the molecular plane. This information is obtained from the fundamental modes in which ν_1 (symmetric stretch) and ν_2 are polarized along the molecular two-fold rotation axis, and ν_3 is polarized along the H-H direction. Infrared spectra of samples 5 and 6 (Figures 7 and 8, respectively) show three prominent bands in the fundamental stretching region (3500-3700 cm^{-1}). The greater breadth of the band in β results from a close overlapping of two bands, which are resolved at 78 K. In addition, the intensity of the band in α at 3689 cm^{-1} correlates with the Type I combination mode at 1898 nm and the band in α at 3574 cm^{-1} correlates with the Type II combination mode at 1903 nm. The observation of four bands in the fundamental stretching region and their correlation with the combination modes near 1900 nm confirm the presence of two different types of molecular H_2O in cordierite. The polarization of the fundamental stretching modes almost entirely in α and β indicates that the molecular planes of both types of H_2O are parallel to (100). Therefore, they only differ in the orientation of their H-H direction, either parallel (Type I) or perpendicular to (Type II) the channel axis in the (100) plane.

The Type II fundamental modes are obtained using the correlation between the combination mode at 1903 nm and the band at 3574 cm^{-1}, and the intensity relationships among the remaining infrared bands. These correlations indicate that ν_1 and ν_2 occur in α at 3574 and 1630 cm^{-1}, respectively, and ν_3 occurs at 3632 cm^{-1} in β. The combination mode from $(\nu_2 + \nu_3)$ expected in β at 1900 nm is observed in β at 1903 nm.

The Type I fundamental modes are more difficult to identify. ν_1 and ν_2 are expected in β and ν_3 is expected in α based on the complete polarization of the combination mode at 1898 nm in α. ν_3 is easily identified at 3689 cm^{-1}

in α based on its intensity correlation with the combination band. Low temperature spectra suggest that ν_1 occurs near 3650 cm^{-1} in α and is less intense than ν_3 at 3689 cm^{-1}. The subordinate intensity of ν_1 explains why there exists an excellent correlation between the main peak in β (ν_3 of Type II) and ν_1 of Type II H_2O. The fundamental bending mode of Type I H_2O, expected in β is also much less intense that ν_3. It is predicted to be at 1580 cm^{-1} based on the difference between the combination mode ($\nu_2 + \nu_3$) at 1898 nm (5269 cm^{-1}) and ν_3 at 3689 cm^{-1}. Three features occur in β at 1550, 1600 and 1638 cm^{-1}, which disappear with the other fundamental modes as the sample is dehydrated, also show a correlation with ν_3 of Type I at 3689 cm^{-1}. We do not understand the marked distinction between the two types of H_2O in the fundamental bending region. Nevertheless, the polarization of the fundamental stretching modes and the combination modes near 1900 nm clearly indicate that the molecular plane of each type of H_2O is parallel to (100).

Relationship to other channel constituents

Wood and Nassau (1967) found a correlation between the alkali content and the amount of Type II H_2O in beryl. They proposed that the presence of an alkali ion in the channel reorients an H_2O molecule into a Type II position. A similar correlation is also found in cordierite (Figure 9) in which the alkali content is dominantly Na. The unusually high Na content of sample 6 explains the dominance of the Type II H_2O absorption bands in this sample (Figure 6). The scatter about the alkali trend in Figure 9 is further reduced by accounting for the channel Fe^{2+} content of each sample. The channel Fe^{2+} content for each sample was obtained based on the amount determined from the Mössbauer data of sample 3, the ratio of optical band intensities for channel Fe^{2+}, and a correction for differences in density. The excellent correlation that results suggests that the Type II H_2O content is controlled by the

positively charged ions that reside in the channels. Further evidence for this control is suggested from the cordierites studied by Berg and Wheeler (1976). Spectroscopic examination of those samples confirms their suggestion that these cordierites are nearly anhydrous, and their microprobe data indicate that these samples contain only 0.02 percent Na_2O.

The least-squares solution to the data in Figure 9 is:

$$Abs/cm = 13.51[CAT] + 1.58$$

where [CAT] is the concentration (in moles/liter) of Na, Ca and Fe^{2+} in the channels. The observation that this trend does not intersect the origin suggests that other ions are present in the channels which are involved in this relationship. The relationship between the concentration of Type II H_2O and [CAT] is obtained by dividing the above equation by the ε value for this absorption band, which is determined in the next section.

Relative amounts of Type I and Type II H_2O

The relative proportion of each type of H_2O can be determined from infrared spectra once the ε values are known. They can be determined from two or more samples using the absorption band intensity for each type of H_2O and the total H_2O content. This has been done for the Type I band at 1898 nm in α and the Type II band at 1903 nm in β for samples 1, 3 and 6. The H_2O contents were determined by conventional thermogravimetric analyses of powdered material for sample 1 (G. V. Gibbs, personal communication) and sample 6 (Iiyama, 1960), and by dehydration of a single slab in which weight loss and infrared spectra were sequentially monitored (sample 3, this study). Microprobe analyses of the dehydrated slab of sample 3 did not detect alkali loss. The least-squares solution to this problem, written in matrix notation as,

$$\begin{matrix} \text{Absorbance/cm} & & & & H_2O \\ \text{Type I} & \text{Type II} & & & \text{(moles/liter)} \end{matrix}$$

$$\begin{pmatrix} 31.36 & 4.04 \\ 21.91 & 3.87 \\ 12.68 & 20.06 \end{pmatrix} \begin{pmatrix} 1/\varepsilon_I \\ 1/\varepsilon_{II} \end{pmatrix} = \begin{pmatrix} 2.84 \\ 2.31 \\ 3.62 \end{pmatrix}$$

is: $\varepsilon_I = 13.1$ and $\varepsilon_{II} = 7.54$. These results indicate that 84, 77 and 27 percent of the total H_2O content is Type I in samples 1, 3 and 6, respectively. The low proportion of Type II H_2O in most samples is consistent with the NMR results of Tsang and Ghose (1972) who failed to detect Type II H_2O. They studied a sample from the same locality as sample 3. It should be pointed out that these calculations are strongly biased by the accuracy of the data for sample 6. Any loss of CO_2 during dehydration will also affect these results.

The least-squares solution to the data in Figure 9 given in the previous section is divided by ε_{II} resulting in

$$[C]_{H_2O}^{\text{Type II}} = 1.79[CAT] + 0.21 \quad .$$

The nearly 2:1 ratio between the concentration of Type II H_2O and [CAT] suggests that most of the channel cations, located in or near the center of the six-membered rings (Gibbs, 1966), are additionally coordinated to one Type II H_2O molecule in the cavity above and one in the cavity below the ring. This would result in a more uniform coordination about the channel cation. Assuming a 2:1 ratio, and by accounting for other cations in the channels by moving the least-squares line in Figure 9 to the origin with the same slope, the relative amounts of Type I H_2O in samples 1, 3 and 6 are determined to be 79, 75 and 18 percent, respectively. Hence, there is good agreement in calculating the relative proportions of both types of H_2O using the spectral intensities and from an intuitively reasonable coordination relationship between the channel cations and the Type II H_2O.

STRUCTURAL STATE

Miyashiro (1957) suggested that cordierite exists in all intermediate structural states between orthorhombic and hexagonal symmetries and attributed the variation to Al/Si ordering in the six-membered rings. Miyashiro defined a distortion index, Δ ($\Delta = 2\theta_{(131)} - (2\theta_{(421)} + 2\theta_{(511)})/2$), measured from X-ray diffractograms, to represent the deviation from hexagonal symmetry. Later structural refinements (Gibbs, 1966; Meagher, 1967) found the same Si/Al ordering in samples having very different Δ values, which led Stout (1975) to suggest that Δ is also dependent upon compositional factors, such as H_2O in the channels.

Optical spectra must also be sensitive to differences in structural state. In a hexagonal crystal, all directions normal to the channel axis are equivalent and the channel Fe^{2+} bands in β and γ must merge into one band (i.e. $\gamma/\beta = 1$). Therefore, γ/β ratios of the channel Fe^{2+} bands from optical spectra also represent deviations from hexagonal symmetry. However, there does not appear to be any correlation between this "optical" hexagonality of cordierite based on the γ/β ratios and the dimensional hexagonality, as measured by the Δ index. Therefore, these scales are measuring different phenomena. It must be remembered that Δ (and $\underline{a} - \sqrt{3}b$) can be equal to zero in which case the crystal is dimensionally hexagonal but still may possess orthorhombic symmetry.

ORIGIN OF COLOR

Smith and Strens (1976) suggested that the color and pleochroism in cordierite are due to intervalence charge-transfer between Fe^{2+} in the octahedral site and Fe^{3+} in the T_1 tetrahedral site. There are two T_1 sites that each share one edge with the octahedron such that the metal-metal vectors make angles of 31.5° with [010] in the (001) plane. Three independent observations support this interpretation. First, the structural refinement of Gibbs (1966) indicates that T_1 is an Al-rich tetrahedron, and therefore is a likely site for Fe^{3+}. The presence of Fe^{3+} in this site is consistent with the electron paramagnetic resonance (EPR) data of Hedgecock and Chakravartty (1966). Second, the energy of this charge-transfer band (17,500 cm^{-1}) is significantly higher than most intervalence charge-transfer bands arising from adjacent octahedral sites (Loeffler et al., 1976). Third, components of the charge-transfer process should occur in β and γ, but not in α, as is observed. The observed β:γ intensity ratio of 2.67 is exactly the value predicted using the squares of the direction cosines of the metal-metal vector with [010] and [100]. Despite this strong support for an octahedral-tetrahedral intervalence charge-transfer mechanism, optical spectra taken on slabs of heat-treated cordierite do not support this interpretation.

Sequential heating experiments conducted in air on a (100) slab of sample 5 were performed to moniter changes in the intervalence band intensity, the oxidation of Fe^{2+}, and the loss of H_2O. After heating, samples were cooled to room temperature and spectroscopically examined. The sample was almost totally dehydrated after 2 hours at 800 °C. Examination of another slab, used to better define the dehydration temperature, did not detect H_2O loss up to 775 °C. Changes in the intervalence charge-transfer and Fe^{2+} band intensities are summarized in Figure 10. Octahedral and channel Fe^{2+} begin to oxidize above

1150 and 200 °C, respectively. The intervalence intensity decreases slightly near 500 °C, but continuously increases above 500 °C.

Spectroscopic evidence was presented in an earlier section to suggest that Fe^{2+} occurs in only the octahedral and channel sites. The continuous decrease of the channel Fe^{2+} absorption bands after heating suggests that Fe^{3+} is being produced in the channels. Note that octahedral Fe^{2+} does not begin to oxidize below about 1150 °C. Above 500 °C, these data suggest that the intervalence charge-transfer in cordierite is due to octahedral Fe^{2+} and channel Fe^{3+}. Support for this interpretation comes from the observation that the same intervalence band at 570 nm increases as more Fe^{3+} is produced in the channels. Furthermore, the same sharp bands of low intensity in the 400-450 nm region, attributed to spin-forbidden transitions of Fe^{3+}, also increase after heating. It is most important to realize that new intervalence and Fe^{3+} absorption bands were not produced after heat treatment. Therefore the observation of the same intervalence and Fe^{3+} bands in all unheated samples indicates that the color and pleochroism in cordierite are due to intervalence charge-transfer between octahedral Fe^{2+} and channel Fe^{3+}.

It is particularly interesting to note that there is an excellent correlation between the oxidation of Fe^{2+} in the channels and the increase in intervalence charge-transfer intensity only above 800 °C, the temperature at which the sample was dehydrated. Below 800 °C, the intervalence intensity remained nearly the same. The slight decrease near 500 °C may arise from difficulties in accounting for overlapping absorptions on either side of the intervalence band in β polarization. It is proposed that the larger channel cations (Na, Ca and Fe^{2+}) occur at or near the center of the six-membered rings (Gibbs, 1966) and are coordinated to Type II H_2O molecules as discussed in a previous section. Smaller cations, such as Fe^{3+}, are suggested to already be present in the channel cavities based

on the presence of intervalence bands in all unheated samples. It is reasonable to expect that these ions would situate near the unsatisfied O_4 and O_5 oxygens that bridge Al- and Si-rich tetrahedra. They would then be in the same (001) plane at z = 1/4 as the octahedral sites, and the resulting Fe^{2+} - Fe^{3+} vectors would be similar to those between the octahedral and T_1 sites to produce a similar pleochroism. Most of the Fe^{3+} that is produced from oxidation by heating remains in the rings due to the coordination by Type II H_2O. The characteristic absorption band intensity of Fe^{3+} in the rings is suggested to be low because it is isolated from interacting with Fe^{2+}, and hence, is not observed. After dehydration at 800 °C, these cations continuously migrate to the walls of the cavities to produce the dramatic increase in the intervalence charge-transfer intensity. There is an indication of electron density loci near the walls of the cavities of sample 1 at fractional coordinates (0.11, 0.16, 0.25) and the symmetry related positions from room temperature data (G. V. Gibbs, personal communication). X-ray data for a dehydrated sample, particularly a Na-rich sample, is required to evaluate the model proposed above. The above interpretation does not preclude the presence of tetrahedral Fe^{3+}. It does suggest that any tetrahedral Fe^{3+} that is present is not responsible for the color and pleochroism in cordierite.

DISCUSSION

Structural models

Stout (1975, 1976) proposed a model to explain the increase in the distortion index (Δ) that occurs when cordierite powders were heated in air for 2 hours at 900 °C. The model attributes the structural readjustment to the loss of H_2O and its influence on the crystal structure from hydrogen bonding to the aluminosilicate framework in the channel cavities. Langer and Schreyer (1976) objected to the influence of H_2O on the crystal structure pointing out that the infrared frequencies of H_2O in cordierite suggested only weak hydrogen bonding interactions. Both authors left open the possibility that compositional factors other than Al/Si ordering may be responsible for the observed structural readjustment after heating.

The model proposed in the previous section provides a plausible explanation of Stout's observations in terms of cation migration from the center of the six-membered tetrahedral rings to the wall of the channel cavities after dehydration. The migration is suggested to occur mainly after dehydration in which the coordinating influence of Type II H_2O with these cations is no longer present. Note that the loss of Na or Fe was not detected from slabs dehydrated at 800 °C for 2 hours. Evidence for cation migration after dehydration is based on the rapid increase in intervalence charge-transfer. This increase is interpreted in terms of the oxidation of Fe^{2+} to Fe^{3+} in the rings which migrate to the cavity wall after dehydration. The incorporation of these ions near the cavity wall is a likely mechanism to affect the lattice geometry without invoking an Al/Si redistribution in nearly totally ordered cordierites.

Quantitative aspects of H_2O

The relative proportions of the two types of H_2O were determined for three samples using their total H_2O content, the spectral intensities of the combination bands, and the suggested 2:1 relationship between Type II H_2O and the channel cations. These results are used to determine the ε values for the fundamental modes of sample 6, which are tabulated in Table 3. Only ν_3 for Type I H_2O was readily observed for a determination of ε. It is important to realize that the ε values for ν_3 of both types of H_2O are about the same, considering the probable errors in their determination. Consequently, the relative proportion of each type of H_2O can be readily determined from infrared spectra of powdered cordierite.

Yinogradov and Linnell (1971) suggested that hydrogen bonding decreases the intensities of overtones. We suggest that this relationship may be used to interpret the intensities of combination bands. For example, the ε values of the combination bands of both types of H_2O in cordierite are greater than those of liquid water (ε~0.9). An ε value of approximately 5 is observed for the combination band in joaquinite (Rossman, 1975a), which is interpreted to have weakly hydrogen bonded H_2O based on fundamental stretching frequencies.

Quantitative aspects of Fe^{2+}

Goldman and Rossman (1977b) indicated that the ε values for Fe^{2+} become greater as the site becomes larger and more distorted. Hence, the ε value for channel Fe^{2+} in cordierite is expected to be very large. The Mössbauer data for the powder of sample 3 indicate that 5.8 percent of the total iron content is Fe^{2+} in the channels. Using the optical data for this sample (Figure 1) and this site distribution, an ε value of 294 is determined. This is the largest ε value that we have determined. For comparison, the ε values for Fe^{2+} in the highly distorted grunerite M4 site and orthopyroxene M2 site are 150 and

40, respectively. The ε value for octahedral Fe^{2+} in cordierite is 3.5 for the higher energy band, and is nearly independent of composition.

CONCLUSIONS

(1) Fe^{2+} is present in both the octahedral ($\varepsilon \sim 3.5$) and channel ($\varepsilon > 200$) sites in cordierite. Channel Fe^{2+} accounts for less than about 5 percent of the total iron content in most samples.

(2) The calculated intensities of the absorption lines in single crystal Mössbauer spectra better match the observed intensities by assuming that all of the iron is present in the octahedral site and by constraining one of the principal EFG axes to coincide with the symmetry axis of the octahedral site.

(3) Two types of molecular H_2O are present in the channels. They are oriented in the (100) plane with their H-H directions parallel to [001] (Type I) and [010] (Type II). Type II is less abundant in most samples and is correlated to the amount of channel cations. It is suggested that there are two Type II H_2O molecules, one in the cavity above and one in the cavity below the six-membered tetrahedral ring, that coordinate a cation in the ring.

(4) Optical spectra provide a measure of the hexagonality of cordierite, but a relationship between this "optical" hexagonality and the Δ index was not found.

(5) The origin of color and pleochroism is suggested to arise from intervalence charge-transfer between octahedral Fe^{2+} and channel Fe^{3+}.

(6) It is suggested that after dehydration, the channel cations in the six-membered rings migrate to the wall of the channel cavities.

(7) The ε values for the asymmetric stretching mode are nearly the same for both types of H_2O indicating that their relative proportions can be determined from infrared spectra of powdered samples.

ACKNOWLEDGEMENTS

I greatfully acknowledge G.V. Gibbs (V.P.I.), E.P. Meagher (U.B.C.), R.F. Dymek (Cal Tech), J.H. Berg (U. Mass.) and R.H. Currier (San Marino, Cal.) for supplying many of the samples used in this study. I am especially indepted to R.M. Housely (Rockwell International) for obtaining the Mössbauer data, to W.A. Dollase (UCLA) for doing the calculations for the single crystal Mössbauer experiments, and to G. R. Rossman (Cal Tech) for taking some of the infrared data, I thank these people for numerous discussions during the course of this study and also G. E. Brown (Stanford) and J.H. Stout (Minn.).

FOOTNOTES

[1]We refer to the six-coordinate metal site described by Gibbs (1966) as the "octahedral" site to distinguish it from the "channel" site. This does not preclude the possibility of six-coordination for the channel site.

[2]There is a regular decrease in the energies of the octahedral Fe^{2+} bands as the total iron concentration increases (Figure 3). This result is consistent with the octahedral site becoming larger as it accommodates more Fe^{2+}.

[3]The resulting parameters from the powder Mössbauer spectrum of sample 3 for quadrupole splitting, isomer shift and relative area are: (channel Fe^{2+}) 1.60, 1.21 mm/sec and 5.8 percent; (octahedral Fe^{2+}) 2.31, 1.22 mm/sec and 94.2 percent. The peak half-widths are 0.31 mm/sec and χ^2 for 200 channels is 648 with ~4 x 10^6 background counts. The presence of Fe^{3+} is suggested in the 0.4-0.5 mm/sec region. Upon removing the intensity constraint for the components of the channel Fe^{2+} doublet, the low-velocity component became more intense suggesting additional resonance in this region. However, an Fe^{3+} doublet was not fitted because its peak positions are not known at 295 K and it accounts at most for only a few percent of the total resonance.

REFERENCES CITED

Berg, J. H. and E. P. Wheeler (1976) Osumilite of deep-seated origin in the contact aureole of the anorthositic Nain Complex, Labrador. Amer. Mineral. 61, 29-37.

Cohen, J. P., F. K. Ross and G. V. Gibbs (1977) An X-ray and neutron diffraction study of hydrous low cordierite. Amer. Mineral. (in press).

Damon, P. E. and L. L. Kulp (1958) Excess helium and argon in beryl and other minerals. Amer. Mineral. 43, 433-459.

Duncan, J. F. and J. H. Johnston (1974) Single-crystal ^{57}Fe Mössbauer studies of the site positions in cordierite. Austral. J. Chem. 27, 249-258.

Farrell, E. F. and R. E. Newnham (1967) Electronic and vibrational absorption spectra in cordierite. Amer. Mineral. 52, 380-388.

Faye, G. H. (1972) Relationship between crystal-field splitting parameter, "Δ_{VI}", of absorption spectra of Fe^{2+}-bearing materials. Canad. Mineral. 11, 473-487.

Faye, G. H., P. G. Manning and E. H. Nickel (1968) The polarized optical absorption spectra of tourmaline, cordierite, chloritoid and vivianite: Ferric-ferrous electron interaction as a source of pleochroism. Amer. Mineral. 53, 1174-1201.

Gibbs, G. V. (1966) The polymorphism in cordierite I: The crystal structure of low cordierite. Amer. Mineral. 51, 1068-1087.

Goldman, D. S. and G. R. Rossman (1977a) The spectra of iron in orthopyroxene revisited: The splitting of the ground state. Amer. Mineral. 62, 151-157.

Goldman, D. S. and G. R. Rossman (1977b) The identification of Fe^{2+} in the M(4) site of calcic amphiboles. Amer. Mineral. 62, 205=216.

Grant, R. W., R. M. Houseley and U. Gonsor (1969) Nuclear field gradient and mean square displacement of the iron sites in sodium nitroprusside. Phys. Rev. 178, 523-530.

Greenwood, N. N. and T. C. Gibb (1971) Mössbauer Spectroscopy. Chapman and Hall, London.

Hedgecock, N. E. and S. C. Chakravartty (1966) Electron spin resonance of Fe^{3+} in cordierite. Canad. J. Phys. 44, 2749-2755.

Heinrich, E. W. (1950) Cordierite in pegmatite near Micanite, Colorado. Amer. Mineral. 35, 173-184.

Iiyama, J. T. (1960) Researches sur le rôle de l'eau dans la structure et le polymorphisme de la cordierite. Bull. Soc. Franc. Min. Crist. 83, 155-178.

Langer, K. and W. Schreyer (1976) Apparent effects of molecular water on the lattice geometry of cordierite: A discussion. Amer. Mineral. 61, 1045-1050.

Leake, B. E. (1960) Compilation of chemical analyses and physical constants of natural cordierites. Amer. Mineral. 45, 282-298.

Loeffler, B. M., R. G. Burns and J. A. Tossell (1976) Metal-metal charge transfer transitions: Interpretation of visible region of the Moon and lunar materials. Proc. 6th Lunar Sci. Conf. 3, 2663-2676.

Meagher, E. P. (1967) The crystal structure and polymorphism of cordierite. Ph.D. Thesis. The Pennsylvania State University, University Park, PA.

Miyashiro, A. (1957) Cordierite-indialite relations. Amer. J. Sci. 255, 43-62.

Newton, R. C. (1966) BeO in pegmatitic cordierite. Min. Mag. 35, 920-927.

Pollack, H. (1976) Charge transfer in cordierite. Phys. Stat. Sol. 74, K31-34.

Pryce, M. W. (1973) Low-iron cordierite in phlogopite schist from White Well, Western Australia. Min. Mag. 39, 241-243.

Pye, E .G. (1957) Geology of the Manitouwadge area. Ont. Dept. Mines Rept. 66, part VIII, 1-114.

Rossman, G. R. (1975a) Joaquinite: The nature of its water content and the question of four-coordinated ferrous iron. Amer. Mineral. 60, 435-440.

Rossman, G. R. (1975b) Spectroscopic and magnetic studies of ferric iron hydroxy sulfates: Intensification of color in ferric iron clusters bridged by a single hydroxide ion. Amer. Mineral. 60, 698-704.

Schreyer, W. and H. S. Yoder (1964) The system Mg-cordierite-H_2O and related rocks. Nues. Jahrb. Mineral. Abstr. 101, 271-342.

Smith, G. and R. G. J. Strens (1976) Intervalence transfer absorption in some silicate, oxide and phosphate minerals. In The Physics and Chemistry of Minerals and Rocks. R. G. J. Strens (ed.). John Wiley and Sons, 583-612.

Smith, J. V. and W. Schreyer (1962) Location of argon and water in cordierite. Min. Mag. 33, 226-236.

Speer, J. A. (1975) The contact metamorphic aureole of the Kiglapait intrusion. In. The Nain Anorthosite Project, Labrador: Field report 1974. S. A. Morse (ed.) University of Massachusetts, 17-26.

Stanek, J. and T. Miskovsky (1964) Eisenreicher cordierit aus pegmatit bei Dolni Bory, Westmähren (tschechisch). Cas. Mineral. Geol. 9, 191-192.

Stout, J. H. (1975) Apparent effects of molecular water on the lattice geometry of cordierite. Amer. Mineral. 60, 229-234.

Stout, J. H. (1976) Apparent effects of molecular water on the lattice geometry of cordierite: A reply. Amer. Mineral. 61, 1041-1044.

Strunz, H., Ch. Tennyson and P. J. Vebel (1971) Cordierite. Morphology, physical properties, structure, inclusions, and oriented intergrowths. Minerals, Science and Engineering 3, 3-18.

Sugiura, K. (1959) Water in cordierite. Tokyo Kogyo Daigaku Gakuho, Ser. B, No. 1, 26pp.

Tsang, T. and S. Ghose (1972) Nuclear magnetic resonance of ^{1}H and ^{27}Al and Al-Si order in low cordierite, $Mg_2Al_4Si_5O_{18}\cdot nH_2O$. J. Chem. Phys. 56(7), 3329-3332.

Wertheim, G. K. (1961) Hyperfine structure of Fe^{57} in paramagnetic and antiferromagnetic FeF_2 from the Mössbauer effect. Phys. Rev. 121, 63-66.

Wood, D. L. and K. Nassau (1967) Infrared spectra of foreign molecules in beryl. J. Chem. Phys. 47(7), 2220-2228.

Yinogradov, S. N. and R. H. Linnell (1971) Spectroscopic Manifestation of Hydrogen Bonding, Van Nostrand, Reinhold Co., New York. Ch 3, p 47.

Zimmerman, J. L. (1972) Petrogenetic application of the study of water and carbon dioxide release from cordierties. C. R. Acad. Sci. Ser. D, 275, 519-522.

Zory, P. (1965) Nuclear electric-field gradient determination utilizing the Mössbauer effect (Fe^{57}). Phys. Rev. 140A, 1401-1407.

TABLE 1. Cordierite analyses

	1	2	3	4	5	6	7	8
	weight percent of oxides							
SiO_2	50.37	49.70	49.54	49.97	49.38	48.75	48.16	46.41
TiO_2	--	0.04	--	--	.09	--	0.04	--
Al_2O_3	34.24	32.91	33.47	33.03	33.05	30.69	31.77	32.29
MgO	13.72	12.66	12.42	12.06	10.49	8.99	7.19	2.55
FeO	1.03	2.28	2.46	2.99	5.30	7.35	10.13	16.71
MnO	0.05	--	0.06	0.03	0.31	0.49	0.33	0.68
CaO	--	0.03	0.02	0.01	0.01	0.01	0.02	0.03
Na_2O	0.20	0.36	0.22	0.15	0.21	1.53	0.04	0.55
	99.66	98.00	98.78	98.24	98.85	97.82	97.69	99.22
	formula proportions (Σcations-Na-Ca = 11)							
Si	4.94	5.00	4.97	5.02	5.00	5.05	5.04	4.97
Al	3.96	3.90	3.96	3.91	3.94	3.75	3.92	4.07
Ti	--	--	--	--	0.01	--	--	--
Mg	2.01	1.90	1.86	1.81	1.58	1.39	1.12	0.41
Fe^{2+}	0.08	0.19	0.21	0.25	0.45	0.64	0.89	1.49
Mn	--	--	--	--	0.03	0.04	0.03	0.06
Na	0.04	0.07	0.04	0.03	0.04	0.31	0.01	0.11
Σ^+	35.86	36.02	35.94	35.96	36.02	36.16	36.01	36.12
ρ (g/cm^3)	2.570	2.583*	2.584*	2.587*	2.603*	2.665	2.649*	2.738*
Δ ($2\theta°$)†	0.25	0.27	0.24	0.25	0.27	0.12	0.22	0.22
a (Å)	17.079			17.08		17.036		17.20
b (Å)	9.730			9.74		9.758		9.83
c (Å)	9.356			9.38		9.323		9.30
γ/β**	2.31	2.25	2.03	2.05	2.08	2.12	1.73	2.04

1. *White Well, Australia. Occurs in a phlogopite schist near intrusive granite (Pryce, 1973). X-ray and neutron diffraction data are reported in Cohen et al. (1977).*
2. *Tanga area near Umba River, Tanzania. Occurs with mica schists in alluvial deposits.*
3. *Mt. Tsilaizina, Malagasy Republic.*
4. *Malagasy Republic. Mössbauer, X-ray and chemical data are reported in Duncan and Johnston (1974).*
5. *Manitouwadge, Ontario, Canada. Occurs in a garnet-anthophyllite schist (Pye, 1957).*
6. *Haddam, Connecticut, U.S.A. Occurs in a pegmatite in a biotite gneiss (Heinrich, 1950). X-ray diffraction data are from Meagher (1967). This sample contains 0.52 BeO (Newton, 1966) resulting in 0.13 Be formula units.*
7. *Snyder group northwest of the Kiglapait intrusive, Nain, Labrador. Occurs with biotite and andalusite in a contact aureole (Speer, 1975).*
8. *Dolni Bory, Moravia, Czechoslovakia. Occurs in a pegmatite as massive layers separated by mica (±anthophyllite). (Heinrich, 1950; Stanek and Miskovsky, 1964). Cell axes are reported in Strunz et al. (1971).*

**Calculated density (see text). †Δ is the distortion index of Miyashiro (1957). **γ/β is the intensity ratio of the channel Fe^{2+} optical absorption bands near 950 nm.*

TABLE 2. Comparison of observed and calculated single-crystal Mössbauer spectral intensities.

#	g.a[a]	g.b	g.c	OBS[b]	CAL[c]	DIF	CAL(D&J)[d]	DIF(D&J)
1	1.000	0.000	0.000	0.603	0.604	-0.001	0.569	0.034
2	0.891	0.454	0.000	0.602	0.598	0.004	0.588	0.014
3	0.743	0.669	0.000	0.602	0.590	0.011	0.595	0.007
4	0.707	0.000	0.707	0.448	0.463	-0.016	0.457	-0.009
5	0.616	0.788	0.000	0.582	0.585	-0.003	0.592	-0.010
6	0.391	0.921	0.000	0.576	0.578	-0.002	0.590	-0.014
7	0.174	0.985	0.000	0.573	0.574	-0.001	0.582	-0.009
8	0.000	1.000	0.000	0.571	0.573	-0.002	0.573	-0.002
9	0.000	0.966	0.259	0.554	0.556	-0.003	0.559	-0.005
10	0.000	0.866	0.500	0.510	0.510	-0.001	0.517	-0.007
11	0.000	0.500	0.866	0.394	0.385	0.009	0.405	-0.011
12	0.000	0.259	0.966	0.346	0.340	0.007	0.363	-0.017
13	0.000	0.000	1.000	0.310	0.323	-0.012	0.346	-0.036
14	-0.259	0.000	0.966	0.351	0.342	0.009	0.359	-0.008
15	-0.500	0.000	0.866	0.390	0.393	-0.003	0.401	-0.011
						0.007 rms		0.016 rms

a. *direction cosines of gamma-ray beam relative to crystal axes.*
b. *fraction of doublet area represented by higher energy peak, as observed by Duncan & Johnston (1974).*
c. *higher energy peak fraction calculated from model proposed in this study.*
d. *higher energy peak fraction calculated by Duncan & Johnston from their model.*

Table 3. ε values for H_2O in cordierite*

Type	Mode	cm^{-1}	ε^a	ε^b
I	ν_3	3689	204	308
	$\nu_2 + \nu_3$	5269	13.1**	
II	ν_1	3574	256	228
	ν_2	1630	584	520
	ν_3	3632	269	239
	$\nu_2 + \nu_3$	5255	7.5**	

Spectral data are from sample 6 (Figure 8).

**Determined from a least-squares solution to the data from samples 1, 3 and 6.*

a. *Based on the spectral intensity determination from which 27 percent of the total H_2O content is Type I.*

b. *Based on the assumed 2:1 relationship between Type II H_2O and the channel cation content from which 18 percent of the total H_2O content is Type I.*

FIGURE CAPTIONS

1. Room temperature optical spectra of a low-Fe cordierite from Mt. Tsilaizina, Malagasay Republic (sample 3). Crystal thickness = 1.20 mm.
2. Room temperature optical spectra of a high-Fe cordierite from Dolni Bory, Moravia, Czechoslovakia (sample 8). Crystal thickness = 0.70 mm.
3. Upper: Intensity data for the Fe^{2+} absorption bands from optical spectra as a function of the total iron concentration for channel Fe^{2+} near 950 nm in β (Δ) and γ ($\square$), and octahedral Fe^{2+} near 1170 nm in α ($\bullet$). Gaussian-fitted intensities to the octahedral Fe^{2+} bands in α near 1000 nm (o) and 1170 nm (+) are also presented. The half-filled squares and triangles are corrections to the intensity of the channel Fe^{2+} bands (see text for explanation).

   Middle: Intensity of the intervalence charge-transfer band in β near 570 nm.

   Lower: Energies of the octahedral Fe^{2+} absorption bands in α near 1000 nm (o) and 1170 nm (+) from Gaussian fits.
4. Correlation of channel Fe^{2+} absorption bands. Symbols are described in Figure 3.
5. Upper: Single crystal Mössbauer spectrum of a high-iron cordierite from Dolni Bory, Moravia, Czechoslovakia (sample 8) taken at room temperature on a 0.180 mm thick (001) slab.

   Middle: Single crystal Mössbauer spectrum of a low-iron cordierite from Mt. Tsilaizina, Malagasay Republic (sample 3) taken at room temperature on a 1.128 mm thick (001) slab.

   Lower: Powder Mössbauer spectrum of a low-iron cordierite from Mt. Tsilaizina, Malagasay Republic (sample 3) taken at room temperature.
6. Room temperature optical spectra of cordierite from Haddam, Connecticut (sample 6). Crystal thickness = 0.70 mm.

7. Room temperature infrared spectra of cordierite from Manitouwadge, Ontario Canada (sample 5) showing the fundamental stretching and bending modes of water. Crystal thickness = 0.050 mm.

8. Room temperature infrared spectra of cordierite from Haddam, Connecticut (sample 6) showing the fundamental stretching and bending modes of water. Crystal thickness = 0.025 mm.

9. Correlation of the Type II water band intensity at 1903 nm in β and the amount of Na + Ca (●) and the amount of Na + Ca + Fe^{2+} (o) in the channels in cordierite.

10. Results of heating experiments conducted in air on a (100) slab of sample 5. The absorption band intensities for channel Fe^{2+} at 950 nm in β (Δ), octahedral Fe^{2+} at 1170 nm in α (●), and intervalence charge-transfer at 570 nm in β (o) were monitored after each heating step. Water loss was not detected until 800 °C. After 2 hours at 800 °C, the sample was completely dehydrated. Crystal thickness represented = 0.5 mm.

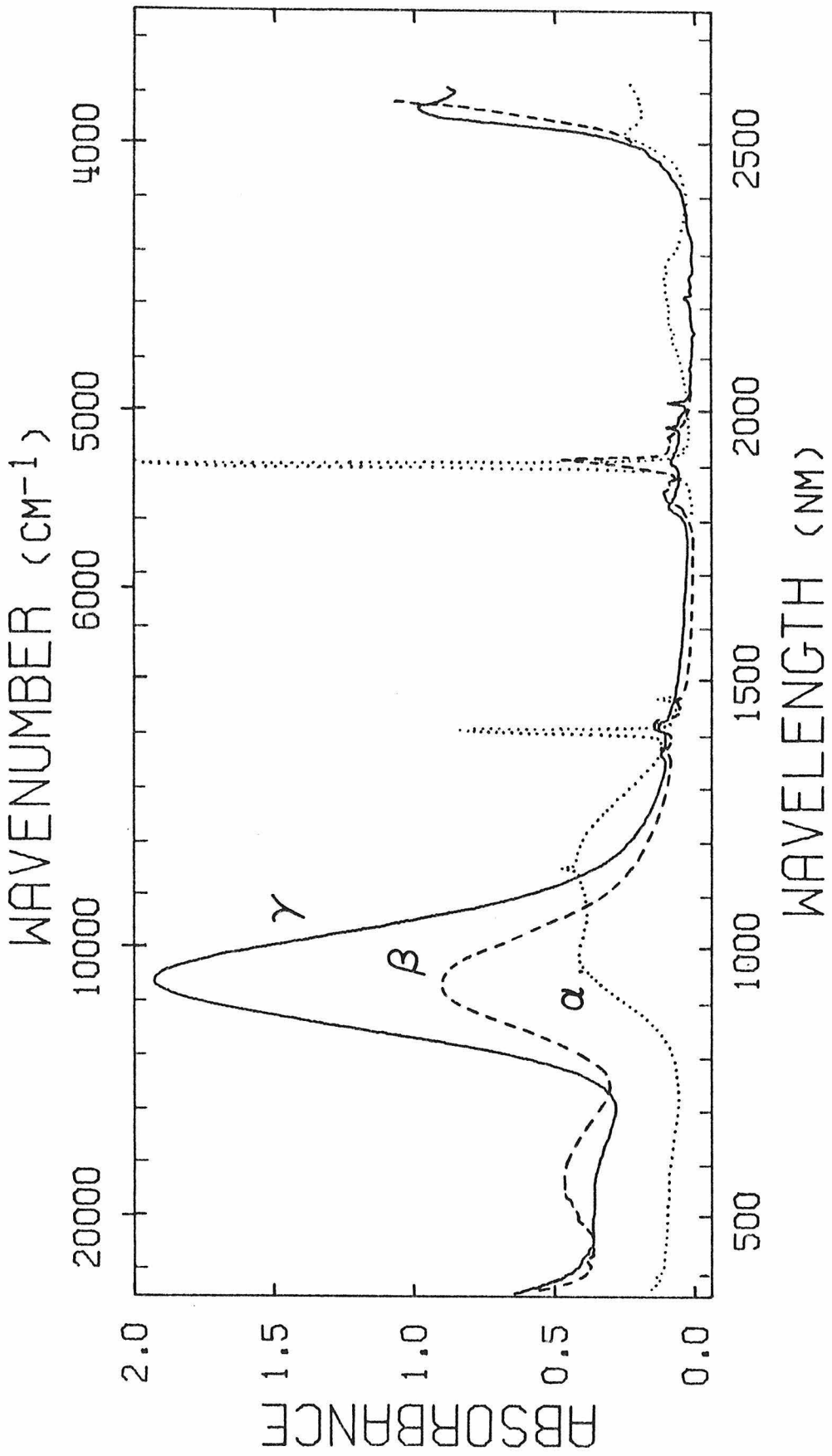
WAVENUMBER (CM-1)
20000
10000
6000
5000
4000
WAVELENGTH (NM)
500
1000
1500
2000
2500
ABSORBANCE
0.0
0.5
1.0
1.5
2.0
γ
β
α

Figure 1

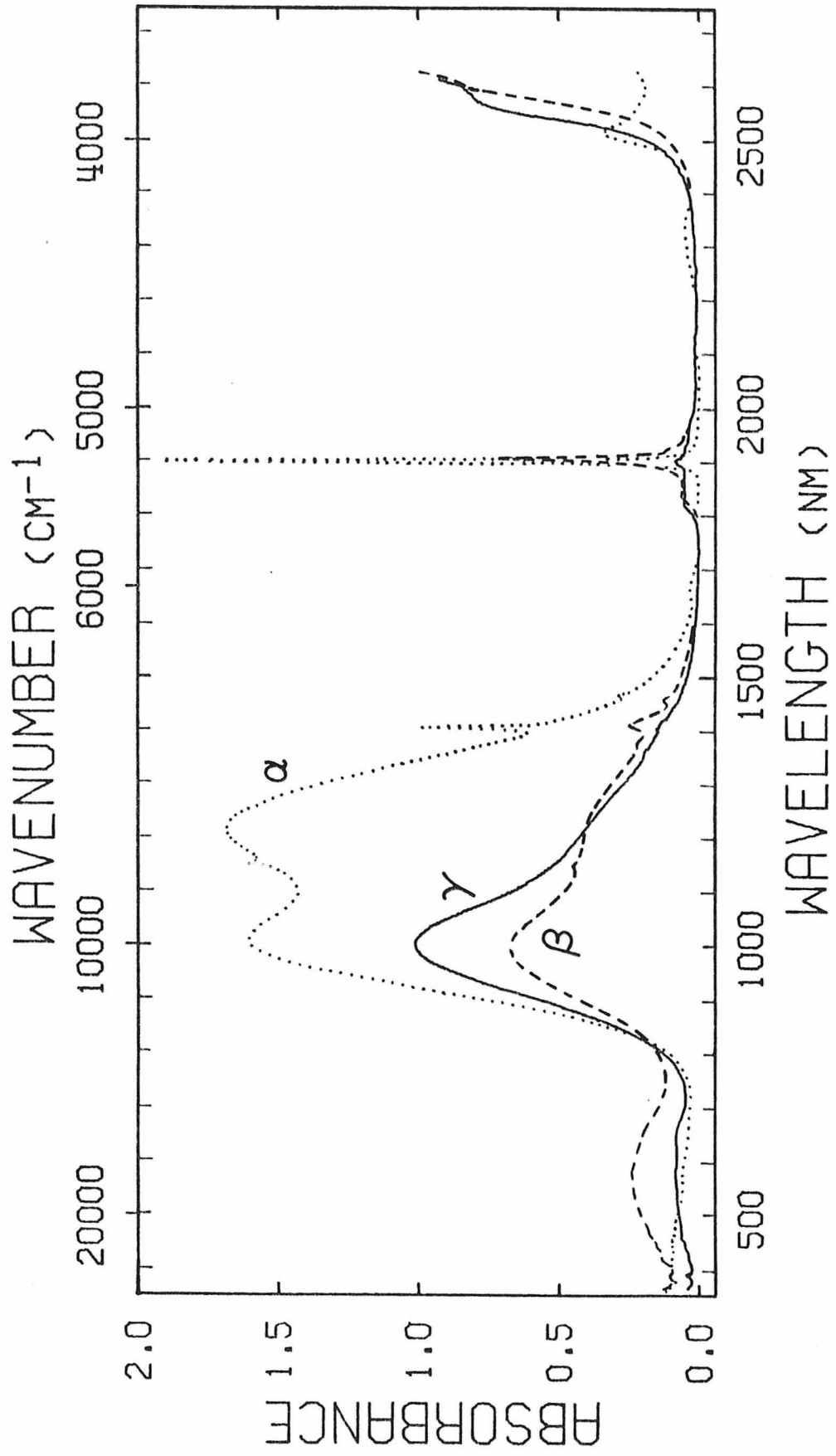
WAVENUMBER (CM-1)
20000
10000
6000
5000
4000
WAVELENGTH (NM)
500
1000
1500
2000
2500
ABSORBANCE
0.0
0.5
1.0
1.5
2.0
α
β
γ

Figure 2

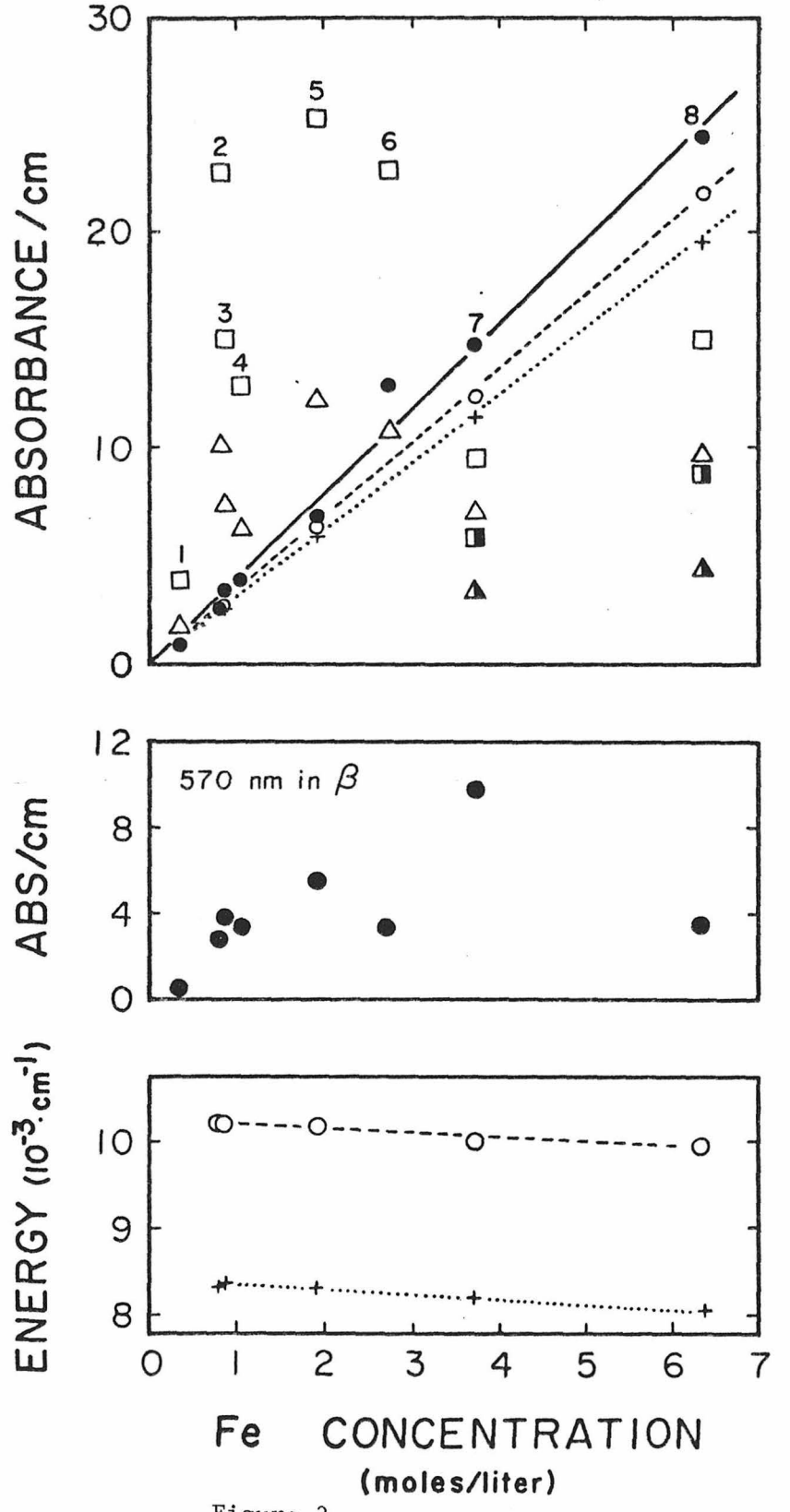
ABSORBANCE/cm
30
20
10
0
1
2
3
4
5
6
7
8
ABS/cm
12
8
4
0
570 nm in β
ENERGY (10⁻³·cm⁻¹)
10
9
8
0
1
2
3
4
5
6
7
Fe CONCENTRATION
(moles/liter)

Figure 3

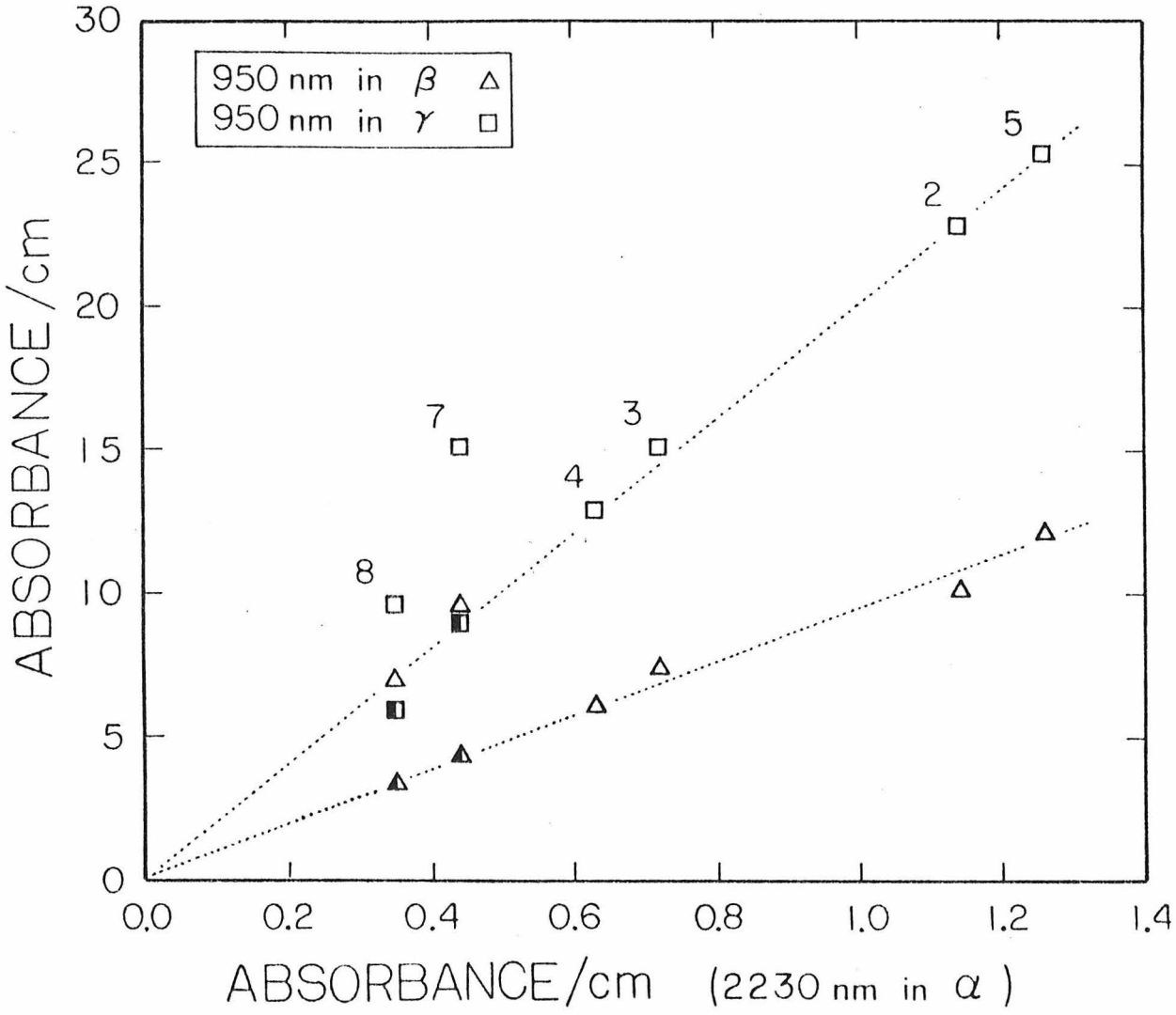
950 nm in β △
950 nm in γ □
ABSORBANCE/cm
ABSORBANCE/cm (2230 nm in α)
0
5
10
15
20
25
30
0.0
0.2
0.4
0.6
0.8
1.0
1.2
1.4
2
3
4
5
7
8

Figure 4

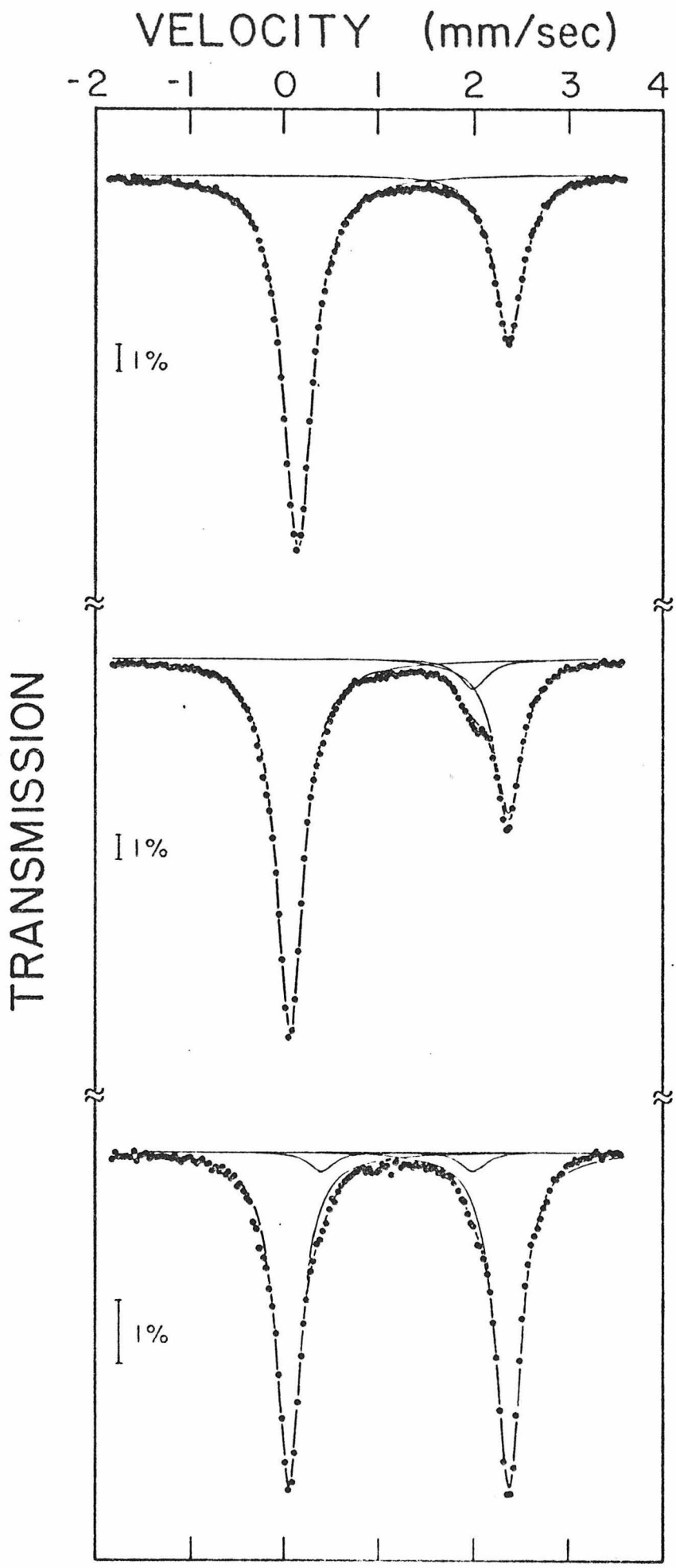

Figure 5

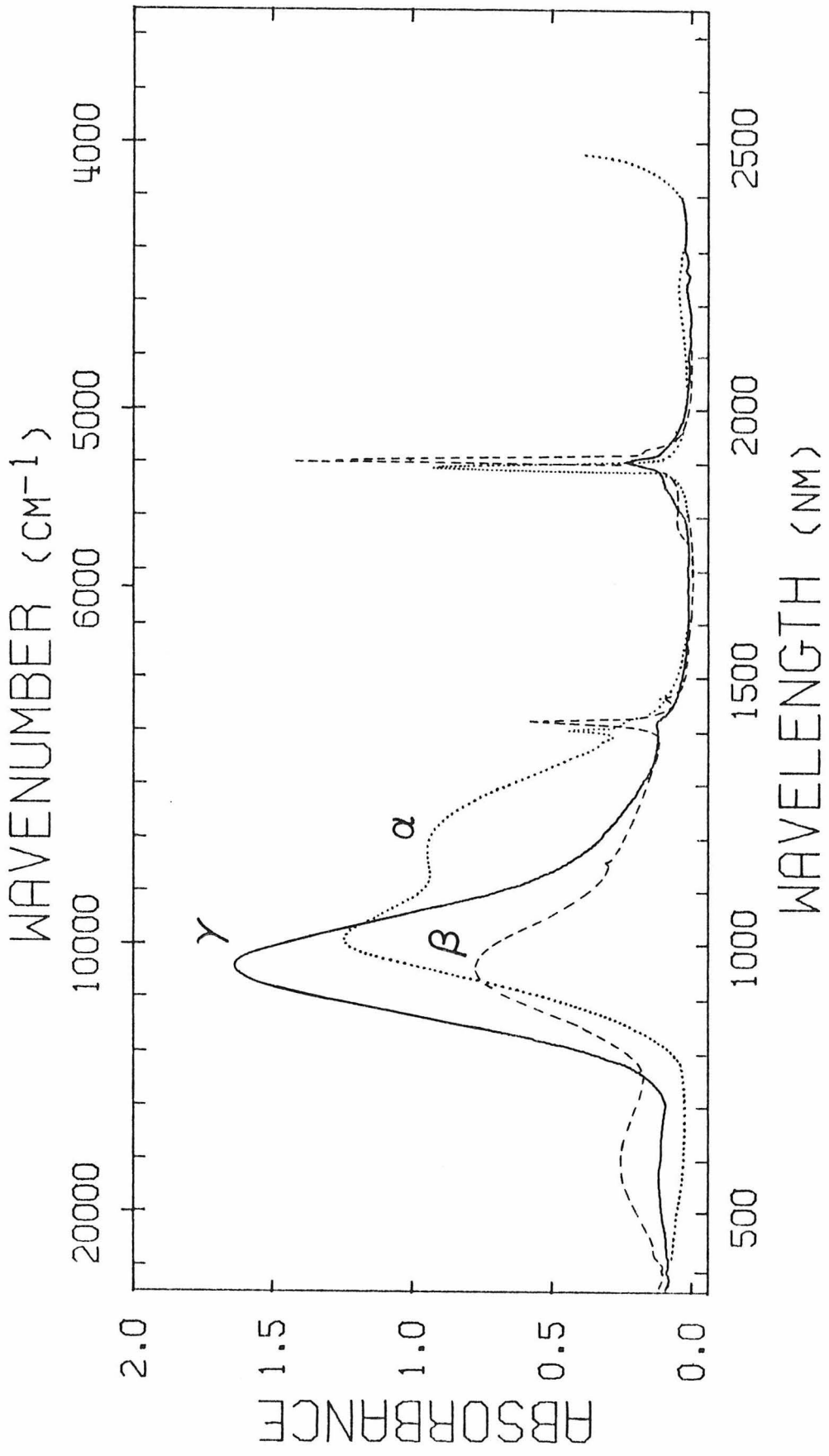
WAVENUMBER (CM-1)
20000
10000
6000
5000
4000
WAVELENGTH (NM)
500
1000
1500
2000
2500
ABSORBANCE
0.0
0.5
1.0
1.5
2.0
γ
β
α

Figure 6

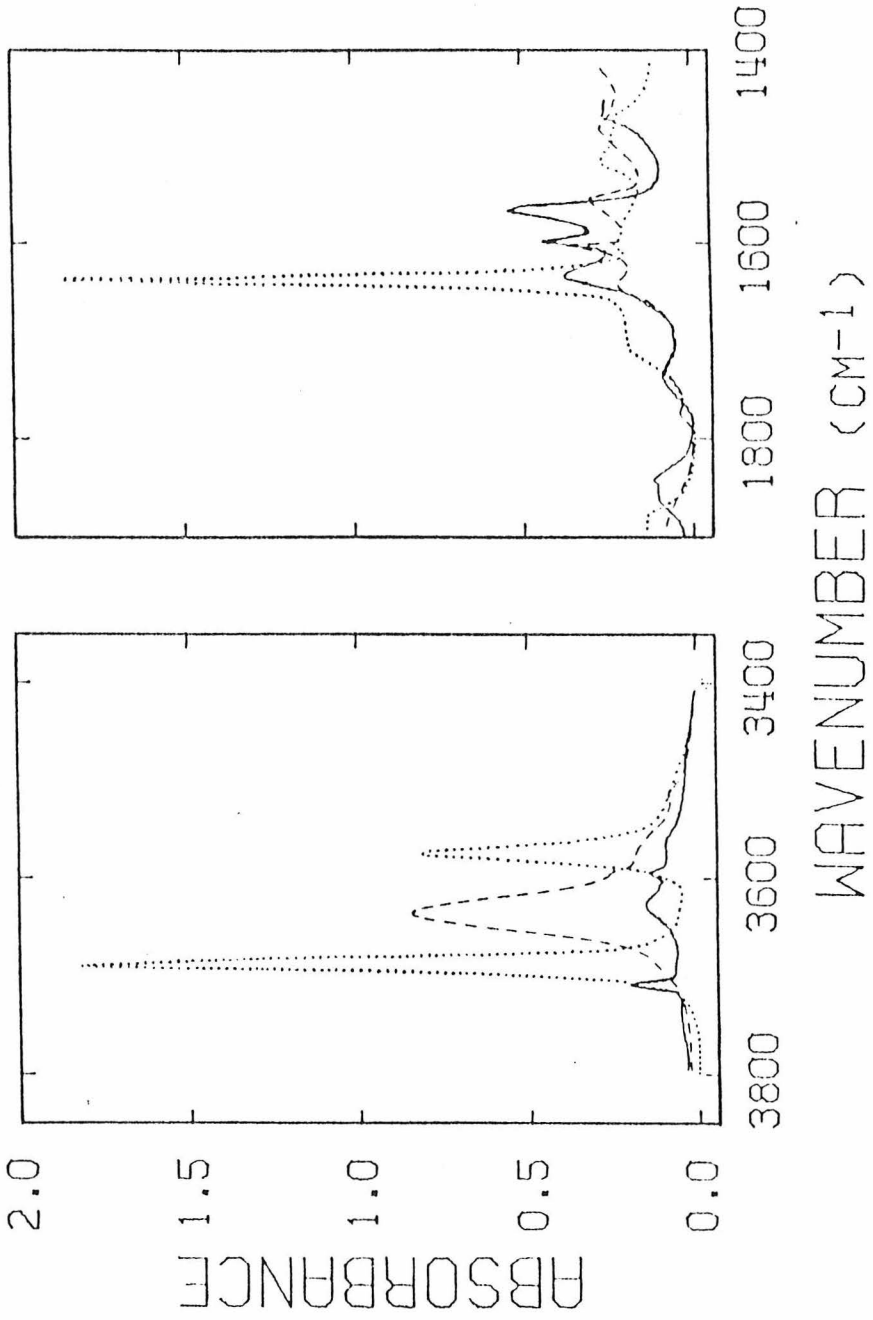
ABSORBANCE
2.0
1.5
1.0
0.5
0.0
3800
3600
3400
1800
1600
1400
WAVENUMBER (CM-1)

Figure 7

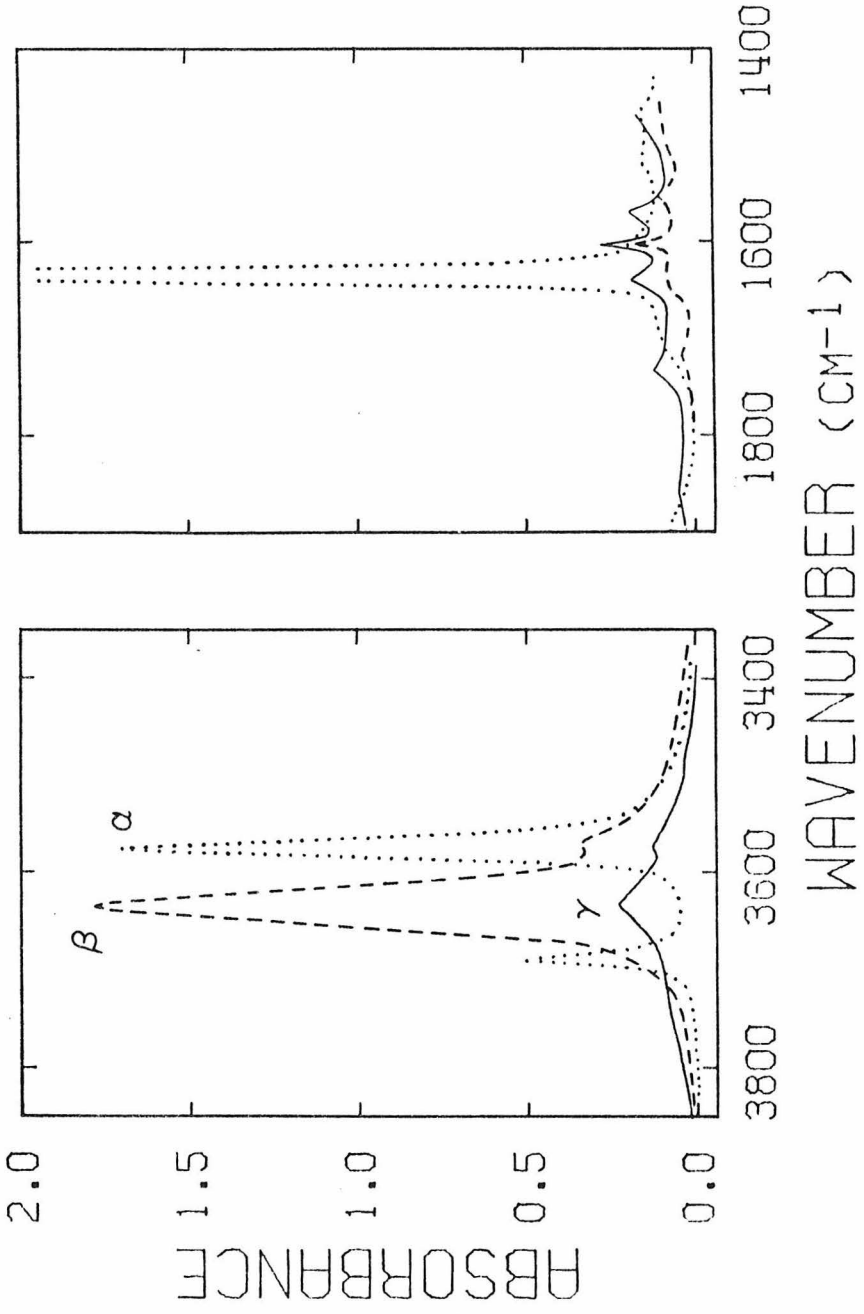
ABSORBANCE
2.0
1.5
1.0
0.5
0.0
3800
3600
3400
1800
1600
1400
WAVENUMBER (CM-1)
α
β
γ

Figure 8

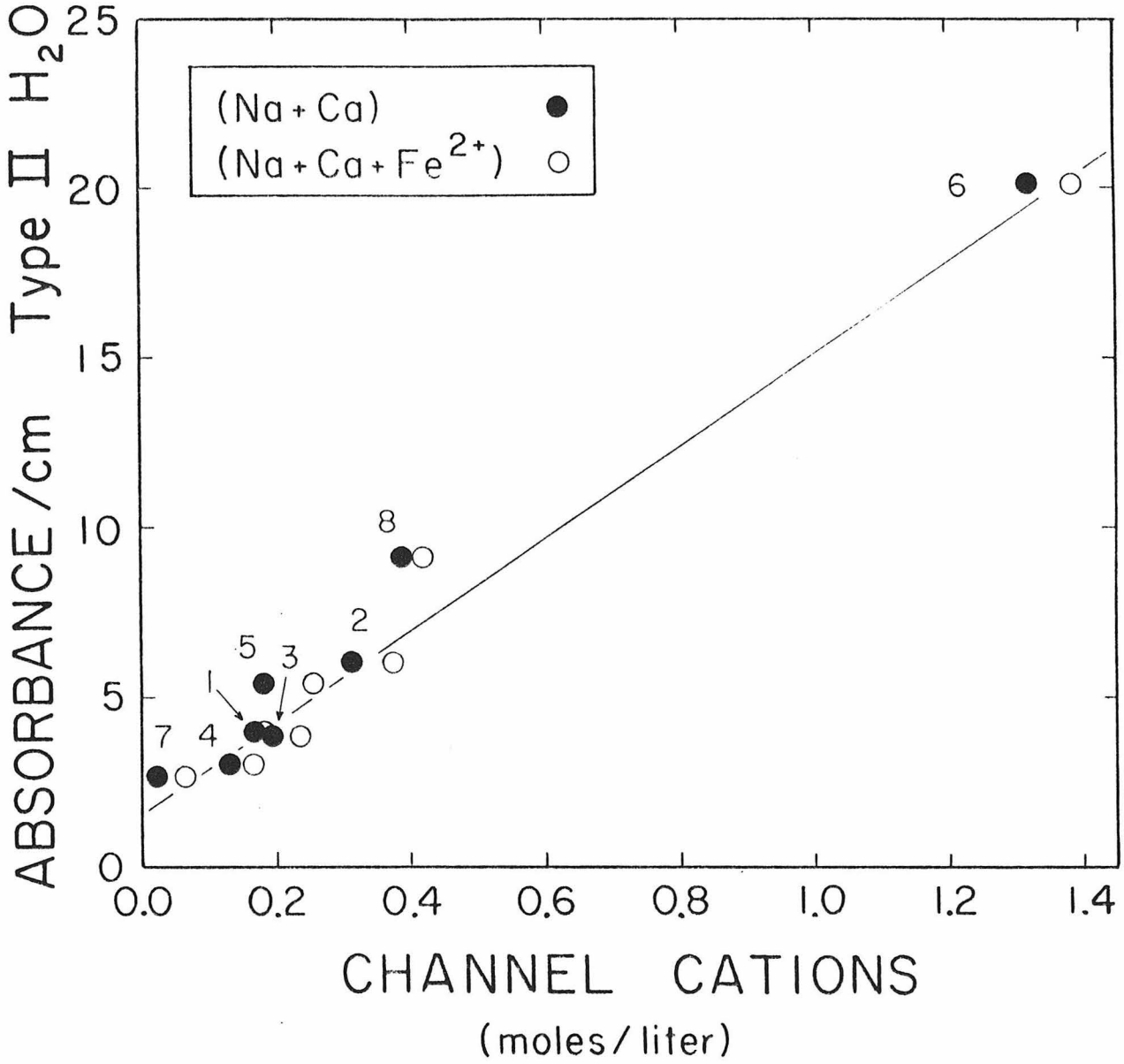
ABSORBANCE /cm Type II H_2O
25
20
15
10
5
0
(Na + Ca)
(Na + Ca + Fe^{2+})
1
2
3
4
5
6
7
8
0.0
0.2
0.4
0.6
0.8
1.0
1.2
1.4
CHANNEL CATIONS
(moles / liter)

Figure 9

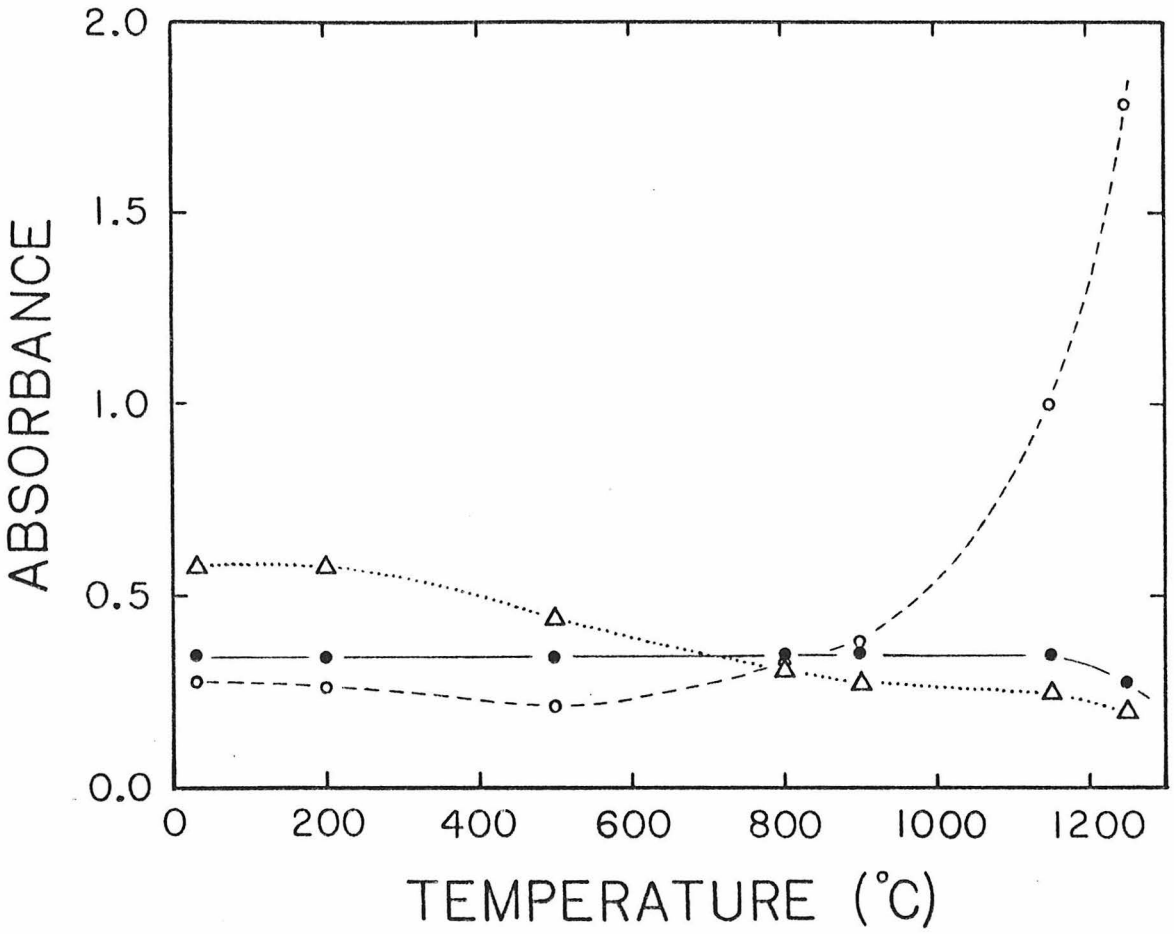
2.0
1.5
1.0
0.5
0.0
ABSORBANCE
0
200
400
600
800
1000
1200
TEMPERATURE (°C)

Figure 10

CHAPTER 9

THE SITE DISTRIBUTION OF IRON AND STRUCTURAL STATE VARIATIONS IN OSUMILITE

INTRODUCTION

Osumilite, $K(Mg,Fe)_2(Al,Fe^{3+})_3(Si,Al)_{12}O_{30}$, is a rare mineral found in rhyolite or rhyodacite volcanic rocks, high grade metamorphic rocks in contact aureoles, and an iron meteorite (see Berg and Wheeler, 1976). The crystal structure of osumilite (Brown and Gibbs, 1969) is similar to that of cordierite and beryl, because it contains channel-like cavities that are formed by the tetrahedral framework. In cordierite and beryl, the channels are formed by a superposition of six-membered tetrahedral rings whereas the channels in osumilite are formed by a superposition of double hexagonal rings (Figure 1). The tetrahedral rings in these minerals are linked together by octahedra and additional tetrahedra.

In the first paper in this series examining cordierite, Goldman et al. (1977) concluded that 1) Fe^{2+} occurs in the octahedral and channel sites, 2) there are two types of water molecules in the channels that differ in crystallographic orientation and interaction with other channel constituents, 3) the blue color of cordierite originates from intervalence charge-transfer between octahedral Fe^{2+} and channel Fe^{3+}, and 4) electronic spectra should be sensitive to structural state, but major differences in structural state were not evident from spectroscopic analyses. These interpretations provide a basis for the study of osumilite.

Samples of osumilite from the type locality in Sakkabira Japan (Miyashiro, 1956), Obsidian Cliffs, Oregon and Nain, Labrador (Berg and Wheeler) are used in this study. The former two samples occur in volcanic rocks, are blue in color, exhibit uniaxially positive optic figures, and are inferred to contain Fe^{3+} in tetrahedral coordination based on stoichiometry (Olsen and Bunch, 1970) and X-ray (Brown and Gibbs) considerations. In contrast to these samples, the Nain osumilite occurs in a granulite, is pink in color, exhibits

biaxially positive optic figures with 2V measurements ranging from 13 to 40° for different crystals in one hand specimen, and is inferred to contain (Mg,Fe^{2+}) in tetrahedral coordination, but little Fe^{3+} (Berg and Wheeler).

This paper reports the findings of a combined electronic absorption and Mössbauer study of the three osumilite samples to examine the site distribution of iron and the origin of color. Changes in the electronic absorption spectra are compared to variations in 2V and inferences are made regarding structural state. In addition, infrared spectra have been taken to evaluate the contention by Olsen and Bunch that osumilite is primarily an anhydrous mineral, and to see if spectral differences exist between the uniaxial and biaxial samples.

EXPERIMENTAL METHODS

Methods of sample preparation, data reduction and data presentation have been described previously (Goldman and Rossman, 1977 a,b). The Sakkabira (Stanford collection number 7753) and Obsidian Cliffs osumilites are uniaxial and polarized electronic absorption spectra were taken on polished ac slabs. There are three different optic directions in the Nain osumilite. Zero and upper level precession photographs were taken on one of the slabs used to obtain electronic spectra (2V=30°) to determine the optic orientation. Deviations from hexagonal $P_{6/mcc}$ symmetry were not apparent, so that the orientation of the α and β indicatrix directions in the plane normal to c is not known. γ is parallel to the c axis. The γ direction for spectroscopic measurement was obtained by first orienting a slab to center the Bxa figure and then rotating this slab 90° about β to obtain a centered flash figure. After obtaining the γ spectrum, the sample was rotated 90° to reproduce the centered Bxa figure, and thinned for measurement of the α and β spectra. Electron microprobe data were taken on the slabs used for the optical spectra and these results are presented in Table 1. Microprobe data for Nain osumilites having 2V's of 24, 30 and 36° were taken to see if variations in 2V can be related to compositional differences, but no such correlation is evident. Microprobe analyses of a Nain osumilite heated at 700°C for 13 hours did not differ from the analyses of the unheated samples. 494, 561 and 520 μg of the Sakkabira, Obsidian Cliffs and Nain samples, respectively, were each ground with 200 mg of KBr and pressed into a pellet for infrared spectroscopic investigation. The pellets were heated in vacuo at 80°C overnight, and repressed to minimize water absorption. All infrared spectra were taken against a KBr reference pellet. Concentrations for the Obsidian Cliffs and Nain samples used in the Mössbauer experiments are about

2.3 and 1.3 mgFe/cm^2 with the off-resonance regions having about 2.9 X 10^6 and 1.1 X 10^6 counts/channel, respectively. All Mössbauer spectra and parameters are reported relative to metallic iron. A Mössbauer spectrum of the Nain osumilite was also taken after heat treatment at 813°C for 13 hours, but significant Fe^{3+} resonance was not observed.

SITE DISTRIBUTION OF IRON

Electronic absorption spectra

The electronic absorption spectra of the uniaxial osumilites from Sakkabira, Japan and Obsidian Cliffs, Oregon are presented in Figures 2 and 3, respectively. They consist of absorption features at 10,280, 15,480, 22,220 and 24,150 cm^{-1} (973, 646, 450 and 414 nm) in ω polarization and 4650, 7020 and 10,280 cm^{-1} (2150, 1425 and 973 nm) in ω polarization. Faye (1972) attributed the asymmetry and greater breadth of the band at 15,480 cm^{-1} in the ω spectrum of the Obsidian Cliffs sample to a superposition of two absorption bands. The dominant, lower energy band was assigned to intervalence charge transfer between tetrahedral Fe^{3+} and octahedral Fe^{2+}, and the subordinate higher energy band was assigned to tetrahedral Fe^{3+}. Faye assigned the weak band near 22,220 cm^{-1} to tetrahedral Fe^{3+} and the band near 10,280 cm^{-1} to octahedral Fe^{2+}.

The electronic absorption spectra of an osumilite from Nain, Labrador having a 2V of 40° (Figure 4) clearly illustrate the three distinct optical directions. The γ spectrum (which has the same crystallographic orientation as ε in Figures 2 and 3) consists of bands at 4686, 7020 and 10,280 cm^{-1} (2135, 1425 and 973 nm). Peak maxima differ slightly for the main band in α and β polarizations and occur at 10,360 and 10,400 cm^{-1} (965 and 962 nm), respectively. The band in the visible region in α and β has a broad maximum between 18,000 and 21,000 cm^{-1} and has a weak shoulder at 22,220 cm^{-1} (450 cm^{-1}), corresponding to the position of the band observed in ω in the other samples. Some of the intensity of the 4686 cm^{-1} band occurs in α, but it is only observed in very thick sections.

Absorptions due to Fe^{2+} can be assigned using the criteria established for cordierite by Goldman *et al.* Therefore, the bands at 10,280 and 7020 cm^{-1}

in γ (or ε) are assigned to Fe^{2+} in the octahedral site. Bands in the 10,200-10,400 cm^{-1} region in α and β (or ω) and the 4650-4700 cm^{-1} region in γ (or ε) are assigned to Fe^{2+} in the channels. The two absorption bands arising from each type of Fe^{2+} are considered to represent electronic transitions to the components of the split $^5\underline{E}_{\underline{g}}$ state. The barycenter (mean) energies of the two transitions for octahedral and channel Fe^{2+} are 8650 and 7590 cm^{-1}, respectively. For comparison, the barycenter energy for octahedral Fe^{2+} in cordierite is about 9200 cm^{-1} (Goldman et al.). The larger barycenter energy in cordierite reflects smaller size of the octahedral site (2.12Å; Gibbs, 1966) than in osumilite (2.15Å; Brown and Gibbs). The barycenter energy can be used as an estimator of 10Dq, the theoretical energy difference between the $^5\underline{T}_{\underline{2g}}$ and $^5\underline{E}_{\underline{g}}$ electronic states, if the splitting of the $^5\underline{T}_{\underline{2g}}$ state is small or similar among the samples to be compared (Faye, 1972). It should therefore vary as $1/\bar{a}^5$, where $\bar{a}$ is the average metal-oxygen bond distance of the coordination site. Using the cordierite data, a barycenter energy of 8575 cm^{-1} is expected for octahedral Fe^{2+} in osumilite from the ideal $1/\bar{a}^5$ dependence. These results support the assignment of the octahedral Fe^{2+} bands in osumilite spectra. In both minerals, the two octahedral Fe^{2+} bands are polarized parallel to the c axis and have similar intensities between each other.

The barycenter energy of channel Fe^{2+} in osumilite of about 7600 cm^{-1} is slightly larger than observed in cordierite (∿ 7200 cm^{-1}). In both minerals, the higher energy band is polarized in the plane normal to the c axis and is much more intense than the lower energy band, which is polarized parallel to the c axis. As in cordierite, heating experiments support the assignment to channel Fe^{2+} in osumilite. After heating an αγ slab in air at 700°C for 13½ hours, the sample was cooled to room temperature and

spectroscopically examined. The bands assigned to octahedral Fe^{2+} retained the same intensity after heat-treatment, whereas both bands assigned to channel Fe^{2+} reduced to about 85 percent of their intensity prior to heating.

Berg and Wheeler suggested from the presence of graphite and pyrrhotite in the rock, that Fe^{3+} is "virtually absent" in the Nain osumilite. Using this assumption and the molar absorptivity determined for octahedral Fe^{2+} in cordierite of 3.5, the intensity of the octahedral Fe^{2+} band at 10,280 cm^{-1} indicates that only about 60 percent of the total iron in the Nain osumilte is in the octahedral site and 40 percent is in the channels. Spectroscopic evidence for tetrahedral Fe^{2+} is not observed. The site distribution of iron in the Nain and Obsidian Cliffs osumilites will now be analyzed using Mössbauer spectroscopy.

Mössbauer spectroscopy

The Mössbauer spectrum of the Nain osumilite (Figure 5) supports the contention of Berg and Wheeler that Fe^{3+} is negligible in this osumilite. The Fe^{2+} resonant absorption is more intense in the low velocity region although both regions have asymmetry in their absorption profiles with the high velocity absorption being broader. It is unlikely that the intensity asymmetry is produced by preferred orientation in the absorber because these crystals do not possess good cleavage. These observations suggest that Fe^{2+} occurs in multiple environments.

A two doublet fit to the spectrum is presented in Figure 5a and the resulting spectral parameters are listed in Table 2. The areas of the two lines of each doublet and the halfwidths of all peaks were constrained to be equal. The large halfwidths of the peaks (0.42 mm/sec) and the inability to fit the main peak intensities and the region near +0.6 mm/sec suggests that this fit is inadequately modeling the data. This poses a problem because the

electronic absorption spectra of osumilite suggest that Fe^{2+} resides in only two types of sites; the octahedral and channel sites. Although a three doublet fit to the spectrum (Figure 5b) provides a better overall spectral fit, a physically meaningful interpretation for each of the three doublets is unclear. In addition, the peak half-width in the three doublet fit (0.38 mm/sec) is still broad for Fe^{2+} in a single site. It is possible that spectral broadening results from variations in next-nearest neighbor chemistry, as has been proposed in clinopyroxenes (Dowty and Lindsley, 1973), orthorhombic Mg-Fe amphiboles (Seifert, 1977) and calcic amphiboles (Goldman, 1977). It is suggested that the outer doublet arises mostly from Fe^{2+} in the octahedral site based on the similar quadrupole splitting and isomer shift found for octahedral Fe^{2+} in cordierite (Goldman et al.), and the inner two doublets are mostly due to Fe^{2+} in the channels. The smaller quadrupole splitting and isomer shift values of the inner doublet(s) are consistent for the more distorted channel environment. The results from the two and three doublet fits indicate that about 68 and 53 percent of the total iron is octahedral Fe^{2+}, respectively. Considering that the three doublet fit probably underestimates octahedral Fe^{2+} content due to increased peak overlap and vice versa for the two doublet fit, an approximate value of 60 percent of the iron in the Nain osumilite being in the octahedral site is reasonable. This would then be in agreement with the site distribution predicted from the electronic absorption spectra.

The Mössbauer spectrum of the Obsidian Cliffs osumilite (Figure 6) also shows asymmetry in the profile and intensity of the Fe^{2+} resonance which is again fitted with three doublets. The three doublets have similar quadrupole splitting and isomer shift values (Table 2) as found in the Nain sample, and the area ratio of the outer doublet to the total Fe^{2+} resonance is 56 percent,

which is also similar to that found in the Nain osumilite. In addition, octahedral Fe^{2+} (the outer doublet) accounts for about 45 percent of the total iron in agreement with value predicted from the electronic absorption spectra (41 percent). The Obsidian Cliffs Mössbauer spectrum contains two additional peaks, not found in the Nain spectrum, that occur near +0.9 and -0.8 mm/sec and have equal intensities. Fitting a doublet to these peaks results in isomer shift and quadrupole splitting values of 0.25 and 1.71 mm/sec, respectively. The isomer shift is indicative of high-spin Fe^{3+}, but this value is much smaller than expected for Fe^{3+} in octahedral coordination ($\sim$ 0.4-0.5 mm/sec). This doublet is assigned to Fe^{3+} in tetrahedral coordination based on the similar parameters reported for tetrahedral Fe^{3+} in ferri-diopside (Hafner and Huckenholz, 1971) and sapphirine (Bancroft et al., 1968), although this assignment is not consistent with the data reported for iron orthoclase (Brown and Pritchard, 1969). Peaks at +0.5 and -0.1 were placed in the spectrum for "octahedral" Fe^{3+} to improve the fit, but whether this doublet represents Fe^{3+} in the octahedral or channel sites is uncertain.

The molar absorptivity in the electronic absorption spectra for octahedral and channel Fe^{2+} in osumilite from the site distribution determined from the Nain sample is 3.5 and 130, respectively.

STOICHIOMETRY

The average of the three electron microprobe analyses of the Nain osumilite (Table 1) has been normalized to the theoretical 30 oxygens in which all iron is considered to be Fe^{2+} based on the Mössbauer data. The resulting formula is:

$$(Na_{0.10}K_{0.89}Fe^{2+}_{0.37})^{XII}(Mg_{1.43}Fe^{2+}_{0.53}Mn_{0.01})^{VI}(Al_{2.66})^{IV}(Si_{10.24}Al_{1.76})O_{30}$$

There is clearly more Fe^{2+} and Mg available than can be accommodated in the octahedral site. Berg and Wheeler placed the excess in the tetrahedral (T2) site with Al. They based this interpretation from a plot of osumilite formulas with regard to two coupled substitutions: the first involves (Mg,Fe) replacing Al in tetrahedral coordination and Si replacing Al; and the second involves (Na,K) entering the channels with Al replacing Si. The observation that natural osumilites have more than 2.0 formula units of Mg and Fe^{2+} suggested the presence of these ions in tetrahedral coordination. However, the results of the present study do not indicate the presence of tetrahedral Fe^{2+}, and therefore, Fe^{2+} should not be included in the first coupled substitution. In this case, natural osumilite compositions would plot in the field (Mg <2) which does not necessitate tetrahedrally coordinated Mg, although some of this substitution may occur. The 0.34 vacancies in the T2 site only amounts to 2 percent vacancies in the 15 tetrahedral sites. The resulting octahedral Fe^{2+} to total Fe ratio of 59 percent in consistent with the determinations from Mössbauer and electronic absorption spectra.

The resulting formula of the Obsidian Cliffs osumilite using an Fe^{3+}/Fe^{T} ratio of 0.20 determined from the Mössbauer spectrum is:

$$(Na_{0.06}K_{0.69}Fe^{2+}_{0.10})^{XII}(Mg_{0.75},Fe^{2+}_{1.01}Fe^{3+}_{0.06}Ti_{0.01}Mn_{0.17})^{VI}(Al_{2.66}Fe^{3+}_{0.23})^{IV}$$

$$(Si_{10.30}Al_{1.70})^{IV}O_{30}$$

The resulting site distribution of Fe^{2+} from this formula does not agree with the distribution expected from Mössbauer and electronic absorption spectra, and the reason for the discrepancy is unclear. Again, there appear to be vacancies in the T2 site containing the Al and Fe^{3+} ions, which is in general agreement with the findings of Olsen and Bunch for natural osumilites. The formula for the Sakkabira osumilite may be found in Olsen and Bunch and will not be analyzed herein without knowledge of the Fe^{3+}/Fe^{2+} ratio.

WATER

Olsen and Bunch found that the weight percent of the oxides in microprobe analyses of osumilites summed near 100 percent, and concluded that natural osumilites are virtually anhydrous. Infrared spectra of single crystals of osumilite support this interpretation. The fundamental stretching modes of water occur in the 3300--3700 cm^{-1} region, but this region is free of absorption features in the Sakkabira and Obsidian Cliffs osumilites. The Nain osumilite does have water absorptions in this region, but the water content is calculated to be less than 0.01 percent (by weight) using the molar absorptivity for water determined in cordierite by Goldman et al. The presence of the combination mode at 5250 cm^{-1} in γ (Figure 4) indicates that this water is oriented with its H-H direction parallel to the c axis.

Brown and Gibbs found electron density in the center of cavities between the double hexagonal ring groups and attributed it to (Na,K,Ca) ions. They also found electron density near the center of the cavity within the double hexagonal rings and attributed it to H_2O. However, the results of this study indicate that the Sakkabira osumilite is anhydrous. This suggests that cations also occur within the double hexagonal rings.

ORIGIN OF COLOR

Heating experiments on cordierite (Goldman et al.) suggested that the blue color originates from intervalence charge transfer between octahedral Fe^{2+} anc channel Fe^{3+}. Heating experiments were conducted on the Obsidian Cliffs osumilite at 813°C, but after prolonged heat treatment the intensity of the spectral features in ω remained the same. The Nain osumilite was heated for one hour at 813°C and then one hour at 869°C. Intensities of the octahedral features remained the same after heat treatment, but significant changes occurred in the unpolarized spectrum normal to the c axis, as shown in Figure 7. The channel Fe^{2+} band near 10,400 cm^{-1} reduced in intensity and the sample turned from pink to blue in color after heat-treatment. Analagous to the results for cordierite, this suggests that the blue color in osumilite is due to intervalence charge transfer between octahedral Fe^{2+} and Fe^{3+} in the cavities between the double hexagonal ring groups. The origin of the pink color in the Nain osumilite is unclear. The possibility that an intervalence charge transfer between octahedral Fe^{2+} and Fe^{3+} in the adjacent tetrahedral site is responsible for some of the blue color in the Sakkabira and Obsidian Cliffs osumilites cannot be excluded. It may be a possible cause for the asymmetry of the main charge-transfer band.

It is interesting to note that water in the channels appears to correlate with the ease at which channel Fe^{2+} will oxidize upon heating. Channel Fe^{2+} was not oxidized at 869°C in the anhydrous Obsidian Cliffs osumilite. About 15 percent of the channel Fe^{2+} was oxidized at 700°C in the Nain osumilite, which contains minor amounts of water. Nearly 45 percent of the channel Fe^{2+} is oxidized at these temperatures in water-bearing cordierites.

STRUCTURAL STATE

There exists an interesting discrepancy between the electronic absorption and X-ray data concerning the structural state of the Nain osumilite. X-ray precession photographs of the Nain osumilite taken as a part of this study are consistent with a hexagonal $P_{6/mcc}$ space group. This result has been independently confirmed by Professor Gordon Brown (personal communication) at Stanford University. However, the three distinct optic directions indicate that the overall symmetry must be lower than hexagonal. In the Sakkabira sample, there are only two optic directions and the 2V is zero. Therefore, if the Nain osumilite was truly hexagonal, the bands in α and β due to channel Fe^{2+} near 10,400 cm^{-1} would have equal intensities, being in the plane normal to the c axis. Since the Nain samples exhibit a wide range of 2V, the relationship between 2V and the β/α intensity ratio of the channel Fe^{2+} bands was explored, and the results are presented in Figure 8. The hexagonal Sakkabira and Obsidian Cliffs osumilites are also included in this correlation, which shows that the intensity asymmetry in the plane normal to c increases as the 2V increases. The trend is not linear and appears to have an upward curvature. This trend intersects typical values for cordierite which have asymmetry values near 2.0 with 2V values of 80-90°.

The correlation in Figure 8 was not expected initially because the band intensity differences are due to the effect of the coordination about the channel Fe^{2+} ion on its electronic structure whereas 2V is determined by differences in refractive index along the different crystal directions in the visible region. For instance, the refractive indices along α and β must have changed after the Nain samples became blue in color from heating. Nevertheless, the 2V remained the same after heating. It is important to realize that cordierite, which has a completely ordered Al and Si tetrahedral framework (Gibbs), has a large 2V and band intensity difference. In contrast,

the Sakkabira osumilite, which has a disordered tetrahedral framework (Brown and Gibbs), has a 2V equal to zero and no difference in band intensity. These results suggest that the Nain osumilites have variable degrees of Al and Si order in the double hexagonal rings which control the overall optics of the crystal. A greater degree of order is expected in the slowly cooled Nain osumilite compared to the quickly cooled volcanic osumilites from Sakkabira and Obsidian Cliffs.

The infrared spectra of the three osumilites have been taken to see if differences exist between the Nain sample (Figure 9) and the hexagonal osumilites from Sakkabira (Figure 10) and Obsidian Cliffs (Figure 11). Although differences exist in the band near 1150 cm^{-1} and in the 800-500 cm^{-1} region among these samples, major differences in band complexity in the Nain sample are not apparent.

ACKNOWLEDGMENTS

Professor W. A. Dollase (UCLA) kindly took the Mössbauer spectra used in this study and fitted the spectrum of the Obsidian Cliffs sample, although I take full responsibility for any errors in its interpretation. I also thank Dr. J. Berg (U. Mass.) for providing a large hand specimen containing the Nain osumilite, Professor Gordon Brown for the crystals of the Sakkabira osumilite and many discussions concerning osumilite crystal chemistry, and Professor George Rossman for taking some of the infrared data as well as numerous discussions during the course of this study. J. Huneke kindly provided additional material from the Oregon locality.

REFERENCES

Bancroft, G. M., R. G. Burns and A. J. Stone (1968). Applications of the Mössbauer effect to silicate mineralogy-II. Iron silicates of unknown and complex crystal structures. Geochim. Cosmochim. Acta, 32, 547-559.

Berg, J. H. and E. P. Wheeler (1976). Osumilite of deep-seated origin in the contact aureole of the anothositic Nain complex, Labrador. Am. Mineral., 61, 29-37.

Brown, G. E. and G. V. Gibbs (1969). Refinement of the crystal structure of osumilite. Am. Mineral. 54, 101-116.

Brown, F. F. and A. M. Pritchard (1969). The Mössbauer spectrum of iron orthoclase. Earth Planet. Sci. Lett., 5, 259-260.

Dowty, E. and D. H. Lindsley (1973) Mössbauer spectra of synthetic hedenbergite-ferrosilite pyroxenes. Am. Mineral. 58, 850-868.

Faye, G. H. (1972). Relationship between crystal-field splitting parameter, "Δ_{V1}", and M_{host} -O bond distance as an aid in the interpretation of absorption spectra of Fe^{2+}- bearing materials. Canad. Mineral., 11, 473-487.

Gibbs, G. V. (1966). The polymorphis in cordierite I: The crystal structure of low cordierite. Amer. Mineral., 51, 1068-1087.

Goldman, D. S. and G. R. Rossman (1977a). The spectra of iron in orthopyroxene revisited: The splitting of the ground state. Am. Mineral. 62, 151-157.

Goldman, D. S. and G. R. Rossman (1977b). The identification of Fe^{2+} in the M(4) site of calcic amphiboles. Am. Mineral. 62, 205-216.

Goldman, D. S. (1977) . A re-evaluation of the Mössbauer spectroscopy of calcic amphiboles. Am. Mineral. 62 (in press).

Goldman, D. S., G. R. Rossman and W. A. Dollase (1977). Channel constituents in cordierite. Am. Mineral. 62 (in press).

Hafner, S. S. and H. G. Huckenholz (1971). Mössbauer spectrum of synthetic ferri-diopside. Nature, 233, 9-11.

Miyashiro, A. (1956) Osumilite, a new silicate mineral and its crystal structure. Am. Mineral. 41, 104-116.

Olsen, E. and T. E. Bunch (1970) Compositions of natural osumilites. Am. Mineral. 55, 875-879.

Seifert, F. (1977) Compositional dependence of the hyperfine interaction of ^{57}Fe in anthophyllite. Phys. Chem. Minerals, 1, 43-52.

TABLE 1. ELECTRON MICROPROBE ANALYSES OF OSUMILITE

oxide	weight percent				
	Labrador 2V=36°	Labrador 2V=30°	Labrador 2V=24°	Japan	Oregon
SiO_2	60.3	61.2	60.8	60.6	60.7
TiO_2	0.2	0.2	0.2	0.0	0.1
Al_2O_3	22.0	22.2	22.4	22.0	21.8
MgO	5.7	5.7	5.6	3.0	3.0
MnO	6.3	6.4	6.6	9.4	9.7
FeO*	0.1	0.1	0.1	1.0	1.2
Na_2O	0.2	0.4	0.3	0.7	0.2
KaO	4.0	4.3	4.2	3.2	3.2
	99.0	100.5	100.1	99.9	99.9

*total iron reported as FeO

TABLE 2. MÖSSBAUER PARAMETERS

Sample	Peaks	Isomer Shift	Quadrupole Splitting	Half-Width	% Area	X^2
Nain	AA'	1.20	2.35	0.42	68	392*
Labrador	BB'	1.14	1.86	0.42	32	
Nain	AA'	1.21	2.41	0.38	53	313*
Labrador	BB'	1.16	2.03	0.38	35	
	CC'	1.17	1.48	0.38	12	
Obsidian	AA'	1.19	2.33	0.33	45	539**
Cliffs	BB'	1.20	1.86	0.33	20	
Oregon	CC'	1.21	1.40	0.33	15	
	DD'	0.25	1.71	0.33	16	
	EE'	0.40	0.60	0.33	4	

*200 channels fitted **330 channels fitted

FIGURE CAPTIONS

1. The tetrahedral framework in cordierite and osumilite (after Brown and Gibbs, 1969).
2. Room-temperature electronic absorption spectra of an osumilite from Sakkabira, Japan. Optic orientation: ε = $\underline{c}$; ω = $\underline{a}$. Crystal thickness = 0.01 mm.
3. Room-temperature electronic absorption spectra of an osumilite from Obsidian Cliffs, Oregon. Optic orientation: ε = $\underline{c}$; ω = $\underline{a}$. Crystal thickness = 0.01 mm.
4. Room temperature electronic absorption spectra of an osumilite from Nain, Labrador. Optic orientation: γ = $\underline{c}$; α and β occur in the plane normal to the $\underline{c}$ axis. Crystal thickness = 0.01 mm. $2V = 40^{o}$.
5. Room temperature Mössbauer spectrum of osumilite from Nain, Labrador, fitted with two (a) and three (b) quadrupole doublets due to Fe^{2+}.
6. Room temperature Mössbauer spectrum of osumilite from Obsidian Cliffs, Oregon.
7. Electronic absorption spectra of an osumilite from Nain, Labrador, before heat treatment and after heating at 813°C for 1 hour and then for 1 hour at 869°C. The sample turned from pink to blue after heating.
8. Correlation between 2V and the intensity ratio of the channel Fe^{2+} absorption bands in the plane normal to the $\underline{c}$ axis in osumilite.
9. Room temperature infrared spectrum of osumilite from Nain, Labrador.
10. Room temperature infrared spectrum of osumilite from Sakkabira, Japan.
11. Room temperature infrared spectrum of osumilite from Obsidian Cliffs, Oregon.

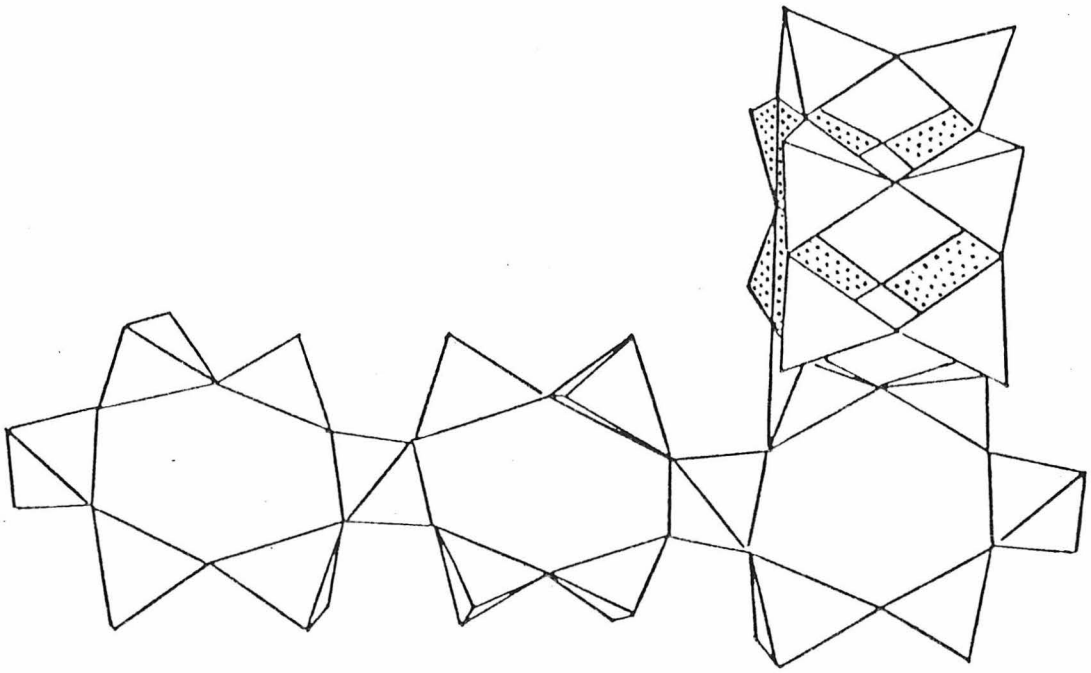

OSUMILITE

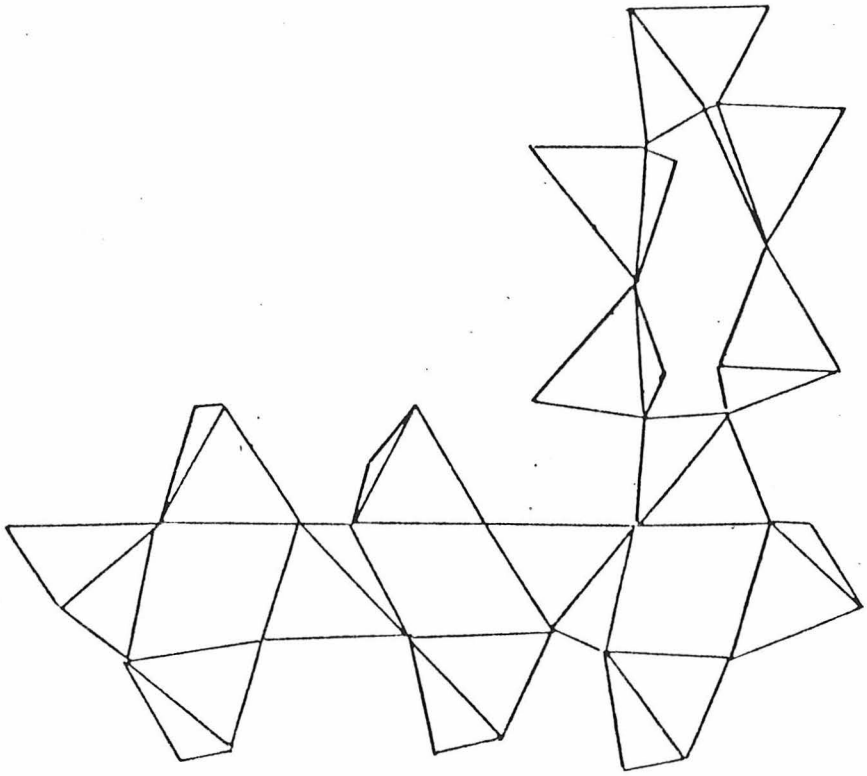

CORDIERITE

Figure 1

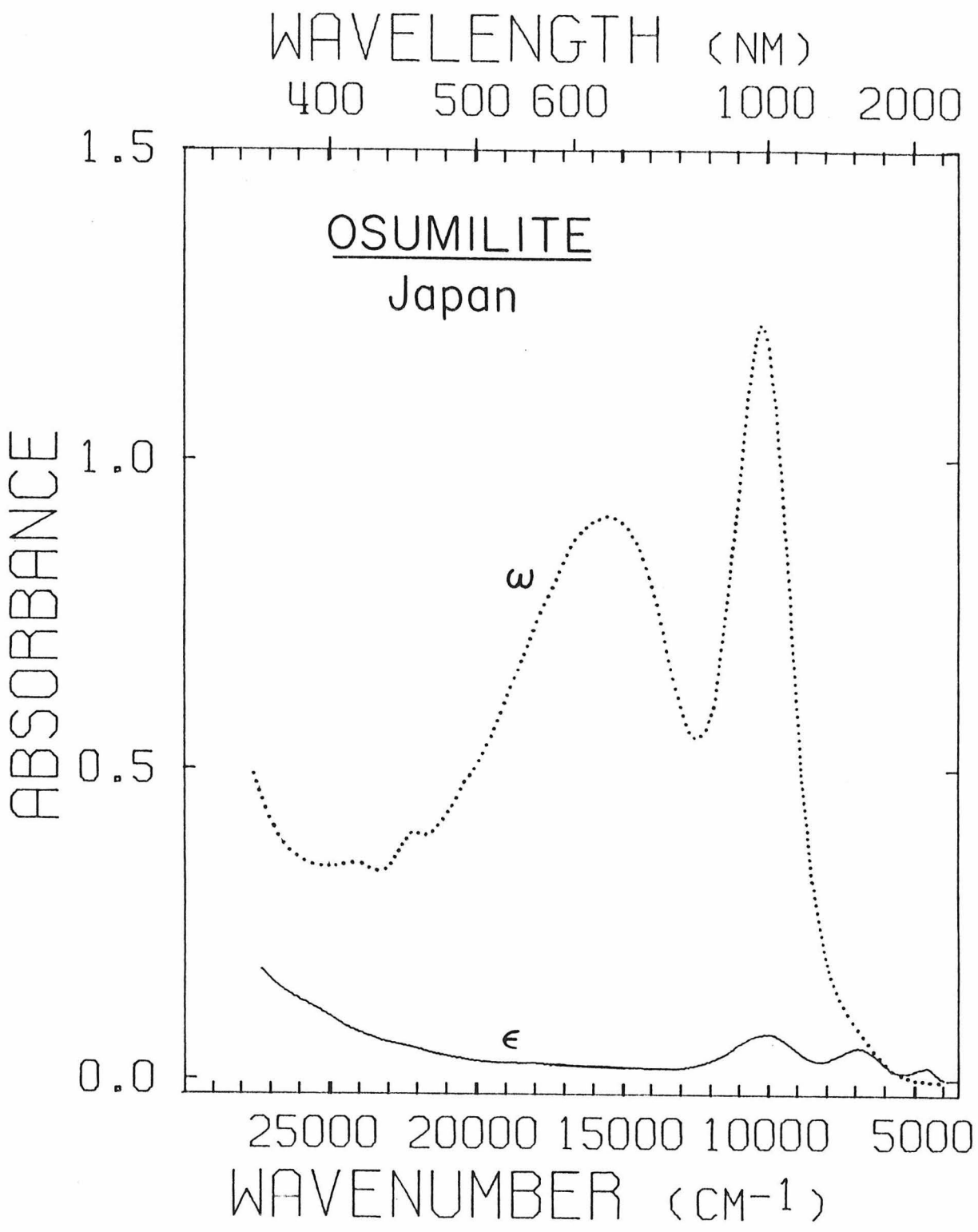
WAVELENGTH (NM)
400
500
600
1000
2000
1.5
OSUMILITE
Japan
ABSORBANCE
1.0
0.5
0.0
ω
ϵ
25000
20000
15000
10000
5000
WAVENUMBER (CM-1)

Figure 2

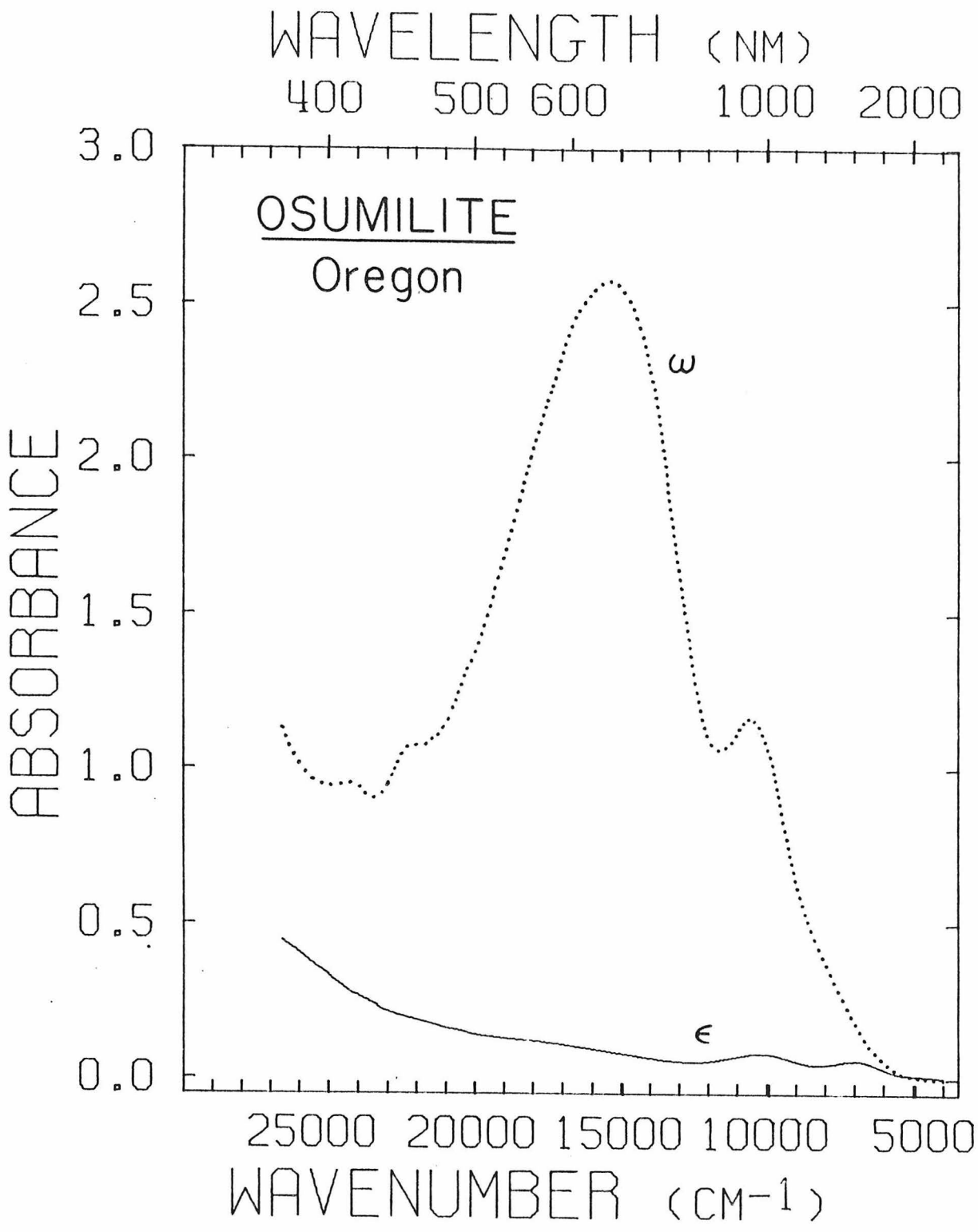
WAVELENGTH (NM)
400 500 600 1000 2000
OSUMILITE
Oregon
ω
ε
ABSORBANCE
3.0
2.5
2.0
1.5
1.0
0.5
0.0
25000 20000 15000 10000 5000
WAVENUMBER (CM-1)

Figure 3

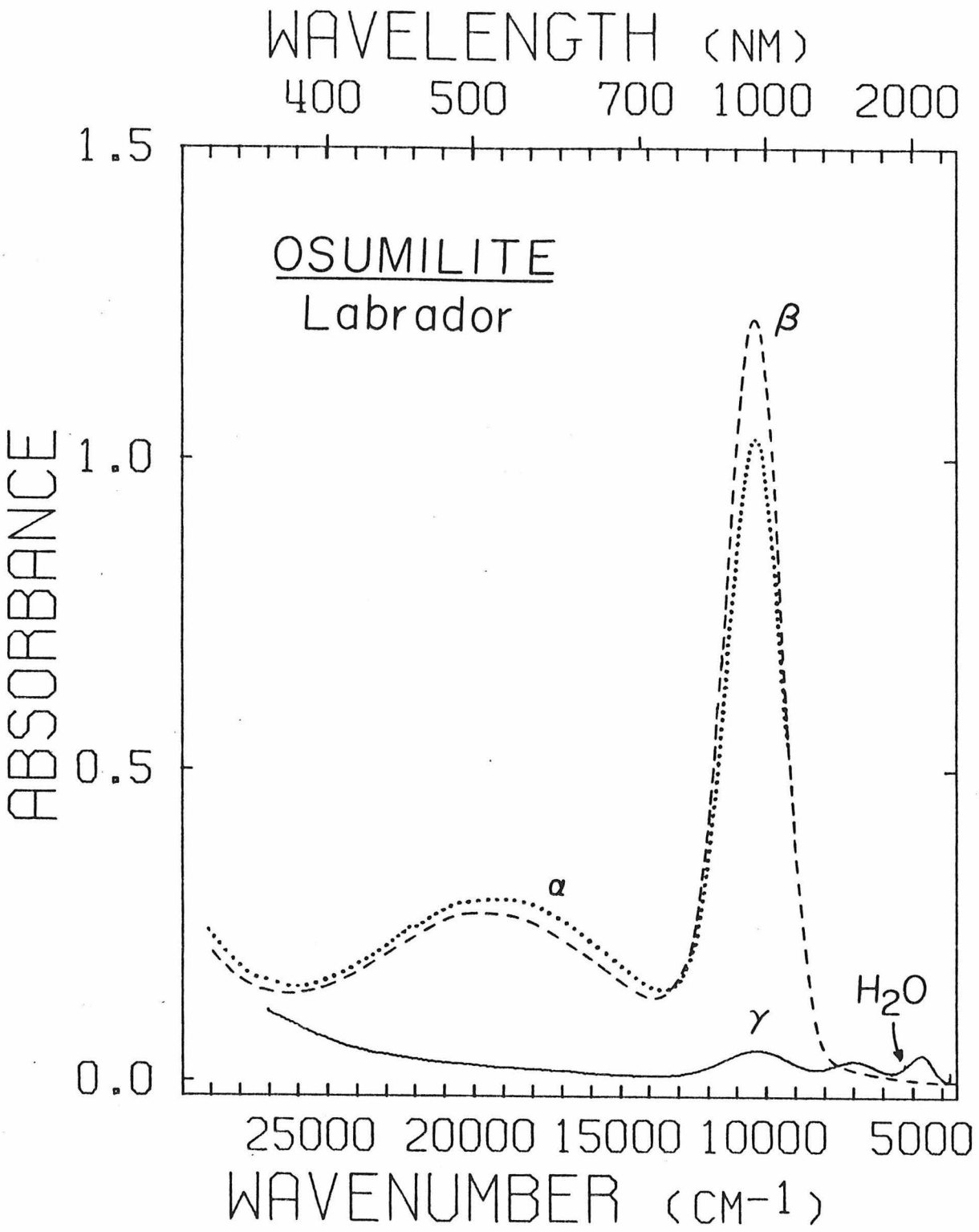
WAVELENGTH (NM)
400 500 700 1000 2000
1.5
OSUMILITE
Labrador
β
ABSORBANCE
1.0
0.5
α
γ
H2O
0.0
25000 20000 15000 10000 5000
WAVENUMBER (CM-1)

Figure 4

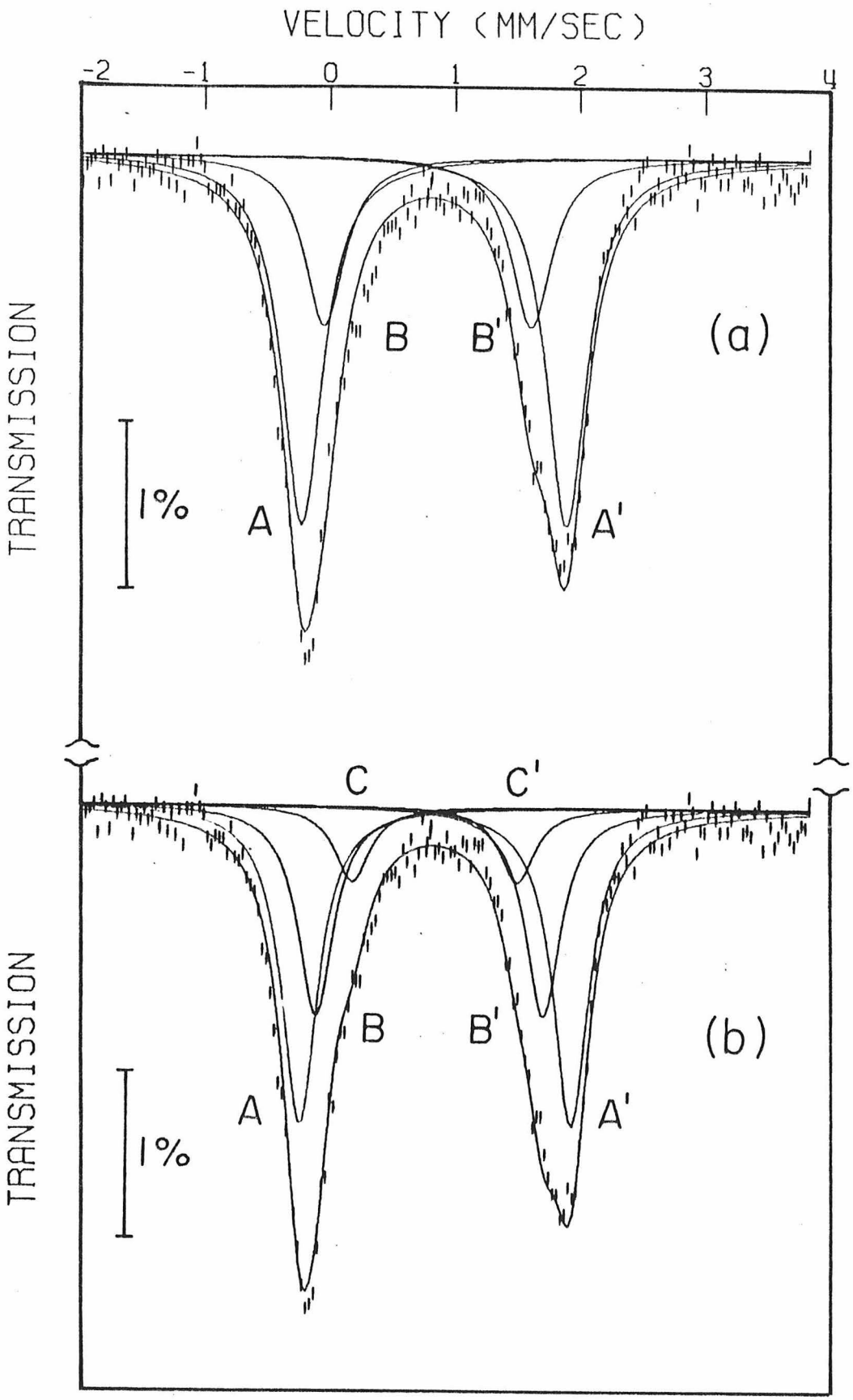
VELOCITY (MM/SEC)
-2
-1
0
1
2
3
4
TRANSMISSION
1%
A
B
B'
A'
(a)
C
C'
TRANSMISSION
1%
A
B
B'
A'
(b)

Figure 5

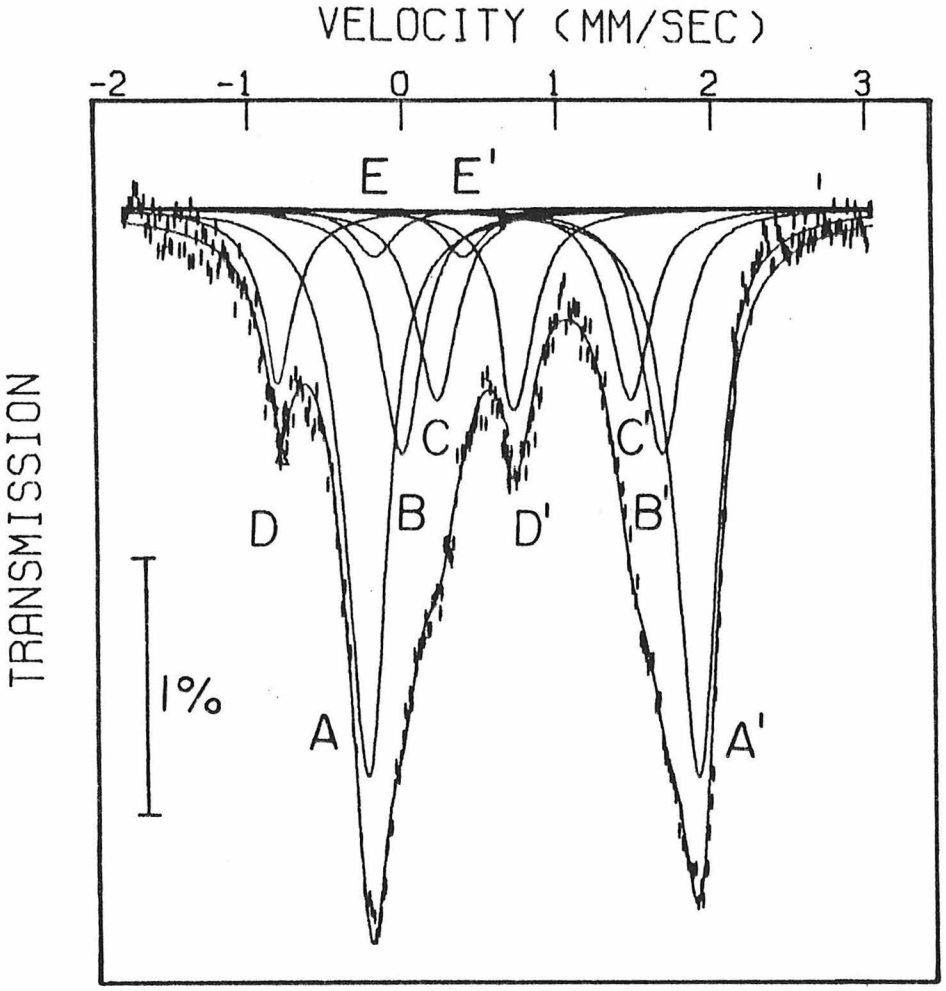

Figure 6

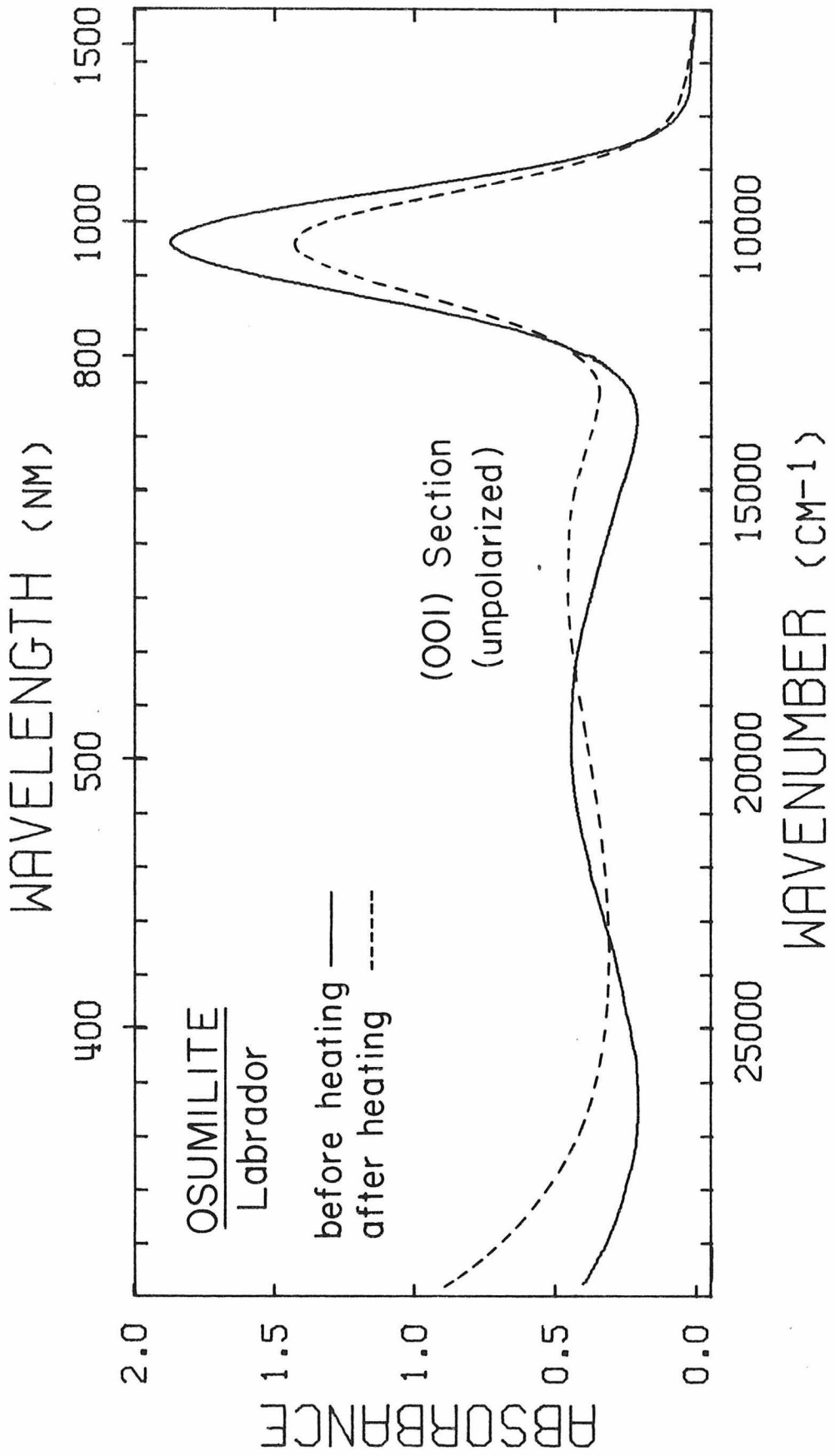
WAVELENGTH (NM)
400
500
800
1000
1500
WAVENUMBER (CM-1)
25000
20000
15000
10000
ABSORBANCE
2.0
1.5
1.0
0.5
0.0
OSUMILITE
Labrador
before heating
after heating
(001) Section
(unpolarized)

Figure 7

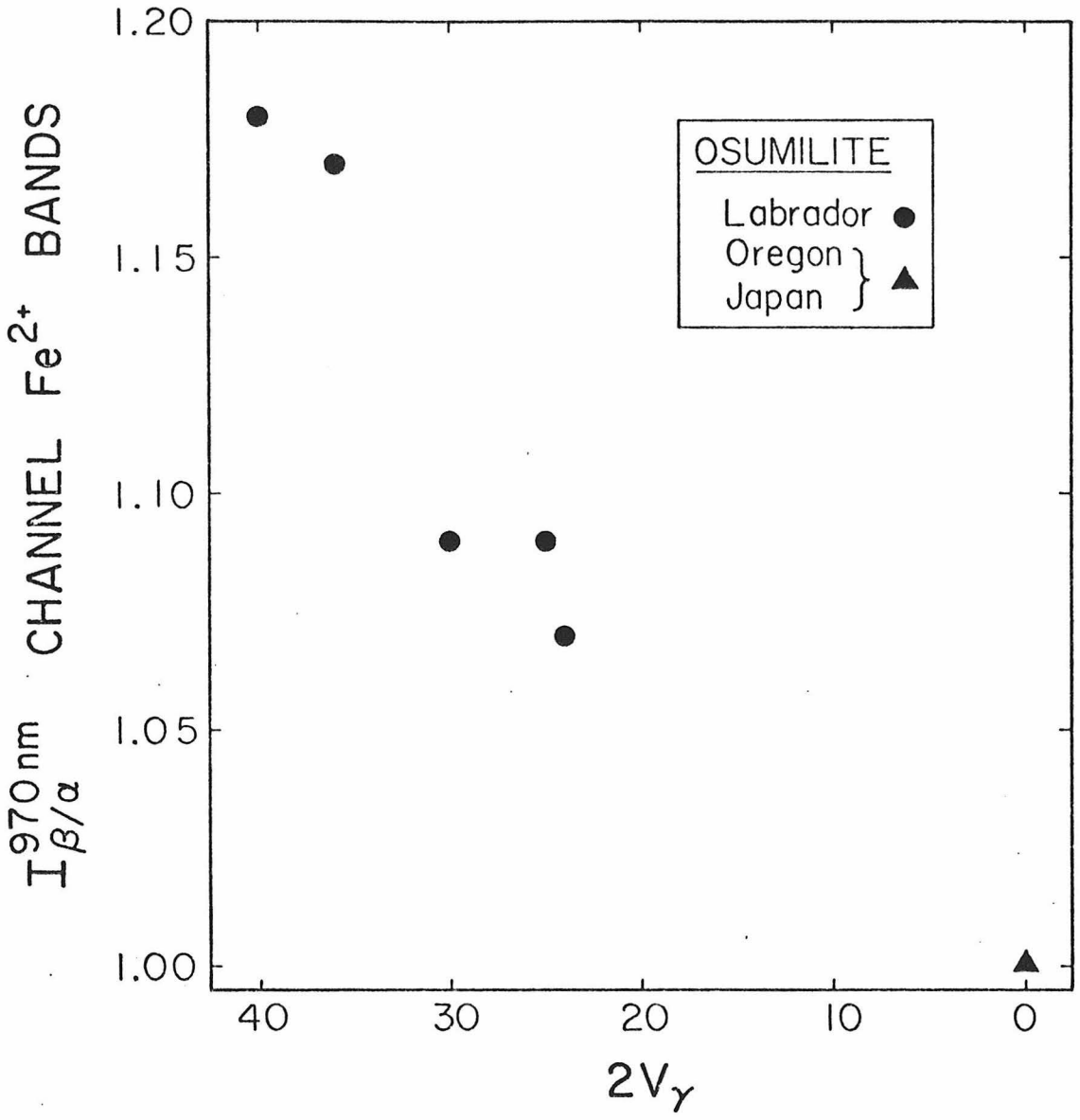
1.20
1.15
1.10
1.05
1.00
40
30
20
10
0
$2V_\gamma$
$I^{970\,nm}_{\beta/\alpha}$ CHANNEL Fe^{2+} BANDS
OSUMILITE
Labrador
Oregon
Japan

Figure 8

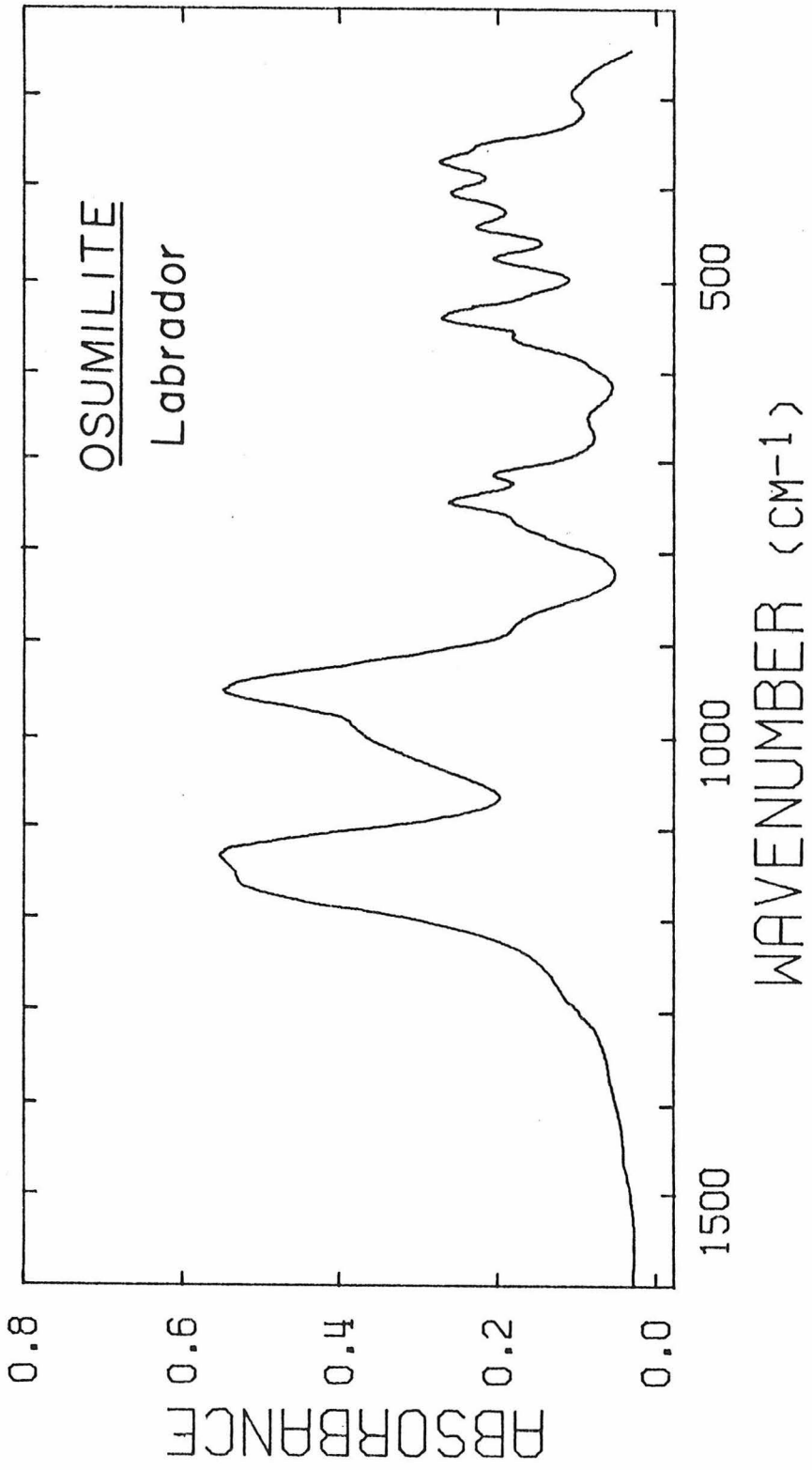
OSUMILITE
Labrador
ABSORBANCE
0.0
0.2
0.4
0.6
0.8
1500
1000
500
WAVENUMBER (CM-1)

Figure 9

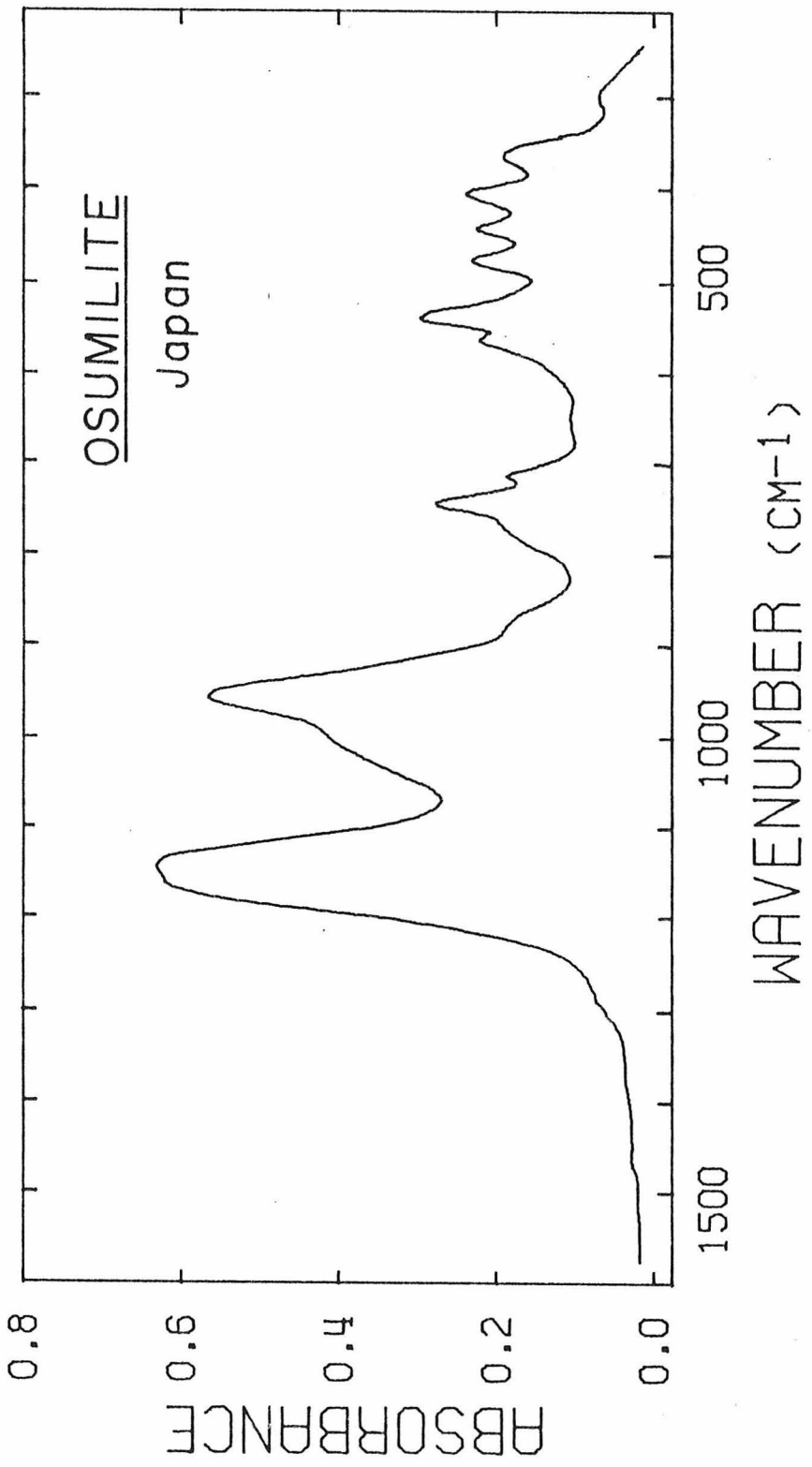
OSUMILITE
Japan
ABSORBANCE
0.0
0.2
0.4
0.6
0.8
1500
1000
500
WAVENUMBER (CM-1)

Figure 10

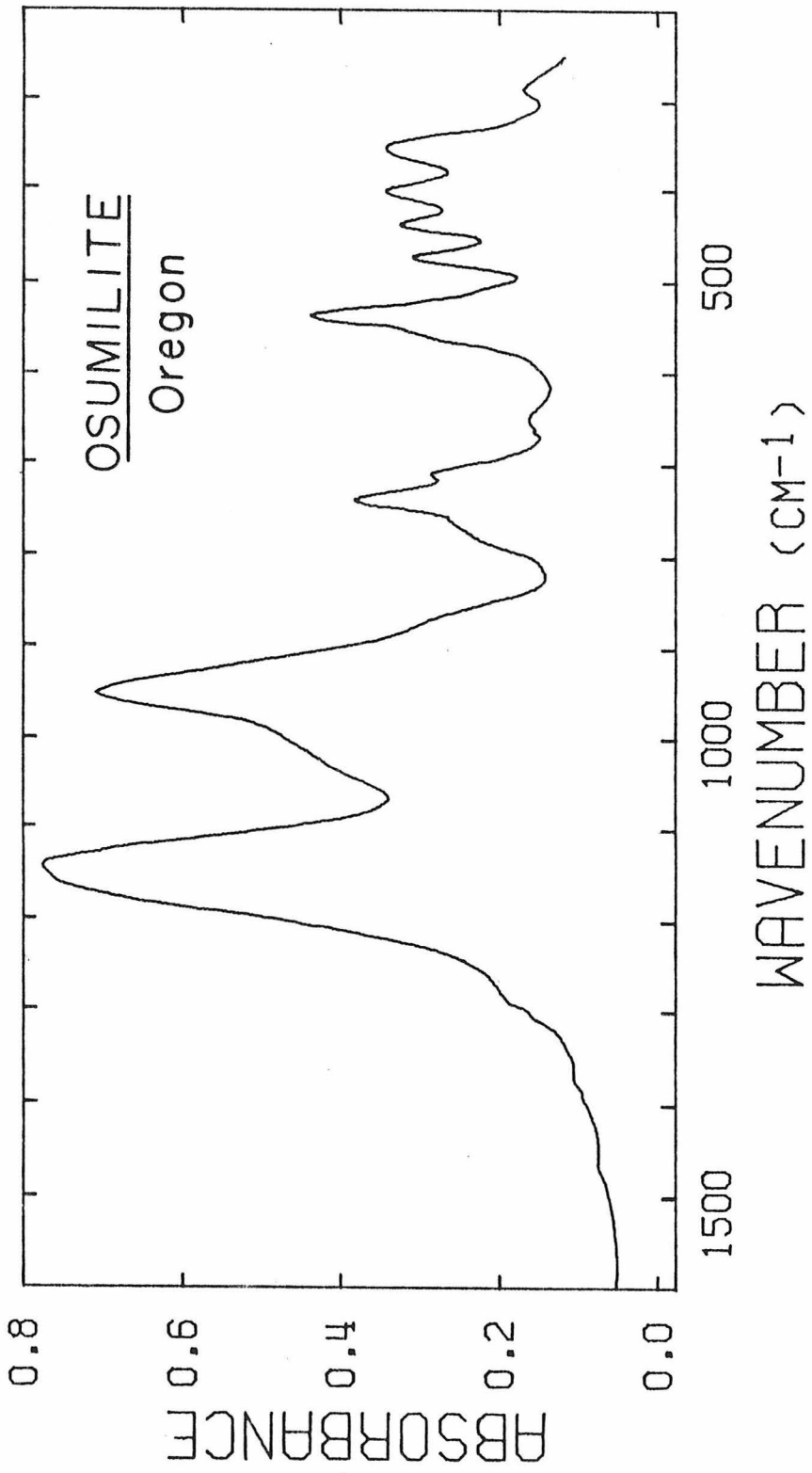
OSUMILITE
Oregon
ABSORBANCE
0.8
0.6
0.4
0.2
0.0
1500
1000
500
WAVENUMBER (CM-1)

Figure 11

CHAPTER 10

Fe^{2+} BAND ASSIGNMENTS IN BERYL

ABSTRACT

The electronic absorption spectra of Fe^{2+} in non-chromium beryls are examined. Bands at about 830 and 1000 nm in ε polarization are assigned to Fe^{2+} in the Al-rich octahedral site, and bands at 830 nm in ω and 2100 nm in ε are assigned to Fe^{2+} in a position in the channel. A band at 620 nm in ε that is responsible for the blue coloration in some beryls (Wood and Nassau, 1968) is interpreted in terms of an Fe^{2+}/Fe^{3+} intervalence charge-transfer.

INTRODUCTION

The variation in intensity among the absorption features in the 600-1000 nm region in non-chromium varieties of beryl, $Be_3Al_2Si_6O_{18}$, has been attributed to ferrous iron in multiple sites (Wood and Nassau, 1968). A band at 810 nm (ω) was assigned to Fe^{2+} in the Al-rich octahedral site. A broad band centered at 810 nm (ε) was assigned to Fe^{2+} in a position in the channels, and a band at 620 nm (ε) was assigned to Fe^{2+} in a different channel site. These spectral features varied independently among the samples examined. These features are similar to those observed in cordierite (Goldman et al., 1977) and osumilite (chapter 9). However, the band assignments for cordierite and osumilite are not consistent with those for beryl, and this apparent discrepancy forms the basis for this study.

EXPERIMENTAL METHODS

Sections of a golden beryl from Goyaz, Brazil (GRR5/25/76) and a yellow beryl from an unknown locality (GRR11/11/74) were oriented in the ac plane using external morphology and conoscopic interference figures. These crystals were thinned, polished and spectroscopically examined at room temperature. Additional spectroscopic data from other beryl samples were provided by Professor George Rossman (Cal Tech).

SPECTRAL INTERPRETATION

The spectra of a yellow beryl from an unknown locality and a golden beryl from Goyaz, Brazil are presented in Figures 1 and 2, respectively. Sharp bands between 900 and 2000 nm have been attributed to vibrations of water molecules in the channel cavities by Wood and Nassau (1967). These figures demonstrate that the two bands in ε at about 830 and 1000 nm are related to each other, and therefore originate from the same Fe^{2+} ion. They are not related to the band in ω at 830 nm, which must arise from a different Fe^{2+} ion.

The two bands in cordierite (Goldman et al) and osumilite (chapter 9), attributed to Fe^{2+} in the octahedral sites of these minerals, occur in the direction parallel to the c axis in the 900-1500 nm region. Based on these interpretations, the two bands in beryl at 830 and 1000 nm in ε are assigned to Fe^{2+} in the octahedral site. The barycenter (mean) energy of the two bands from octahedral Fe^{2+} in these minerals decreases as the size of the site becomes larger (Figure 3).

A band at 830 nm in ω is assigned to Fe^{2+} in a channel site. The bands due to channel Fe^{2+} in this region in cordierite and osumilite are also polarized in the direction normal to the c axis. Due to the large size of the channel site, the remaining band from the splitting of the ^5E_g electronic state is expected to occur in the 2000 nm region. It is expected to be polarized parallel to the c axis based on the cordierite and osumilite spectra. It is apparent from Figures 1 and 2 that the yellow beryl, which has an intense channel Fe^{2+} band at 830 nm in ω, also has broad intensity in ε in the 1800-2300 nm region. In contrast, the channel Fe^{2+} band in the golden beryl is weak, and there is not appreciable intensity in the 1800-2300 nm region. To test whether the

second ^5E_g component of channel Fe^{2+} occurs in this region, the intensity at 2100 nm in ε has been compared to the intensity of the channel Fe^{2+} band at 830 nm in ω for a number of samples, and the results are presented in Figure 4. The resulting linear correlation indicates that both bands are produced by the same Fe^{2+} ion. Their barycenter energy of about 8400 cm^{-1} supports their assignment to a position in the large channels.

The band at 620 nm reported by Wood and Nassau (1968) probably originates from an Fe^{2+}/Fe^{3+} intervalence charge-transfer process. It is unlike the assigned charge-transfer bands in cordierite and osumilite because it is polarized parallel to the c axis, and not normal to it. This may suggest that the Fe^{2+} - Fe^{3+} couple occurs in the channel parallel to the c axis. Because there is also a "cavity" between the octahedral sites along the c axis (independent of the channels), a possible couple between Fe^{3+} in this cavity and Fe^{2+} in the octahedral site may also be responsible for the 620 nm band. Clearly, more data are required to examine these possibilities.

CONCLUSION

The results of the spectral study of silicates that contain large, channel-like cavities show that Fe^{2+} occurs in both the octahedral site and the channels. No evidence was found for the presence of tetrahedral Fe^{2+}. Although the blue color in many of these minerals probably arises from Fe^{2+} interacting with channel Fe^{3+}, more work is required to identify the positions of the metal ions in these intervalence couples.

REFERENCES CITED

Goldman, D.S., G.R. Rossman and W.A. Dollase (1977) Channel constituents in cordierite. Am. Mineral. (submitted)

Wood, D.L. and K. Nassau (1967) Infrared spectra of foreign molecules in beryl. J. Chem Phys. 2220-2228.

Wood, D.L. and K. Nassau (1968) The characterization of beryl and emerald by visible and infrared absorption spectroscopy. Am. Mineral. 53, 777-800.

FIGURE CAPTIONS

1. Room temperature electronic absorption spectra of a yellow beryl from an unknown locality. Crystal thickness = 5.0 mm.
2. Room temperature electronic absorption spectra of a golden beryl from Goyaz, Brazil. Crystal thickness = 5.0 mm.
3. Correlation between the barycenter energy of the octahedral Fe^{2+} absorption bands and the size of the octahedral site in beryl, osumilite and cordierite.
4. Correlation between the intensity of the absorption bands assigned to Fe^{2+} in the channel site in beryl.

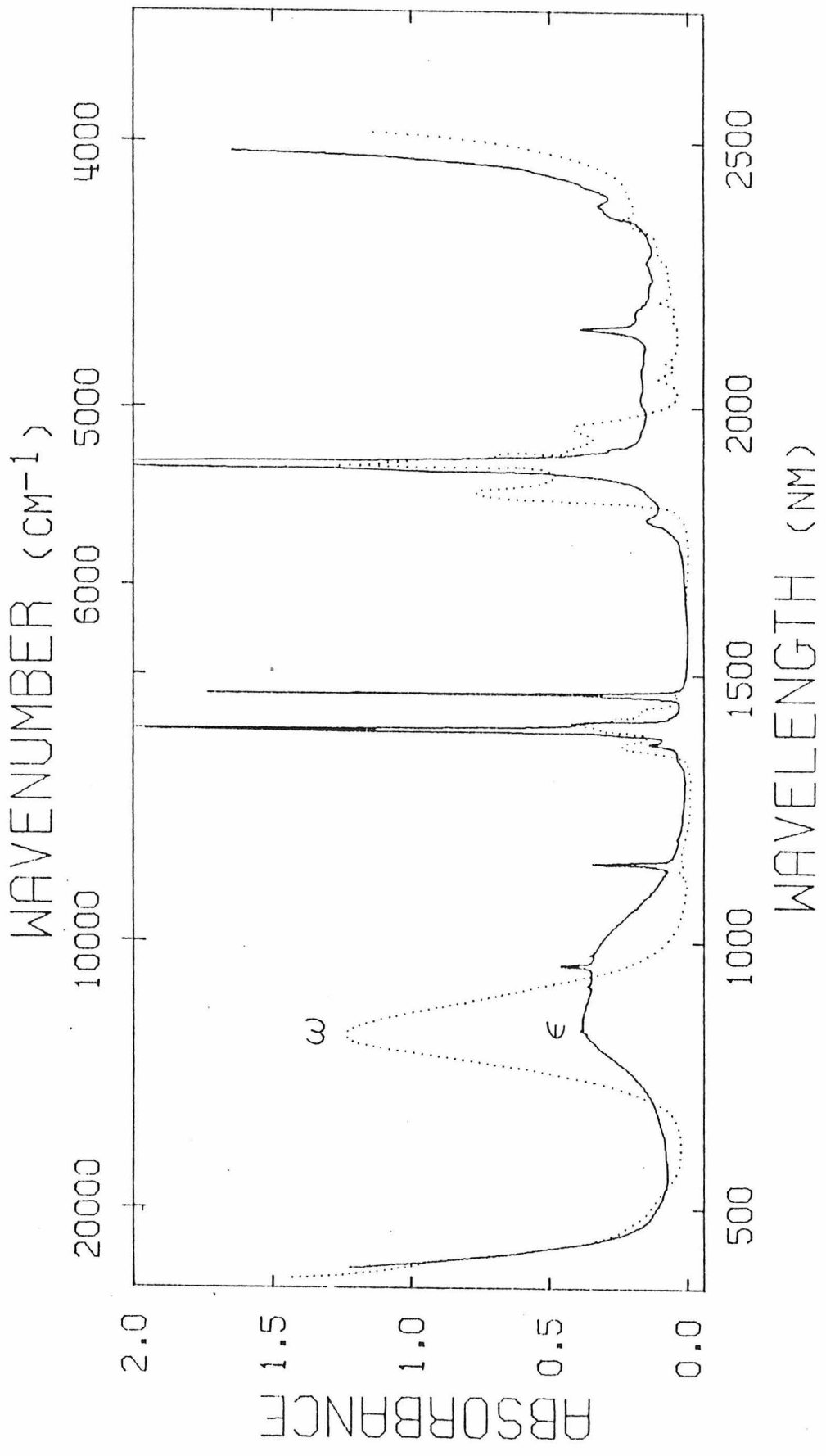
WAVENUMBER (CM-1)
20000
10000
6000
5000
4000
WAVELENGTH (NM)
500
1000
1500
2000
2500
ABSORBANCE
0.0
0.5
1.0
1.5
2.0
ω
ε

Figure 1

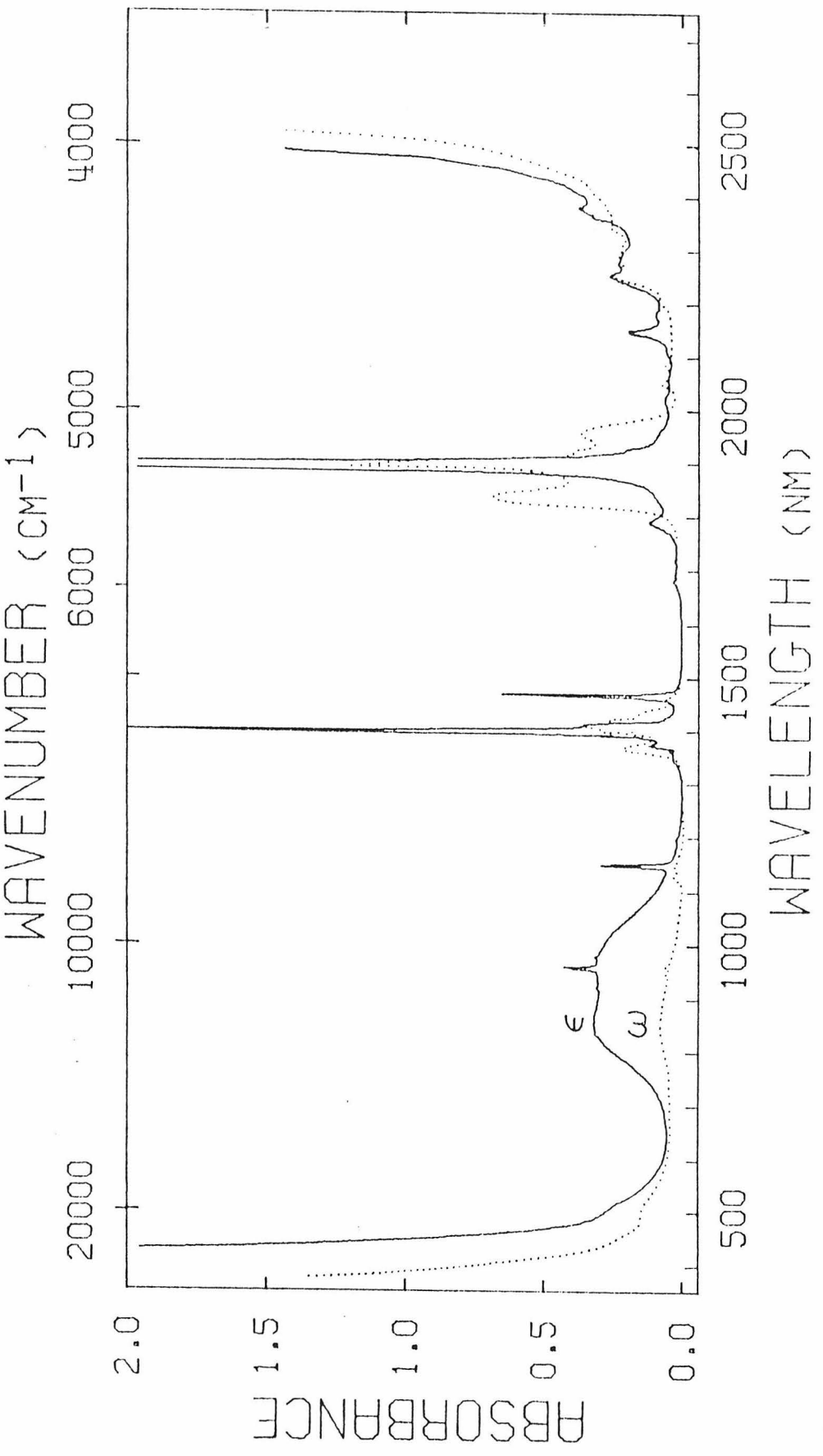
WAVENUMBER (CM-1)
20000
10000
6000
5000
4000
WAVELENGTH (NM)
500
1000
1500
2000
2500
ABSORBANCE
0.0
0.5
1.0
1.5
2.0
ε
ω

Figure 2

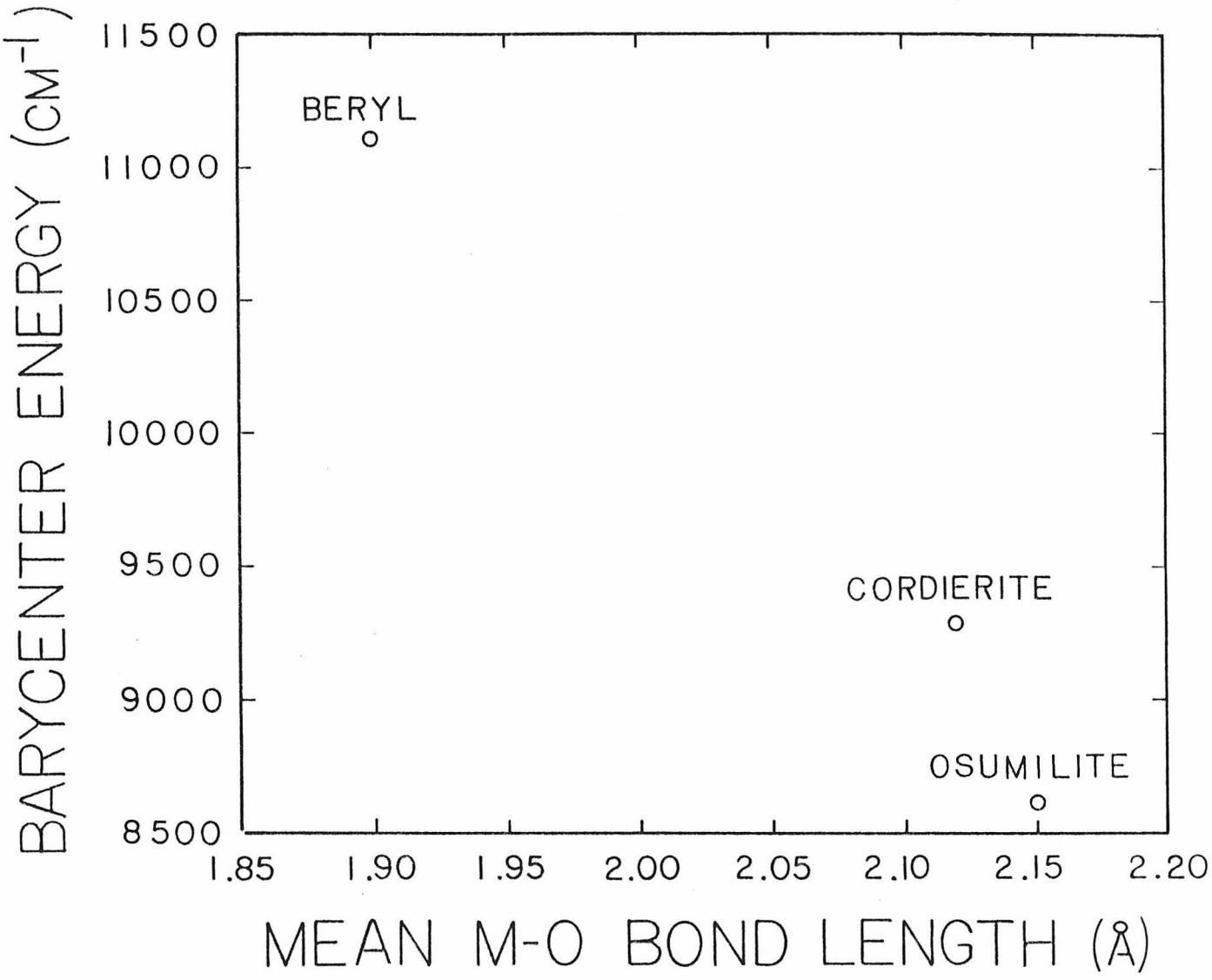
BARYCENTER ENERGY (CM⁻¹)
11500
11000
10500
10000
9500
9000
8500
BERYL
CORDIERITE
OSUMILITE
1.85
1.90
1.95
2.00
2.05
2.10
2.15
2.20
MEAN M-O BOND LENGTH (Å)

Figure 3

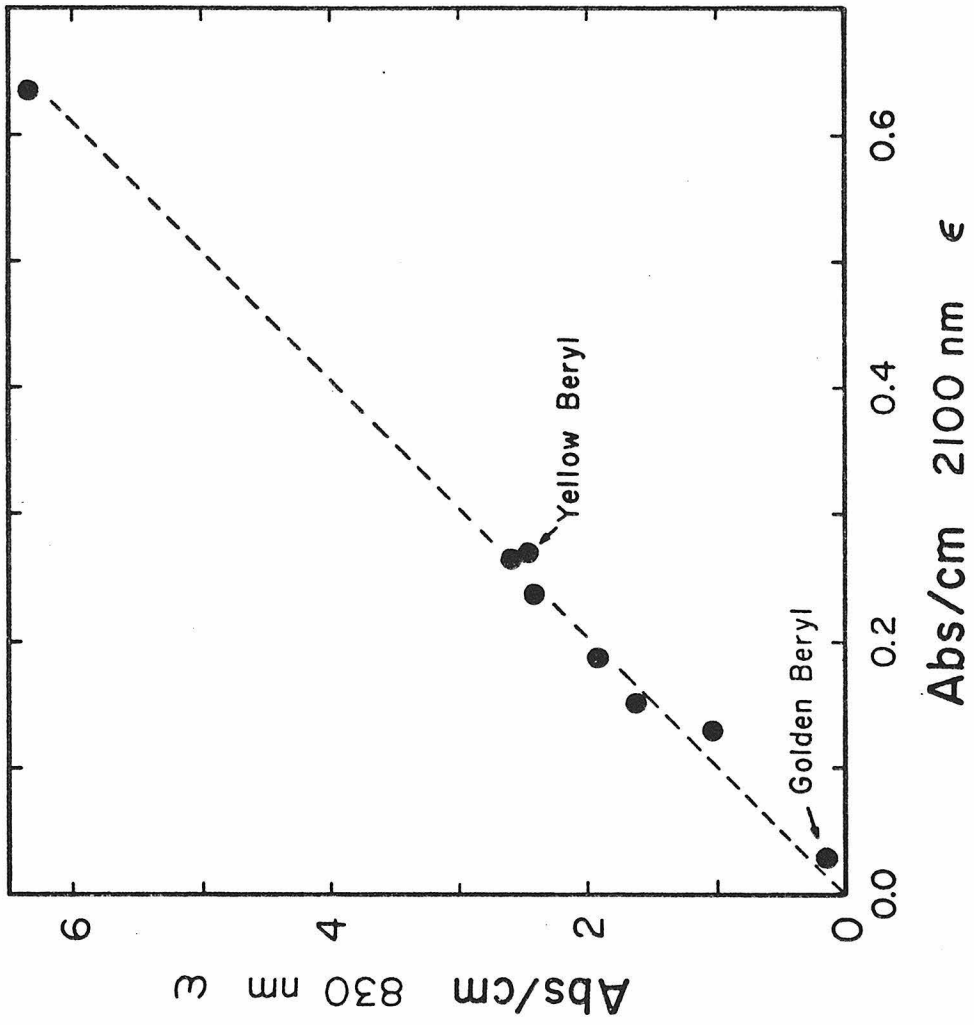
Abs/cm 830 nm ε
0
2
4
6
Yellow Beryl
Golden Beryl
0.0
0.2
0.4
0.6
Abs/cm 2100 nm ε

Figure 4

CHAPTER 11

THE EFFECT OF SITE DISTORTION ON THE ELECTRONIC PROPERTIES OF FERROUS IRON

ABSTRACT

The effect of site size and distortion are correlated with the properties of ferrous iron in the electronic absorption spectra of minerals and compounds. Site size affects band positions and site distortion enhances band intensity and polarization anisotropy. In addition, as band intensity increases due to a greater distortion of the site, the quadrupole splitting from Mössbauer spectra is found to decrease. The results of this study suggest that as a site becomes larger, it becomes more distorted.

INTRODUCTION

The electronic absorption spectroscopy of ferrous iron in minerals and compounds exhibits a varied array of absorption band positions, polarization properties and intensities. These spectroscopic characteristics are related to the size and geometry of the coordination site in which ferrous iron resides. The size of the site affects band positions, with larger sites producing bands at longer wavelengths (lower energies). The further distortion of a site from octahedral geometry enhances absorption band intensity and polarization anisotropy.

This study correlates the effect of site size and distortion on the spectroscopic properties of ferrous iron in minerals and compounds. The quadrupole splitting parameter in Mössbauer spectroscopy is also considered to be sensitive to the distortion of a site from octahedral geometry (Ingalls, 1964), and it will also be incorporated into the correlation. The properties of ferrous iron in cubic (e.g. garnet; White and Moore, 1972), tetrahedral (e.g. staurolite; Burns, 1970a) and square planar (e.g. gillespite; Burns *et al.*,1966) coordinations have special spectroscopic characteristics and therefore, they will not be discussed herein.

OLIVINES AND BORACITES: SPECTROSCOPIC ANOMALIES?

The absorption pattern of Fe^{2+} in the near infrared region is nearly always characterized by two absorption bands that result from a removal of the degeneracy of the $^5\underline{E}_g$ electronic state. The interpretation of the spectra of Fe^{2+} in boracites and olivines provide notable exceptions. The spectra of a fayalite from Coso, California are presented in Figure 1. The bands and shoulders in the 850-920 and 1050-1280 nm regions have been assigned to Fe^{2+} in the M(1) site and the main band in γ polarization in the 1040-1080 nm region has been assigned to Fe^{2+} in the M(2) site by Burns (1970a,b; 1974). Burns considered the spectroscopic symmetry of the M(2) site to be C_{3v}, in which case the degeneracy of the $^5\underline{E}_g$ electronic state is not removed. As Burns pointed out, the M(1) assignments are supported by the spectra of monticellite, $Ca(Mg,Fe)SiO_4$, which is isostructural with olivine (Onken, 1965) and only contains Fe^{2+} in the M(1) site.

The mineral triphylite, $LiFe(PO_4)$, is also isostructural with olivine, but it only has Fe^{2+} in the M(2) site (Finger and Rapp, 1970). The spectra of triphylite from New Hampshire (Figure 2) show two bands near 1070 and 1380 nm. Hare (1976) studied the spectra of triphylite and concluded from the presence of these bands that the main band in γ in olivine (1040-1080 nm) and the prominent shoulder near 1250 nm in γ originate from Fe^{2+} in the M(2) site.

Pisarev et al. (1970) studied the spectra of iron boracites, $Fe_3^{2+}B_7O_{13}X$, where X is Cl, Br or I. They found one absorption

band near 910 nm and assigned it to the $^5\underline{T}_{2g} \rightarrow {}^5\underline{E}_g$ electronic transition of Fe^{2+} in the large, octahedral site. In contrast to these observations, the unpolarized spectrum ($\sim 30^o$ off ω) of a synthetic iron fluoroboracite (Bither and Young, 1974) in Figure 3 shows two bands at 933 and 2675 nm. The latter band has a half-width (full-width at half-maximum intensity) of about 1100 cm^{-1}, which is consistent for an Fe^{2+} absorption band. In addition, this band is not present fluoroboracites containing Cr^{2+} in place of Fe^{2+}. These observations suggest that both bands originate from Fe^{2+} in the octahedral site.

SITE SIZE AND BAND POSITION

The energy separation between the $^5\underline{T}_{2g}$ and $^5\underline{E}_g$ electronic states theoretically varies as $1/\bar{a}^5$, where $\bar{a}$ is the average metal-ligand bond distance of the site (Figgis, 1966, page 35). Ideally, the barycenter (mean) energy of the two near-infrared absorption bands represents the energy of the $^5\underline{E}_g$ state. Therefore, the barycenter energy will also vary as $1/\bar{a}^5$, if the $^5\underline{T}_{2g}$ state remains degenerate. Although the $^5\underline{T}_{2g}$ state is probably split in most minerals (e.g. orthopyroxene; Goldman and Rossman, 1977a), a regular trend is expected for a correlation between $\bar{a}$ and the barycenter energy if the $^5\underline{T}_{2g}$ splitting is either small or similar among the samples compared. Faye (1972) found a nearly linear, negative correlation between these parameters, after adjusting $\bar{a}$ for the substitution of other ions in the site (e.g. $\bar{a}$ for Fe^{2+} in a dominantly Mg site was increased by 0.03Å). However, many of the spectral assignments used by Faye are considered to be incorrect and have been reinterpreted by the author. Using the spectral data collected by the author and the X-ray data reported in the literature (Table 1), the resulting correlation between $\bar{a}$ and the barycenter energy is presented in Figure 4. The filled circles represent spectral data for sites that are mostly occupied by Fe^{2+}, and the $\bar{a}$ values represent X-ray data for sites that are nearly fully occupied by Fe.[1] The open circles represent spectral and X-ray data for Fe^{2+} in Mg-rich sites and the half-filled circles represent data for Fe^{2+} in sites that have approximately equal proportions of Fe^{2+} and Mg. The values of $\bar{a}$ for the M(1) sites in ortho- and clinopyroxenes (samples 8

and 9, respectively) were determined by interpolating between the Mg and Fe end-member values (shown by the bars) to the Fe^{2+} occupancy of the site in the sample used for the spectral study. The triangle represents Fe^{2+} in the Al-rich site in beryl. For most of these data a regular, but not linear, negative correlation is evident. The curvature extends toward higher values of $\bar{a}$ at lower barycenter energies. A similar curvature is obtained assuming a $1/\bar{a}^5$ dependence using a barycenter energy of 10,000 cm^{-1} for a site with $\bar{a}$ equal to 2.1Å as a basis for calculation. The trend defined by the Fe-rich samples is similar to the data presented by Faye after making adjustments to $\bar{a}$. Beryl (sample 12) plots significantly off this trend because $\bar{a}$ represents the Al^{VI}-O, but not Fe^{2+}-O bond lengths from the X-ray data. The deviation of beryl from the trend of the other data ($\sim$0.22Å) is consistent with the difference in effective ionic radii of Al and Fe^{2+} in six-fold coordination (Shannon and Prewitt, 1969). The deviation of anthophyllite (sample 4) from the trend may be related to its unusual seven-fold coordination and three long bonds (Finger, 1970). The deviation of the fluoroboracite (sample 15) may result from the replacement of two <u>trans</u> oxygen ligands by fluorine ions, although the hexaquo coordination about Fe^{2+} in $FeSiF_6 \cdot 6H_2O$ does not produce a deviation from the trend.

The relationship between the $^5\underline{E}_g$ splitting is compared to $\bar{a}$ and the barycenter energy in Figures 5 and 6, respectively. The $^5\underline{E}_g$ splitting appears to be independent of site size in the 2.1-2.2Å range, but it shows a positive correlation with sites that are larger than 2.2Å. There is a negative correlation

between the barycenter energy and $^5\underline{E}_g$ splitting in Figure 6, although there is considerable scatter in the data. This scatter may result from differences in distortion of sites having similar size.

SITE DISTORTION AND BAND INTENSITY

The intensification of absorption features of Fe^{2+} in sites lacking centers of symmetry is a well known phenomenon in the spectroscopy of minerals (Burns, 1970a). Goldman and Rossman (1977b) indicated that molar absorptivity (ε) increases as a site becomes larger. The ε value for the most intense absorption band for each site is also listed in Table 1. It was calculated from the peak intensity and the concentration of iron in that site determined from either Mössbauer or X-ray data or the stoichiometry of that sample. The correlation between $\bar{a}$ and ε is presented in Figure 7 in which centrosymmetric and non-centrosymmetric sites are plotted with open and closed circles, respectively. The ε values for Fe^{2+} in non-centrosymmetric sites regularly increase (except for anthophyllite, sample 4) as $\bar{a}$ increases. These results indicate that sites become more distorted as they become larger. The ε values for Fe^{2+} in centrosymmetric sites are less than 12, regardless of the size of the site. This result is consistent with the fact that electronic transitions in centrosymmetric sites are orbitally forbidden by selection rules, and intensity must come about by vibronic coupling or intensity stealing (Figgis, 1966, page 203).

One way by which distortions occur in mineral sites is from an elongation of two <u>cis</u> metal-ligand bonds so that increased distortion involves a greater metal-ligand bond range. The range of bond distances, normalized to $\bar{a}$, is plotted against ε in Figure 8 which shows a regular trend for the data (except for anthophyllite and $Fe_3B_7O_{13}F$).

SITE DISTORTION AND BAND ANISOTROPY

It became apparent as more polarized spectroscopic data were collected that the higher energy $^5\underline{E}_g$ component became more intense than the lower energy $^5\underline{E}_g$ component as the site became more distorted. This relationship is presented in Figure 9 in which the low/high energy intensity ratio for the near-infrared bands approaches unity as the ε value of the higher energy band decreases. For the large, distorted sites, the lower energy band is mostly polarized in a different direction than the higher energy band.

MÖSSBAUER AND OPTICAL CORRELATION

The quadrupole splitting parameter determined in Mössbauer spectra is expected to decrease as a site becomes distorted from octahedral geometry (Ingalls, 1964). It should therefore correlate with the molar absorptivity determined from electronic absorption spectra. This correlation is presented in Figure 10 in which centrosymmetric and non-centrosymmetric sites are designated by open and filled circles, respectively. The quadrupole splitting data were obtained at room temperature either by the author on the same samples used to determine ε, or from values reported in the literature on samples of similar chemistry. The centrosymmetric sites in Figure 10 do not show a correlation because ε for Fe^{2+} in these sites is typically small. The data for the non-centrosymmetric sites show that as the quadrupole splitting decreases below about 2 mm/sec, ε begins to increase rapidly. However, for ε values that are less than about 5, it appears that the quadrupole splitting may take on a wide range of values.

DISCUSSION

The results of this study point to the importance of the size of the coordination site in controlling the spectroscopic properties of ferrous iron. Smaller sites ($\bar{a}$ < 2.15 Å) generally have $^5\underline{E}_{\underline{g}}$ splittings of less than 3000 cm^{-1}, ε values that are less than 10, and nearly equal intensities of the two near-infrared bands which are polarized in the same direction. In contrast, the larger sites generally have $^5\underline{E}_{\underline{g}}$ splittings that are greater than 5000 cm^{-1}, ε values that are typically much greater than 40, and large differences in the intensities of the two main $^5\underline{E}_{\underline{g}}$ components which are polarized in different directions. These results may suggest that the Jahn-Teller mechanism remains the dominant spectroscopic control in the smaller sites, despite the fact that their symmetries are lower than $\underline{O}_{\underline{h}}$. The spectroscopy of ferrous iron in the larger sites appears to be controlled by the distortion (i.e. the low symmetry) of the site.

The distortion common to most larger silicate sites results from an elongation of two <u>cis</u> metal-oxygen bonds. In these sites, the most intense absorption band is polarized in the direction of the elongation, and the resulting spectroscopy overall conforms to the polarizations expected in $\underline{C}_{\underline{2v}}$ symmetry. Difficulties arise in attempting to analyze the polarization properties of the bands due to ferrous iron in the smaller sites. For example, many of these sites have $\underline{C}_2$ point-group symmetry. This symmetry would require at least one of the $^5\underline{E}_{\underline{g}}$ components to be polarized parallel to the $\underline{C}_2$ axis of the site. However, both bands are found (e.g. cordierite, clinopyroxene M1, clinoamphibole M1,M2,M3) to be polarized in the plane normal to the C_2 axis and have nearly equal intensity. The success in modeling the spectroscopy of iron in the larger sites and the failure to do so in the smaller sites supports the contention that different mechanisms are operable in each case.

CONCLUSION

The size and distortion of a coordination site are found to have a pronounced influence upon the spectroscopic properties of ferrous iron in terms of band position, intensity and polarization anisotropy. There is an overall relationship between the size of the site and these properties, because larger sites are generally more distorted than smaller sites. The spectroscopic properties of ferrous iron in large and small sites are clearly different suggesting that different mechanisms are dominating the spectroscopy in each case.

ACKNOWLEDGEMENTS

I thank G.R. Rossman for showing me his earlier work on iron-bearing olivines and triphylites and for the interpretation that Fe^{2+} in the olivine M(2) site actually produces two near-infrared bands. I also thank him for pointing me to the literature on iron boracites.

REFERENCES

Bancroft, G.M., A.J. Maddock, and R.G. Burns (1967) Applications of the Mössbauer effect to silicate mineralogy-I. Iron silicates of known crystal structure. Geochim. Cosmochim. Acta. 31, 2219-2246.

Bither, T.A. and H.S. Young (1974) Nitrato- and fluoroboracites $M_3B_7O_{13}NO_3$ and $M_3B_7O_{13}F$. J. Solid State Chem. 10, 302-311.

Brown, G.E. and G.V. Gibbs (1969) Refinement of the crystal structure of osumilite. Am. Mineral. 54, 101-116.

Burnham, C.W., Y. Ohashi, S.S. Hafner and D. Virgo (1971) Cation distribution and atomic thermal vibrations in an iron-rich orthopyroxene. Am. Mineral. 56, 850-876.

Burns, R.G., M.C. Clark and A.J. Stone (1966) Vibronic polarization in the electronic spectra of gillespite, a mineral containing iron (II) in square-planar coordination. Inorg. Chem. 5, 1268-1273.

Burns, R.G. (1970a) Mineralogical Applications of Crystal Field Theory. Cambridge University Press.

Burns, R.G. (1970b) Crystal field spectra and evidence of cation ordering in olivine minerals. Am. Mineral. 55, 1608-1633.

Burns, R.G. (1974) The polarized spectra of iron in silicates: Olivine. A discussion of neglected contributions from Fe^{2+} ions in the M(1) sites. Am. Mineral. 59, 625-629.

Cameron, M., S. Sueno, C.T. Prewitt and J.J. Papike (1973) High-temperature crystal chemistry of acmite, diopside, hedenbergite, jadeite, spodumene, and ureyite. Am. Mineral. 58, 594-618.

Deer, W.A., R.A. Howie and J. Zussman (1966) An Introduction to the Rock-Forming Minerals. John Wiley and Sons, New York. page 474.

Dowty, E. and D.H. Lindsley (1973) Mössbauer spectra of synthetic hedenbergite-ferrosilite pyroxenes. Am. Mineral. 58, 850-868.

Faye, G.H. (1972) Relationship between crystal-field splitting parameter, "Δ_{vi}", and M_{host}-O bond distance as an aid in the interpretation of absorption spectra of Fe^{2+} materials. Canad. Mineral. 11, 473-487.

Figgis, B.N. (1966) An Introduction of Ligand Fields. Interscience. New York.

Finger, L.W. (1969) The crystal structure and cation distribution of a grunerite. Mineral. Soc. Amer. Spec. Pap. 2, 95-100.

Finger, L.W. (1970) Refinement of the Crystal structure of an anthophyllite. Carnegie Inst. Wash. Year Book. 68, 283-290.

Finger, L.W. and G.R. Rapp, Jr. (1970) Refinement of the crystal structure of tryphylite. Carnie Inst. Wash. Year Book. 68, 290.

Ghose, S. (1961) The crystal structure of a cummingtonite. Acta Crystallogr. 14, 622-627.

Ghose, S. (1965) Mg^{2+}-Fe^{2+} order in an orthopyroxene, $Mg_{0.93}Fe_{1.07}Si_2O_6$. Zeits. Kristallogr. 122, 81-99.

Ghose, S. and J. Weidner (1972) Mg^{2+}-Fe^{2+} order-disorder in cummingtonite, $(Mg,Fe)_7Si_8O_{22}(OH)_2$: A new geothermometer. Earth and Planet Sci. Lett. 16, 346-354.

Gibbs, G.V. (1966) The polymorphism in cordierite I: The crystal structure of low cordierite. Am. Mineral. 51, 1068-1087.

Gibbs, G.V., D.W. Breck and E.P. Meagher (1968) Structural refinement of hydrous and anhydrous synthetic beryl, $Al_2(Be_3Si_6)O_{18}$ and emerald, $Al_{1.9}Cr_{0.1}(Be_3Si_6)O_{18}$. Lithos. 1, 275-285.

Goldman, D.S. (1977) A reevaluation of the Mössbauer spectroscopy of calcic amphiboles. Am. Mineral. (in press)

Goldman, D.S. and G.R. Rossman (1977a) The spectra of iron in orthopyroxene revisited: The splitting of the ground state. Am. Mineral. 62, 151-157.

Goldman, D.S. and G.R. Rossman (1977b) The identification of Fe^{2+} in the M(4) site of calcic amphiboles. Am. Mineral. 62, 205-216.

Goldman, D.S., G.R. Rossman and W.A. Dollase (1977) Channel constituents in cordierite. Am. Mineral. (in press).

Grant, R.W., H. Wiedersich, A.H. Muir, Jr., U. Gonsor and W.N. Delgass (1966) Sign of the nuclear quadrupole splitting constants in some ionic ferrous compounds. J. Chem. Phys. 45, 1015.

Hamilton, W.C. (1962) Bond distances and thermal motion in ferrous fluorosilicate hexahydrate: A neutron diffraction study. Acta Crystallogr. 15, 353-360.

Hare, J.W. (1976) Crystal field applications to biochemical and geochemical systems: Electronic structure of blue copper proteins and iron group olivines. Ph.D. Dissertation. California Institute of Technology.

Ingalls, R. (1964) Electric-field gradient tensor in ferrous compounds. Phys. Rev. 133A, 787-795.

Ito, T., H. Morimoto and R. Sadanaga (1951) The crystal structure of boracite. Acta Crystallogr. 4, 310-316.

Landolt-Börnsten (1955) Zehlenwerte und Funktionen Vol. 1, Part 4, Springer, Berline-Gottingen-Heidleberg, page 140.

Morimoto, N. and K. Koto (1969) The crystal structure of orthoenstatite. Zeits. Kristallogr. 129, 65-83.

Onken, H. (1965) Verfeinerung der kristallstruktur von monticellit. Tchermak's Mineral. Petrogr. Mitt. 10, 344-44.

Papike, J.J. and M. Ross (1970) Gedrites: Crystal structures and intracrystalline cation distributions. Am. Mineral. 55, 1945-1972.

Pisarev, R.V., V.V. Druzhinin, N.N. Nesterova, S.D. Prochorova and G.T. Andreeva (1970) Optical absorption of ferro-electrical iron boracites. Phys. Stat. Solids. 40, 503-512.

Seifert, F. (1977) Compositional dependence of the hyperfine interaction of ^{57}Fe in anthophyllite. Phys. Chem. Minerals. 1, 43-52.

Shannon, R.D. and C.T. Prewitt (1969) Effective ionic radii in oxides and fluorides. Acta Crystallogr. B25, 925-946.

Smyth, J.R. (1975) High-temperature crystal chemistry of fayalite. Am. Mineral. 60, 1092-1097.

Virgo, D. and S.S. Hafner (1969) Fe^{2+},Mg order-disorder in heated orthopyroxenes. Mineral. Soc. Amer. Spec. Pap. 2, 67-82.

White, W.B. and R.K. Moore (1972) Interpretation of the spin-allowed bands of Fe^{2+} in silicate garnets. Am. Mineral. 57, 1692-1710.

FOOTNOTES

1. The spectrum of iron fluoroboracite was taken on synthetic $Fe_3B_7O_{13}F$. The X-ray data used for this sample were taken on a natural Mg-rich boracite.

TABLE 1. Spectral Data

	MATERIAL	1	2	3	4	5	6	7
1.	Faylite M(2)	2.179	0.216	8580	1860	18.1	2.90	0.51
2.	Faylite M(1)	2.157	0.098	9380	3550	2.3	2.90	1.18
3.	Gedrite M(4)	2.183	0.401	7730	5820	16.8	1.85	0.27
4.	Anthophyllite M(4)	2.349	0.871	7550	6400	28.5	1.82	
5.	Grunerite M(4)	2.293	0.769	7030	6260	149.5	1.55	0.12
6.	Cummingtonite M(4)	2.306	0.657	7170	6270	118.1	1.64	
7.	Orthopyroxene M(2)	2.224	0.482	7740	5960	40.8	1.96	0.24
8.	Orthopyroxene M(1)	2.092*	0.128*	10750	4100	4.6	2.48	
9.	Ferrosalite M(1)	2.109*	0.076*	9540	1690	4.3	2.22	0.95
10.	Cordierite (Oct.)	2.119	0.011	9310	1840	3.5	2.31	0.92
11.	Osumilite (Oct.)	2.150	0.0	8660	3290	3.5	2.35	0.67
12.	Beryl (Oct.)	1.903	0.0	11000	1810	3.1		0.82
13.	Siderite	2.180	0.0	7750	9260	2.1	1.80	
14.	$FeSiF_6 \cdot 6H_2O$	2.150	0.0	9750	1400	2.0	3.39	
15.	$Fe_3B_7O_{13}F^2$	2.370	0.980	7230	6980	11.0**		

1 Mean metal-ligand bond distance (Å)
2 Range in bond length (Å)
3 Barycenter energy (cm^{-1})
4 ^5E_g splitting (cm^{-1})
5 Molar absorptivity
6 Quadrupole splitting at 295 K (mm/sec)
7 Band intensity ratio (see text)

* These values have been determined by interpolating the X-ray data for the Mg and Fe end-members using the occupancy of Fe in this site.

** Determined from $Fe_3B_7O_{13}Cl$ in Pisarev et al. (1970)

TABLE 2. Data references

Materials	Site Distribution	X-ray Data	Mössbauer Data	Chemical Data
1. Fayalite M(2)	Stoichiometry (all Mn in M(2)	Smyth (1975)	Bancroft et al (1967)	Present study*
2. Fayalite M(1)	Stoichiometry (all Mn in M(2)	Smyth (1975)	Bancroft et al (1967)	Present study*
3. Gedrite M(4)	Papike and Ross (1970)	Papike and Ross (1970)	Seifert (1977)	Papike and Ross (1970)
4. Anthophyllite M(4)	Finger (1970)	Finger (1970)	Bancroft et al (1967) Seifert (1977)	Finger (1970)
5. Grunerite M(4)	Goldman (1977)	Finger (1969)	Goldman (1977)	Goldman (1977)
6. Cummingtonite M(4)	Ghose and Weidner (1972)	Ghose (1961)	Bancroft et al (1967)	Ghose and Weidner (1972)
7. Orthopyroxene M(2)	Chapter 4	Ghose (1965) Burnham et al (1971)	Burnham et al (1971)	Virgo and Hafner (1969)
8. Orthopyroxene M(1)	Chapter 4	Morimoto and Koto (1969) Burnham et al (1971)	Burnham et al (1971)	Virgo and Hafner (1969)
9. Ferrosalite M(1)	Stoichiometry	Cameron et al (1973)	Dowty and Lindsley (1973)	Present study**
10. Cordierite (Oct)	Goldman et al (1977)	Gibbs (1966)	Goldman et al (1977)	Goldman et al (1977)
11. Osumilite (Oct)	Chapter 9	Brown and Gibbs (1969)	Chapter 9	Chapter 9
12. Beryl (Oct)	Chapter 10	Gibbs et al (1968)		

TABLE 2. (Continued)

Materials	Site Distribution	X-ray Data	Mössbauer Data	Chemical Data
13. Siderite	Stoichiometry	Landolt-Börnsten (1955)	Grant et al (1966)	Deer et al (1966)
14. $FeSiF_6 \cdot 6H_2O$	Stoichiometry	Hamilton (1962)	Grant et al (1966)	
15. $Fe_3B_7O_{13}F$	Stoichiometry	Ito et al (1951)		

* $Fe_{1.90}Mg_{0.01}Mn_{0.11}Si_{0.98}O_4$

** $Ca_{0.98}Mg_{0.42}Fe_{0.54}Mn_{0.06}Si_{1.98}O_6$

FIGURE CAPTIONS

1. Room temperature electronic absorption spectra of a fayalite from Coso, California. Crystal thickness = 0.06 mm.
2. Room temperature electronic absorption spectra of a tryphylite from New Hampshire. Crystal thickness = 0.1 mm.
3. Room temperature electronic absorption spectrum of synthetic $Fe_3B_7O_{13}F$ taken unpolarized on a section that is approximately 30^o off ω. Crystal thickness = 0.12 mm.
4. Correlation between the barycenter energy of the two near-infrared Fe^{2+} absorption bands and the size of the site, $\bar{a}$. The dashed line represents the trend expected for an ideal $1/\bar{a}^5$ dependence of the barycenter energy (see text).
5. Correlation between the $^5\underline{E}_{\underline{g}}$ splitting and the size of the site.
6. Correlation between the barycenter energy of the two near-infrared Fe^{2+} absorption bands and the energy splitting between them.
7. Intensification of Fe^{2+} absorption bands as a function of the size of the site. Molar absorptivity (ε) values are determined for the most intense Fe^{2+} absorption band.
8. Intensification of Fe^{2+} absorption bands with increased radial distortion in the site determined from the range of metal-ligand bond distances normalized to the mean metal-ligand bond distance. The symbols are described in Figure 7.

9. Relationship between molar absorptivity (ε) and the change in the intensity of the two near-infrared Fe^{2+} absorption bands. The intensity anisotropy was determined by a ratio of the most intense lower energy $^5\underline{E}_{\underline{g}}$ component to that of the higher energy $^5\underline{E}_{\underline{g}}$ component.
10. Relationship between molar absorptivity (ε) determined from electronic absorption spectra and the quadrupole splitting determined in Mössbauer spectra. All data have been obtained from room temperature spectra.

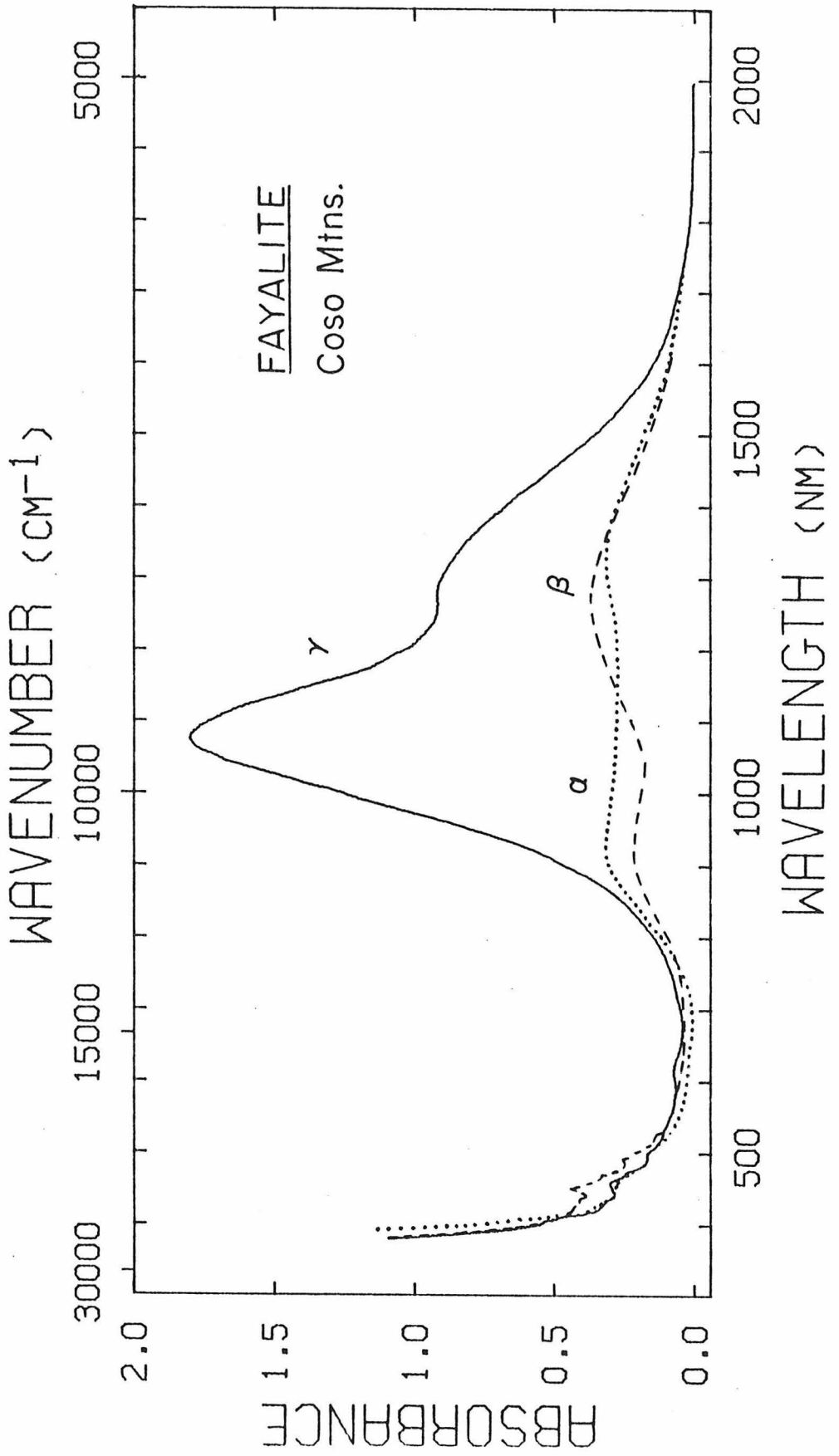
FAYALITE
Coso Mtns.
γ
β
α
WAVENUMBER (CM-1)
30000
15000
10000
5000
WAVELENGTH (NM)
500
1000
1500
2000
ABSORBANCE
2.0
1.5
1.0
0.5
0.0

Figure 1

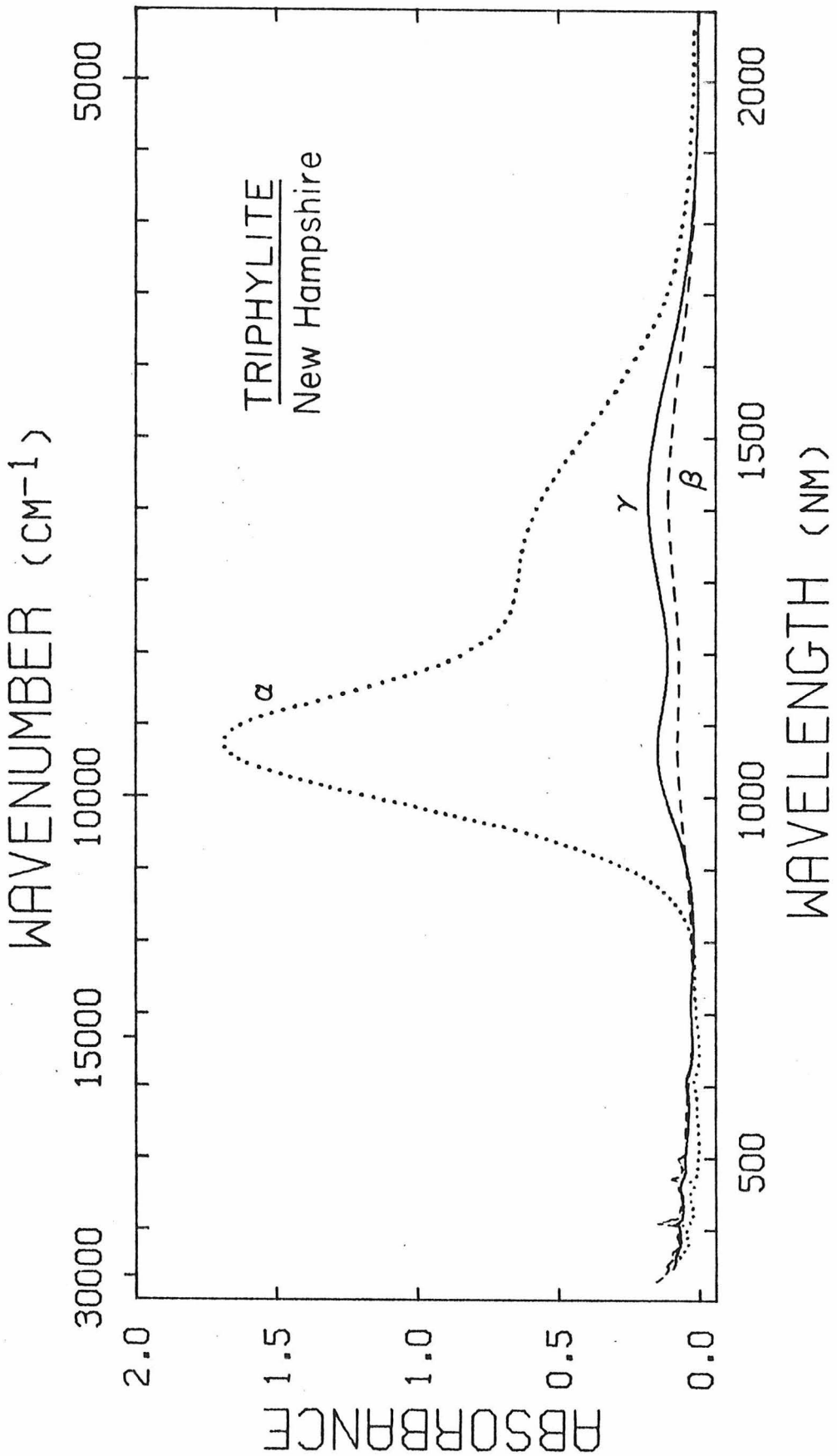
TRIPHYLITE
New Hampshire
α
β
γ
WAVENUMBER (CM-1)
30000
15000
10000
5000
WAVELENGTH (NM)
500
1000
1500
2000
ABSORBANCE
2.0
1.5
1.0
0.5
0.0

Figure 2

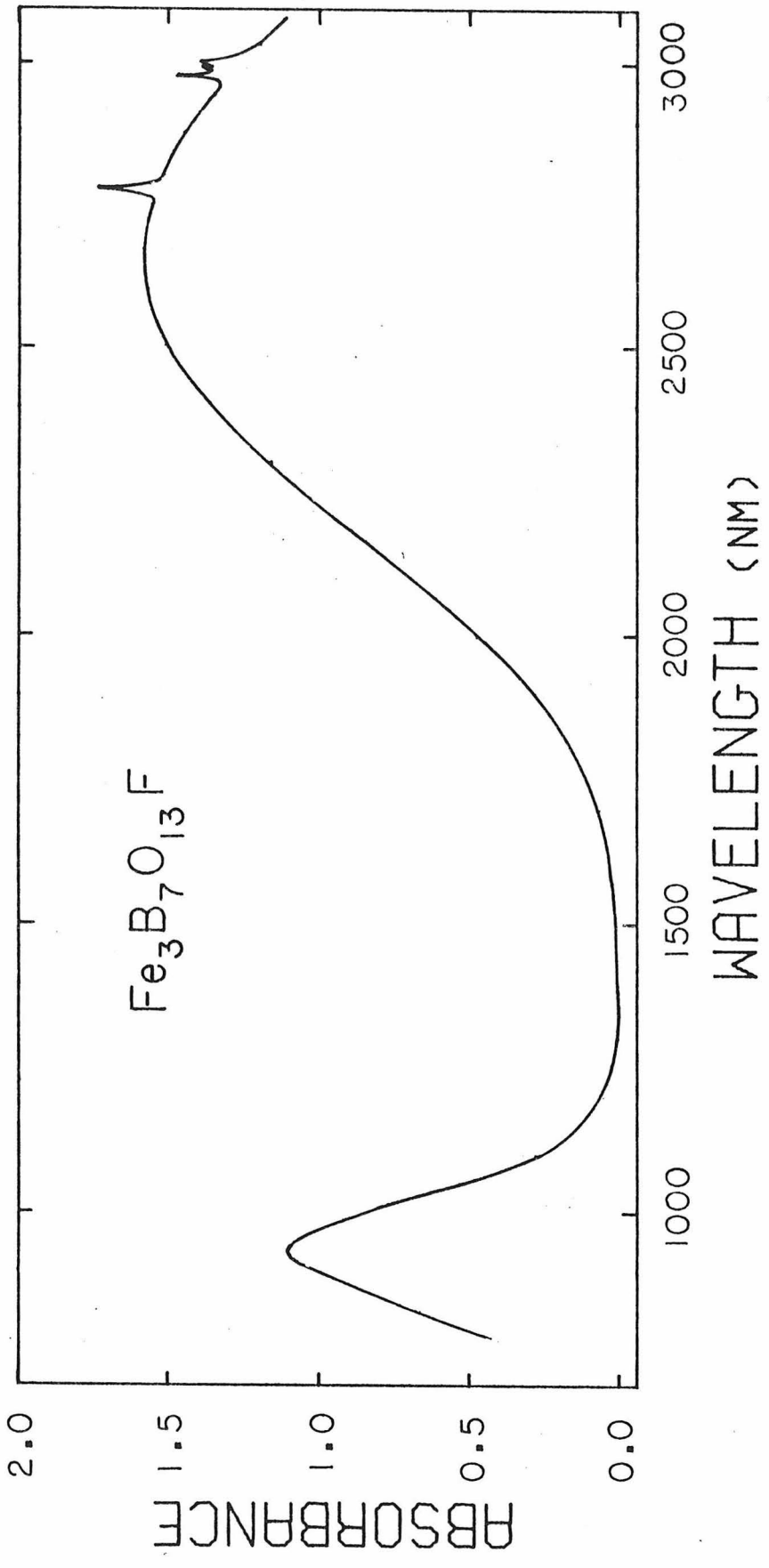
$Fe_3B_7O_{13}F$
ABSORBANCE
0.0
0.5
1.0
1.5
2.0
1000
1500
2000
2500
3000
WAVELENGTH (NM)

Figure 3

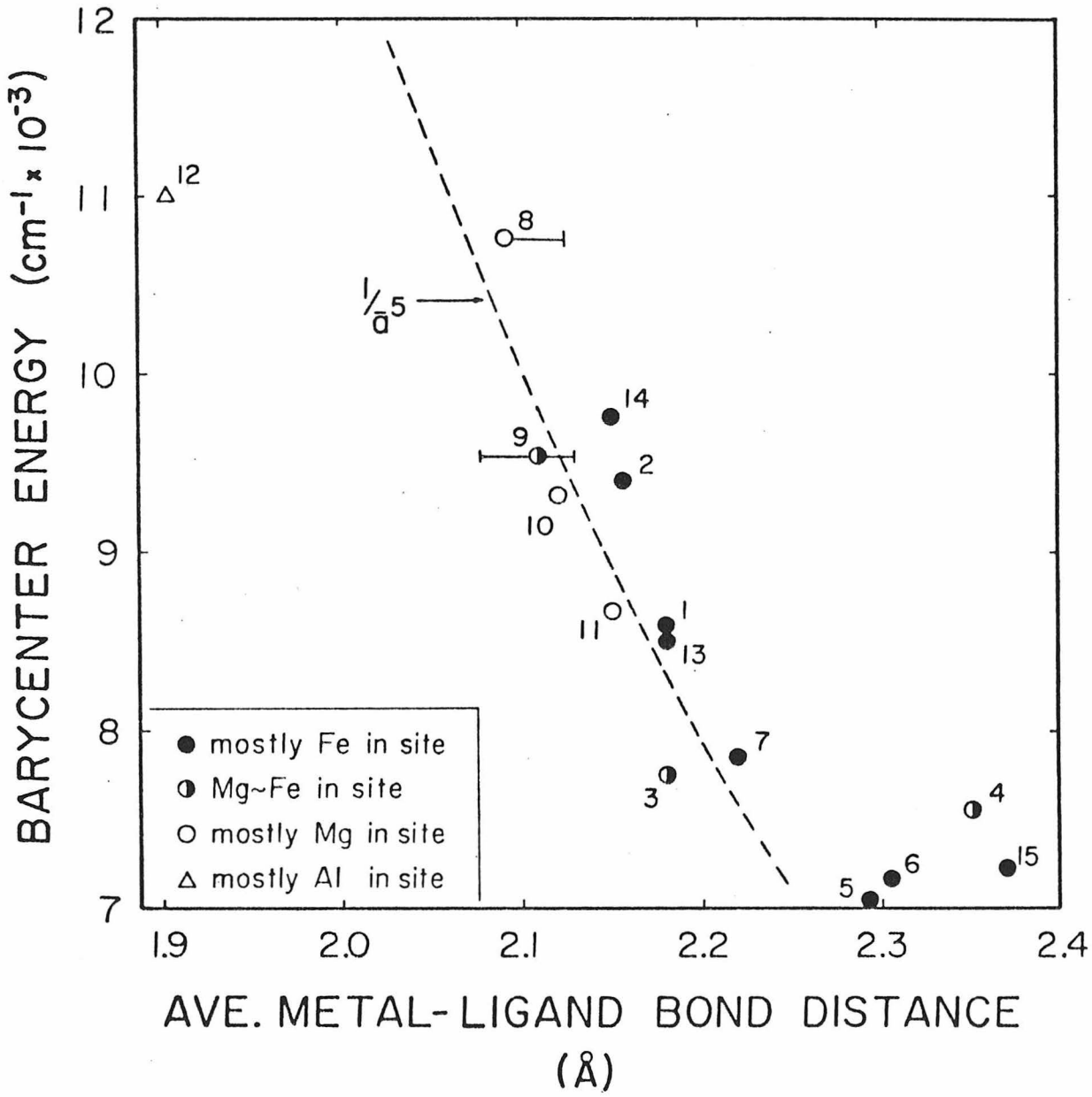
BARYCENTER ENERGY (cm⁻¹ x 10⁻³)
12
11
10
9
8
7
1.9
2.0
2.1
2.2
2.3
2.4
AVE. METAL-LIGAND BOND DISTANCE (Å)
mostly Fe in site
Mg~Fe in site
mostly Mg in site
mostly Al in site
1/ā
1
2
3
4
5
6
7
8
9
10
11
12
13
14
15

Figure 4

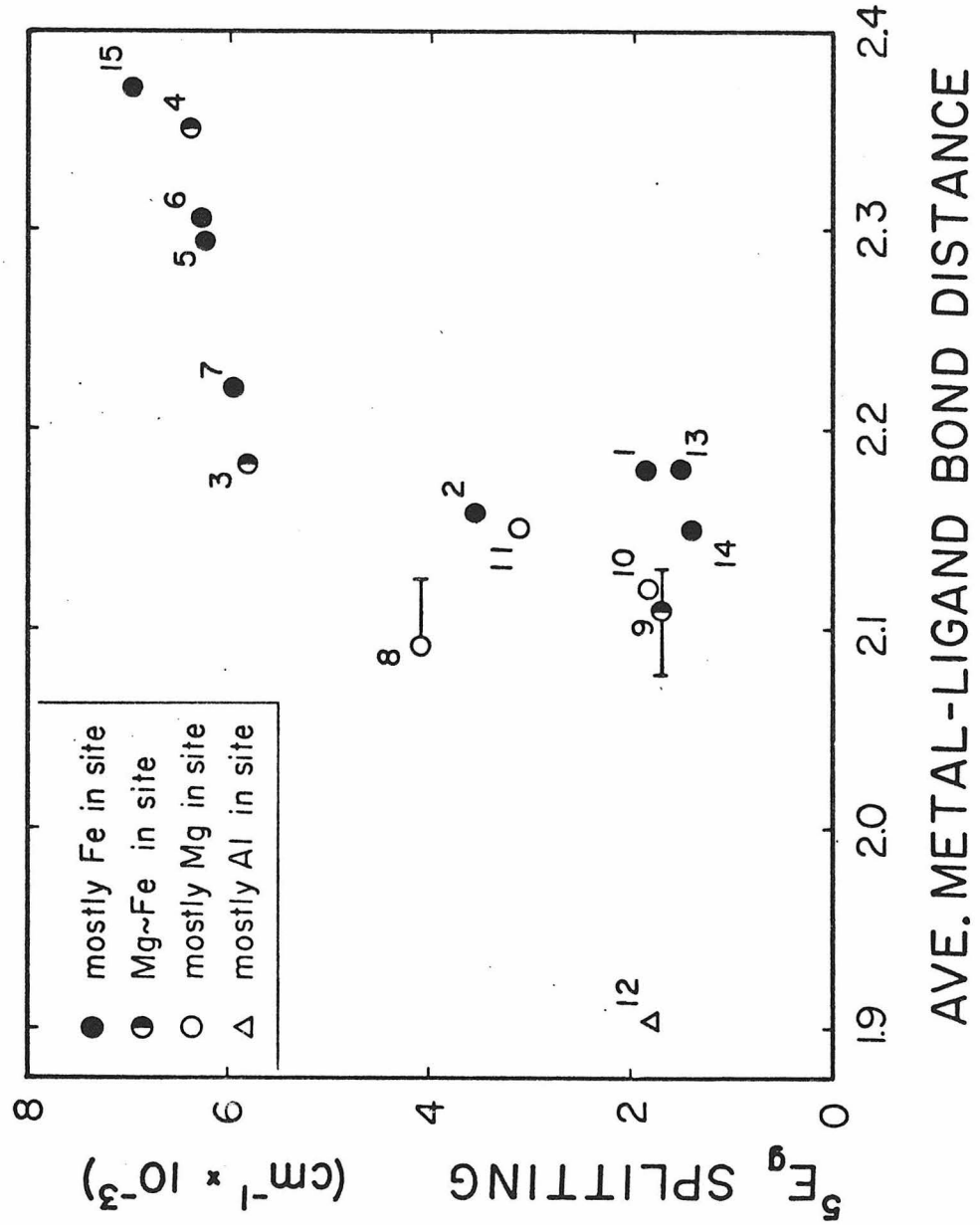
mostly Fe in site
Mg~Fe in site
mostly Mg in site
mostly Al in site
^5E_g SPLITTING ($cm^{-1} \times 10^{-3}$)
AVE. METAL-LIGAND BOND DISTANCE (Å)
0
2
4
6
8
1.9
2.0
2.1
2.2
2.3
2.4
1
2
3
4
5
6
7
8
9
10
11
12
13
14
15

Figure 5

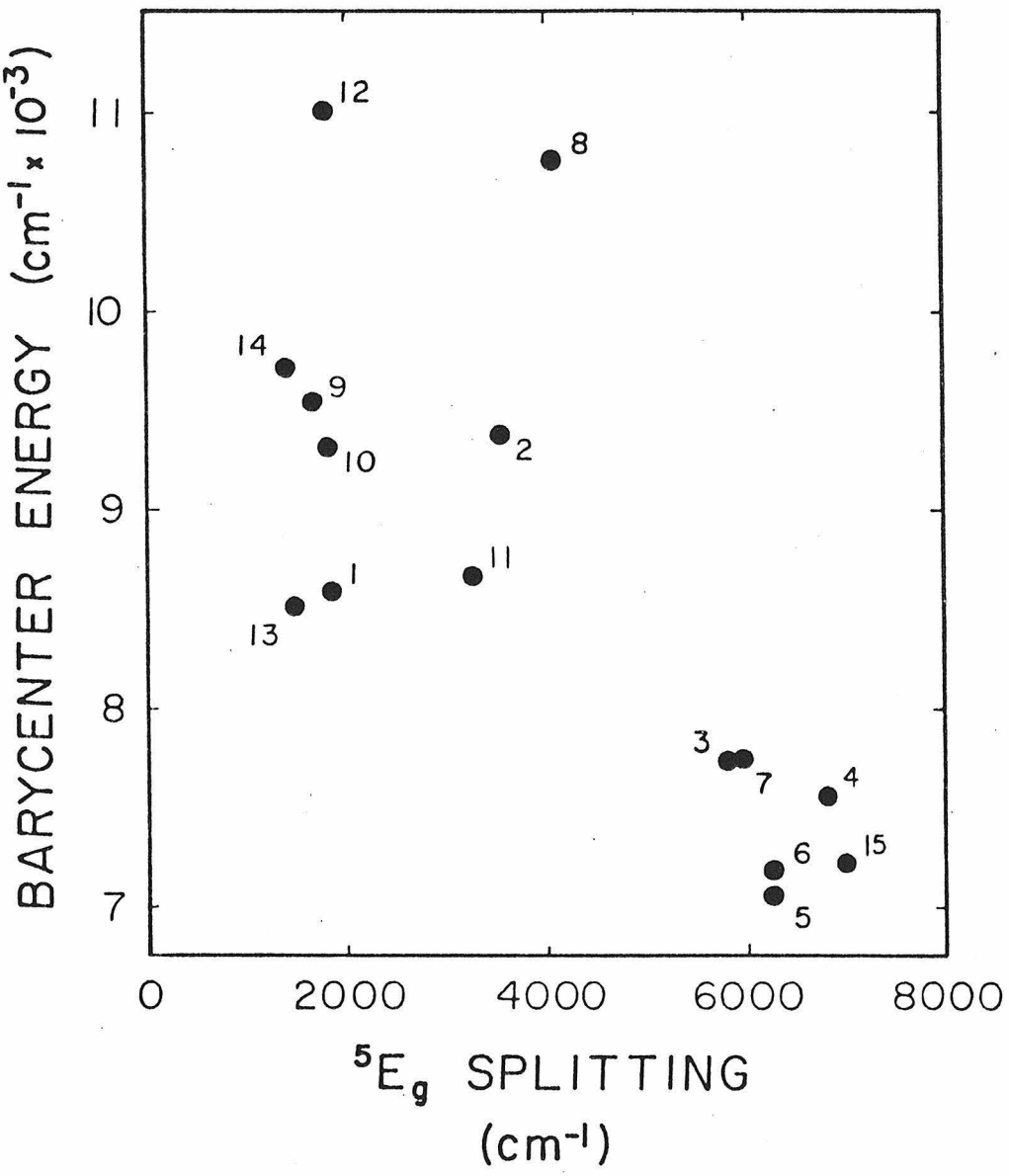
BARYCENTER ENERGY (cm⁻¹ x 10⁻³)
11
10
9
8
7
0
2000
4000
6000
8000
⁵Eg SPLITTING
(cm⁻¹)
12
8
14
9
10
2
11
1
13
3
7
4
6
15
5

Figure 6

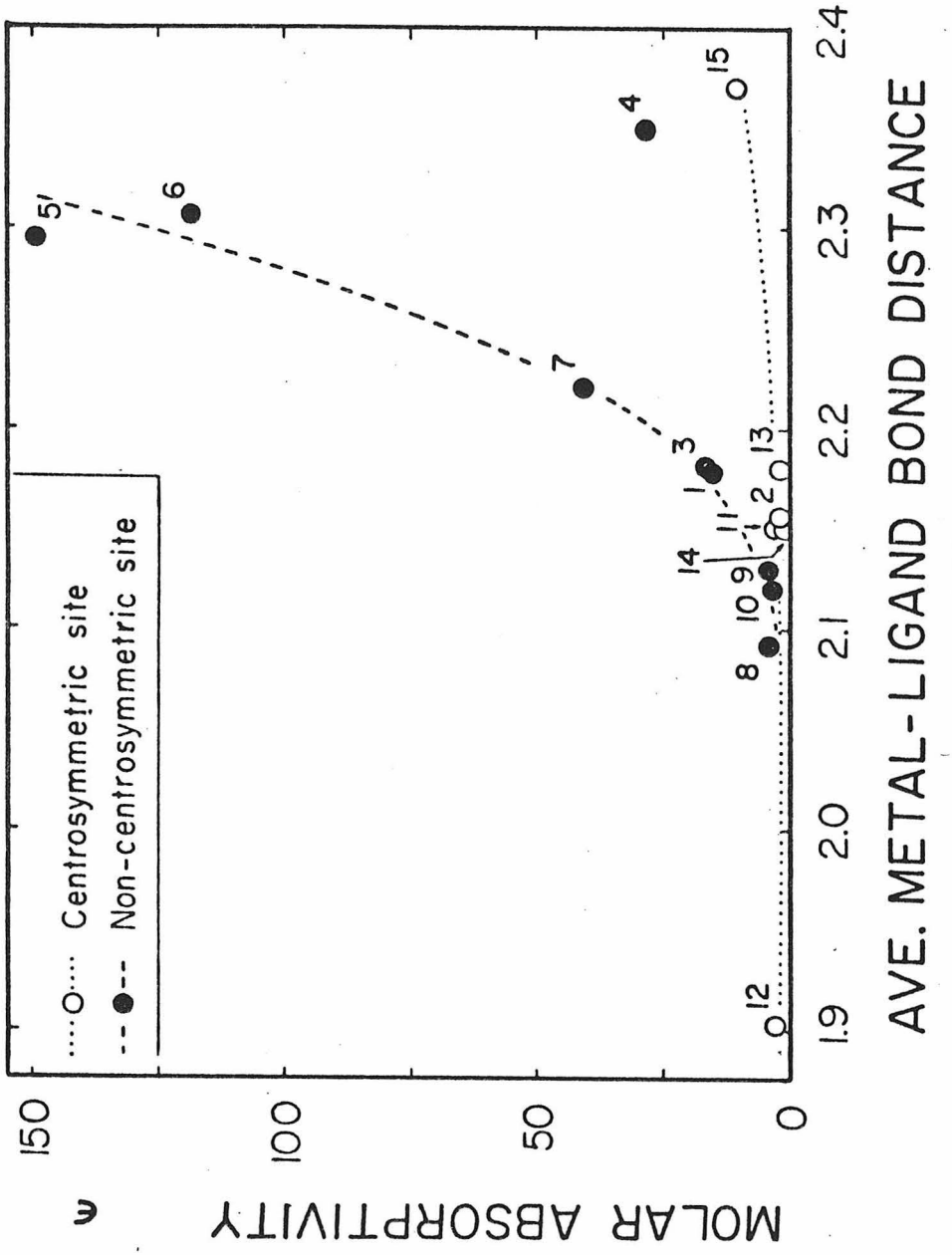
Centrosymmetric site
Non-centrosymmetric site
MOLAR ABSORPTIVITY
ε
150
100
50
0
1.9
2.0
2.1
2.2
2.3
2.4
AVE. METAL-LIGAND BOND DISTANCE
(Å)
1
2
3
4
5
6
7
8
9
10
11
12
13
14
15

Figure 7

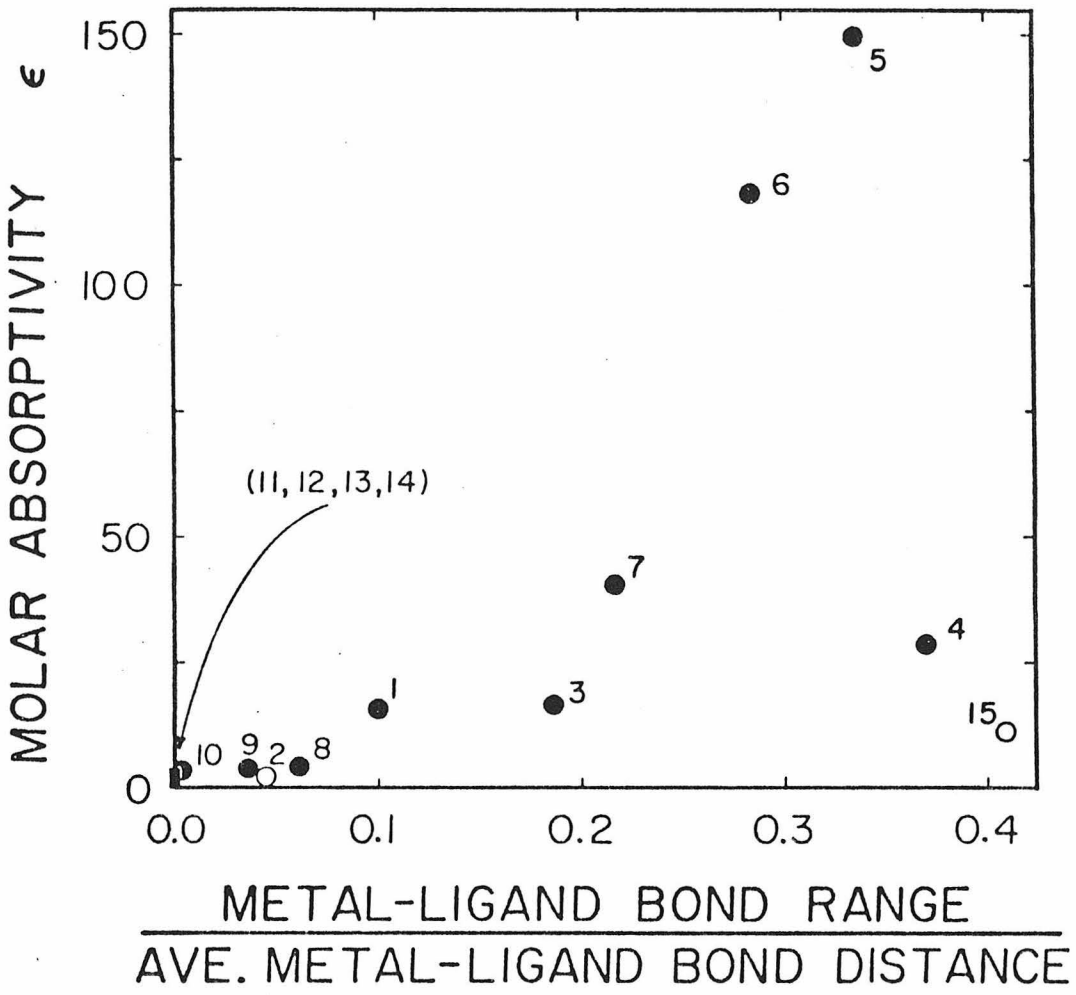
MOLAR ABSORPTIVITY ε
150
100
50
0
0.0
0.1
0.2
0.3
0.4
(11, 12, 13, 14)
10
9
2
8
1
3
7
6
5
4
15
METAL-LIGAND BOND RANGE
AVE. METAL-LIGAND BOND DISTANCE

Figure 8

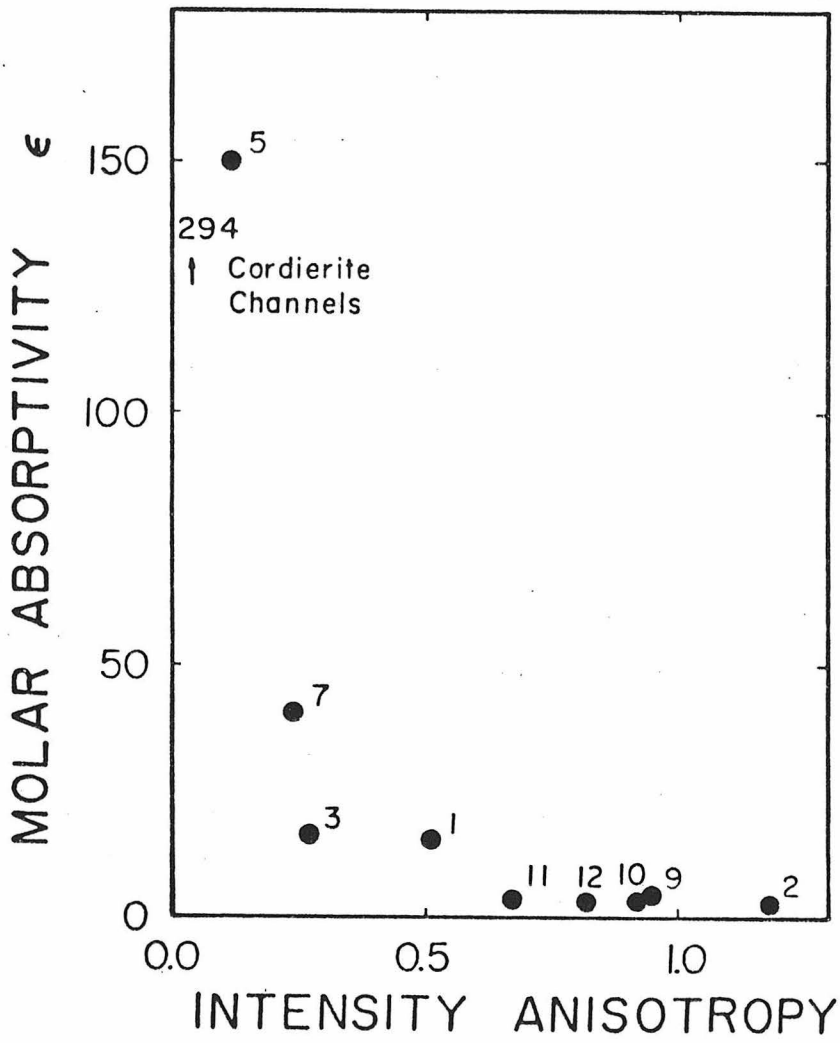
MOLAR ABSORPTIVITY ε
150
100
50
0
5
294
Cordierite
Channels
7
3
1
11
12
10
9
2
0.0
0.5
1.0
INTENSITY ANISOTROPY

Figure 9

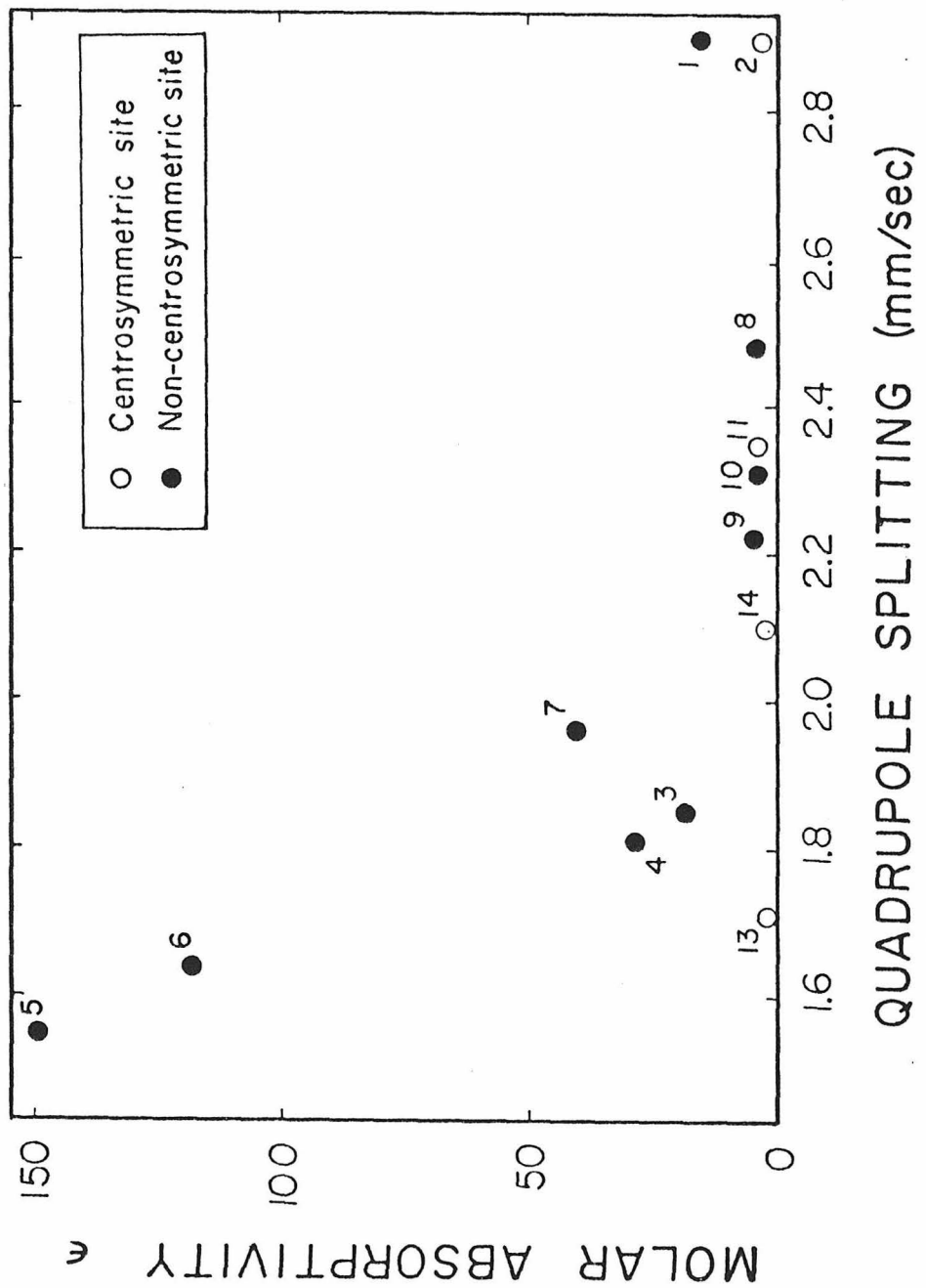
Centrosymmetric site
Non-centrosymmetric site
MOLAR ABSORPTIVITY ε
150
100
50
0
1.6
1.8
2.0
2.2
2.4
2.6
2.8
QUADRUPOLE SPLITTING (mm/sec)
1
2
3
4
5
6
7
8
9
10
11
13
14

Figure 10

APPENDIX: GENERAL EXPERIMENTAL PROCEDURES

Polarized spectra were obtained with Ahrens prism calcite polarizers in a Cary 17I spectrometer in the 300-2700 nm range and gold wire grid polarizers on a silver bromide substrate in a Perkin Elmer 180 spectrometer in the 4000-1000 cm^{-1} region. The Cary 17I is not equipped with polarizing microscopes in the sample and reference chambers, which is a common method used in other laboratories.

Polarized spectra were obtained on oriented single crystals. For pyroxenes and amphiboles, external morphology was used for initial orientation. Aluminum blocks were constructed to fit in a microsaw and to have specific angles so that these crystals can be glued onto the surface with their c axes parallel to the direction of the cutting blade such that the resulting cuts would closely approximate (100) and (010) planes. A Buehler Isomet microsaw with diamond studded 3-4 inch diameter copper blades was used to cut all crystals. After cutting, these crystals were held on a glass slide with black apiezon sealing wax or orthodontic acrylic resin. Glass slabs of thicknesses similar to the crystal were glued onto the four corners of the glass slide using Eastman 910 cyano-acrylate glue to insure uniform thinning of the crystal. The crystal was thinned using 320, 400 and 600 grit sandpaper and polished using 1.0 and 0.3 microm alumina powder until a smooth surface was obtained in reflected light in a microscope with a 40X objective lens. The sample in wax was removed by heating the glass slide on a hotplate at 200°C for a few minutes. It was then flipped over, polished, removed and immersed in M6 organic solvent and then acetone to clean the sample. Samples held in acrylic were pried loose with a razor blade, flipped over and held on a clean glass slide with Eastman 910 (making sure this glue only

adhered to the acrylic and not the crystal). The sample was polished and removed with a razor blade. The polished slabs were reoriented, if necessary, using conoscopic interference figures in a microscope by propping the crystal with tackiwax to center the figure, embedding the crystal and wax in acrylic and polishing as described above. For amphibole and pyroxene grains that were too small to use the aluminum blocks, these crystals were oriented with the acrylic technique on a glass slide. For other minerals such as cordierite, osumilite and beryl which lack good cleavages, the initial orientation was done using their pleochroism characteristics which indicated that the darkest color is normal to their c axes. For these samples orientation was much more dependent upon centering conoscopic interference figures. Acrylic was used for all thinning and polishing work for these samples. Universal stage and X-ray precession photographs of some samples indicated that the final orientations were usually within 5^{o} of the desired direction which suggests that at most only a few percent of the true peak intensity is lost in spectral measurement based upon calculations similar to those at the end of Chapter 4. The thicknesses of the slabs were determined by the ability to obtain all spectral data within the first two pen ranges of the Cary 17I and were measured by a hand held micrometer unless otherwise stated in text.

The oriented crystals were held in place over an aperture in a copper disk, using the largest aperture appropriate for the size of the crystal, with electrical tape or vaseline. Aluminum holders for the calcite polarizers were constructed to fit in the sample and reference chambers of the Cary 17I. The copper disk containing the sample was place on the aluminum holder in the sample chamber between

the calcite polarizer and the detector. The polarization direction of the calcite polarizers is 45° from the polarization direction of the Cary 17I caused by the position of its gratings. In many instances, the copper disk was removed from the aluminum holder and directly transferred to the Perkin Elmer 180 for measurement in the infrared region. Absorbance mode was used in the Perkin Elmer 180 and the absorbance was calibrated with a wire grid screen with a known absorbance at 4000 cm^{-1} (2500 nm) determined in the Cary 17I. The baseline spectra for each experiment were obtained solely with the copper disk without the sample using the same spectrometer settings. Spectral resolution was better than 5 nm for the Cary 17I and 10 cm^{-1} for the Perkin Elmer 180. The spectra were digitized on computer cards and plotted by computer using the program SPPLOT which is briefly described in Chapter 2. A listing of this program may be obtained from the author for the cost of duplication.

Spectra taken at 77 K were obtained in a locally constructed liquid nitrogen dewar. The sample was held in a vacuum on a copper block that is in contact with liquid nitrogen.

A variety of ovens were used to heat single crystals. Temperatures were calibrated against a chromel-alumel thermocouple. The accuracy of the thermocouple was verified at 100°C in boiling H_2O and at other temperatures using the millivolt readout and standard tables. The estimated error in reported temperatures is $\pm$ 10°C.

Electron microprobe data were obtained mostly by the author (A.A. Chodos kindly obtained some of the data for osumilite in Chapter 9) on Cal Tech's computerized MAC5-SA3 electron microprobe using the program ULTIMATE (Chodos et al., 1973). Operating voltage was 15 kV with a current of .05 ma with approximately an 18 micron spot diameter.

Microprobe analyses were taken in the areas on the oriented slabs used for optical work. X-ray precession photographs were obtained in Cal Tech's chemistry department under the supervision of Dr. Sten Samson. Details of the procedure to obtain the Mössbauer data are given in Chapter 5. The Mössbauer data were obtained at the University of California, Los Angeles with Dr. W. A. Dollase and at the Rockwell International Science Center in Thousand Oaks, California with Dr. R. M. Housely.

Absorption peak positions in the electronic absorption spectra were obtained by estimating the slope of the baseline upon which the main peak is superimposed, drawing tangents at a point on the baseline and the main peak, and finding a particular position at which both tangents are parallel to each other. The intensity difference between these two points of tangency is used as the intensity of that absorption band. Gaussian fitted intensities and positions were determined only for some of the cordierite samples because of the closely overlapping octahedral Fe^{2+} bands. However, the results from these computer fits were similar to those estimated using the tangency procedure. The error bars for the intensities of the intervalence bands in calcic amphiboles on page 167 were determined by taking the least possible intensity of the band by drawing a straight line between the tails of the band and a reasonable maximum intensity by giving the baseline a much greater curvature in this region. Typical errors for Fe^{2+} site occupancies from Mössbauer data (Chapter 5, Table 2) are typically less than a few percent when peaks are well separated. Including possible differences in recoil-free fractions among the various sites, the estimated uncertainties in these values probably is less than 10 percent. The Mössbauer data of Bancroft and

Brown (1975) agreed within about 10 percent of the Fe^{3+}/Fe^{2+} ratios determined on their samples from wet-chemical analysis.

REFERENCES

Bancroft, G. M. and J. R. Brown (1975) A Mössbauer study of coexisting hornblendes and biotites: Quuatitative Fe^{3+}/Fe^{2+} ratios. Am. Mineral. 60, 265-272.

Chodos, A.A., A.L. Albee, A.J. Gancarz and J. Laird (1973) Optimization of computer-controlled quantitative analysis of minerals. Proc., Eigth National Conf. Electron Probe Analysis, 45A-45C.